Characterization and Modeling of Water Flow in Sandy Soils for Irrigation Optimization

Meisam Rezaei

.

To Reihaneh and Arad,

My Sweet Home;

To the most wonderful people in my life,

My Family

Supervisors:

Prof. Dr. ir. Piet Seuntjens
Flemish Institute for Technological Research, Environmental Modeling Unit
Ghent University, Department of Soil Management

Prof. dr. ir. Wim Cornelis
UNESCO Chair of Eremology,
Ghent University, Department of Soil Management

Dr. ir. Ingeborg Joris
Flemish Institute for Technological Research, Environmental Modeling Unit

Examination committee: **Prof. dr. ir. Guido Wyseure** *(KU Leuven)*
Prof. dr. ir. Dany Bylemans *(KU Leuven, pcfruit)*
Prof. dr. Peter Finke *(Ghent University)*
Prof. dr. ir. Pascal Boeckx *(Ghent University),* ***Secretary***
Prof. dr. ir. Kris Verheyen *(Ghent University),* ***Chairman***

Faculty of Bioscience Engineering
Dean **Prof. dr. ir. Marc Van Meirvenne**

Ghent University
Rector **Prof. dr. Anne De Paepe**

ir. Meisam Rezaei

Characterization and Modeling of Water Flow in Sandy Soils for Irrigation Optimization

Thesis submitted in fulfillment of the requirements for the degree of

Doctor (PhD) in Applied Biological Science Engineering: Land and Water Management

Academic year 2015-2016

Dutch translation of the title:

Karakterisering en modellering van bodemwatertransport voor optimalisatie van irrigatie

This work should be cited as:

Rezaei, Meisam. 2016. Characterization and Modeling of Water Flow in Sandy Soils for Irrigation Optimization. PhD thesis, 238 pp, Ghent University, Ghent, Belgium.

ISBN: 978-90-5989-918-6

Cover illustration:
Front: irrigation of potato field using standard Reel Gun Sprinkler (Credits: Meisam Rezaei).

Back: a) the classified map of 0–100 cm soil ECa with indication of the 20 soil sampling locations (black bullets) from the ESAP software, the eight additional points along the transect, and the elevation contour intervals (labels in m a.s.l.); b) estimated saturated hydraulic conductivity, K_s from the site-specific empirical (geophysical) relation; c) interpolation of groundwater level, GWL; d) first layer depth, FLD; and e) a map of triggred irrigation (resolution: 10 x 10 m), the outcom of quasi 3D modeling approach.

بسم الله الرَّحمن الرَّحيم

In the name of Allah, most benevolent, ever-merciful

"*We sent down water from the sky in right measure, and caused it to stay in the soil, and We have the power to cause it to drain off (vanish).*"

(Holly Quran: 23:18)

Acknowledgments

"***O my Lord, open my breast for me, and make my task easy for me, and remove the impediment from my tongue so that people may understand my speech, and appoint a counselor for me...*** " (Holly Quran: 20: 25-29)

To be honest, writing the thesis is easier than writing the forewords, enough words do not come to express.

First and foremost, I would like to thank Allah for hidden and apparent assistance and the many blessings that steered me to the right ways allowing to have the contribution to the advantageous knowledge to the human being. With no doubt, God provided everything through my life and crossing my road with supervisors, friends and colleagues.

During the past years of my doctorate study, it has been an honor getting to know all my professors, teachers, the reviewers of the thesis, colleagues, friends and all those who made their noticeable efforts, put finger prints and immense benefits on this work. It would not have been possible to complete without the support of them.

I want to say thank you to Dr. Seyed Alireza Movadedi Naeini for the valuable advice and for persisting and inspiring me with his positive attitude to getting a PhD position abroad. Getting acceptance from Prof. Piet Seuntjens and Prof. Wim Cornelis and thereafter starting the PhD is greatly appreciated. Thanks for opening the door and for continuously showing me the correct way.

I would like to express my deepest appreciation and thanks to my supervisors Prof. Piet Seuntjens, Prof. Wim Cornelis and Dr. Ingeborge Joris. I want to dedicate my special thanks to Piet for encouraging my research, for significantly supporting and guiding me to grow as a research scientist, and for opening my sight on applied science. As Piet, Wim is one of the best teacher I have ever had. I would like to say thanks to him for putting up with me, for giving me feedback and support, and for gently pushing me into the right direction regardless of being a very busy mentor. His smile and laugh is never forgotten. Thanks to critical feedback and insightful talks of Ingeborg. She was always with me in front of VITO juries. They were all so honest and friendly like my brothers and sisters. As the nice model for my future career, their humanity, morality, personality and ability to guide and teach students are deserved to be appreciated.

I would like to thank Prof. Wyseure, Prof. Bylemans, Prof. Boeckx, Prof. Verheyen, Prof. Finke as the members of the Examination board of the PhD defense for spending plenty of their valuable times, for making constrictive comments and providing useful suggestions which resulted in a noticeable improvement of the manuscript. After the pre-defense, I had a meeting with Prof. Wyseure and Prof. Finke separately. Their effort to teach me and to show me the right insight in this research even during the short time is acknowledged.

Furthermore, I would like to thank the farmer and field owner Jacob Van Den Borne and his family for the great support and for providing the opportunity to perform this study at the experimental fields at his farm. His inspiration on precision agriculture is appreciated.

I would like to thank the researchers and my colleagues who had significant finger print, efforts and valuable feedback on this work and on all my publications. Especially, I want to acknowledge Dr. Mojtaba Pakparvar who taught me a lot about the geostatistical analysis using various software, remote sensing and showed me how important a good collaboration is. Special thanks to Dr. Stijn Van Hoey and Jan De Pue for their great contribution on helping me in the modelling approach and on teaching me programing in python.

Special thanks go to Wesley Boënne, Daniel Wilczek, Marten Volckaert, Anne Terryn, Luc Deboosere and Patrick Dossche for their help and support during the many hours of field and lab work, administrative work and other relevant discussions.

From VITO, I would like to acknowledge all the people who contributed in my work, had valuable discussions and support, and helped me in different aspects. I would nominate them as, Dr. Jan Bronders, Dr. Ilse Van Keer, Dr. Goedele Verreydt, Dr. Filip Lefebre, Dr. Bino Maiheu, Dr. Clemens Mensink, Wim Peelaerts, Inge Uljee, Dr Siavash Atashgahi, Dr. Ann Gobin, Dr. Uwe Schneidewind, Alistair Beams, Sivee Chawla, Maurits Ceuppens, Katrien Bultynck, Johan Vos, Dr. Jeremy de Valck, Dr. Ghulam Mustafa, Dr. Sareh Rezaei among many others.

From Ghent university a special thanks goes to my friends for sharing their experience, for handing in my research, for nice discussion during lunch times, for nice parties, for nice traveling for conferences and contribution to this work. Mesfin, Jeroen, Nele, Sofie, Phoung, Ellen, Stany, Linh, Lisa, Bashar, Lidong, Mararten, Yves-Dady, Jasmin, Muhammed, Mansonia, Nick, Geofry, Linda, Timothy, Emmanuel, Masuda (Emily), Hui, Philippe, Marthe,

Samuel, Peter, Darren, Azita, Mathias, MohammadReza, Mojtaba, Sami, Hojjat, Hadi, Razieh, Elham; Thank you so much.

Outside Ghent university, I wish to express my gratitude to my friends and their families: Khaleh Foozieh, Abbas, Jafar, Naweer, Sajad, Hojjat, Ali, Mohammad, Sasan, Siamak, Karim, Amir, Farzad, Reza, Hadi, Hamidreza, Mehdi, Hassan, Ali, Mojtaba, Hadi, sadegh, Hatef, Ali, Davood, Simon, Dacil, Jessica.

This work was funded by the Ministry of Science, Research and Technology (MSRT) of Iran, Ghent University and Flemish Institute for Technological Research (VITO) of Belgium. I am grateful to all study participants for their contributions.

A super special thanks to my family. I am deeply indebted to my parents, Reza and Batool, and my parents-in-law, Ahmad and Robabeh. Their prayers, guidance, patience, relentless and unconditional love, compassion and encouragements allowed me to reach where I am today. Words cannot express how grateful I am to them. They have provided the most important support in giving the energy and motivation for being progressive in my life. I also acknowledge my brother; Masoud, sister; Mahya, sisters –in-law; Hengameh and Sharareh, and brother-in-law; Pedram. I am especially grateful to Hengameh who did all my administrative work in Iran. May the Almighty God bless all of them abundantly.

Next to all, for the last but not least, I should remember the devoted patience of my wife Reihaneh for paving the road for all stages of my studies. I appreciate Reihaneh for her love, tolerance and understanding towards me. She has encouraged me during the past few years of my PhD career. Thank you to Reihaneh for taking care of our son Arad during my time away from home and looking after him during the weekends and holidays, allowing me to concentrate on my thesis. Our darling child Arad, who was born in 2014, motivates me to try harder and make the difference in life. His everyday smiles have kept me strong all through.

اَللّهُمَّ اَخْرِجْنی مِنْ ظُلُماتِ الْوَهْمِ وَ اَکْرِمْنی بِنُورِ الْفَهْمِ اَللّهُمَّ افْتَحْ عَلَیْنا اَبْوابَ رَحْمَتِكَ وَانْشُرْ عَلَیْنا خَزائِنَ عُلُومِكَ بِرَحْمَتِكَ یا اَرْحَمَ الرّاحِمینَ

Gent, Belgium, September 2016

Meisam Rezaei

Table of Contents

List of Figures

List of Tables

List of Acronyms and Symbols

1-D model	One dimentional model
2/3-D model	Two/Three dimensional model
CAS	Central Absolute Sensitivity
CEC	Cation exchange capacity
CET	Central European Time
CPRS	Central Parameter Relative Sensitivity
CTRS	Central Total Relative Sensitivity analysis
CV	Coeficient of variation
DOE	Depth of exploration
DWS	Degree of water stress
EMI	Electromagnetic induction
FAO	Food and agriculture organization
FLD	First layer depth of soil profile
FPI	The fuzziness performance index
FSE	Fortran Simulation environment
GSA	Global sensitivity analysis
GWL	Groundwater level
HP	Hydraulic properties
IDW	The inverse distance weighting
IPCC	Intergovernmental Panel on Climate Change
LAI	leaf area index
LSA	Local sensitivity analysis
LSD	Least significant difference
M	Mean
Max	Maximum
MEE	Mean estimation error
Min	Minimum
MPE	Modified partition entropy
MVG	Mualem-van Genuchten
OAT	One-At-a-Time approach
OC	Organic carbon
OK	Ordinary point kriging

pdf	Probability density function
PTFs	Pedotransfer functions
RMSE	Root-mean-square errors
RSSD	Response-surface sampling design
SA	Sensitivity analysis
SD	Standard deviation
SE	Standard error of estimation
SSE	Sum of square error
SWRC	Soil water retention curve
SWS	Soil-water storage
TDR	Time Domain reflectometry
TI	Tension disc infiltrometer
WRB	World reference base

a	Effective range
C_0	Nugget variance
$C_0 + C_1$	Sill
C_e	Nash–Sutcliffe coefficient of model efficiency
ECa	Apparent soil electrical conductivity
ET	Evapotranspiration
ET_a	Actual crop evapotranspiration
ET_o	Reference evapotranspiration
ET_p	Potential evapotranspiration
ϕ	Soil porosity
h	Pressure head
$h_0(t)$	Inlet pressure head
h_i	Initial pressure head
j	Particular measurement set
K(h)	Unsaturated hydraulic conductivity function
K_c	Crop coefficient
K_{fs}	Field saturated hydraulic conductivity
K_{ls}	Laboratory saturated hydraulic conductivity

K_s	Saturated hydraulic conductivity
Ky	Crop yield factor (for grass Ky=1),
l	Pore connectivity and tortuosity parameter
L_r	Rooting depth
M	Number of different sets of measurements
n	Pore size distribution index
N_i	Number of measurement in a particular measurement set i
O	Observed values
P	Significant level
Pc	Crop price
pf	Perturbation factor
phi	fuzziness exponent
$p_j^*(t_i)$	Specific measurement at time t_i
Q	Quasi-steady infiltration rate
q	Quasi-steady state water fluxes
r	Radius of the disc
R(Irr)	Revenue of irrigation function
R(x)	Root distribution function
r^2	Coefficient of determination
S	Simulated values
S(h)	Sink term of Richards'equation
S_e	Effective saturation
SF(t)	Sensitivity function
t	Time
T_p	Potential transpiration
v_i	Weighting coefficient associated with a particular measurement set *i*
vj	Weighting coefficient associated with a particular measurement set *j*
w(h)	Water stress response function
w_{ij}	Weighting coefficient associated with a particular measurement set *j* and *i*
x	Parameter in SF(t) function

x_j	Parameter value
Y	Crop yield
y(t)	Output variable
Y_a	Actual crop yield,
Y_m	Maximum crop yield in optimal condition,
z	Radial and vertical space coordinate taken positive downward
α	Inverse of air entry value, parameter of the van Genuchten-Mualem
n	Shape parameters for the van Genuchten-Mualem
α_G	Slope of *K(h)* function in semi logarithmic form of Gardner's equation
α_{vG}	van Genuchten inverse of air entry value
β	Vector of optimized parameters β
Δx_j	Perturbation
θ	Actual volumetric water content
θ*(h)*	Water content function
θ_f	Final water content at the end of the experiment,
θ_i	Initial water content
θ_r	Residual water content
θ_s	Saturated water content
ρb	Bulk density
σ_j^2	Measurement variances
Φ	Objective function
λ	Macroscopic capillary length

Summary

Monitoring and modeling tools may improve irrigation strategies in precision agriculture. The main aim of this thesis was to develop and test methods for optimizing the irrigation efficiency using a combination of non-invasive soil sensors and process-based soil hydrological models integrated with crop growth models. Soil-water content fluctuations and crop yield was predicted in a heterogeneous sandy grassland and potato field under supplementary irrigation.

In the first step, we used non-invasive soil moisture monitoring, a crop growth and a soil hydrological model to predict soil-water content fluctuations and crop yield in a heterogeneous sandy grassland soil under supplementary irrigation. The sensitivity of the soil hydrological model to hydraulic parameters, water stress, crop yield and lower boundary conditions was assessed for a one-dimensional soil column. The results showed that the effect of the position of the groundwater level was dominant in soil-water content prediction and associated water stress. A time-dependent sensitivity analysis of the hydraulic parameters showed that changes in soil water content are mainly affected by the soil saturated hydraulic conductivity K_s and the Mualem-van Genuchten (MVG) retention curve shape parameters n and α. in a two-layered soil. Results further showed that different parameter optimization strategies (two-, three-, four- or six-parameter optimizations) did not affect the calculated water stress and water content as significantly as does the bottom boundary. In this case, a two-parameter scenario, where K_s was optimized for each layer under the condition of a constant groundwater depth at 135-140 cm, performed best. Numerical results showed that optimal irrigation scheduling using the aforementioned water stress calculations can save up to 12-22% irrigation water as compared to the current irrigation regime. This resulted in a yield increase of 4.5-6.5%, simulated by the crop growth model.

In the second step, the correspondence between K_s and the apparent electrical conductivity (ECa) was assessed to estimate the spatial distribution of hydraulic properties at the field scale. To predict the *Ks* for the whole field, spatial distributions of *Ks* and its relationship between co-located soil ECa measured by a DUALEM-21S sensor were investigated. Results demonstrated the large spatial variability of all studied properties with K_s being the most variable one (CV = 86.21%) followed by ECa (CV $\geq$ 53.77%). A significant negative correlation was found between ln-transformed K_s and ECa ($r = 0.83$; $P \leq 0.01$) at two depths of exploration (0-50 and 0-100 cm). This site-specific relation between ln K_s and ECa was used to predict saturated hydraulic conductivity over 0-50 cm depth for the whole field. The empirical relation was validated using an independent dataset of measured K_s. The statistical results demonstrate the robustness of this empirical relation with mean estimation error MEE=0.46 (cm h^{-1}), root-mean-square errors RMSE = 0.74 (cm h^{-1}), coefficient of determination $r^2 = 0.67$ and coefficient of model efficiency $C_e = 0.64$. The relationship was then used to produce a detailed map of K_s for the whole field. The result will allow model predictions of spatially distributed water content in view of irrigation management.

In the third step, to identify proper sets of hydraulic parameters and to evaluate their relevance on hydrological model performance for irrigation management purposes we analyzed and

compared soil hydraulic properties obtained by traditional laboratory experiments and inverse optimization tension infiltrometer data along the vertical direction within two profiles in a potato field. The main goal was to identify proper sets of hydraulic parameters and to evaluate their relevance on hydrological model performance for irrigation management purposes. Tension disc infiltration experiments were carried out at four and five different depths for both profiles at consecutive negative pressure heads of 12, 6, 3 and 0.1 cm. At the same locations and depths undisturbed samples were taken to determine MVG hydraulic parameters (residual water content θ_r, saturated water content θ_s, shape parameters α and n, and lab saturated hydraulic conductivity K_{ls}) in the laboratory. Results demonstrated horizontal differences and vertical variability of hydraulic properties. The tension disc infiltration data fitted well in inverse modeling using Hydrus-2D/3D in combination with final water content at the end of the experiment, θ_f. Four MVG parameters (θ_s, α, n and field saturated hydraulic conductivity K_{fs}) were estimated (θ_r set to zero), with estimated K_{ls} and α values being relatively similar to values from Wooding's solution which used as initial value and estimated θ_s corresponded to (effective) field saturated water content. The laboratory measurement of K_{ls} yielded 2 – 30 times higher values than the field method K_{fs} from top to subsoil layers, while there was a significant correlation between both K_s values (r = 0.75). We found significant differences of MVG parameters θ_s, n and α values between laboratory and field measurements, but again a significant correlation was observed between laboratory and field MVG parameters namely K_s, n, θ_s ($r \geq 0.59$). Assessment of the parameter relevance in 1-D model simulations, illustrated that the model over predicted and under predicted top soil-water content using laboratory and field experiments data sets respectively. The field MVG parameter data set resulted in better agreement to observed soil-water content as compared to the laboratory data set at nodes 10 and 20 cm. However, better simulation results were achieved using the laboratory data set at 30 to 60 cm depths. Results of our study do not confirm whether laboratory or field experiments data sets are most appropriate to predict soil water fluctuations in a complete soil profile, while field experiments are preferred in many studies.

In the fourth step, a quasi 3D modeling approach was developed by integrating a crop growth (LINGRA-N) and a one dimensional soil hydrological model (Hydrus-1D) to simulate and visualize the water flow, water storage, water stress and crop yield over the entire heterogeneous sandy field. The approach illustrates how prior information on soil hydraulic properties, soil layer thickness and groundwater level with different resolutions can be used in water flow modeling for managing irrigation more effectively and practically in precision farming. In this modeling setup, the field is represented by a collection of parallel non-interacting vertical columns representing different field conditions in terms of soil saturated hydraulic conductivity (K_s) groundwater level (GWL) and root zone-first layer depth (FLD) which were obtained from previous steps. We assessed the computational efficiency and uncertainty when simulating water flow on the large field scale with low to high resolution of input factors and evaluated four irrigation scenarios (no, current, optimized and triggered irrigation scenarios) to find the optimal and most cost-effective irrigation scheduling.

The results showed that the uncertainty in model output (quasi 3D modeling approach) was reduced when using the high-resolution information while a fast performance was achieved.

Results further showed that this approach can accurately determine the field scale irrigation requirements, taking into account spatial variations of model parameters and of boundary conditions across the field. We found that a uniform distribution of water is not an efficient approach since at locations with shallow groundwater, the amount of water applied will be excessive as compared to the crop requirements, while in locations with a deeper groundwater table, the crop irrigation requirements will not be met. Numerical results showed that optimal irrigation scheduling is obtained by triggered irrigation, using the aforementioned water stress calculations and soil pressure heads resulting in saving up to ~300% irrigation water as compared to the current irrigation regime, while yield was not significantly affected (increase of ~1%). Overall, the presented approach can be a useful to help decision makers and applicants in answering what resolution of data is adequate for precision agriculture management, what the optimal irrigation scheduling is and what the economic benefits will be.

Chapter 1. ***General introduction***

1.1 Introduction

Water is the main factor limiting crop production when rainfall is insufficient to meet crop demand (FAO, 2012b). The increased pressure on available water resources, resulting from population growth, represents a major challenge in water management (Falkenmark, 1997). Water availability is also a challenging issue because of human-induced climate change (Hanasaki et al., 2013; Oki and Kanae, 2006). It was reported that 1.8 billion people could be living under conditions of acute water scarcity and two-thirds of the world population could be under stress conditions by 2025 (FAO, 2015). In fact, world agriculture wastes (through inadequate water conservation, losses in distribution, and inappropriate times and rates of irrigation) about 1500 trillion liters of water, 60% of the 2500 trillion liters of water it uses each year (Greenwood et al., 2010). Irrigation is the most important sector accounting for about 70% of the global freshwater withdrawals (the world's accessible water) and 90% of consumptive water uses (Siebert et al., 2010).

Intensive industrial farming in Northwestern Europe is thought to have a lower vulnerability to climate change, because farmers can compensate the impacts with management and technology (Olesen et al., 2011; Reidsma et al., 2010). But it has been shown that a sharp increase in extreme heat and drought is projected by the end of the century, with the potential to significantly reduce yields under current technologies (Gobin, 2012). On the other hand, there is considerable uncertainty about how to adjust timing and rates of irrigation in different cropping systems using such advanced technology.

Accordingly, advanced monitoring and modeling may promote efficient water utilization and an optimal water supply/distribution to increase food and fodder productivity which is crucial when being confronted with worldwide water scarcity, climate change, growing populations and increasing water demands (FAO, 2011). This chapter begins with highlighting the global to regional problems in terms of water management and irrigation, and then introduces general irrigation methods shortly. Further it discusses hydrological and crop growth models and their applications in precision agriculture along with principles of modeling approaches and methods of providing input parameters for such models. Furthermore, the objectives, statement of problem and the outlines of the thesis are presented.

1.2 Water resources: from climate change - global warming to regional water scarcity

Weather and climate are uncontrollable factors which affect the quantity and quality of agricultural production. Agriculture is the most climate–sensitive sector among all economic sectors (Potopová et al., 2015). Therefore the risks of climate change are the major challenges especially for societies of which their population, economic activities and livelihoods depend either directly or indirectly on agriculture (IPCC, 2013b). Climate change plays a diversity of roles all affecting the water cycle and water availability (UNEP, 2014).

According to the latest scientific insights, climate change is leading to changes in the frequency, intensity, length, timing and spatial coverage of extreme weather events (UNEP, 2012). This means that extreme climate events such as droughts, heat waves and flash floods are going to be more modal with higher peaks as compared to the past (IPCC, 2012). Climate change may affect food security and it emphasizes the need to propose local and region-specific management/adaptation strategies in terms of water management. Studies of the impact of global warming on water use and availability have identified the regions vulnerable to water scarcity and have projected future scarcity (Hanasaki et al., 2013).

Climate change is expected to alter hydrological regimes (Mora et al., 2014)and the availability of freshwater, with impacts on both rain fed and irrigated agriculture (FAO, 2012a). With climate change, rainfall levels are expected to decline in many places or to occur in more intense events, while both evaporation and transpiration rates are projected to increase (FAO, 2013). These changes will reduce the availability of soil moisture for plant growth. In addition, changes in the global water cycle in response to warming over the twenty-first century will not be uniform. The contrast in precipitation between wet and dry regions and between wet and dry seasons will probably increase. Climate change is adding heat to the climate system and on land much of that heat goes into drying (Trenberth et al., 2014). The higher temperatures will also increase the rate of soil organic matter decomposition, especially near the soil surface, which will affect the soil’s potential capacity to sequester carbon, retain water and supply vital nutrients to plants (FAO, 2013). A natural drought should therefore set in quicker, become more intense, and may last longer. Droughts may be more extensive as a result. Droughts will have major effects on agricultural production, with a decrease of production in certain areas and increased variability of production to the extent that important changes may need to be

made in the geographic area where crops are cultivated. Local impacts will bring global imbalances (FAO, 2013).

1.2.1 Drought

Drought is a major natural hazard that can have devastating impacts on regional agriculture, water resources and the environment (Sternberg, 2011). Drought is a complex phenomenon which is difficult to monitor. But it can be simply considered in term of soil water storage (Iñiguez et al., 2016). Several definitions of drought can be found in literature. The definition of drought is different in meteorology, hydrology and agriculture (Rossi et al., 1992). Further according to Intergovernmental Panel on Climate Change, IPCC (IPCC, 2007), these three different definitions of drought, which emphasize the relative roles of precipitation, evapotranspiration (ET) and runoff caused by climatic factors, are presented as: i) agricultural drought in terms of moisture (soil water) deficits in the vadose zone or the root zone that impacts crops, ii) meteorological drought is mainly a prolonged deficit of precipitation, and iii) hydrologic drought is related to below-normal streamflow, lake and groundwater levels. However, hydrological drought can also be linked to soil moisture and therefore soils can response to drought differently. This responses is called “the resilience or resistance to drought” and is defined by Iñiguez et al. (2015) as the time needed to recover to its pre-drought state of water content once that rainfall has started in a continuous way to exceed the vegetation water demand.

In addition, climatological (precipitation shortage in absolute amounts for a given period) and atmospheric (defined in terms of precipitation shortages, temperature, humidity and wind speed) are other drought categories (Zamani et al., 2015). Drought can be quantified or defined in terms of the probability distribution function of a drought indicator such as soil water content or stream flow. For a drought not only the amount of water in terms of volume is relevant, but also its availability at the time it is mostly needed (Fischer et al., 2013). In other words, in a drought situation available soil water content reduces on average due to decreasing regional precipitation and increasing evapotranspiration or global warming (if the availability of soil water content is inadequate, part of any extra energy goes into raising temperatures, thereby amplifying warming). Therefore, in the medium to long term, drought will affect water resources and reduce the availability or reliability of water supplies in many places subjected to water scarcity. The impact of drought as a result of climate change is presented in Figure 1-1.

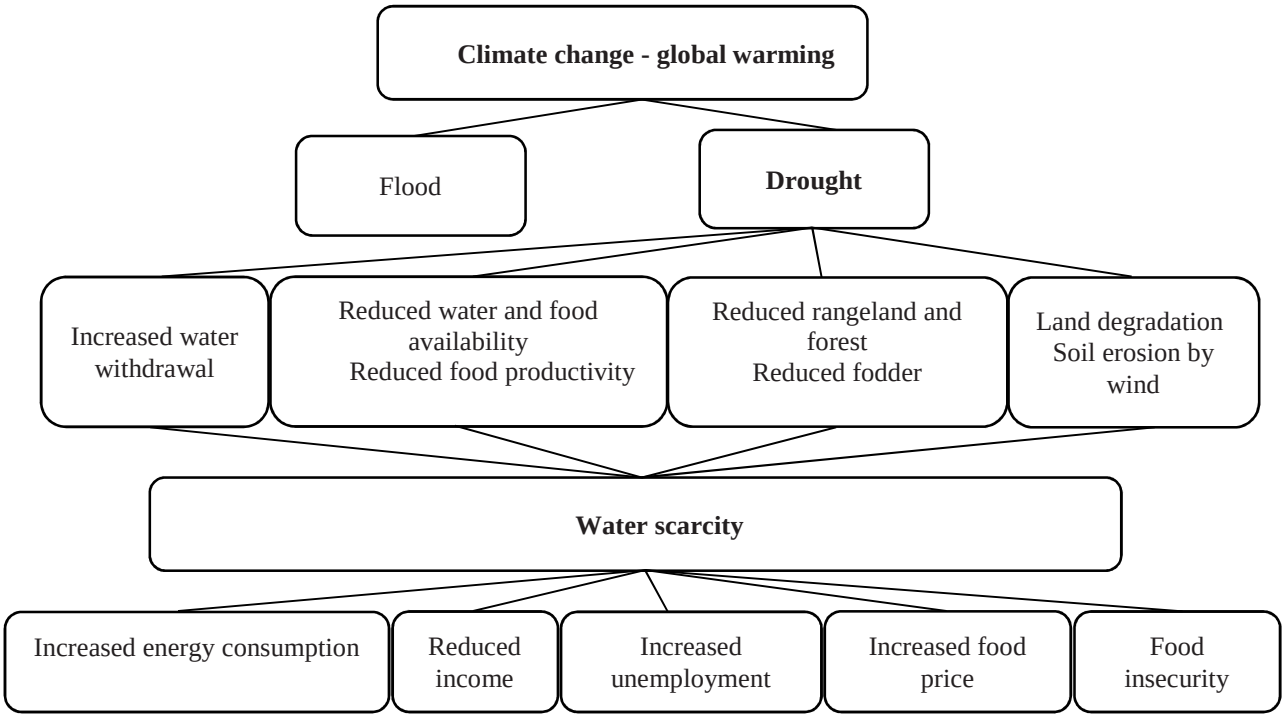

Figure 1-1. The impact of drought as a result of climate change. Source: own.

Although agriculture is highly dependent on climate, it is also strongly influenced by factors unrelated to climate, especially management practices, technological advances, market prices and agricultural policies (FAO, 2013). These factors all have more immediate impacts on water (Bates et al., 2008). For this reason, it is important to understand the current status of water (i.e. water scarcity) and organize efficient water management including irrigation planning in agriculture.

1.2.2 Water scarcity

Agriculture is the main economic sector where water scarcity has the greatest relevance. Figure 1-2 shows significant variations of water availability per capita between countries. This emphasizes the potential of water scarcity over the world which impacts on crop yields (Figure 1-3). Generally, water scarcity is defined as an imbalance between available supply and expressed demand of freshwater in a specified domain, under prevailing institutional arrangements (including both resource 'pricing' and retail charging arrangements) and infrastructural conditions (FAO, 2012a). This definition involves two main types of water scarcity, i.e. physical and economic scarcities which are related to each other. Water scarcity and the presence of water of good quality is a serious public concern since it determines the availability of water to society. Water scarcity especially in arid climates and due to extreme

droughts related to climate change drive water use technologies such as irrigation to become more efficient and sustainable.

Two related terms of water scarcity can be addressed here. One is **water shortage,** i.e., a shortage of quantity and quality of water supply at a given place and a given time. The excessive expansion of irrigation areas with free or cheap water for farmers can result in water scarcity. Groundwater exploitation has grown exponentially in scale and intensity over recent decades. Groundwater's capacity to provide flexible, on-demand water in support of irrigation has been seen as a major advantage by farmers. While intensification of groundwater use has contributed to improved livelihoods of millions of rural people (FAO, 2012a), it has also resulted in long-term groundwater levels declining and aquifer depletion, groundwater pollution and saltwater intrusion into important coastal aquifers (WWDR, 2015). Another one is **water stress,** i.e., the symptoms of water scarcity or shortage expressed in yield reduction. As discussed above climate change and global warming poses an additional threat to water scarcity due to changing meteorological input dynamics which may lead to significant changes in water supply in many regions (Schewe et al., 2014). Water stress depends on soil water–holding capacity, water demand and antecedent wetness conditions (Barron et al., 2003). Water stress is more extended when not buffered by soil water storage. In rain-fed and irrigated agriculture, if the water availability in the soil cannot buffer the difference between supply and demand, the symptoms of water scarcity can be observed, i.e., the development of plants will be hampered, and in the worst case the plants will wither (Fischer et al., 2013). To shorten the

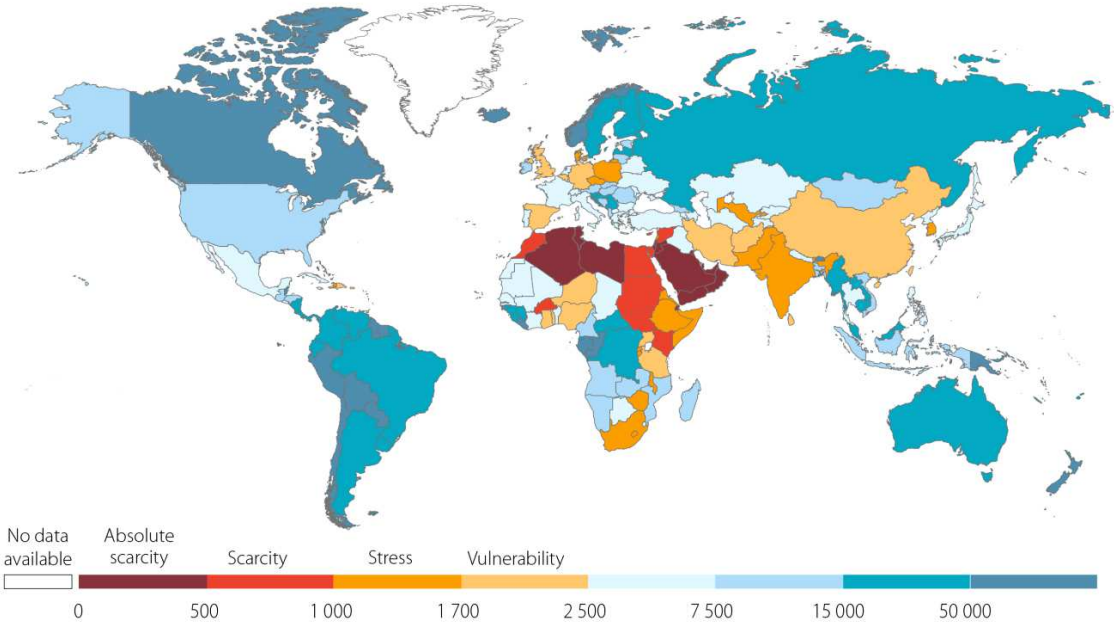

Figure 1-2. Total renewable water resources (fresh water) with variations of water availability between countries in 2013 (per capita in m^3) (WWDR, 2015).

stress period and to cope with water scarcity and drought effects on productivity, adaption in irrigation strategy is crucial.

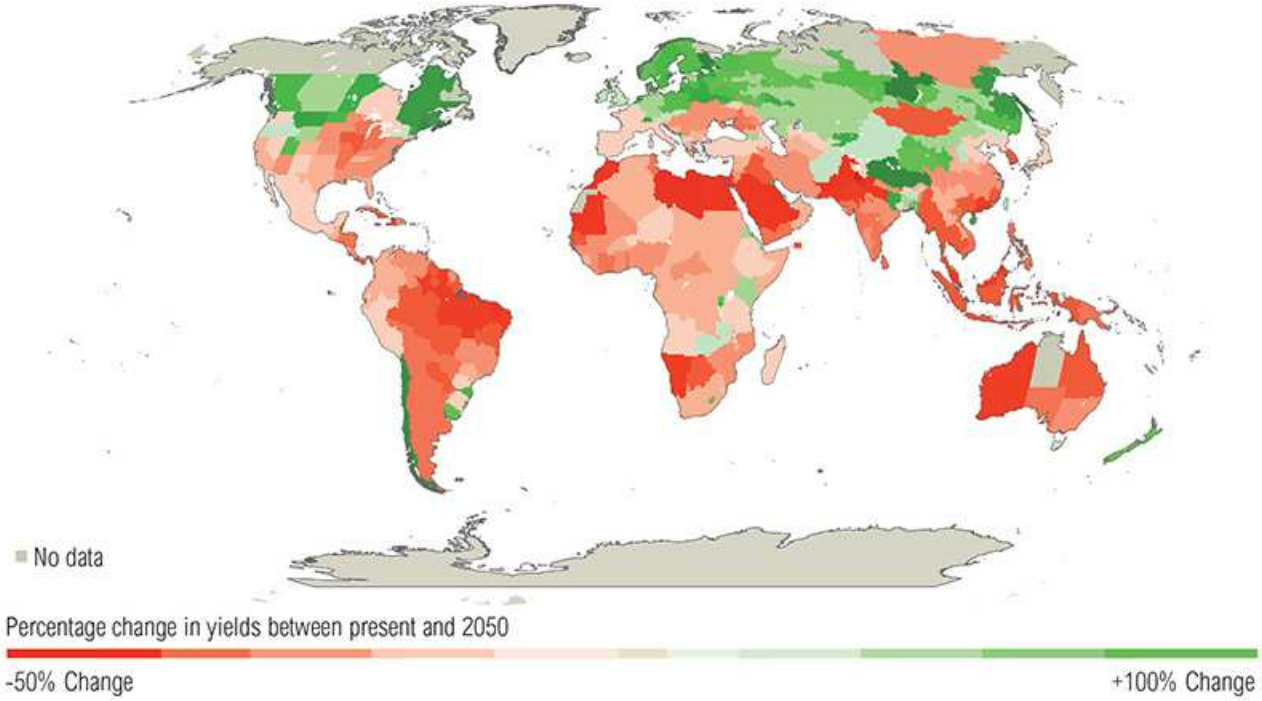

Figure 1-3. Projected impact of climate change (water scarcity) on crop yields between present and 2050 (World Resources Institute; http://ow.ly/rpfMN).

1.2.3 Drought in Belgium

Over the last decades, droughts have had considerable influence on forest and agriculture in Europe (Maracchi et al., 2005; Olesen and Bindi, 2002; Reidsma et al., 2009). Increasing temperature and irregular precipitation patterns during summer will increase the number and intensity of drought events further in Europe (IPCC, 2013a). Over the last two decades, Belgium has experienced more monthly extremes than in any other decade since the observations began in 1833 (Gobin, 2010). Gobin (2010) stated that increasing temperature increases crop development and shortens the growing season. It strongly affects cumulative drainage for both winter and summer crops. Rising temperatures cause higher evapotranspiration rates results in a drier water balance regime with climate change. In that study, average yield losses of 12 to 27% were simulated for sugar beet and 23 to 44% for potatoes owing to drought and heat stress. It has been shown that water stress in a dry summer can decline potato yield of 10 to 40% (Elsen et al., 1995). It is shown that the impacts of the 2003 heat wave in Europe (with temperatures up to 6°C above long-term means) and precipitation deficits up to 300 mm, resulted in an estimated loss of €13 billion for the European agricultural sector (Ciais et al., 2005). The most common drought that occurs in Belgium is

precipitation shortage (meteorological drought) in combination with higher temperature, severe wind and low humidity (atmospheric drought) (Zamani et al., 2015) which leads to water management drought. Therefore this country is exposed to water scarcity and has a high potential of deficit precipitation (cumulative differences between daily evapotranspiration and rainfall) and drought in the summer (1 April-30 September) with increasing in annual temperature (Van Passel et al., 2016).

As we will discuss in the next chapter, to estimate water flow and crop water requirement, reference evapotranspiration (ET_o) and precipitation are two main factors. In Belgium, around early April the average daily evapotranspiration becomes larger than the average daily precipitation; a deficit can therefore accumulate from April onwards. After September, the precipitation deficit tends to decrease as evapotranspiration reduces and rainfall increases. In The Netherlands, the precipitation deficit is defined as the cumulative difference between precipitation and evaporation from April to September (Beersma and Buishand, 2007). Zamani et al. (2015) used the precipitation deficit to identify droughts during summer (April-September) in Belgium and showed the extent and regional variability of drought (Figure 1-4). In Figure 1-4, a 20-years return level of extreme precipitation deficit of grass and surface water provides information on the probability of accordance and magnitude of drought which may be closely linked to soil water shortage and stress.

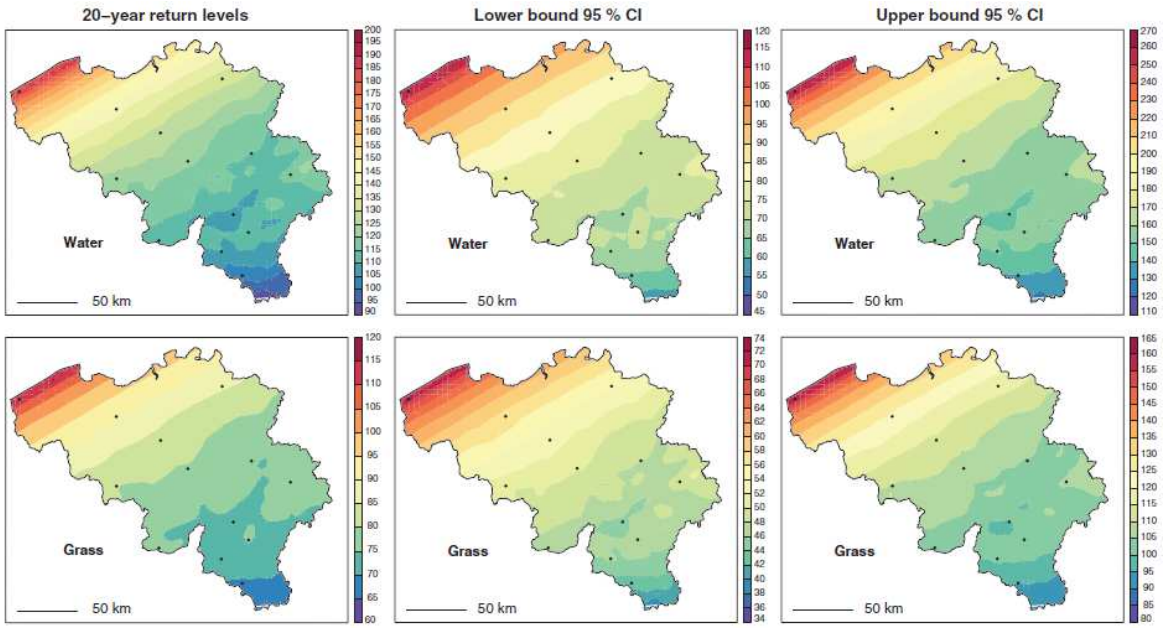

Figure 1-4. 20-Year return level maps, and bounds of the 95% confidence intervals (CI) for precipitation deficit (mm) of Belgium (adapted from Zamani et al. (2015)). Dots on maps show the positions of weather stations where the data obtained.

1.3 Water resource management: adaptation in irrigation scheme

The agricultural sector will face water shortage due to increasing demand from agriculture and non-agriculture sectors, and the uncertainties in water management brought by climate change (Bakkes et al., 2009). For climate change adaptation through enhancing land and water management and increasing agricultural productivity, optimizing irrigation through advanced technology seems to be crucial. Presently, without irrigation global production of dates, rice, cotton, citrus, sugar cane and cereal would decrease by 60%, 39%, 38%, 32% 31%, and 20%, respectively (Siebert and Döll, 2010) while today about 24% of the total harvested cropland is irrigated (Jagermeyr et al., 2015). Increasing water use efficiency is one of the principles for increasing production, while adapting to climate change (FAO, 2013; Fereres et al., 2011). Indeed excessive water withdrawal for agriculture can further exacerbate water scarcity and therefore, efficient irrigation techniques and optimized irrigation programming can have a dramatic impact on reducing water demand (reducing water loss), and consequently increase yield (food, feed, fiber and fuel production per unit of land) and income (more crop per volume of water applied) (WWDR, 2015).

Many researchers investigated the various factors influencing irrigation and how to improve irrigation efficiency of many crops (Akhtar et al., 2013; Banedjschafie et al., 2008; Greenwood et al., 2010; Stewart and Nielsen, 1990). It is reported that despite gradual improvement of water use efficiency in irrigation (using sprinkle or gravity systems), more than half of the irrigated cropland is still irrigated traditionally. However, current irrigation efficiencies are below 50% with most water being lost in the conveyance system or through inefficient application (Jagermeyr et al., 2015). In addition, more than 90% of the farmers do not assess crop irrigation requirements using more efficient on-farm water management practices such as moisture-sensing devices and commercial irrigation-scheduling services (Schaible and Marcel, 2012). For irrigation optimization, a manageable issue is to prevent water losses, which is mostly neglected (Frederiksen and Allen, 2011; Simons et al., 2015). Reducing non-beneficially consumed water (i.e. lost water in any way) can increase crop yields (Al-Said et al., 2012; Luquet et al., 2005; Molden et al., 2010). These strategies can inevitably reduce flow return as well (Jagermeyr et al., 2015).

1.3.1 Crop water productivity

Several approaches can be addressed to increase water use efficiency-crop water productivity, including i) breeding and certain agronomic practices to increase crop yield without increasing

evapotranspiration and water supply (plant breeding to improve yield under drought (Cattivelli et al., 2008)). These propose for developing new crop phenotyping/screening protocols to make better use of deep stored water. They also explore which root traits are most likely to be valuable for improving water uptake to increase yield, and efficient ways to select for these traits in breeding (optimum root system for delivering the highest yield); ii) proper irrigation methods and strategies to reduce water losses; and iii) considering the relationships between crop yield and applied water and irrigation design to increase economic productivity of water. The two latter approaches are further discussed here.

There are various definitions for crop water productivity, or in other words irrigation water use efficiency, and it is therefore difficult to compare studies (Perry et al., 2009). Shortly, crop water productivity can be defined as the ratio between applied water and crop yield. While irrigation efficiency can be translated to the amount of water stored in the root zone compared to the amount of applied water (Pardossi et al., 2009) or the ratio between water consumption (evaporation, transpiration and interception) and water withdrawal (e.g., Jagermeyr et al., 2015). The water efficiency indicators are time and space dependent. It is reported that under optimal practices, irrigation efficiency can be as high as 95%, while the average irrigation efficiency in good field practices, i.e. under sprinkler and drip irrigation, is estimated to be ~65-75%. Furrow and flood irrigation can only achieve an efficiency of ~30-40% (FAO, 2013).

The applied water separates into evaporation from soil, transpiration by crop, surface and lateral runoff and drainage or deep percolation. In a potential evapotranspiration condition, supplying sufficient amount of water to reduce water loss and in/on time water application can be considered as effective efficient irrigation. Two important aspects which affect irrigation efficiency are the type of irrigation and irrigation scheduling. Optimizing the design of irrigation systems can maximize crop yield and decrease the volume of applied water. Under-irrigation results in reducing yield and its quality while over-irrigation increases the nutrient losses, and consequently increase nutrient requirements, and the crop's vulnerability to diseases, the energy costs for water pumping and distribution, water loss and environmental pollution due to the leaching of nutrients. Anyhow, farmers have a tendency to over-irrigate, as to overcome any water shortage regardless of many other aspects (short-sight policy). They must be made aware that due to water scarcity, the limited irrigation water availability and the high pressure on reducing irrigation water as a policy, optimizing water application under frequent (deficit) irrigation is important to derive maximum crop yield (Garcia-Vila et al.,

2009). However, excessive irrigation might not produce greater yield or optimal economic benefit (Sun et al., 2006). Therefore water productivity can be expressed in terms of money (Vazifedoust et al., 2008) or the ratio between the value of the product and water application (Rodrigues and Pereira, 2009; Zwart and Bastiaanssen, 2004). The income term plays an important role in irrigation management. Using full- or over-irrigation, sharply increases yield , but productivity reaches its maximum at a given amount of water supply and then decreases or remains at a constant level even with further increasing water supply (Geerts and Raes, 2009). Since crop yield (Y, unit weight per area) multiplied by crop price (P_c, price per unit weight) is equal to gross income (Eq. 1-1), the relation between irrigation and gross income will show the same trend. The revenue of irrigation function R(Irr) can be written as (English and Raja, 1996):

$$R(Irr) = P_c\, Y(Irr) \qquad (1\text{-}1)$$

Subtracting the irrigation cost e.g., operation cost, from the revenue function gives the maximum income. Figure 1-5 shows the relation between marketable yield and water supply (irrigation and rainfall). In section A, water is insufficient and crop will not fully develop. Once a minimum amount of water is applied (rainfall or irrigation), yield starts to increase with increasing water application (section B). In section C the production function can become nearly linear with additional water application with sharp slope; In section D, the slope of yield often decreases with water application, as observed for many crops. At this stage the yield is maximized with applied water. Additional water application will not produce more yield from the middle of this stage. In section E, applying more water not only will not increase yield but also water losses and will decrease the revenue.

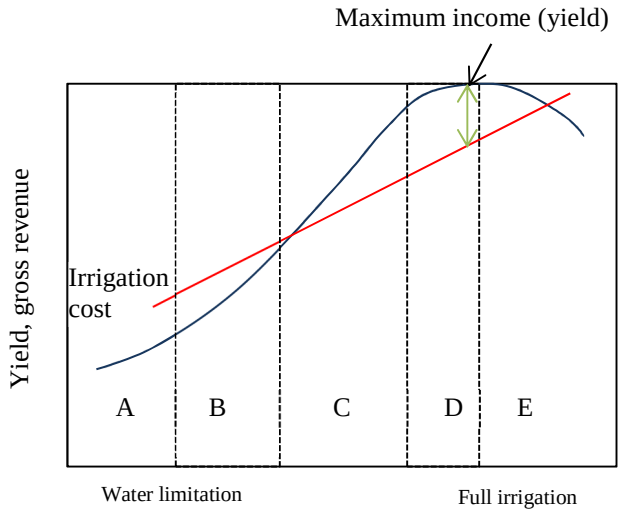

Figure 1-5. General shape of crop production and revenue as a function of water application (adaptet from: English and Raja, 1996; Geerts and Raes, 2009).

1.3.2 Irrigation methods

When talking about irrigation, we generally mean the artificial application of water to cropland and soil. This includes the time, the duration, the intensity or discharge rate and thus the amount of applied water. First of all, the irrigation method is considered to be an important factor in irrigation and agricultural practices for sustainable and economical crop production. Irrigation methods vary regionally and depend on factors like natural conditions (i.e. water availability, soil properties, water quality, climate and topography), type of crop, type of technology, running cost, investment size (Burt et al., 2000) and the farmer's economic income and preferences or experiences. Surface irrigation, sprinkler irrigation and (sub)surface drip/trickle irrigation are the main irrigation methods (Brouwer et al., 1988).

Surface irrigation or flood irrigation is one of the most popular methods for crop irrigation. In this method, water is distributed over the soil surface by gravity flow. Water is pumped or brought to the fields and is allowed to flow along the ground in between the crops. The irrigation water is introduced into level or graded furrows (e.g. to grow vegetables) or basins (e.g. to grow rice) or strips of land (borders, e.g. to grow pasture and alfa alfa), using siphons, gated pipes, or turnout structures, and is allowed to advance across the field. Surface irrigation is best suited to flat land, and medium to fine textured soil types which promote the lateral spreading of water down the furrow or across the basin. Soil evaporation is supposed to be high for this method. This method is simple and cheap, and is widely used by societies in less developed parts of the world as well as in the U.S. This method has a low water use efficiency due to poor irrigation management and some problems such as leveling, low soil infiltration rates and runoff potential (Brouwer et al., 1988; Keller and Bliesner, 1990).

Surface drip/trickle irrigation systems are methods of micro-irrigation wherein water is conveyed under pressure through emitters (which are closed to the plant) to the soil surface as drops or small streams (the immediate root zone of each plant is moistened). The main objective of the drip irrigation design is the uniform distribution of water delivered through the emitters which is affected by design parameters like pressure, discharge variation and emitter characteristics (Carrion et al., 2013; Keller and Bliesner, 1990; Pereira et al., 2002). The discharge rate of the emitters or drippers is slow so this irrigation method can be used on all soil types. Drip irrigation is suited to a wide range of cultivations, for instant individual plants, trees or row crops such as vegetables, cotton and sugarcane.

Subsurface drip/trickle irrigation consists of methods whereby irrigation water is applied below the soil surface and hence increases the water application efficiency with the lowest soil evaporation. The specific type of irrigation method varies depending on the depth of the water table. When the water table is well below the surface, drip or trickle irrigation emission devices can be buried below the soil surface within the plant root zone. However, these systems show higher investment costs than other pressurized irrigation systems. It has been demonstrated that crop yield in this method was greater than or equal to other irrigation methods, and less water was required in most cases (Camp et al., 2000; Lamm and Trooien, 2003). The highest water use efficiency was reported for this method among other methods (O'Neill et al., 2008).

Sprinkler irrigation is a planned irrigation system in which water is pumped through a pipe system and then sprayed over or under the crop canopy, or sprinkled through the air in rain like drops. The system aims to have high uniformity distribution. Of course, the uniformity of the applied water depends on the layout and spacing between sprinklers, wind speed and direction, pressure change, which directly affects sprinkler discharge, and the water distribution pattern of the sprinkler. The water distribution pattern depends on sprinkler type, nozzle type, rotation rate, crop interference, malfunctioning sprinkler heads, and non-vertical risers (Hanson et al., 2011; Keller and Bliesner, 1990; Pereira et al., 2002). The spray and sprinkling devices can be permanently set in place (solid set), temporarily set and then moved after a given amount of water has been applied (portable set or intermittent mechanical move or mobile-gun sprinkler), or they can be mounted on booms and pipelines that continuously travel across the land surface (wheel roll, linear move, center pivot) (Keller and Bliesner, 1990). This method is adaptable to any sloped farm. It is best suited to sandy soils with high infiltration rates. This method is not suitable for soils which easily form a crust, and under very windy and warm conditions.

1.3.3 Irrigation in Belgium and strategic crops

In many parts of Europe, irrigated agriculture is central to the local economy. Traditional water management using sprinkler and drip irrigation systems are mostly used for outdoor and greenhouse, respectively, with an efficiency of 70 to 90%. Increasing irrigation efficiency is one way to improve the irrigation system and sustainable water management. It has been shown that in Belgium the total area equipped for irrigation is 23830 ha (~2% of total agricultural area), of which 13864 ha is irrigated with groundwater (Siebert et al., 2013) which is highly increasing. Therefore, the quantity of groundwater may deteriorate rapidly. In Belgium, 60% of the land is occupied by agricultural area. Grassland (temporary and permanent) covers ~43%

of the agricultural area and annual crops ~55% (Peeters, 2010). Normally, full irrigation water is applied to match the crop water demand at the certain time with almost homogeneous distribution all over the field.

Peltonen-Sainio et al. (2010) concluded that for potato, one of the strategic crops in western and north-eastern agricultural regions of Europe, tuber formation was constrained by reduced precipitation. Using long-term datasets, they found that elevated temperatures had harmful effects on yield and revealed whether there are commonalities across the European agricultural regions for major field crops. Marshall (2015) reported that potato production has further revised down of about 24.8 Mt in 2015 which is now 1.5% below the five years average in North-Western Europe. For Belgium, potato yielded 16% less than previous year i.e., 2014. Potato is highly sensitive to water stress which likely suffers from global climate change.

Grass is one of the most widely cultivated crop in Belgium for livestock production, e.g. meat and dairy. As ryegrass is relatively sensitive to drought stress (Frame and Laidlow, 2011; Norris, 1982), it is almost impossible to achieve its maximum or optimum yield without irrigation. Grass irrigation can lead to excessive water consumption using conventional water management/irrigation. Overall, seasonal crops such as grass and potato put more pressure on groundwater resources. The large amount of required irrigation water has encouraged the development and application of efficient irrigation strategies.

1.3.4 Effective irrigation scheduling

Irrigation scheduling in terms of efficient irrigation, refers to the determination of the applied amount of water to a crop and the timing for application (Pardossi et al., 2009). The goal of irrigation scheduling is to approach an optimal water supply and distribution for achieving higher productivity (soil moisture being maintained close to the upper available water content or field capacity) (Jones, 2004; Schütze and Schmitz, 2010). Generally, four different approaches are used in irrigation management: i) controlling soil-water content in the root zone by its direct or indirect measurement in soil, i.e., “soil-based”, ii) using meteorological data and mathematical models that calculate evapotranspiration (Nosetto et al., 2012), i.e., “weather-based”, iii) sensing of the plant response to water deficits by measuring crop parameters such as stem diameter, leaf thickness; stem sap flow, or root pattern, i.e., “crop-based”, and iv) canopy temperature-based via infrared thermometers on land or boarded on aircrafts and/or satellites, i.e., ‘remote–sensing based” (Evett et al., 2008; Jones, 2004; Mohanty et al., 2013; Pardossi et al., 2009). The advantages and disadvantage of each method

are summarized in Table 1-1. Using a combination of these approaches is increasingly popular. It helps to optimally distribute limited irrigation water during the growing season. This irrigation scheme is adapted to actual weather conditions, soil properties and drought or water shortage conditions and crop status (crop water demand) to achieve high yields and less water loss. Sometimes heterogeneous distribution of irrigation is necessary due to heterogeneity, topography and other soil and field properties. Controlled deficit irrigation is an optimized strategy of irrigation scheduling where water is mainly applied during drought sensitive growth stages of a crop (Geerts and Raes, 2009). Outside these periods, irrigation is limited if precipitation provides a minimum supply of water (English, 1990).

Table 1-1. Summary of main advantages and disadvantages of irrigation scheduling approaches (adapted from Jones (2004)).

Irrigation method	Advantages	Disadvantages
Soil-based: soil water content/potential (TDR, gravimetric and soil water content probe, tensiometer)	Easy to apply; Precise; Availability of commercial system; Automated sensors; Indicate how much water to apply	Extensive monitoring program; Requires many sensors due to soil heterogeneity; Some difficulty in selecting the root zone representation; Sensors do not generally measure water status at root surface
Weather-based: based on soil water balance calculation (needs estimate of water supply and evapotranspiration)	Easy to apply; Indicate how much water to apply	Not so accurate as direct measurements; Required local estimates of precipitation; Evapotranspiration, crop coefficients; Errors are cumulative; Regular recalibration is needed
Crop-based: include plant stress sensing (Tissue water status e.g., visible wilting, pressure chamber, physiological response, etc. e.g., stomatal conductance, growth rate, etc.)	Measure the plant response directly; Somehow easy to detect; Widely accepted reference technique; Sensitive indicator for water deficit	Does not indicate how much water to apply; Labor intensive and slow; Required to determine control thresholds; Not so precise in some cases; Yield reduction often occurs before symptoms, Hard to automate; Need high level skill; Required sophisticated equipment; Expensive
Remote sensing: satellite-based	Remote application; Easy to apply; Scaling up to large area/fields; Correlated to evapotranspiration; Involve wide range of vegetation; suitable for studies of spatial and temporal patterns; Less expensive and time consuming	Does not indicate how much water to apply; Should combine with water balance study (dependency); Recalibration is necessary; Indirect method; Limitations in satellite imagery; Observation are not always captured at ideal items and times; Difficult to identify small irrigated area (resolution imagery 15-60 m from satellite)

1.4 Irrigation scheduling: modeling approach

A balance between water supply and water demand is the key factor for efficient management of water resources in agriculture. The vadose zone is a complex system involving highly non-

linear processes and interactions. Due to limitations of irrigation scheduling methods (Table 1-1) and their application, e.g., expenses of installing sensors in the field, in situ or laboratory measurement difficulties, etc. a modeling approach can be used to simulate the timing of irrigation and amount of irrigation. During the last decades, noticeable shifts can be seen from allocation approaches to quantitative management irrigation scheduling (Elmaloglou and Malamos, 2003; Li et al., 2012; Paudyal and Dasgupta, 1990; Raman et al., 1992; Sanaee-Jahromi et al., 2001). The fundamental step to guide quantitative irrigation is developing and using developed mathematical, numerical, physically-based and conceptual models. These models can be used individually or coupled to crop growth and/or hydrological models to efficiently manage water resources in agriculture. These models have been applied to manage irrigation systems.

1.4.1 Crop growth modeling

A crop model is a simple presentation of a crop which is used to study crop growth and to calculate growth response to chemical and water applications. Several models have been developed during the past three decades to simulate crop growth and soil water processes (Vazifedoust et al., 2008). There are various crop growth models that differ in complexity, including statistical, mechanistic, deterministic, stochastic, dynamic, static, simulation, descriptive and explanatory models designed for different purposes (Murthy, 2004). Crop models facilitate the evaluation of irrigation strategies or climate scenarios and generalized crop production. Crop growth models are generally based on a soil water balance and include yield-water functions. These model are applied in decision support systems for irrigation and fertilization scheduling (Darouich et al., 2014), to predict possible impact of climate change on agriculture (Gobin, 2010; Semenov, 2009), to design or manage irrigation systems (Darouich et al., 2014; Li et al., 2011; Shang and Mao, 2006), to assess water saving practices (Fang et al., 2010; Gongalves et al., 2007), and to evaluate the feasibility of deficit irrigation (Geerts et al., 2010; Salemi et al., 2011). In Table 1-2, examples of crop growth models and their application are summarized.

1.4.1.1 LINGRA-N: a crop growth model

The grassland growth model LINGRA (LINTUL GRAssland) was developed by the DLO Institute for Agrobiology and Soil Fertility (AB-DLO) (Bouman et al., 1996), now Alterra Wageningen UR. LINGRA was developed to predict growth and development of perennial rye grass across the member states of the EU at the level of potential and water-limited production.

The model is based on the LINTUL (Light INTerception and UtiLisation simulator) concept as proposed by Spitters (1988); Spitters (1990). It also is the extension of CGMS (Crop Growth Monitoring System) to include the estimation of productivity of grasslands using WOFOST model. The model was calibrated and evaluated on experimental field data collected throughout Europe. The LINGRA-N model, which is extended and developed from LINGRA by Wolf (2012), is a simple crop growth model which can calculate grass growth and yield under potential (i.e. optimal), water limited (i.e. rain fed) and nitrogen limited growing conditions. In both situations, the crop is optimally protected against pests, diseases and weeds. LINGRA-N is a generic model which can be used for different grass types growing under a large range of soil and weather conditions with different management regimes.

LINGRA was written in the Fortran Simulation Environment (FSE) standard. This model simulates grass growth, development and biomass yield as a function of weather, soil, management and variety-specific coefficients (Bouman et al., 1996). Within a given region, crop and soil characteristics and farm management are relatively constant over years, and the function of the tool is to quantify the effect of varying weather conditions on crop growth. The main principle of this concept is that crop growth is proportional to the amount of light intercepted by the canopy. The growth rate in the LINGRA model follows the source-sink concept. Growth depends on the strength of both the source (photosynthesis and remobilization of reserves) and the sinks (the carbon-demand of growing tillers and leaves). The assimilation production from photosynthesis is set be the amount of intercepted radiation and a light use efficiency (LUE) factor, which in turn is determined by the CO_2-concentration in the air, the air temperature, the light intensity. LUE is also sensitive to drought and decreases with increasing water stress. More details are given by Schapendonk et al. (1998). A simulation with the LINGRA-N program uses in general the file BATCHG.inp to read the specifications (in particular, the years, soil, weather, crop, and management) of the run. The routines CROPG.dat (crop data such as emergence, phenology, green area, radiation use efficiency, death rate), SoilG.dat (soil data such as water retention data, infiltration rate, initial soil water content and maximum rooting depth, rooting, water and nitrogen use), MANAGG.dat (input file for N application, irrigation water application and cutting regime) and STATR.dat (daily weather data such as solar radiation, minimum and maximum temperature, vapour pressure, wind speed and precipitation) are used in the batch setup. The daily output is produced by the model (in DAILOUT.out). The components of the grass production (kg/ha), development stage, leaf are index, LAI (m^2/m^2), components of water balance (mm) soil water content (cm^3/cm^3) are given

in that output file. For a thorough overview on this crop growth simulation model, the reader is referred to Bouman et al. (1996) and Wolf (2012).

Table 1-2. Examples of most commonly used crop growth models and their application.

Model	Description	Application	Review literature
WOFOST (Van Keulen and Wolf, 1986)	WOrld FOod STudies	A mechanistic-simulation model for the quantitative analysis of water use, the growth and production of annual field crops	Castaneda-Vera et al. (2015); Eitzinger et al. (2013); Li et al. (2012); Mishra et al. (2015); Peltonen-Sainio et al. (2015); Rotter et al. (2012); van Diepen et al. (1989); Wang et al. (2015a)
CGMS (Hooijer and van der Wal, 1994)	Crop Growth Monitoring System	A combination of GIS and WOFOST model for spatial yield prediction	Technow et al. (2015); Hutchings et al. (2012)
SUCROS (Spitters et al., 1989)	Simple and Universal Crop Simulator	Simulates potential growth of a crop under supplied water and nutrients and prevailing weather condition	Burguete et al. (2014)
SIMCOY (Brown and 1969; Place and Brown, 1987)	SIMulation of COrnYileld	Simulate yields under different management options	Wang et al. (2015a)
CERES (Jones and Kiniry, 1986)	Crop Environment REsource Synthesis	The explanatory and dynamic crop model to simulate phenological development, formation of leaf and stem and root biomass, available soil water content and nitrogen balance for cereals (barley, maize, sorghum, millet, rice and wheat)	Castaneda-Vera et al. (2015); Eitzinger et al. (2013); Hasegawa et al. (2000); Jamieson et al. (1998); Laurila (1995); Quiring and Legates (2008); St'astna et al. (2002); Wang et al. (2015a)
APSIM (McCown et al., 1996)	Agricultural Production System sIMulator	Allows models of crop and pasture production, residue decomposition, soil water and nutrient flow, and erosion to be readily re-configured to simulate various production systems and allows soil and crop management to be dynamically simulated using conditional rules	Keating et al. (2003); Wang et al. (2002); Wang et al. (2015a)
Beta model (Gao et al., 1992)		Similar to WOFOST, uses multiplicative functions to describe the interaction between temperature and photoperiod effects under different management	Wang et al. (2015a); Zheng et al. (2000)
SWACROP (Huygen, 1992)	Soil WAter Content and Crop	Simulates root-water uptake functions, crop yield, solute transport	Hack-ten Broeke (2001); Pinthong and Clemente (2014); Utset et al. (2000)
MACROS (Penning de Vries et al., 1989)	Modules of an Annual CROp Simulator	Processes of crop growth and water movement for a range of crop types and weather variables. Estimates water balance for well drained and partially saturated soils	Ebrahim (2008); Matthews and Wassmann (2003)
CROPWAT (Smith, 1991)	CROP WATer	A decision support tool for the calculation of crop water requirements and irrigation requirements based on soil, climate and crop data	Abedinpour et al. (2014); George et al. (2000); Kloss et al. (2012); Kuo et al. (2006); Loukas et al. (2015); Luo et al. (2015)

Model	Description	Application	Review literature
ISAREG (Teixeira and Pereira, 1992)	Irrigation Scheduling REGen	Performs the water balance for a multilayered soil; Used for irrigation scheduling simulation, impacts of water stress and salinity on yield0	Darouich et al. (2014); (Gongalves et al., 2007); Pereira et al. (2009); Valverde et al. (2015)
BUDGET (Raes, 2002)		A set of validated subroutines describing the various processes involved in water extraction by plant roots and water movement in the soil profile. Calculates the water storage and salt content in a cropped soil profile as affected by input and withdrawal of water	Malekpour and Babazadeh (2011); Raes et al. (2006a)
OSIRI (Chopart et al., 2007)	Outil Simplifié pour une Irrigation Raisonnée et Individualisée (i.e. simple decision-making tool for sustainable individual monitoring of irrigation)	A simple tool aimed at optimizing irrigation water and rainfall use, taking into account heterogeneities of the irrigation parameters and of the environmental factors	Lebourgeois et al. (2010)
ISM (George et al., 2000)	Irrigation Scheduling Model	Irrigation scheduling model under various management options for both single and multiple fields	Dogrul et al. (2011); Raul et al. (2012)
PILOTE (Mailhol et al., 1996)		An operative water balance model which predicts actual evapotranspiration and yield of crops; Determines the water stress index	Bouazzama et al. (2013); Feng et al. (2014); Kloss et al. (2012); Mailhol et al. (1997); Mailhol et al. (2011)
SIMDualKc (Rosa et al., 2012)	Simulation (soil water balance) Dual crop coefficient (Kc)	Simplifying implementation of the computation of the crop coefficient and crop evapotranspiration using the dual crop coefficient approach over a range of cultural practices and to provide ET information for use in irrigation scheduling and hydrologic water balances	Gonzalez et al. (2015); Pereira et al. (2016); Qiu et al. (2015)
AquaCrop (Raes et al., 2009)		The FAO crop-model to simulate yield response to water of several herbaceous crops; Estimation of crop productivity in relation to water supply and agronomic management in a framework based on current plant physiological and soil water budgeting concepts	Abedinpour et al. (2014); Akhtar et al. (2013); Castaneda-Vera et al. (2015); Eitzinger et al. (2013); Pereira et al. (2016); Tavakoli et al. (2016)
DAISY (Abrahamsen and Hansen, 2000)		A mechanistic-dynamic model for simulation of water and nitrogen dynamics and crop growth in agro-ecosystems. The model aims at simulating water balance, nitrogen balance and losses, development in soil organic matter and crop growth and production in crop rotations under alternate management strategies	Angulo et al. (2014); Kloss et al. (2012); Plauborg et al. (2010); Rotter et al. (2012)

Model	Description	Application	Review literature
AFRC-Wheat (Weir et al., 1984)		A mechanistic model that incorporates crop response to water and nitrogen constraints. Model processes include phenological development, partitioning of photosynthesis, growth of leaf and stems, senescence, biomass accumulation, and root system dynamics.	Atkinson et al. (2005); Butterfield and Morison (1992); Jamieson et al. (1998); Laurila (1995)
APSIM	**A**gricultural Production Systems Simulator	A farming systems model that consists of several modules integrated to perform farming systems simulation including water balance, N and P transformations, soil pH, erosion and a full range of management controls	Araya et al. (2015); Brown et al. (2011); Keating et al. (2003); Kloss et al. (2012)
CROPGRO (Hoogenboom et al., 1992)	CROP GROwth	A generic, physiological, process-oriented legume crop growth model	Amiri et al. (2015); Scholberg et al. (1997); Thorp et al. (2015)
CropSyst (Stockle et al., 1994)	Crop System	A multi-year, multi-crop, daily time step cropping systems simulation model developed to serve as an analytical tool to study the effect of climate, soils, and management on cropping systems productivity and the environment	Bouazzama et al. (2013); Castaneda-Vera et al. (2015); Donatelli et al. (1997); Eitzinger et al. (2013); Stockle et al. (2003)
LINTUL (van Oijen, 1992)	Light INTerception and UtiLization simulator	A generic and simple crop growth model that can simulate crop growth under both potential, water limited and nitrogen limited conditions and under climatic change; The main simulated processes are: photosynthesis, phenological development, assimilate distribution to crop organs, water uptake, nitrogen uptake, evapotranspiration, soil water balance, and nitrogen balance	Angulo et al. (2014); Franke et al. (2013); Hijmans et al. (2003); Kooman and Haverkort (1995); Zhao et al. (2015)
SIRIUS (Brooking et al., 1995)		Responses to environmental variations, and in practice by farmers to optimize water and nitrogen applications	Brown et al. (2011); Jamieson et al. (1998); Stratonovitch et al. (2012)
CoupModel (Jansson and Karlberg, 2001)	Coupled heat and mass transfer model for soil-plant-atmosphere system	A process-oriented, dynamic model which describes water-heat-carbon and nitrogen flows in the soil-plant-atmosphere system as a function of climate at various time and spatial scales	(Conrad and Fohrer, 2009; Karlberg et al., 2006)
CENTURY (Parton et al., 1992)		A general model of plant-soil nutrient cycling which is being used to simulate carbon and nutrient dynamics for different types of ecosystems including grasslands, agricultural lands, forests and savannas	Cong et al. (2014)
EPIC (Williams et al., 1983)	Erosion-Productivity Impact Calculator	A cropping systems model that was developed to estimate soil productivity as affected by erosion	Angulo et al. (2014); Eitzinger et al. (2013)

Model	Description	Application	Review literature
DSSAT (Tsuji et al., 1994)	Decision Support System for Agrotechnology Transfer	Soil water balance and crop management; Includes the CERES models for cereals and the CROPGRO models for legumes (dry bean, soybean, peanut and chickpea); and models for root crops (cassava, potato) and other crops (sugarcane, tomato, sunflower and pasture)	Angulo et al. (2014); Araya et al. (2015); Eitzinger et al. (2013); Jame and Cutforth (1996); Rotter et al. (2012)
InfoCrop (Aggarwal et al., 2006)		A generic crop model designed to simulate the effects of weather, soils, agronomic management (including planting, nitrogen, residues and irrigation)	Boomiraj et al. (2010); Tsarouchi et al. (2014)
Expert-N (Baldioli et al., 1994)	The nitrogen balance modeling tool for agricultural and forest ecosystems	A development system with the aim to improve the process understanding of the turnover and transport of matter and the energy fluxes in the soil-plant-atmosphere system; The focus are the simulations of matter cycling in forest, grassland, and crop ecosystems from the field to the regional scale	Gayler et al. (2002); Priesack et al. (2007); Wöhling et al. (2013)
HERMES (PC-Agrar., 1994)		A model to describe plant growth and water and nitrogen dynamics in the soil-plant system.	Eitzinger et al. (2013); Hlavinka et al. (2014); Nendel et al. (2011); Rotter et al. (2012)
LPJmL (Sitch et al., 2003)	Lund-Potsdam-Jena managed Land	Simulates the global terrestrial carbon cycle and the response of carbon and vegetation patterns under climate change	Forkel et al. (2015); Langerwisch et al. (2008); Sitch et al. (2003)
MONICA (Nendel et al., 2011)		A dynamic, process-based simulation model which describes the transport and bio-chemical turn-over of carbon, nitrogen and water in agro-ecosystems	Rotter et al. (2012); Specka et al. (2015)
SALUS (Hoffmann et al., 1993)	System Approach to Land Use Sustainability	Designed to model continuous crop, soil, water and nutrient conditions under different management strategies for multiple years	Eitzinger et al. (2013); Hoffmann et al. (1993); O'Leary et al. (2015)
LINGRA-N (Wolf, 2012)	LINtul-GRAssland-Nitrogen	A simple generic grass growth model which can calculate grass growth and yields under potential (i.e. optimal), water limited (i.e. rain fed) and nitrogen limited growing conditions	Barrett et al. (2004); Barrett et al. (2005); Schapendonk et al. (1998)
SIMPLACE (Gaiser et al., 2013)	Scientific Impact assessment and Modeling PLatform for Advanced Crop and Ecosystem management	A modular modeling framework to support decisions for the management of a wide range of crops and ecosystems under changing resource availability and climate conditions; The framework is developed with standard technologies, which reduce the effort in model development and customization	Rezaei et al. (2015); Zhao et al. (2015)

1.4.2 Hydrological modeling

Crop growth models are sophisticated plant production modules but mostly use simplified soil hydrological concepts, i.e., available water and field capacity. In the vadose zone, modeling soil water content, water flow and solute transport has been under development since 1970s (Bultot and Dupriez, 1976; Neuman et al., 1974; Toksoz and Kirkham, 1971; Zaradny and Feddes, 1979). Hydrological modeling started earlier than 1960s before modelers began to develop conceptual models, e.g. the Stanford Watershed Model (Crawford and Burges, 1966).

Hydrological models are classified based on model input and parameters and on the extent of physical principles applied in the model. Hydrologicals model can be classified according to Jajarmizadeh et al. (2012) as i) based on equations: deterministic (simulate same output for a single set of input values) and stochastic (simulate different values of output for a single set of inputs) models; ii) based on time: static (exclude time) and dynamic (include time divided in two groups: continuous and event-based) models; iii) based on laws and assumptions: empirical (metric model), conceptual (parametric model) and physically-based models; iv) based on parameters: distributed and lumped models; and v) based on the procedure of computation: analytical and numerical models.

The **empirical models** which are called data-driven models, are observation oriented models which take only the information from existing data without considering the features and processes of the hydrological system (Todini, 2007). They involve mathematical equations derived from concurrent input and output time series. Statistically based methods use regression and correlation models and are used to find the functional relationship between inputs and outputs, while **conceptual models** describe all of the component of the hydrological processes. They consist of a number of interconnected physical elements of porous media with rainfall, infiltration, percolation, evaporation, runoff, drainage and etc. Normally, semi empirical equations are implemented in these models and a large number of meterological and hydrological records are needed for calibration. The **physically based models,** also called mechanistic models, are mathematically idealized representations of the real phenomenon. They use state variables which are measurable and are functions of both time and space. The hydrological processes of water movement are represented by finite difference or element equations. They reqiure extensive hydrological, meteorological data and hydraulic parameters describing the physical characteristics of the porouse media and catchment for their calibration and evaluation (Devia et al., 2015; Todini, 2007). They normally require a huge amount of data

such as soil water content, groundwater depth and topography to provide large amount of information. **Analytical models** are mathematical models that have a closed-form solution of the govering equations, i.e. the solution to the equations used to describe changes in a system can be expressed as a mathematical analytic function. **Numerical models** are mathematical models that use some sort of numerical time-stepping procedure to solve the governing equations. The numerical solution is represented by a generated table and/or graph. These models provide outputs only at a finite number of points in both space and time. The numerical soil hydrological models have increased our understanding of irrigation and drainage processes in the context of soil–plant–atmosphere systems during past decades (Bastiaanssen et al., 2004). The most widely used hydrological models are presented in Table 1-3.

Table 1-3. Examples of most commonly used hydrological models and their application.

Model	Description	Application	Review literature
SWAP (van Dam et al., 1997)	Soil-Water-Atmosphere-Plant	Simulates transport of water, solutes and heat in unsaturated/saturated soils at field scale level, during growing seasons and for long term time series	Huo et al. (2012); Vazifedoust et al. (2008)
SWAT (Arnold et al., 1993)	Soil And Water Assessment Tool	Predicts the effect of management decisions on water, sediment, nutrient and pesticide yields with reasonable accuracy on large, ungauged river basins	Abbaspour et al. (2015); Krysanova et al. (1998); Maharjan et al. (2016); Napoli et al. (2013)
VIC (Liang et al., 1994)	Variable Infiltration Capacity	A semi distributed grid based hydrology model which uses both energy and water balance equations; The processes like infiltration, runoff, base flow are based on various empirical relations	Haddeland et al. (2006); Nijssen et al. (2001); Shukla et al. (2011)
HydroGeoSphere (Therrien et al., 2009)		A three-dimensional surface-subsurface soil hydrological model to simulate the observed rainfall-runoff process impacted by a runoff water harvesting technique, while simultaneously simulating the soil moisture redistribution in the subsurface	Brunner and Simmons (2012); Li et al. (2008); Partington et al. (2009); Rosenbom et al. (2009); Verbist et al. (2012); Zhu et al. (2012)
MACRO (Jarvis and Larsson, 1998)		A detailed mechanistic dual-porosity model of water and solute transport in a macroporous soil; A non-steady state simulation of water flow and solute transport in a one-dimensional (vertical) heterogeneous-layered field soils	Merdun and Quisenberry (2005); Siimes and Kamari (2003); Steffens et al. (2014)
HYSWASOR (Dirksen et al., 1993)		The numerical simulation model for hysteretic water and solute transport in the root zone; Simulation root water uptake under non-uniform soil water osmotic and pressure heads in hysteretic conditions	Feddes and Roats (2004); Homaee (2004); Homaee et al. (2002); Homaee and Feddes (1999)
DHSVM (Wigmosta et al., 1994)		A distributed hydrologic model that explicitly represents the effects of topography and vegetation on water fluxes through the landscape	Schnorbus and Alila (2004a); Schnorbus and Alila (2004b); Thyer et al. (2004); VanShaar et al. (2002); Waichler and Wigmosta (2003); Whitaker et al. (2003)
CREST (Wang et al., 2011)	Coupled Routing and Excess STorage	A distributed hydrologic model developed to simulate the spatial and temporal variation of atmospheric, land surface, and subsurface water fluxes and storages by cell-to-cell simulation	Xue et al. (2013)
SWMS2D (Šimůnek et al., 1994)	The Variably-Saturated Two-Dimensional Water Flow and Transport Model	Simulates water and solute movement in two-dimensional variably saturated media; The program numerically solves the Richards' equation for saturated-unsaturated water flow and the convection-dispersion equation for solute transport	Zhu et al. (2013); Zhu et al. (2012)
GSFLOW (Markstrom et al., 2008)	Ground-water and Surface-water FLOW model	Simulates coupled groundwater/surface-water flow in one or more watersheds by simultaneously simulating flow across the land surface, within subsurface saturated and unsaturated materials, and within streams and lakes	Hassan et al. (2014); Tian et al. (2015a); Tian et al. (2016); Tian et al. (2015b); Wu et al. (2015a)

Model	Description	Application	Review literature
VS2DI (Healy and Essaid, 2012)		Simulates water, solute, and heat transport through soils or other porous media under conditions of variable saturation	Butkus and Konstantinova (2008); Dowman et al. (2003); Healy (2008); Kulasekera and Parkin (2011); Schulz et al. (2008)
MODFLOW (McDonald and Harbaugh, 1983)	Modular Groundwater Flow Model	A three-dimensional finite-difference ground-water model; Simulates steady and nonsteady flow in an irregularly shaped flow system in which aquifer layers can be confined, unconfined, or a combination of confined - unconfined	Lee (2015); Liu et al. (2013); Luo and Sophocleous (2011); Perkins and Sophocleous (1999); Switzman et al. (2015); Xu et al. (2012)
WBM-WTM (Fekete et al., 1999)	Water Balance/Transport Model	Gridded water balance model using climate input forcings that calculate surface and subsurface runoff and ground water recharge for each grid cell. horizontal transport	Fekete et al. (2010); Vorosmarty et al. (1996)
FEFLOW (Diersch and Kolditz, 1998)	Finite Element subsurface FLOW system	Simulates groundwater flow, mass transfer and heat transfer in porous media and fractured media; The program uses finite element analysis to solve the groundwater flow equation of both saturated and unsaturated conditions	An et al. (2012); Awan et al. (2015); Liu et al. (2012); Ren et al. (2012); Sulzbacher et al. (2012); Sun et al. (2011); Zhu et al. (2012)
MIKE-SHE (Refsgaard and Storm, 1995)	Systeme Hydrologique European	An advanced integrated hydrological modeling system; A deterministic, physically based, spatially distributed model; Simulation of coupled hydrologic processes with emphasis on surface water - groundwater interactions, channel flow, unsaturated zone flow and groundwater flow	Kourgialas and Karatzas (2015); Mertens et al. (2005)
IWFM (Dogrul, 2007)	Integrated Water Flow Model	A water resources management and planning model that simulates groundwater, surface water, stream-groundwater interaction, and other components of the hydrologic system	Miller et al. (2009); Scherberg et al. (2014)
SPAW (Saxton et al., 1974)	Soil-Plant-Air-Water	Simulates a daily hydrologic budget for agricultural fields with a moderate level of complexity to account for the most important hydrologic processes that will be impacted by the field characteristics; For an agricultural field/watershed plus a wetland/pond/reservoir model	Andersen et al. (2010a); Andersen et al. (2010b); Rao and Saxton (1995); Saxton et al. (1992)
SVAT (Noilhan and Planton, 1989)	Soil Vegetation Atmosphere Transfer	Developed to understand the heat and water regimes in a river basin scale through hydrological modeling	Bormann (2012); Danierhan et al. (2013); Gong et al. (2012); Hashemian et al. (2015); Kloss et al. (2014); Li et al. (2013)
Hydrus 1/2/3D (Šimůnek et al., 2006b)		The one/two/three-dimensional finite element model for simulating the movement of water, heat, and multiple solutes in variably saturated media	Akhtar et al. (2013); Ebrahimian and Noory (2015); Kandelous et al. (2012); Sadeghi and Jones (2012); Seuntjens (2002); Tafteh and Sepaskhah (2012); Wang et al. (2015b); (Wyseure and Chou, 2010)

1.4.2.1 Soil hydrological model

During past several decades, considerable progress has been made in the conceptual understanding and mathematical description of water flow and solute transport processes in the vadose zone. A variety of analytical and numerical models are now available to predict water and/or solute transport within the soil profile from soil surface to ground water table. The most popular models use Richards equation (Richards, 1931) for variably saturated flow, and the Fickian-based convection-dispersion equation for solute transport. Deterministic solutions of these classical equations have been used, and likely will continue to be used in the near future, for predicting water and solute movement in the vadose zone, and for analyzing specific laboratory or field experiments. Models of this type are also helpful tools for extrapolating information from a limited number of field experiments to different soil, crop and climatic conditions, as well as to different tillage and water management schemes (Šimůnek et al., 2013b). This modeling approach ranges from simple analytical models to more complex numerical codes that permit consideration of a large number of simultaneous nonlinear processes such as for transient water flow or nonequilibrium solute transport with nonlinear reactions (van Genuchten et al., 2014).

Even with well-documented numerical computer models available, one major problem often preventing the use of such codes is the extensive work required for data preparation, finite element grid design, and graphical presentation of the output results. Hence, a more widespread use of numerical models requires techniques which make it easier to create, manipulate and display large data files, and which facilitate interactive data management. To avoid or simplify the preparation and management of relatively complex input data files and to graphically display final simulation results, an interactive graphics-based user-friendly interface Hydrus-1D for the MS Windows environment was developed by Šimůnek et al. (2006b). The tool numerically solves the Richards equation for variably-saturated water flow and advection-dispersion type equations for heat and solute transport. The flow equation incorporates a sink term to account for water uptake by plant roots. The flow equation may also consider dual-porosity type flow in which one fraction of the water content is mobile and another fraction immobile, or dual-permeability type of flow involving two mobile regions, one representing the matrix and one the macropores. The program may be used to analyze water and solute movement in unsaturated, partially saturated, or fully saturated porous media. The flow region may be composed of non-uniform soils. Flow and transport can occur in the vertical, horizontal,

or a generally inclined direction. The water flow part of the model can deal with prescribed head and flux boundaries, boundaries controlled by atmospheric conditions, as well as free drainage or constant head boundary conditions. The governing flow and transport equations are solved numerically using Galerkin-type linear finite element schemes (Celia and Binning, 1992). In addition, this model also includes a Levenberg-Marquardt (Levenberg, 1944; Marquardt, 1963) type parameter optimization algorithm for inverse estimation of soil hydraulic and/or solute transport and reaction parameters from measured transient or steady-state flow and/or transport data (Šimůnek et al., 2013b). The Hydrus-1D is a one-dimensional version of the Hydrus-2D and Hydrus-2D/3D codes simulating water, heat and solute movement in two- or three-dimensional variably saturated media (Šimůnek et al., 2006a; Šimůnek et al., 2006b). Further details about the model, governing equations and their functions can be found in Chapters 2 and 4.

1.4.3 Inverse modeling - parameter estimation

To optimize water use efficiency using hydrological models, hydraulic properties need to be determined (Šimůnek and Hopmans, 2002). Due to the highly parameterized framework of numerical hydrological models, direct measurement of its parameters in the laboratory and/or even in the field may be inaccurate, insufficient or inefficient for predictions at the field scale (Verbist et al., 2012; Wöhling et al., 2008). The calibration process, i.e., adjusting a model by manipulating the input parameters such as soil hydraulic parameters, and initial and boundary conditions within a reasonable range to find the least mismatch between simulated and observed soil water content (Šimůnek et al., 2012), is crucial for application in the field. Traditionally, calibration of hydrological models has been performed manually using a trial and error parameter adjustment procedure. The process of manual calibration, however, may be very tedious and time-consuming, depending on the number of model parameters and their interaction. Furthermore, due to the subjectivity involved, it is difficult to explicitly assess the confidence of the model simulations. Consequently, a great deal of research has been directed to the development of more efficient and more objective automatic calibration procedures (Mertens et al., 2005). These can be overcome by conducting inverse modeling (automatic calibration process). An example is the Levenberg–Marquardt optimization for single-objective inverse parameter estimation (Abbasi et al., 2004; Abbasi et al., 2003b; Jacques et al., 2012; Šimůnek et al., 2013b).

In the last few decades, unsaturated soil hydraulic parameters have been estimated with inverse modeling. The inverse modeling approximates soil hydraulic properties from transient experiments in the laboratory or in situ in the field. Inverse modeling was defined by Hopmans et al. (2002) as a general mathematical method to determine unknown causes on the basis of observations of their effects, as opposed to modeling of direct problems whose solution involves finding effects on the basis of a description of their causes.

Water flow and contaminant transport in the vadose zone depends on soil hydraulic parameters, e.g., soil water retention, and saturated and unsaturated hydraulic conductivity (Hopmans et al., 2002). Inverse modeling usually includes the prediction of the soil water retention and unsaturated soil hydraulic conductivity characteristics using Richards' equation. Some advantages of inverse modeling can be: a) more flexibility in boundary conditions on the transient experiment; b) allow simultaneous estimation of both unsaturated hydraulic conductivity function and soil water retention curve; c) increase speed and accuracy of parameter optimization; d) apply in field experiments under different boundary conditions. Excellent overviews of the inverse modeling procedure can be found in Hopmans et al. (2002); Šimůnek and Hopmans (2002); Vrugt et al. (2008); Wöhling and Vrugt (2011).

Soil scientists are often confronted with issues of non-uniqueness and ill-posed terms in parameterization – optimization processes, leading to identifiability problems (Hopmans et al., 2002). In the optimization process, an objective function is measuring an agreement between measured and simulated data (see Chapter 2 and 4 for more details). It is directly or indirectly related to the adjustable parameters to be fitted. Minimizing the objective function generates the best-fit parameters. Maximum probability density function (pdf) and a minimum least-squares criterion should be achieved (Šimůnek and Hopmans, 2002). When multiple local minima or a global minimum occur in a range of parameter values on the basis of the convexity of the objective function (which can be increased by inclusion of prior information (**initial input values of parameters**)), the model solution is called **nonunique**. When a similar system response is caused by different combinations of parameters, the parameters are said to be **nonidentifiable** (leads to a nonunique solution). If small errors in the model or system result in large changes in the optimized parameters, e.g., optimized parameters are sensitive to measurement error, the solution is called **unstable**. The inverse problem is **ill-posed** if the identified parameters are unstable and/or nonunique. Nonuniqueness can be reduced by decreasing the number of parameters to be estimated based on sensitivity analysis. It is caused

by lack of sensitivity analysis of flow variables on particular parameter sets (Hopmans et al., 2002). Nonuniqueness is influenced by the type of measured data, applied values of weighting factor and the suitability of boundary conditions. More information can be found in (Carrera and Neuman, 1986). Sensitivity is affected by the type and number of optimized parameters, model and input variable errors. To that end, systematical sensitivity analysis has been used to better estimate values, to better understand and reduce uncertainty (Rocha et al., 2006) and to investigate the effects of various parameters or processes on water flow and transport (van Genuchten et al., 2012). To reduce the number of parameters that need to be optimized, **sensitivity analyses** are often performed that evaluate model output for each parameter perturbation in a one-at-a-time approach.

1.4.4 Initial values of soil hydraulic parameters

Modeling soil water dynamics, water movement and solute transport requires not only knowledge of soil-water-atmosphere-plant relationships but also their individual characteristics. In a modeling approach, estimates of initial parameter must be reasonably close to their true values, and measurement variables errors such as soil water content must be small. Optimized parameters in inverse solutions strongly dependent on their initial estimation or measurement. Providing well-constrained initial estimates is crucial in forward and inverse modeling of water and solute transport as well as heat and mass transport near the soil surface.

Soils are intrinsically heterogeneous, and some heterogeneities, such as macropores and hydraulic properties control the ability of the soil to store and conduct water at the field scale. Heterogeneity causes variability, and the efficient techniques of the characterization of soil physical variability remains the object of scientific pursuit (Teixeira et al., 2014).

A long array of methods to determine soil hydraulic properties has been earlier presented in (Dane and Topp, 2002; Klute, 1986), and several methods have been added since as presented in the state-of-the-art review by Minasny et al. (2013). We will not repeat them here, but an overview of those methods is summarized in Table 1-4 and Table 1-5. In fact, soil hydraulic properties determination/measurements are expensive, time consuming and labor intensive. Therefore, scientists have attempted to find more efficient ways of characterizing soil hydraulic properties and their spatial and temporal dynamics. In modeling approaches using numerical models, normally shape parameters of soil water retention curve, SWRC, are needed as initial input parameter values. They can be obtained by fitting-closed form analytical expressions containing several parameters to discrete SWRC data sets, which can be obtained through field

or laboratory experiments or from pedotransfer functions (PTFs) (Cornelis et al., 2005). A comparison of closed-form unimodal analytical expressions to describe SWRC can e.g. be found in Cornelis et al. (2005) and Khlosi et al. (2008). Further details about these parametric models to derive SWRC and the hydraulic conductivity function, *K(h)*, are presented in chapter three of Dane and Topp (2002).

Table 1-4. An overview of soil hydraulic parameters determinations (measurement techniques).

			K*		SWRC*	
			Application	**Review literature**	**Application**	**Review literature**
Measurements	**Direct**	**Laboratory**	Constant Head Soil Core Method, Falling Head Soil Core Method, Steady Flow Soil Column Method, Long Column, Steady-State Centrifuge, Wind And Hot-Air Methods, Suction Crust Infiltrometer, Bypass Flow, Tension Disc Infiltrometer, Evaporation Method	Fodor et al. (2011); Jačka et al. (2014); Kelishadi et al. (2014); Reynolds (2008); Reynolds et al. (2000); Schindler et al. (2010); Šimůnek et al. (1999)	Hanging Water Column (*Haines Apparatus)*, Pressure Cell, Pressure Plate Extractor, Long Column, Suction Table, Sand Box, Controlled Liquid Volume, Freezing Method, , Steady-State Centrifuge, Wind And Hot-Air Methods, Suction Crust Infiltrometer, Bypass Flow, Tension Disc Infiltrometer	Schindler et al. (2010); Schwen et al. (2014); Šimůnek et al. (1999)
		Field	Single-ring and double- or Concentric-ring infiltrometers, pressure infiltrometer, constant head well permeameter, the rainfall simulator, Invers/auger-hole method, Piezometer Method, Mini Disc Infiltrometer, Instantaneous Profile, Plane Of Zero Flux, Constant Flux Vertical Time Domain Reflectometry, Guelph Permeameter, Tension Disc Infiltrometer	Fodor et al. (2011); (2014); Reynolds et al. (2000); Reynolds and Elrick (1985b); Ronayne et al. (2012); Verbist et al. (2010); Verbist et al. (2013b); Verbist et al. (2012); Zadeh et al. (2007)	Instantaneous Profile, Plane of Zero Flux, Constant Flux Vertical Time Domain Reflectometry, Tension Disc Infiltrometer	Angulo-Jaramillo et al. (2000); Jabro et al. (2009); Kelishadi et al. (2014); Latorre et al. (2015); Morgan et al. (2001); Zhang (2015)
	Indirect	**Inverse modeling**	Multistep Outflow Method, Evaporation Method, Tension Disc Infiltrometer, Field Drainage, Evaporation Method	Ramos et al. (2006); Schindler et al. (2010); Schwartz and Evett (2002); Schwartz and Evett (2003); Šimůnek and van Genuchten (1996); Šimůnek and van Genuchten (1997)	Multistep Outflow Method, Evaporation Method, Tension Disc Infiltrometer, Field Drainage, Evaporation Method	Angulo-Jaramillo et al. (2000); Ghezzehei et al. (2007); Latorre et al. (2015); Rashid et al. (2015); Rucker et al. (2005); Schindler et al. (2010); Schwartz and Evett (2003); Šimůnek and van Genuchten (1996); Šimůnek and van Genuchten (1997); Verbist et al. (2009b)

Table 1-5. An overview of soil hydraulic parameters determinations (estimation techniques).

	Application	Description	Review literature
Estimation/prediction	**Geostatistics**	Spatial interpolation methods to estimate hydraulic properties and provide their tempo-spatial maps	Bardossy and Li (2008); Botors et al. (2009); Cooke et al. (1993); Gumiere et al. (2014); Herbst et al. (2006); Horta et al. (2014); Miháliková et al. (2015); Romano (1993); Skoien and Bloschl (2006); Voltz and Goulard (1994)
	Proximal soil sensing and Remote sensing	Finding a correspondence between soil hydraulic properties, and an easily measurable parameters e.g., ECa, using sensors such as EMI, GPR and models like DEM to predict high resolution spatial and temporal soil properties	Archie (1942); Brosten et al. (2011); Chaplot et al. (2011); Cosentini et al. (2012); Dafflon et al. (2009); Doolittle and Brevik (2014); Farzamian et al. (2015); Gooley et al. (2014); Jonard et al. (2015); Lesmes and Friedman (2005); Mawer et al. (2015); Mohanty (2013); Morin et al. (2010); Niu et al. (2015); Niwas and Celik (2012); Purvance and Andricevic (2000a); Santanello et al. (2007); Scheibe and Chien (2003); Schmugge (2013); Sudduth et al. (2013); Wildenschild et al. (2000)
	Pedotransfer functions and soil inference systems	Prediction hydraulic parameters from more easily measurable and more readily available soil properties like particle size distribution, organic matter content, dry bulk density, etc., using simple to such sophisticated models in aim of e.g., Neural network analysis	Botula et al. (2014); Bouma (1989); Cornelis et al. (2001); Cresswell et al. (2006); Gupta and Larson (1979); Gwenzi et al. (2011); Moreno et al. (2014); Nguyen et al. (2015); Ostovari et al. (2015); Schaap et al. (1998); Schaap et al. (2001); Vereecken et al. (2010); Weynants et al. (2009); Wosten et al. (1999)
	Digital soil mapping and assessments	Describe approaches that seek to map soil properties with aid of digital techniques (data processing, GIS)	Abdu et al. (2008); Chaplot et al. (2010); Finke (2012); Friedman and Seaton (1998); Gooley et al. (2014); Shin et al. (2013)
	Markov Chain Monte Carlo simulation	Sampling method for sets of hydraulic parameters feeding into the model	Coppola et al. (2009); Harter and Yeh (1998); Mertens et al. (2005); Shin et al. (2013); Verbist et al. (2012); Wöhling and Vrugt (2008)
	Pedogenetic modeling	Regional to Global modeling of soil change; it helps making spatial prediction of soil properties, quantifying the uncertainty of prediction and delineating area of risks	Finke and Hutson (2008); Mirus et al. (2009); Nimmo et al. (2009)
	Inverse modeling	Indirect modeling to approximate hydraulic properties in combination with another methods such as PTF or monte carlo simulation	Carrera et al. (2005); Mirus et al. (2009); Romano (1993); Shin et al. (2013); Verbist et al. (2012); Vrugt et al. (2004); Wöhling and Vrugt (2008)

1.4.5 Sensitivity analysis

Sensitivity analysis (SA) is the study of how a given model output depends on the changes in input parameters or initial conditions which are often poorly known. In general, SA is used to increase the confidence in the model and its predictions. SA is closely linked to uncertainty analysis. The latter aims to quantify the overall uncertainty associated with the response of the

model to model input uncertainties (Rocha et al., 2006). Dane and Hruska (1983) questioned the uniqueness of the inverse solution and concluded that the sensitivity of the optimized parameters depended on the prescribed boundary conditions. Moreover, a higher sensitivity will result in quicker convergence of inverse modeling (Hopmans et al., 2002). Sensitivity is influenced by the type and number of optimized parameters, and by the model (e.g., adjustable factors and/or model structure) and input measurement errors (Russo et al., 1991). To avoid the nonuniqueness of the model solution, the number of parameters to be optimized should be minimized (Schwartz and Evett, 2003) and insensitive parameters should be fixed to the measured or the initial value.

It is important to correctly parameterize water flow equations for irrigation management, specifically for dry periods (which are essential for a correct irrigation management). The application of a time variant sensitivity analysis is crucial to this respect. Therefore, SA is, among other purposes, used to find the most relevant parameters for relevant periods of time which enable a reduction of the number of parameters that need to be optimized in hydrological models. Many studies did aggregate the sensitivities into summarizing sensitivity indices, e.g., Abbasi et al. (2003a); Li et al. (2012); Mertens et al. (2005); Rocha et al. (2006); Šimůnek and van Genuchten (1996); Verbist et al. (2012); Zhou et al. (2012). Parameter SA can be divided into two large categories: global and local sensitivity analysis, each having their strengths and weaknesses.

1.4.5.1 Parameter sensitivity analysis

1.4.5.1.1 Global sensitivity analysis

Global sensitivity analysis (GSA) is the process of apportioning the uncertainty in outputs to the uncertainty in each input factor over their entire range of interest. A sensitivity analysis is considered to be global when all the input factors are varied simultaneously and the sensitivity is evaluated over the entire range of each input factor -ranges of existence- (Saltelli et al., 2008). GSA quantifies the importance of model inputs and their interactions with respect to model output. It provides an overall view on the influence of inputs on outputs as opposed to a local view of partial derivatives as in local sensitivity analysis. The sampling-based method (Monte Carlo) (Spear and Hornberger, 1980), the screening method or one-at-a-time (OAT) approach (Morris, 1991) (computing a number of local sensitivities), the Sobol method (Sobol, 1993), and the response surface method (Kleijnen et al., 1992) are the most commonly used global methods. Most of GSA are variance-based, which means that the resulting sensitivity reflects

the contribution of the model input to the total variance in the model output. However, some of them are regression-based which mostly used to replace a highly complex model to response surface (Iman and Helton, 1988). A comprehensive literature review on SA is provided by Loosvelt (2013).

1.4.5.1.2 Local sensitivity

Local sensitivity analysis, LSA, is a straightforward methodology, which we consider as an essential step within the modeling workflow to learn about model behavior and to identify key parameters. This method investigates the sensitivity of model output for a specific input scenario, i.e. a fixed set of input. Applying a time variant instead of aggregating the sensitivity in a single metric is crucial to derive this kind of information. To reduce the number of parameters that need to be optimized, LSA is often performed by evaluating model output for each parameter perturbation in a OAT approach (based on partial differentiation of the model, i.e., derivative-based approach). Indeed, various techniques for LSA exist such as (i) the finite difference method, (ii) the direct differential method, (iii) the Green's function method, (iv) the polynomial approximation method, (v) automatic differentiation and (vi) the complex-step derivative approximation method. Details about these techniques can be found in (De Pauw, 2005) and are not repeated here. The use of LSA is explained in detailed in Chapter 2.

1.4.5.2 Model factors sensitivity analysis

In model conceptualization, another sensitivity analysis which can be called classical/manual sensitivity analysis to identify the adjustable factors in the model such as boundary conditions, crop root distribution, profile geometry and spatial discretization is addressed shortly here. This SA on model factors can be conducted by changing the boundary conditions (Carrera-Hernández et al., 2012), e.g. free drainage, different constant heads, deep drainage, crop root distribution, density and root water uptake parameters (Hupet et al., 2002; Wollschlager et al., 2009), leaf area index (LAI) and extinction coefficient, and different discretization (Carrera-Hernández et al., 2012). The aim of this approach is to find the best condition and factors which reduce the mismatch between observed and simulated data.

1.5 Problem statement

Precision irrigation needs new methods and strategy/management of accurate irrigation scheduling. Considerable improvement in current irrigation strategies in Northwestern Europe as well as other parts of the world can be obtained with novel irrigation technology (e.g., Reel Sprinkler Gun irrigation) in combination with monitoring technology (e.g., Diver pressure sensors for groundwater monitoring, soil water content probes and tensiometers for soil water status monitoring and ISARIA crop sensor for crop status and LAI monitoring). A potential problem is that even using a considerable amount of irrigation water, the crop is exposed to water stress during dry periods and optimal yield is not achieved. In addition, the uniform distribution of water at the field scale using a standard gun sprinkler may not be an efficient approach since at locations with e.g. shallow groundwater, the amount of water applied will be excessive as compared to the crop requirements, while in locations with a deeper groundwater table, the crop irrigation requirements will not be met during crop water stress.

However, modern technology can quantify flow process and soil-water status, but in practice, in situ instruments can be installed in a limited number of sites only (due to costs, labor intensity). Moreover, irrigation management strategies under different field conditions (management zones) are needed for a large field with spatial differences in soil properties, groundwater depth and topography. Therefore, the solution is to use a modeling approach to simulate the soil water status for transient climatic conditions using a coupled soil water –crop growth model and to estimate or optimize the timing and amount of irrigation. The generalization of predictions (e.g. scaling up from 1D column at one spot to a large area like a field or region) is required in this respect. To do so, accurate information about the spatial variation of field-scale soil hydraulic properties is required in water management, flow and transport processes. The use of geophysical techniques such as electromagnetic induction as proxy could serve as valuable data source to estimate hydraulic properties for hydrological models to calculate variable irrigation requirements within agricultural fields. However, an integrated approach (based on the combination of crop growth model and hydrological model in a quasi 3D field scale model) for spatially distributed (variable rate) irrigation scheduling is still lacking.

Good modeling practice requires proper initial hydraulic parameter sets as input, parameter sensitivity analysis, conceptualization of the model, proper choice of boundary conditions, and root water uptake parameters. On the other hand, for understanding and enhancing knowledge

of water flow and water status, i.e., soil-water storage and stress at field scale it is necessary i) to accurate determine the bottom boundary condition, both in space and time, ii) to evaluate spatial variability of soil hydraulic parameters due to the soil heterogeneity, iii) to find more efficient methods for soil hydraulic parameters characterization and proper sets of those parameter as input parameter, and iv) to predict hydraulic properties at field scale and scaling up them as input parameter for the model. These approaches aim to optimize variable irrigation requirement within the field using a 2D modeling technique (quasi 3D). The latter may be the most efficient irrigation water management strategy that may help farmers to apply limited amount of (or even no) water in some parts of the field where the crop is not exposed to drought stress, and increase water supply within the zones where the crop is exposed to water stress. The aim is to increase yield, and consequently the revenue of irrigation and income will increase. The present research gives attention to all these issues.

1.6 Research objectives

Varying irrigation water application leads to differences in the yield and biomass component. The hypothesis of the study is: improving irrigation scheduling of water management using a state-of the-art modelling approach can result in a sustainable increase in agricultural water productivity and production under drought/ water deficit conditions and economic benefits. Determining proper timing, location and amount of irrigation is the most important factor for efficient use of water resources, for reducing/optimizing the irrigation cost and for maximizing crop yield. Therefore, the main objective of this dissertation (to support the hypothesis) is to develop and test methods for optimizing irrigation efficiency using a combination of sensors and process-based soil hydrological models integrated with crop growth models. Sensors that will be used are soil moisture sensors and tensiometers that measure water content and water potential in a fully automated field setup for quantitatively identifying flow processes in an agriculture soil. With this dissertation we try to contribute to some of the listed issues concerning modeling approach with a focus on models integration, model calibration and sensitivity analysis, development of methods for predicting hydraulic conductivity within a field, evaluating laboratory and field characterization of hydraulic parameters to find proper input parameter and way to scale up our modeling effort across the field to optimize irrigation strategy. These are very relevant, not only for arid and semi-arid conditions, but also for the management of intensively used agricultural fields in West- and Southern Europe suffering from summer droughts related to climate change.

The specific objectives focus essentially on different aspects of modeling and its effectiveness, and on developing methods needed to provide the required input for field 3D quasi modeling.

The specific objectives are:

1) to evaluate a modeling approach for irrigation optimization, using the Hydrus-1D model in combination with the crop based model LINGRA-N and to particularly
   - to show to what extent the hydrological modeling approach affects the estimations of irrigation requirement and crop yield;

2) to upscale and determine soil hydraulic properties more effectively and precisely at the field scale, based on proximal sensed data and geostatistics

3) to identify proper sets of hydraulic parameters using in situ and laboratory approaches and evaluate their relevance on hydrological model performance for irrigation management purposes and

4) to improve irrigation management at field scale using a modelling approach for water flow and redistribution in soils at field scale and to particularly

   - evaluate cost effects of an optimized irrigation application (from research to application view).

1.7 Dissertation framework

The dissertation is organized based on the research objectives addressed above. Figure 1-6 provides an overview of the thesis which consists of a general introduction, four main research chapters and a general conclusion chapter. Each research chapter contains an introduction followed by a list of specific objectives, provides an overview of the methodology used and presents results and discussions.

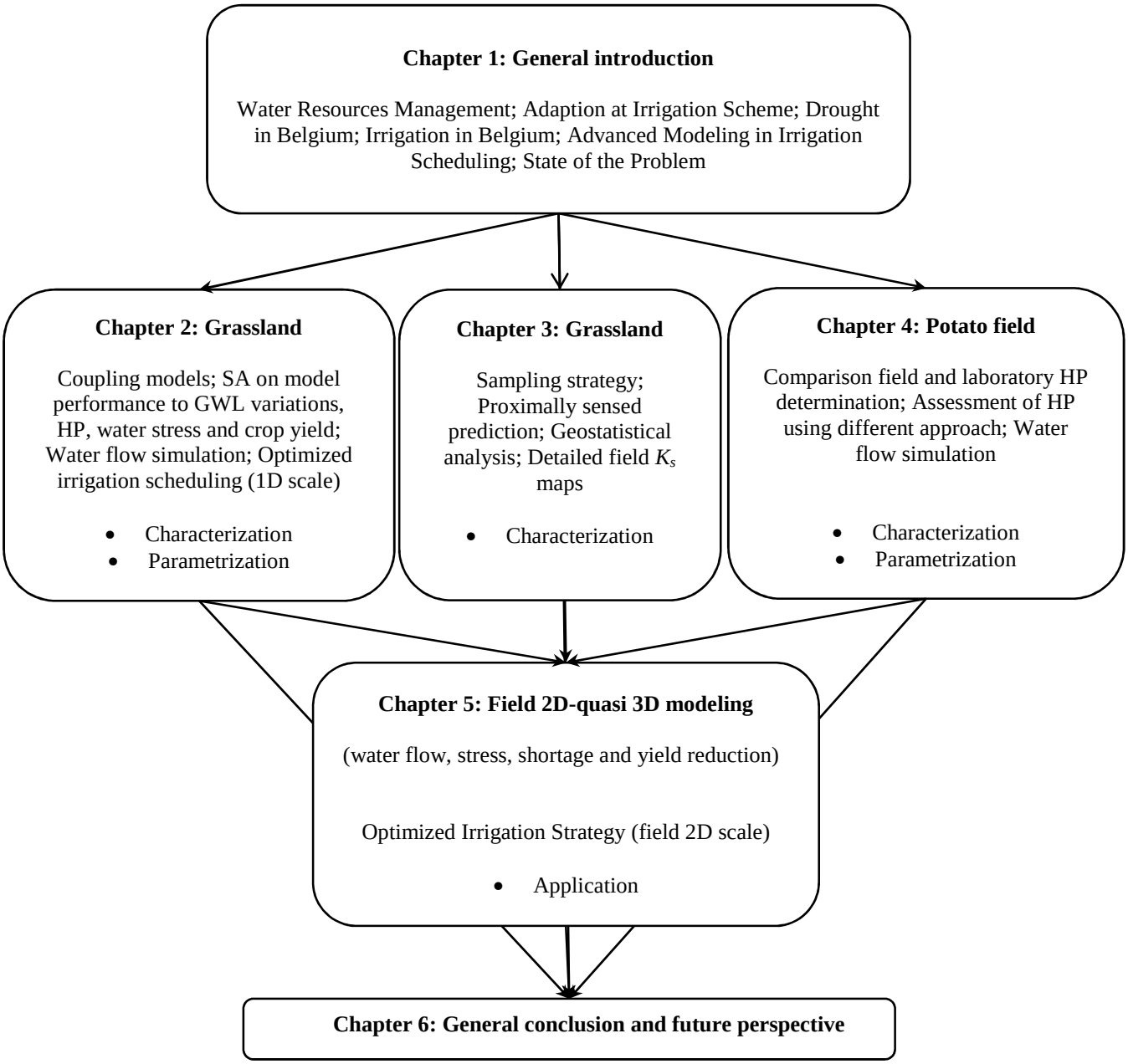

Figure 1-6. The flowchart of the thesis framework. SA, GWL, HP and K_s are sensitivity analysis, groundwater level, hydraulic properties and hydraulic conductivity, respectively.

Research contribution:

All parts of the study including soil sampling, characterization and data analyzing, modeling and so on were fully done by the author, only the ECa survey was done by ORBIT group of soil water management department (Ghent university).

Chapter 2. ***Sensitivity of water stress in a two-layered sandy grassland soil to variations in groundwater depth and soil hydraulic parameters***

This chapter is based on a modified published article:

Rezaei, M., Seuntjens, P., Joris, I., Boënne, W., Van Hoey, S., Campling, P., and Cornelis, W. M. 2016. Sensitivity of water stress in a two-layered sandy grassland soil to variations in groundwater depth and soil hydraulic parameters, Hydrology and Earth System Sciences, 20, 487-503, doi:10.5194/hess-20-487-2016.

2.1 Introduction

Efficient water use and optimal water supply to increase food and fodder productivity are of great importance when confronted with worldwide water scarcity, climate change, growing populations and increasing water demands (FAO, 2011). In this respect, irrigation efficiency which is influenced by the type of irrigation and irrigation scheduling is essential for achieving higher water productivity. In particular, precision irrigation is adopting new methods of accurate irrigation scheduling (Jones, 2004). Various irrigation scheduling approaches such as soil-based, weather-based, crop-based, and canopy temperature-based methods have been presented (Evett et al., 2008; Huo et al., 2012; Jones, 2004; Mohanty et al., 2013; Nosetto et al., 2012; Pardossi et al., 2009).

Numerical models are increasingly adopted in water resource planning and management. They contain numerical solutions of the Richards' equation (Richards, 1931) for water flow and root water uptake (Fernández-Gálvez et al., 2006; Skaggs et al., 2006; Vrugt et al., 2001) or contain reservoir cascade schemes (Gandolfi et al., 2006). Hydrological models require determination of hydraulic properties (Šimůnek and Hopmans, 2002), upper boundary conditions related to atmospheric forcing (evapotranspiration and precipitation) (Brutsaert, 2005; Nosetto et al., 2012) and groundwater dynamics at the lower boundary of the soil profile (Gandolfi et al., 2006). Numerical models such as Hydrus-1D (Šimůnek et al., 2013b) have been used in a wide range of irrigation management applications, for example, by Sadeghi and Jones (2012), Tafteh and Sepaskhah (2012), Akhtar et al. (2013), and Satchithanantham et al. (2014). The tool has been combined with crop-based models for accurate irrigation purposes and for predicting the crop productivity for cotton (Akhtar et al., 2013), vegetables and winter wheat (Awan et al., 2012). The degree of soil-water stress was used for irrigation management by coupling a hydrological model (Hydrus-1D) with a crop growth model (WOFOST) for maize (Li et al., 2012) and wheat (Zhou et al., 2012). The importance of correct average representation of the soil-plant-atmosphere interaction in numerical models has been stressed by (Wollschlager et al., 2009). A combination of crop growth model and the hydrological model makes it possible to calculate calculating crop yield reduction based on soil-water stress derived by the hydrological model.

Direct measurement of hydraulic parameters may be inaccurate for predictions at the field scale (Verbist et al., 2012; Wöhling et al., 2008). As an alternative, parameters can be determined by inverse modeling. A single-objective inverse parameter estimation using the Levenberg–

Marquardt optimization procedures has been used in different studies (Abbasi et al., 2004; Jacques et al., 2012; Šimůnek et al., 2013b). A typical challenge in parameter optimization is the non-uniqueness of the parameters, leading to parameter identifiability problems (Hopmans et al., 2002). Non-uniqueness can be reduced by decreasing the number of parameters to be estimated based on a sensitivity analysis. Sensitivity analysis has been used to optimize parameter estimation, to reduce parameter uncertainty (Rocha et al., 2006), and to investigate the effects of various parameters or processes on water flow and transport (van Genuchten et al., 2012).

In this part of study, we used a combination of soil moisture monitoring and modeling to estimate hydraulic properties and to predict soil-water content in a two-layered sandy soil for precision irrigation management purposes. The objective of this study is to investigate the impact of parameter estimation and boundary conditions on the irrigation requirements, calculated using a soil hydrological model in combination with a crop growth model. The effect of changing bottom boundary conditions on model performance was evaluated in a first step. A systematic local sensitivity analysis was then used to identify dominant hydraulic model parameters. This was followed by a model calibration using inverse modeling with field data to estimate the hydraulic properties. Finally, the degree of soil-water stress was calculated with different parametrization scenarios to show to what extent hydrological model parameter choice and boundary conditions affect estimations of irrigation requirement and crop yield. It is acknowledged that there is no stress in soil-water, whereas the water stress is in the plant, indeed. But similar to a large bulk of papers and reports, we used the soil-water stress term in the present paper instead of water stress in the plants.

2.2 Materials and Methods

2.2.1 Description of the study site

The study site is located in a sandy agricultural area at the border between Belgium and The Netherlands (with central coordinates 51°19′05″ N, 05°10′40″ E), characterized by a temperate maritime climate with mild winters and cool summers. During the study period 2011-2013, the farmer cultivated grass. The farm is almost flat (less than 1% sloping up from NW to SE) and runoff is not considered to be important. The measured depth of the groundwater table was between 80 and 155 cm and the Ap horizon thickness was between 30 and 50 cm below the soil surface at various locations across the field depending on the topography. The field is partly drained by parallel drainage pipes which are placed at 10 to 20 m intervals and at around 90

cm below the soil surface (as measured in the ditch). Drainage pipes are connected to a ditch in the northwest border of the field. Figure 2-1 shows the location, overview of groundwater level (GWL) in relation with apparent soil electrical conductivity (ECa) and layout of the field. The topographic map of the area is given in Appendix-Chapter 1 (Figure A2.1). The ECa was measured at 5 m intervals between the measurement lines with a DUALEM-21S sensor (DUALEM, Milton, ON, Canada) corresponding to 0-100 cm depth of exploration wich is correlated to GWL. Then, ECa data were interpolated using ordinary point kriging (OK) to a 0.5 by 0.5 m grid to produce the field ECa map. More details about this methodology and its procedure can be found in Chapter 3. Reel Sprinkler Gun irrigation (type Bauer rainstar E55, Röhren- und Pumpenwerk BAUER Ges.m.b.H., Austria) was used on a 290 m by 400 m field to improve crop growth in the sandy soil during dry periods in summer. The field was irrigated three times throughout each growing season (2012: 64.5 mm and 2013: 85.4 mm, see Table 2-5).

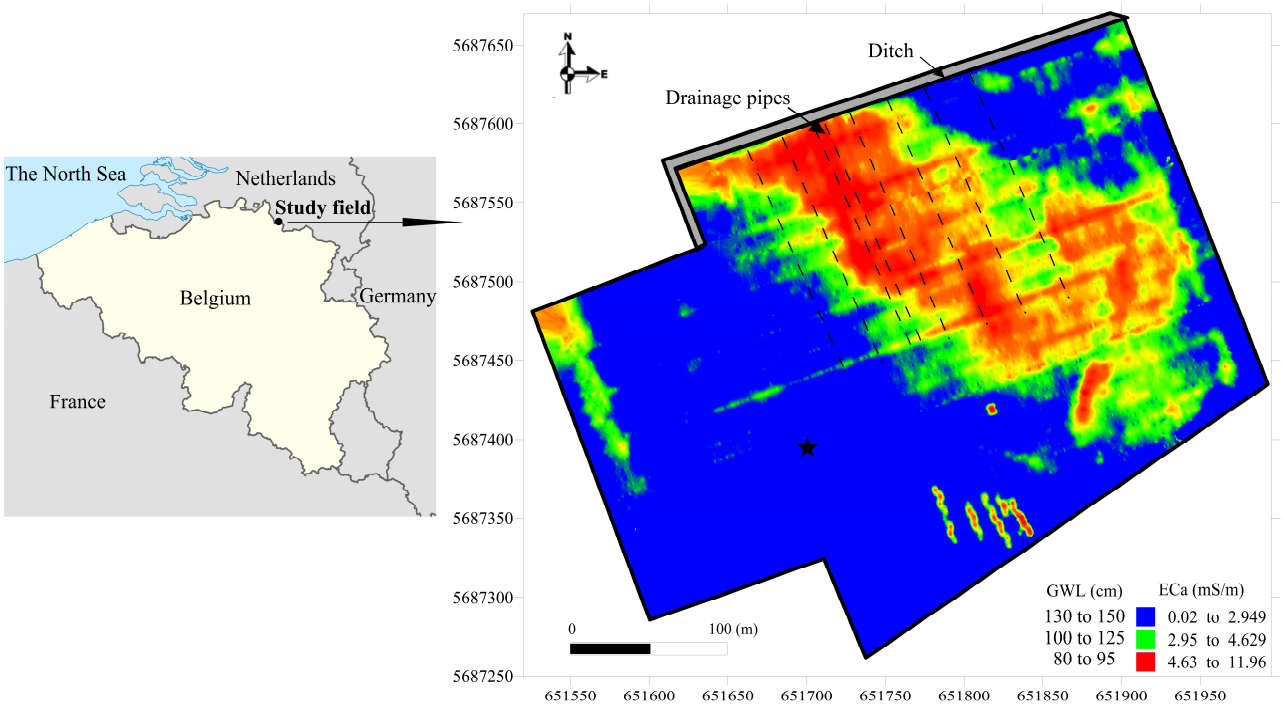

Figure 2-1. Geographical location of the experimental field and the map of the apparent soil electrical conductivity (ECa) of the study site corresponding to three different zones of groundwater levels (GWL). The black star on the ECa map indicates the sensor location.

Figure 2-2 shows the soil profile at a sensors location, indicated by the star on the map in Figure 2-1 (see also next section), a typical Podzol (Zcg-Zbg type according to the Belgian soil classification or Albic Podzols (Arenic) according to WRB, (FAO, 2014)) consisting of a uniform dark brown layer of sandy soil (Ap horizon, 0 to 33 cm) with elevated organic matter content, followed by a yellowish to white sandy soil, including stones and gravels, (C1 horizon, 33 to 70 cm). A deeper horizon is light grey sandy soil (C2 horizon, 70 to 135 cm), including more stones and gravels (max 20%), but having similar hydraulic properties as the C1 horizon (as measured in the laboratory). Maximum grass root density was found at about 6 cm and decreased from 6 to 33 cm (based on field observation during profile excavation). The properties of the two layers are summarized in Table 2-1.

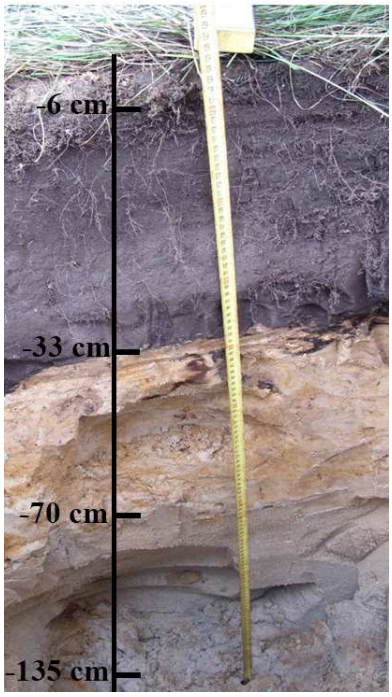

Figure 2-2. Two-layered typical soil profile of the field close to the location of the sensor.

Table 2-1. Average of soil properties of soil profile at sensor location: ρ_b is soil bulk density. θ_r, θ_s are residual and saturated water content, respectively; α and n are shape parameters for the van Genuchten-Mualem equation. K_s denotes the saturated hydraulic conductivity.

	K_s	θ_r	θ_s	α	n	OC	Sand	Silt	Clay	ρ_b
	cm h^{-1}	cm^3cm^{-3}		cm^{-1}			%			gcm^{-3}
Topsoil	9.59	0.09	0.39	0.017	2.72	2.08	91.65	7.0	1.35	1.57
Subsoil	4.74	0.03	0.31	0.021	2.34	0.18	95.7	3.1	1.2	1.76

2.3 Field monitoring system

The site was equipped with two weather stations (type CM10, Campbell Scientific Inc., Utah, USA), one in the study field and another 100 m away from the field. Soil-water content was recorded (from 1 Mar. until 25 Nov. in both 2012 and 2013) using a water content profile probe (type EasyAG50, Sentek Technologies Ltd., Stepney, Australia), placed vertically, that measures soil-water content at 10, 20, 30, 40 and 50 cm depths. The weather stations were connected to a CR800 data logger (Campbell Scientific Inc., Utah, USA) and the water content profile probe provided the soil water content wirelessly. All measurements were taken on an hourly basis and an hourly reference evapotranspiration was calculated based on the Penman–Monteith equation (Allen et al., 1998) using weather station data. The amount of irrigation was derived by subtracting measurements of rain gauges of the field's weather station (i.e. rainfall and irrigation) and the local meteorological station (i.e. only rainfall) outside the study field. Grass yield (dry matter) was measured at each harvesting time (4 times in each growing season) across the field (Figure 2-3).

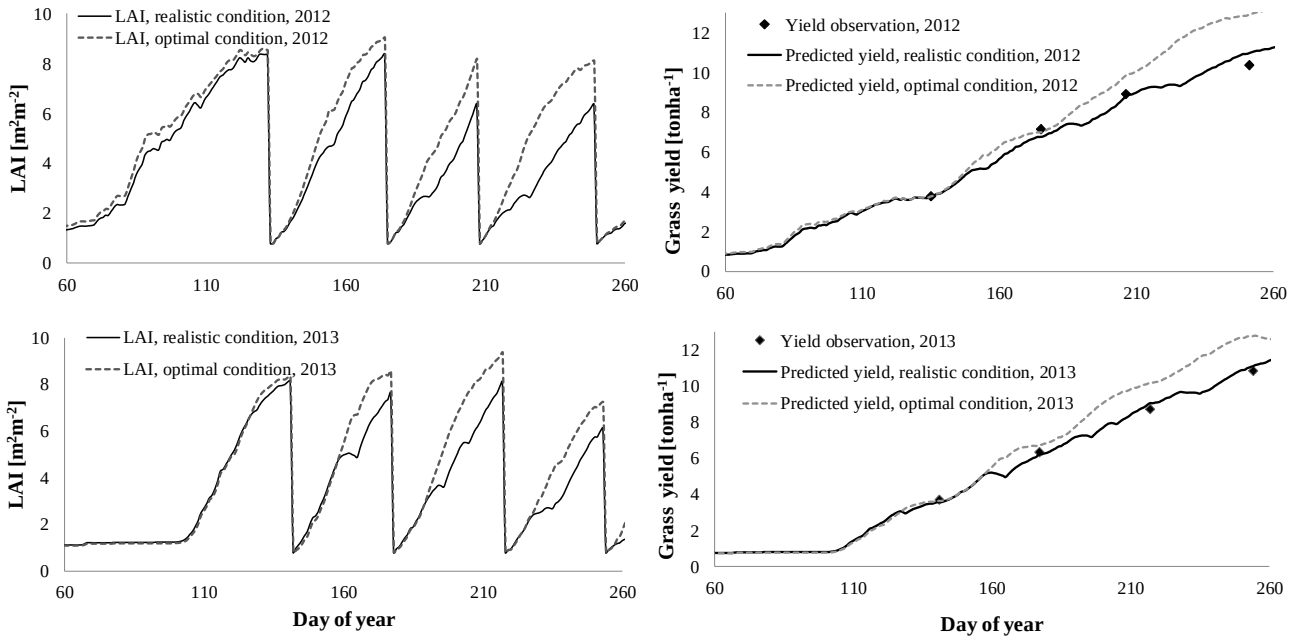

Figure 2-3. Predicted leaf area index, LAI and grass yield using the LINGRA-N model for 2012 and 2013.

At the sensor location (indicated by the star on the map in Figure 2-1), duplicate undisturbed (100 cm^3 Kopecky rings, Eijkelkamp Agrisearch Equipment, Giesbeek, The Netherlands) soil samples were taken to determine the soil saturated hydraulic conductivity and water retention curve, and one disturbed sample to measure soil properties such as texture, dry bulk density and organic matter, from the Ap (topsoil) and C (subsoil) horizons in June 2013. Groundwater

depth at the sensor location was measured four times on 4 June and 5 October 2012 (140 and 136 cm, respectively), and 24 June and 25 October 2013 (135 and 133 cm, respectively) using augering.

The saturated hydraulic conductivity (K_s) was determined using a constant head laboratory permeameter (M1-0902e, Eijkelkamp Agrisearch Equipment, Giesbeek, The Netherlands). The soil water retention curve, (SWRC, $\theta(h)$), was determined using the sandbox method (Eijkelkamp Agrisearch Equipment, Giesbeek, The Netherlands) up to a matric head of -100 cm and the standard pressure plate apparatus (Soilmoisture Equipment, Santa Barbara CA, USA) for matric heads equal to or below -200 cm, following the procedure outlined in (Cornelis et al., 2005). Bulk density was obtained by drying volumetric soil samples (100 cm^3) at 105 °C. Particle size distribution of the mineral component was obtained using the pipette method for clay and silt fractions and the sieving method for sand particles (Gee and Bauder, 1986). The organic matter content was determined by the method of Walkley and Black (1934) .

Soil hydraulic properties were determined according to the van Genuchten (1980) and Mualem (1976) conductivity model (MVG model). The parameters of the water retention equation were fitted to the observed data set using the RETC, version 6.02 (van Genuchten et al., 1991). The MVG model (Mualem, 1976; van Genuchten, 1980) is given by:

$$S_e = \frac{\theta - \theta_r}{\theta_s - \theta_r} \tag{2-1}$$

$$S_e(h) = 1 \qquad h \geq 0 \tag{2-2}$$

$$S_e(h) = (1 + |\alpha h|^n)^{-m} \qquad h < 0;\ \ where\ m = 1 - \frac{1}{n} \tag{2-3}$$

$$K(S_e) = K_s {S_e}^l \left[1 - (1 - S_e{}^{\frac{1}{m}})^m\right]^2 \tag{2-4}$$

where θ_s, θ_r, and θ are the saturated, residual and actual volumetric water content respectively ($cm^3\ cm^{-3}$), α is the inverse of air entry value (cm^{-1}), n is a pore size distribution index > 1, m=1-1/n (dimensionless), S_e is the effective saturation (dimensionless), and l is a pore connectivity and tortuosity parameter in the hydraulic conductivity function, which is assumed to be 0.5 as an average for many soils (Mualem, 1976).

2.3.1 Modeling at monitoring locations

2.3.1.1 Simulation of leaf area index and grass yield

The simple generic grass growth model, LINGRA-N (Wolf, 2012), which can calculate grass growth and yields under potential (i.e. optimal), water-limited (i.e. rain fed) and nitrogen-limited growing conditions, was used to calculate the leaf area index (LAI) and grass yield. This tool was calibrated and tested for perennial rye grass and natural annual grass over Europe (Barrett et al., 2004; Schapendonk et al., 1998). LINGRA-N simulates the growth of a grass crop as a function of intercepted radiation, temperature, light use efficiency and available water (Wolf, 2012). The LAI and crop growth simulations were carried out from 1 January 2012 to 31 December 2013. The model calculated LAI and yield on a daily time intervals using daily weather data, solar radiation (kJ m^{-2} d^{-1}), minimum temperature (˚C), maximum temperature (˚C), vapour pressure (kPa), wind speed (m s^{-1}) and precipitation (mm d^{-1}). A grass crop data file is available mainly derived from WOFOST (section 1.4.1.1). Soil data for our soil were produced using measured values of soil moisture content at air dry (pF=6), wilting point (pF= 4.2), field capacity (pF= 2.3) and at saturation and also percolation (K_s) to deeper soil layers (cm day^{-1}) in the laboratory. The maximum rooting depth was adjusted to 40 cm. Irrigation supply was imposed at the specific applied times with optimal nitrate application. The simulated LAI was scaled to an hourly basis using linear interpolation between two adjacent simulated daily values of LAI. The model was run for optimal (no water limitation) and realistic conditions (actual water inlet i.e. irrigation and rainfall) for each growing season. Figure 2-3 represents predicted LAI and grass yield of 2012 and 2013.

2.3.2 Simulation of water flow

The simulated soil profile in the hydrological model extends to 150 cm depth and is divided into two layers: Layer 1 (0 to 33 cm) and Layer 2 (33 to 150 cm). Simulation of root water uptake and water flow, which is assumed to be in the vertical direction in the vadose zone, was carried out for two growing seasons (from 1 Mar. until 25 Nov. in 2012 and 2013) using Hydrus-1D version 4.16 which solves the 1-D Richards' equation:

$$\frac{\partial \theta}{\partial t} = \frac{\partial}{\partial z}\left[K(h)\left(\frac{\partial h(\theta)}{\partial z} + 1\right)\right] - S(h) \qquad (2\text{-}5)$$

where θ is the volumetric water content (cm^3 cm^{-3}), t is time (h), z is the vertical space coordinate taken positive downward (cm), $K(h)$ is the unsaturated hydraulic conductivity function (cm h^{-1}), h is the pressure head (cm), and $S(h)$ represents a sink term (cm^3 cm^{-3} h^{-1}),

defined as the volume of water removed from a unit volume of soil per unit time due to plant water uptake.

To solve Eq. 2-5, the MVG soil hydraulic model (Eqs. 2-1 - 2-4) without hysteresis was used. The initial pressure head distribution was calculated using the inverse of Eq. (2-3), $h(S_e)$, from the measured initial water content of each observation node. These point values were then interpolated linearly from the deepest observation node to the groundwater level (h=0, GWL). The pore connectivity parameter of the MVG model was fixed at l=0.5. The upper condition for water flow was an atmospheric boundary condition (based on rainfall and irrigation water supply, LAI calculated by LINGRA-N (see 2.3.1) and reference evapotranspiration (ET_o)) with surface runoff. The model performance was assessed using various implemented bottom boundary conditions, i.e. free drainage and incremental constant head conditions, as a manual sensitivity analysis (see section 2.5.1). The Feddes' model (Feddes et al., 1978) without solute stress was used for root water uptake. The default grass parameters values provided by Hydrus-1D were used (Taylor and Ashcroft, 1972).

2.4 Soil-water stress and yield reduction

In the Feddes model (Feddes et al., 1978) the sink term of Richards' equation Eq. (2-5), $S(h)$, is specified in terms of quantify potential root water uptake and water stress, as:

$$S(h) = w(h)R(x)T_p \tag{2-6}$$

where $R(x)$ is the root distribution function (cm), T_p is potential transpiration (cm h^{-1}), and $w_{(h)}$ is the water stress response function ($0 \leq w_{(h)} \leq 1$) which prescribes the reduction in uptake that occurs due to drought stress. Crop-specific values of this reduction function are chosen from the default Hydrus data set. The actual plant transpiration is calculated numerically, as:

$$T_a = \int_{L_r} S(h)dx = T_p \int_{L_r} w(h)R(x)dx \tag{2-7}$$

where L_r is the rooting depth (cm).

By assuming root water uptake is equal to actual transpiration, the ratio of actual to potential transpiration by the root uptake was introduced as a degree of water stress, DWS, (Jarvis, 1989), as:

$$\mathrm{DWS} = \frac{T_a}{T_p} = \int_{Lr} w(h)R(x)dx \quad (2\text{-}8)$$

The effect of the boundary conditions and parameter uncertainty on soil-water stress was evaluated using the ratio between the calculated actual water uptake/actual transpiration and the potential transpiration provided by the model (Li et al., 2012; Zhou et al., 2012). In optimal and stress-free conditions, this ratio should be (close to) unity (>0.90 of maximum reference evapotranspiration).

The ratio between actual crop evapotranspiration and potential evapotranspiration was introduced as a water stress factor equal to the crop yield reduction due to water shortage (Doorenbos and Kassam, 1979), given as:

$$1 - \frac{Y_a}{Y_m} = K_y\,(1 - \frac{ET_a}{ET_p}) \quad (2\text{-}9)$$

Where Y_a is actual crop yield, Y_m is the maximum crop yield in optimal condition, K_y is the crop yield factor (for grass K_y=1), ET_a is actual crop evapotranspiration estimated by the model. The Y_m value was simulated using LINGRA-N in optimal condition (no water stress) for 2012 and 2013 growing seasons. ET_p is potential evapotranspiration and can be calculated from the reference evapotranspiration by:

$$ET_p = ET_0 \times K_c \quad (2\text{-}10)$$

where K_c is the crop coefficient and equal to 1, assuming that grass at our site did not differ much from the reference crop. Accordingly, crop yield reduction of each scenario was calculated using Eq. 9 for both periods to show to what extent different scenarios affect soil water stress and crop yield.

2.4.1 Sensitivity analysis

2.4.1.1 Effect of soil layering and the Groundwater Level (GWL) on Soil Water Content and Water Stress

As a first step, the effect of soil layering was evaluated by changing layered soil profile with the homogeneous profile by calculating the effective hydraulic conductivity and arithmetic average of hydraulic properties based on soil layer thickness. Then, a manual sensitivity analysis of the bottom boundary conditions was conducted by applying various conditions. A

free drainage and various constant head conditions were imposed by setting a zero pressure head value at the GWL ranging from 120 to 150 cm (5 cm interval, i.e., 7 scenarios) below the soil surface to cover the GWL variations (the sensor location was at dryer zone (Figure 2-1)). This small variation is due to the existence of drainage system. The effects of these bottom boundary conditions on soil water stress and water content prediction were evaluated for both calibration and validation periods (2012 and 2013).

2.4.1.2 Parameter Sensitivity

The effect of each input factor or parameter on the model output is determined by a local sensitivity analysis (SA), using a one-at-a-time (OAT) approach. We used this approach because it allows a clear identification of single-parameter effects. Relevant parameters have major effects on output variables with only a small change in their value (Saltelli et al., 2008). SA is, among other purposes, used to find the most relevant parameters which enables a reduction of the number of parameters that need to be optimized. In a local SA, only the local properties of the parameter values are taken into account, in contrast to global SA which computes a number of local sensitivities. Since the interest in this study goes specifically to the measured (parameter) values in the field, a local SA is chosen. Furthermore, an OAT approach (local or global) does not provide direct information about higher- and total-order parameter interaction as is provided by variance-based SA (Saltelli et al., 2008). However, by evaluating the parameter sensitivities in time, insight is given about potential interaction when similar individual effects are observed. The latter can be quantified by a collinearity analysis (Brun et al., 2001), but will be done graphically in this contribution. A dynamic sensitivity function can be written as follows:

$$SF(t) = \frac{\partial y(t)}{\partial x} \tag{2-11}$$

where *SF(t)*, *y(t)*, and *x* denote the sensitivity function, output variable and parameter respectively. If an output variable *(y)* significantly changes (evaluated by calculating the variance or coefficient of determination or by visualizing in a scatter plot) due to small changes of the parameter of interest *x*, it is called a sensitive parameter.

This partial derivative can be calculated analytically or numerically with a finite difference approach by a local linearity assumption of the model on the parameters. Local sensitivity functions evaluate the partial derivative around the nominal parameter values. The central

differences of the sensitivity function are used to rank the parameter sensitivities and can be expressed as follows:

$$\Delta x_j = p_f . x_j \tag{2-12}$$

$$\text{CAS} = \frac{\partial y(t)}{\partial x} = \lim_{\Delta x_{j \to 0}} \frac{y(t, x_j + \Delta x_j) - y(t, x_j - \Delta x_j)}{2\Delta x_j} \tag{2-13}$$

$$\text{CTRS} = \frac{\partial y(t)}{\partial x} . \frac{x_j}{y}, \qquad \text{CPRS} = \frac{\partial y(t)}{\partial x} . x_j \tag{2-14}$$

where p_f is the perturbation factor, x_j is the parameter value and Δx_j is the perturbation, CAS is the Central Absolute Sensitivity, CTRS is the Central Total Relative Sensitivity analysis, and CPRS is a Central Parameter Relative Sensitivity. Since the parameters and variables have different orders of magnitude for which the sensitivity is calculated, direct comparison of the sensitivity indices with CAS is not possible. Hence, recalculation towards relative and comparable values is needed. In order to compare the sensitivity of the different parameters towards the different variables, CTRS is preferred. CPRS is sufficient when the sensitivity of different parameters is compared for a single variable, i.e., soil-water content. Here, a dynamic (time-variable) local sensitivity analysis was conducted by linking Equations (2-11 - 2-14), programmed in Python™ software (https://www.python.org/) to Hydrus-1D (Appendix – Chapter 2).

Given the output accuracy of Hydrus-1D (0.001), a perturbation factor of 0.1 was chosen. To carry out the SA, each hydraulic parameter (K_s, θ_r, θ_s, α, and n) in each layer was varied (measured value ± perturbation factor multiplied by measured value) and its CTRS was calculated (Eq. 2-13 - 2-14), while the values of other parameters were fixed to the measured values. The model was run in forward mode 20 times, i.e., 10 runs for each layer and two runs for each parameter. A weak direct effect of a parameter in SA is denoted by low absolute values close to zero. A positive effect is expressed by a positive value and a negative effect by a negative value.

2.4.2 Model calibration and validation

2.4.2.1 Model calibration

For accurate parameter estimation, a longer period such as a growing season (i.e. 2012) with several drying and wetting events was selected. This was also suggested by Wöhling et al. (2009); Wöhling et al. (2008). Therefore, the period between 1 Mar. 2012 (00:00 h CET) and

25 Nov. 2012 (23:00 h) was used as the calibration period. We used a time interval of 2 hours, resulting in 12960 soil-water content records for four depths (as data for inverse solution), based on hourly precipitation and evaporation input data. Based on our experience this number of data is sufficient for optimization purposes. The objective functions were soil water content and water retention data for both soil layers with unit weighting. In the calibration, we optimized only the values of the most sensitive parameters (K_s, n, and α) of the two layers, taking initial values of hydraulic parameters for each layer equal to the values estimated by the RETC program for the independent field samples, while keeping the insensitive hydraulic parameters fixed to the measured values. Thirty-seven parameter optimization scenarios were selected and analyzed to identify correlations among optimized parameters and to identify the most influential parameter sets on soil water stress and water content in different lower boundary conditions. The 37 scenarios comprised optimizing all six parameters simultaneously (one scenario), four parameters (nine scenarios), three parameters (18 scenarios) and two parameters (nine scenarios). Finally, the best-performing parameter set - based on performance criteria, the correlation between optimized parameters (non-uniqueness of the parameter sets) and the visual inspection of simulated and observed soil-water content - was selected for validation using independent data from 2013 (from 1 Mar. until 12 Sep. 2013).

2.4.2.2 Model Evaluation and Statistical Analysis

The performance of models can be evaluated with a variety of statistics (Neuman and Wierenga, 2003). It is known that there is no efficiency criterion which performs ideally. Each of the criteria has specific pros and cons which have to be taken into account during model calibration and evaluation. It is suggested to use a combination of different efficiency criteria to assess of the absolute or relative volume error (Krause et al., 2005). The root-mean-square errors (RMSE), the coefficient of determination (r^2) and the Nash–Sutcliffe coefficient of model efficiency (C_e) (American Society of Civil Engineers, 1993), are popular and widely used performance criteria to evaluate the difference between observed and modelled data (Gandolfi et al., 2006; Nasta et al., 2013; Verbist et al., 2009a; Verbist et al., 2012; Vrugt et al., 2004; Wöhling and Vrugt, 2011; Wollschlager et al., 2009).They are calculated as follows:

$$C_e = 1 - \frac{\sum_{i=1}^{n}(O_i - S_i)^2}{\sum_{i=1}^{n}(O_i - \bar{O})^2} \qquad (2\text{-}15)$$

$$r^2 = \left(\frac{\sum_{i=1}^{n}(O_i - \bar{O})(S_i - \bar{S})}{\sqrt{\sum_{i=1}^{n}(S_i - \bar{S})^2 \sum_{i=1}^{n}(O_i - \bar{O})^2}}\right)^2 \quad (2\text{-}16)$$

$$RMSE = \sqrt{\frac{\sum_{i}^{n}(O_i - S_i)^2}{n}} \quad (2\text{-}17)$$

where O and S are observed and simulated values at time/place i, respectively.

C_e and r^2 are considered to be satisfactory when they are close to 1, while RSME should be close to 0. C_e may result in negative values when the mean square error exceeds the variance (Hall, 2001).

2.4.3 Effect of optimization scenarios on estimated water stress and yield reduction and irrigation scheduling

2.4.3.1 Scenario analyses on required additional irrigation

Additional irrigation refers to the amount of irrigation that has to be added to the current irrigation to avoid water stress or that has to be subtracted from the current irrigation to avoid water loss. The impact of groundwater depth on the required additional amount was assessed using scenario analysis. The additional required irrigation was calculated by adding an amount of water input as precipitation variable at the start time of water stress and then the model was run several times in forward mode until the calculated water stress was eliminated (by reducing or increasing amount of water supply). This procedure was repeated for each scenario and boundary condition for both years. In addition, crop yield reduction of each scenario was calculated (using Eq. 2-9) for both periods to show to what extent different scenarios affect soil water stress and crop yield.

2.4.3.2 Irrigation scheduling optimization

The value of soil-water stress, and the number and the duration of stress periods was calculated for two growing seasons (2012 and 2013), as an indicator for the performance of the irrigation scheduling (van Dam et al., 2008). To optimize the irrigation scheduling (timing of application), the actual water supply (all irrigation events) was deleted from the model input of the hydrological model. Secondly, the LAI simulated with the LINGRA-N for optimal conditions (no water stress) was used as a variable in the hydrological model. Then, the hydrological model with a constant bottom boundary condition was run with the new input

variables to elucidate water stress without actual water supply. Subsequently, the required irrigation was added to the precipitation at the beginning of each water stress period to exclude water stress from the simulations. To simulate crop yield at the optimized condition, the new precipitation variables (rainfall and required irrigation) were used in LINGRA-N model. The optimal yield obtained using the optimized irrigation scheduling was compared to the actual (simulated and measured) yield of current irrigation management practices.

2.5 Results and Discussion

2.5.1 Effect of soil layering and the GWL on soil water content and water stress predictions

Result showed effects of homogeneous and heterogeneous of free drainage and different constant head conditions on water content estimation (see Appendix –Chapter 2, Fig. A2-1). Generally, the better agreement between the prediction and observation was reached in heterogeneous profile. In the free drainage condition, soil water content is generally underestimated, while in constant head bottom boundary condition simulation agreed well with observation. Pachepsky et al. (2007) found a two layered soil profile was superior than homogeneous profile by carrying out aggregation abstraction in their case, in our ongoing study it confirmed heterogeneous profile is most suitable for water flow simulations. Figure 2-4 shows the effects of free drainage and different constant head conditions on water content estimations made using the uncalibrated hydrological model. In the free drainage condition, soil-water content was generally underestimated, especially at deeper observation nodes. The results further show that a constant head boundary condition yields a much better agreement between the model and the observations due to wetter conditions in the lower part of the profile.

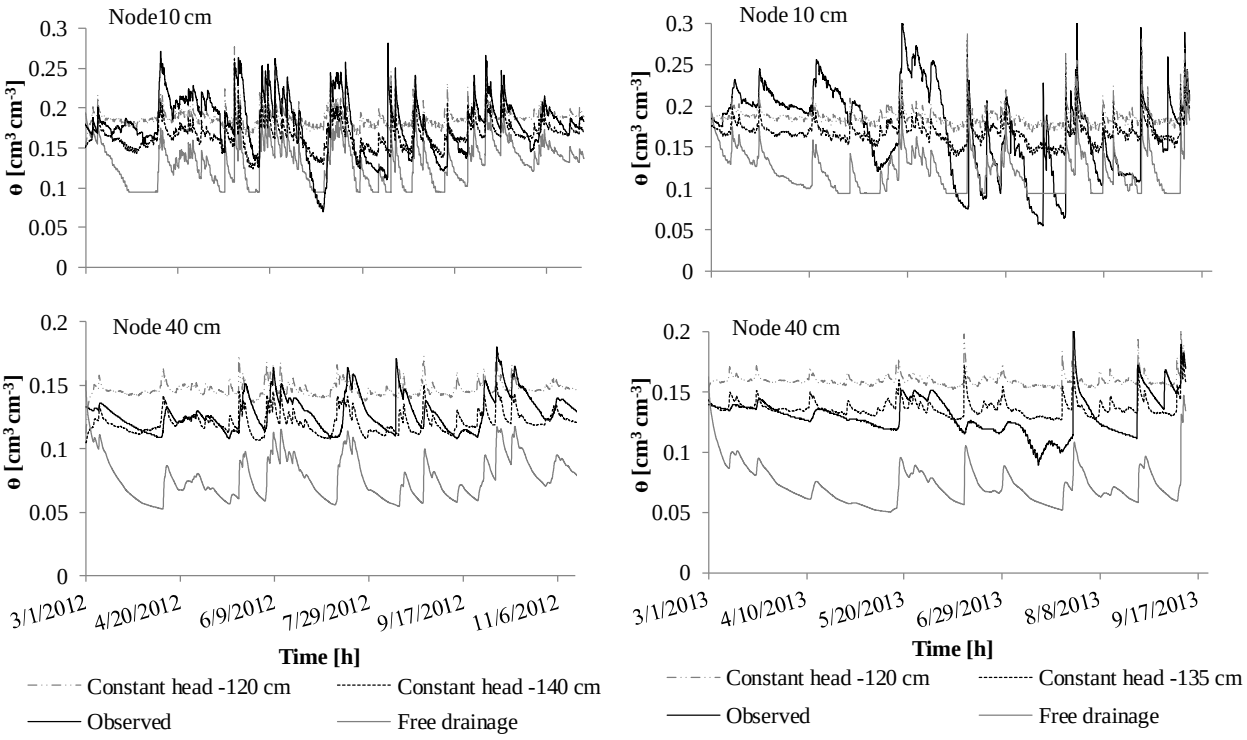

Figure 2-4. Water content estimations at 10 and 40 cm depths using the uncalibrated model for free drainage and different constant head bottom boundary conditions at the soil moisture sensor location.

The constant head condition showing the smallest difference between observations and simulations was in agreement with average groundwater depth observations in 2012 and 2013 (-140 and -135 cm respectively) at the location of the sensor (2012: RMSE=0.018, C_e=0.27, and r^2=0.48; 2013: RMSE=0.024, C_e=0.26 and r^2=0.43). Decreasing the groundwater depth to -120 cm overestimated the soil-water content, especially at the three deepest observation nodes. On the contrary, soil water stress was overestimated in free drainage condition, which means that the plant is exposed to water stress most of the time of growing season. While there is almost no water stress predicted in constant head condition with GWL below 135 cm (Figure 2-5). Obviously, results show constant head boundary condition leads to higher calculated root water uptake as compare as free drainage condition. The results clearly show the great importance of the bottom boundary condition in estimating soil-water content and soil water stress in the soil profile, even for groundwater depths well below 120 cm depth and sandy soils. The effect of the boundary condition may well exceed the impact of uncertain hydraulic parameters in a parameter optimization. Carrera-Hernández et al. (2012) stated that choosing adequate boundary conditions is the first step toward accurately estimation water content and flux using hydrological model; But our result shows, in optimizing the hydraulic model parameters, the effect of the boundary conditions should therefore be assessed simultaneously

and then the appropriate boundary conditions should be chosen in term of root water uptake and soil water content.

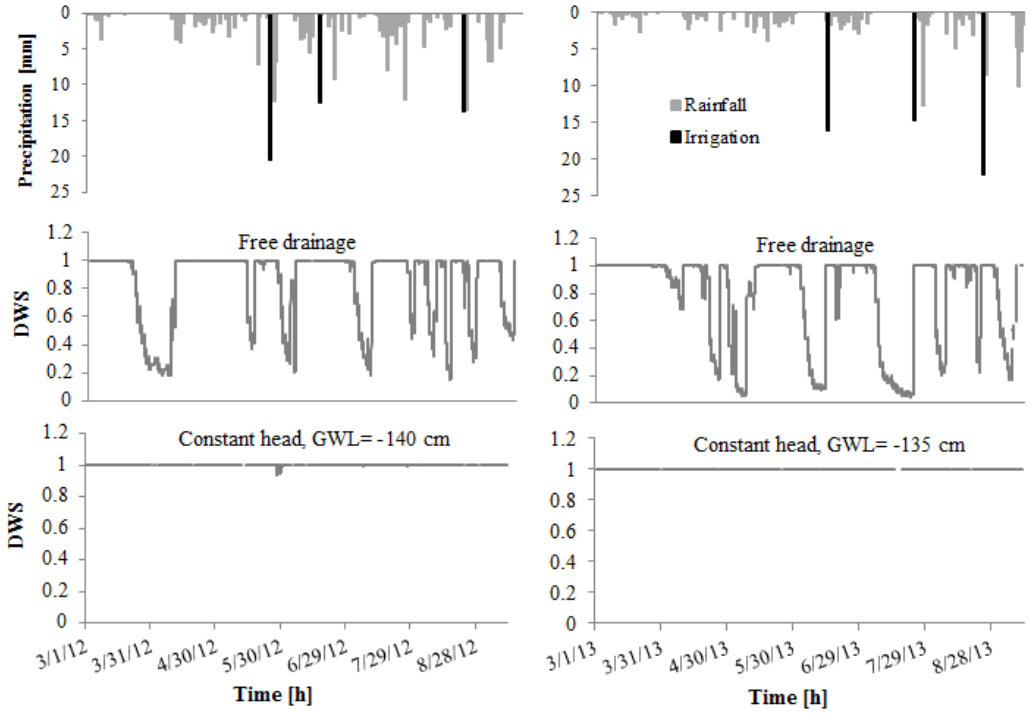

Figure 2-5. Soil water stress calculations using the uncalibrated model for free drainage and constant head bottom boundary condition (GWL= -140 cm) at the soil moisture sensor location. DWS is degree of water stress.

2.5.2 Parameter sensitivity analysis

Due to the variable rainfall, irrigation, evapotranspiration and drainage, the soil-water content changes in the soil profile, and, consequently, parameter sensitivities are time dependent. The soil-water content has a low sensitivity to θ_s and θ_r, especially for the second layer. Low sensitivities to θ_r have been reported by others (Kelleners et al., 2005; Mertens et al., 2006; Wöhling et al., 2008). Figure 2-6 illustrates the results of the sensitivity analysis as a function of time for the most influential parameters α, n, and K_s, and for both soil layers as depicted by the suffix 1 for layer 1 and suffix 2 for layer 2 (see also Appendix-Chapter 2, Figure A2-3 and A2-4). A weak direct effect of a parameter is reflected by low absolute values (close to zero). The results show for all parameters a general change in sensitivity with time with the seasonal changes in irrigation application and rainfall. Generally, all soil hydraulic parameters showed higher sensitivity in dry periods as compared to wet periods. On the other hand, there is a clear effect of parameter variability in layer 1 on water content estimation at 10 cm, and the effect is slightly declining at 20 and 30 cm, which suggests the great importance and influence of upper boundary variables, especially evapotranspiration. Similar results were observed by Rocha et al. (2006). They found that soil water content and pressure heads were most sensitive to

hydraulic parameters variation in the dry period near the soil surface using local sensitivity analysis of Hydrus.

Soil-water content is sensitive to variations of α, n and K_s in both layers. The sensitivity is the largest for n, α and less so for K_s in the first layer. For the second layer, soil-water content was the most sensitive to α followed by n and K_s. Abbasi et al. (2003a) reported that n, θ_s and K_s were most sensitive parameters in their study and that this sensitivity was more pronounced in deeper parts, however they also observed some sensitivity near the soil surface during the drier conditions. The most sensitive parameters were θ_s, n and α and least sensitive parameter was K_s in the study by Schneider et al. (2013) using Hydrus-1D. They found large interaction (correlation) among sensitive parameters. In contrast, Wegehenkel and Beyrich (2014) reported that soil water content predictions were most sensitive to θ_r and θ_s and least sensitive to α, n, and K_s input parameters using Hydrus-1D. Similarly, Caldwell et al. (2013) found that θ_r, n and l were sensitive and θ_s, α and K_s were insensitive to water content simulation. In dry periods, there is a general negative correlation between n and α on the one hand and soil-water content on the other hand, whereas a positive correlation exists between K_s and soil-water content (Figure 2-6). Figure 2-6 shows that in the first layer, the soil-water content is more influenced by rainfall at 10 cm than at 30 cm (higher and lower sensitivity for observation nodes 10 and 30 cm, respectively, within first layer).

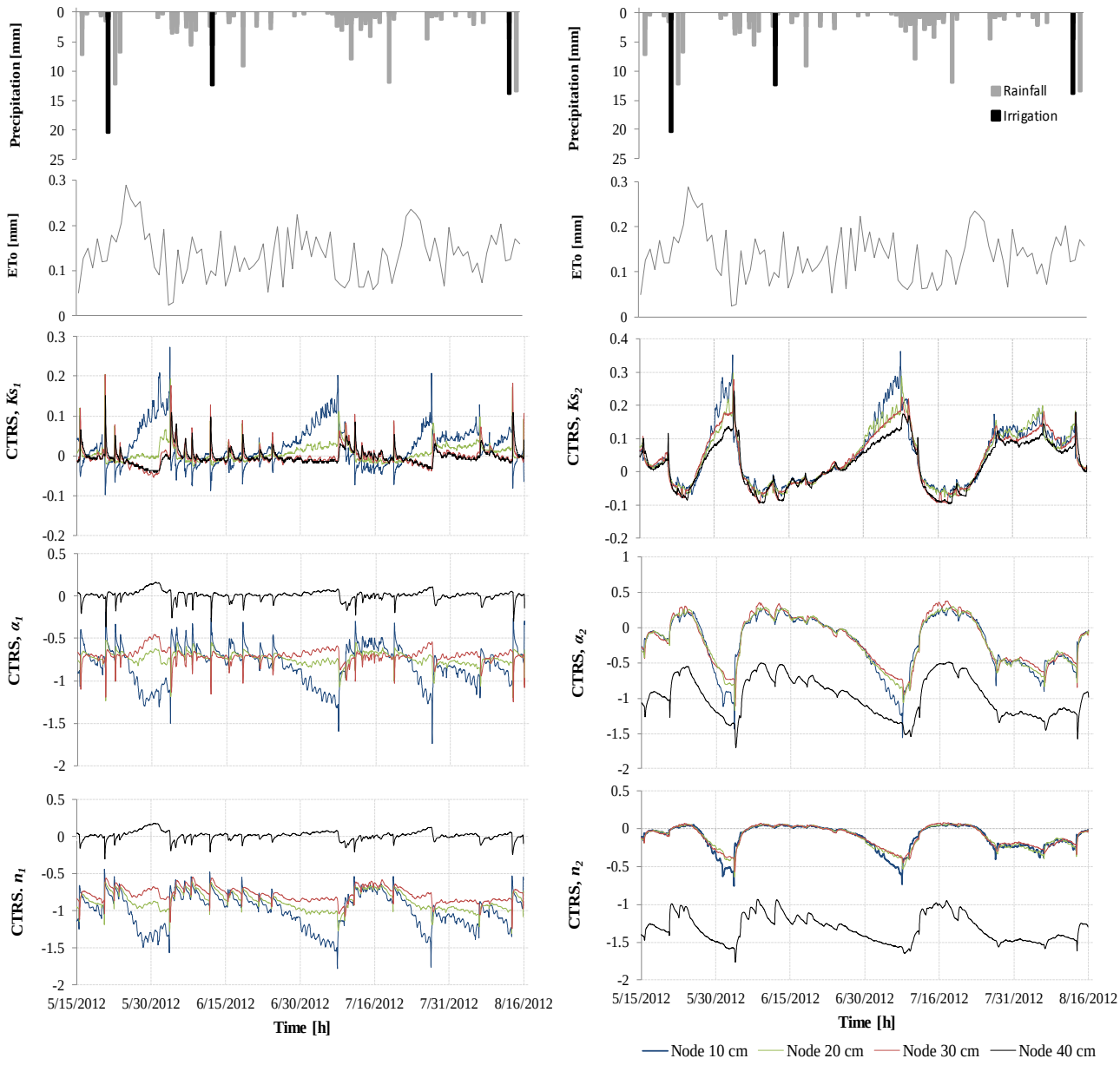

Figure 2-6. Parameter sensitivity as a function of time. The numbers 1 and 2 correspond to the first and second layer, respectively.

The fact that the model predictions in the upper part of the soil profile are extremely sensitive to variations in hydraulic parameters in dry periods, is of great importance to irrigation management. To improve the timing of irrigation in these crucial periods, numerical soil models that are used to determine irrigation requirement, need to be well parametrized for α, n and K_s.

2.5.3 Model calibration

Since soil-water content prediction was insensitive to the parameters θ_s and θ_r, they were fixed to the measured (initial) values (Table 2-1). Similar strategies were used by Schwartz and Evett (2002); Verbist et al. (2012). The model was run inversely using time series of soil-water content with values for α, n and K_s being optimized for the two layers (i.e., six-parameter optimization scenario). A significant correlation appears between optimized α and K_s for both layers (layer 1: r = 0.85; layer 2: r = 0.95 constant head; and layer 1: r = 0.82; layer 2: r = 0.80 free drainage) and between optimized n and α (both layers: r = -0.99 constant head; and layer 1: r = -0.83 and layer 2: r = -0.84 free drainage) within each layer, but not between layers. On the other hand, there is a significant correlation between n and K_s in both layers (layer 1: r = -0.85; layer 2: r = -0.94 constant head; and layer 1: r = -0.75; layer 2: r = -0.98 free drainage). This means that α, n and K_s within one layer cannot be determined independently and different sets of correlated parameters lead to very similar predictions of soil-water content. The high correlation between optimized parameters within a layer leads to a large uncertainty of the final parameter estimates (Hopmans et al., 2002). To avoid non-uniqueness of the inverse solution (Šimůnek and Hopmans, 2002), 36 additional systematic four-, three- and two-parameter optimizations were conducted. All optimizations resulting in correlations among the optimized parameters were removed and only the optimization scenarios with the uncorrelated parameters were kept. This resulted in parameter values as shown in Table 2-2 for a constant head corresponding to a groundwater depth of -140 cm and free drainage. For comparison purposes, six-parameter scenario (all parameters optimized) and only the best performing optimization with two parameters is presented for the other boundary conditions (i.e. GWL = -120 cm).

The performance results of the parameter optimizations according to the performance criteria for all scenarios with uncorrelated parameters and different boundary conditions are presented in Table 2-3, together with the performance of the six-parameter scenario. The results show that a two-parameter optimization (optimizing only K_s in both layers) performs equally well as compared to a six-, four- or three-parameter scenario for all performance criteria and observation depths. However, parameters in the six-parameter scenario are considered unidentifiable due to their correlations. In this case, the model was not able to find a global minimum but found a local minimum (Levenberg-Marquardt method) due to the high dimensionality of the problem (Ritter et al., 2003) and the large uncertainty of the optimized values.

Table 2-2. Optimized values of hydraulic parameters for the optimization scenarios yielding uncorrelated parameters (except for reference scenario with six optimized parameters). Values indicated in italic are values fixed to the measured values close to the sensor location. Numbers between parentheses represent the standard errors of optimized parameter.

Boundary condition	Number of optimized parameters	First soil layer			Second soil layer		
		α_1 (cm^{-1})	n_1	K_{s1} (cm h^{-1})	α_2 (cm^{-1})	n_2	K_{s2} (cm h^{-1})
Constant head (-140 cm)	6	0.023 (0.0004)	2.14 (0.02)	2.87 (0.111)	0.022 (0.0006)	2.15 (0.034)	1.95 (0.14)
	4	*0.017*	2.64 (0.003)	1.54 (0.028)	0.020 (0.00005)	*2.34*	1.43 (0.026)
	3	*0.017*	*2.72*	1.39 (0.026)	0.020 (0.00005)	*2.34*	1.65 (0.031)
	2	*0.017*	*2.72*	1.20 (0.023)	*0.021*	*2.34*	2.17 (0.044)
Constant head (-120 cm)	2	*0.017*	*2.72*	3.45 (0.162)	*0.021*	*2.34*	0.75 (0.0107)
Free drainage	6	0.036 (0.0007)	1.45 (0.003)	16.68 (0.48)	0.013 (0.0005)	1.59 (0.013)	5.10 (0.51)
	4	*0.017*	1.53 (0.003)	5.09 (0.12)	0.003 (0.00013)	*2.34*	0.33 (0.005)
	3	*0.017*	*2.72*	0.97 (0.02)	0.017 (0.00008)	*2.34*	0.22 (0.004)
	2	*0.017*	*2.72*	0.86 (0.022)	*0.021*	*2.34*	0.39 (0.004)

Large differences in model performance were obtained when using free drainage or constant head conditions (Table 2-3). After optimization, the r^2 for different free drainage and constant head conditions and various optimization scenarios was similar, while C_e and RSME were different. Overall, the performance of the model to predict soil-water content at 40 cm was lowest. The model performs well for the 10, 20, and 30 cm depths where the plant roots are concentrated and which are consequently the most critical in terms of irrigation optimization. The model with a constant head (-140 cm) clearly performed better than the free drainage boundary condition. The smallest differences were detected at the top node (10 cm) compared to deeper nodes in constant head and free drainage conditions. The optimization approach showed that the free drainage condition was unsuccessful to predict soil water content sufficiently well in agreement with observations, even using different parameter estimations. The two-parameter scenario requires fewer parameters (one parameter for each layer) to be optimized, performs better as compared to the uncalibrated model and is therefore to be preferred. Large confidence limits indicate uncertain estimations of a particular parameter (Šimůnek and Hopmans, 2002). The optimized K_s with 95% confidence limits (CL) for the first and second layer were 1.20 (1.15–1.24) cm h^{-1}, and 2.17 (2.06–2.26) cm h^{-1}, respectively, in

Table 2-3. Calculated performance criteria describing the correspondence between measured and simulated soil water content for each scenario for various boundary conditions.

	Boundary condition	Number of optimized parameters	Nodes depth cm	RMSE †	C_e †	r^2 †
Uncalibrated (2012)	Constant head (-140 cm)	0	10	0.029	0.34	0.58
			20	0.018	0.44	0.53
			30	0.016	0.18	0.38
			40	0.014	-0.03	0.27
	Constant head (-120 cm)	0	10	0.032	0.2	0.37
			20	0.039	-1.66	0.26
			30	0.029	-1.65	0.16
			40	0.023	-1.76	0.08
	Free drainage	0	10	0.054	-1.32	0.51
			20	0.036	-1.24	0.7
			30	0.055	-8.52	0.6
			40	0.052	-13.51	0.62
Calibration period (2012)	Constant head (-140 cm)	6	10	0.023	0.56	0.62
			20	0.016	0.53	0.74
			30	0.010	0.67	0.69
			40	0.008	0.63	0.64
		4	10	0.024	0.52	0.62
			20	0.016	0.54	0.76
			30	0.010	0.65	0.70
			40	0.008	0.64	0.64
		3	10	0.026	0.45	0.62
			20	0.014	0.65	0.75
			30	0.010	0.65	0.70
			40	0.008	0.63	0.64
		2	10	0.026	0.46	0.63
			20	0.014	0.65	0.75
			30	0.010	0.66	0.69
			40	0.010	0.45	0.63
	Constant head (-120 cm)	2	10	0.022	0.60	0.61
			20	0.031	-0.65	0.72
			30	0.025	-0.97	0.64
			40	0.019	-1.01	0.56
	Free drainage	6	10	0.023	0.57	0.60
			20	0.018	0.46	0.71
			30	0.016	0.19	0.56
			40	0.011	0.34	0.50
		4	10	0.022	0.62	0.64
			20	0.018	0.45	0.71
			30	0.014	0.13	0.55
			40	0.016	-0.11	0.42
		3	10	0.032	0.18	0.54
			20	0.021	0.29	0.62
			30	0.027	0.12	0.50
			40	0.019	-0.95	0.43
		2	10	0.028	0.39	0.51
			20	0.022	0.31	0.59
			30	0.015	0.12	0.51
			40	0.014	-0.98	0.50
Validation period (2013)	Constant head (-135 cm)	2	10	0.042	0.34	0.37
			20	0.027	0.30	0.40
			30	0.020	0.24	0.33
			40	0.016	0.11	0.29

†RMSE, C_e and r^2 are the root-mean-square deviation (cm^3cm^{-3}), the Nash–Sutcliffe coefficient of efficiency and the coefficient of determination.

the two-parameter scenario with -140 cm GWL. Therefore, this optimization result was considered the best and was chosen for the evaluation run.

2.5.4 Model evaluation

The validation results (using the same hydraulic parameter values as in the calibration period) under different upper (rainfall and water supply, ET_o, LAI) and lower (groundwater depth, i.e. -135 cm) boundary conditions, show that model performance during the calibration was superior to the validation period at all observation depths (Figure 2-7, Table 2-3). The same result was reported by, Wöhling et al. (2008), Wöhling et al. (2009).

Similar to the calibration period, soil-water content was predicted better during the rain and irrigation period than in the dry period. Specifically, soil-water content was overpredicted during summer months (June-August) and underpredicted during winter and spring. Wöhling et al. (2009) explained that the differences can be partly attributed to non-uniqueness of the optimization process, inadequacy of the model structure, the large number of optimized parameters, different information content in the calibration and evaluation data, and seasonal changes in soil hydraulic properties. The extent to which the soil water content prediction affects the calculated irrigation requirements, is dealt with in the next section.

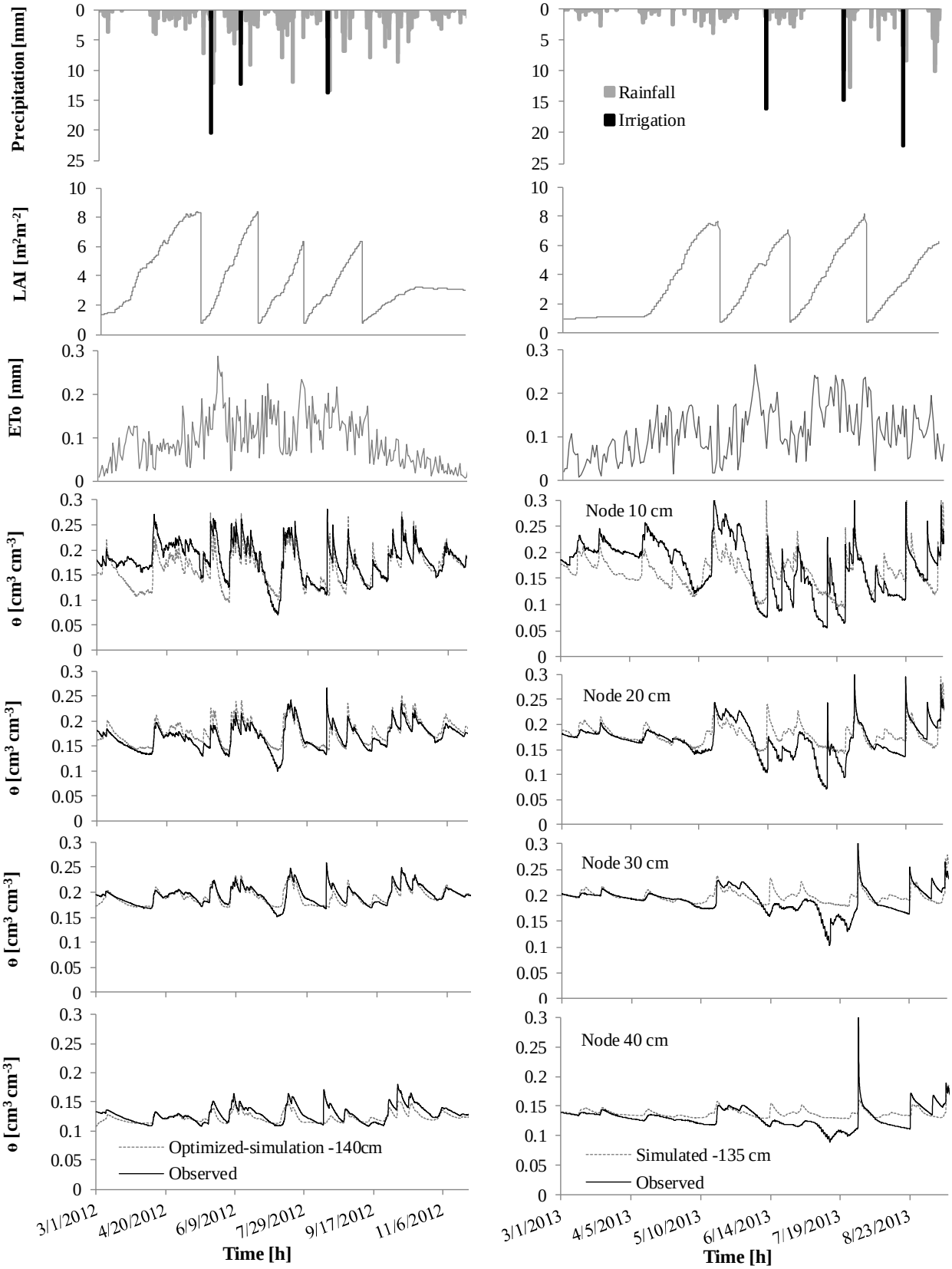

Figure 2-7. Observed and simulated time series of soil water content with calibration using the two-parameter K_s scenario for 2012 and validation results of 2013.

2.5.5 Effect of optimization scenarios on estimated water stress and yield reduction

Using the two-parameter optimization scenario (Table 2-4), the calculated potential-reference evapotranspiration (ET_o) values for 2012 and 2013 (same period from 1 Mar. to 12 Sep.) were 523 and 524 mm, respectively. The cumulative actual transpiration and evaporation, provided by the hydrological model, were 353 and 86 mm for the calibration (2012) and 343 and 114 mm for validation (2013) periods. Calculated cumulative actual fluxes across the bottom of the soil profile were -15.4 mm (outflow/drained) and 63.3 mm (upward inflow/capillary rise), for 2012 and 2013 respectively. The calculations are valid for the location where the soil moisture sensor was placed, i.e., in the drier part of the field with groundwater depths below 120 cm. The sum of irrigation and precipitation over the simulation period was 463 mm (64.5 mm irrigation and 398.5 mm precipitation) in 2012 and 428.7 mm (85.4 mm irrigation and 343.3 mm precipitation) in 2013. In 2013, the amount of water from irrigation and rainfall was lower as compared to 2012, resulting in a larger recharge from the groundwater. Overall, the periods of water stress totaled 671 h in 2012 and 675 h in 2013 (Table 4). Despite the similarity, the extent of soil water stress was larger in 2013 as compared to 2012. This can be attributed to the fact that the first water stress event in 2012 with about 328 h duration is not related to soil water availability but is also due to climate limitations (low temperature and light-radiation limitation because growth is function of radiation, temperature, light and then water; see sections 1.4.1.1 and 2.3.1.1). No significant reduction or increase in yield and LAI was achieved during this first water stress event in current and optimum conditions (Figure 2-3).

There was a significant effect of the bottom boundary condition on the calculated water stress. A free drainage condition resulted in a larger number, longer duration of stress conditions (Figure 2-8 and Table 2-4) and overestimated water stress due to excessive recharge to the groundwater (more than 148 mm). On the other hand, a shallower imposed groundwater level (-120 cm) creates less estimated water stress (Figure 2-8 and Table 2-4), because this boundary condition allows inflow (upward flow) from groundwater table. When the GWL was -140 cm the outflow of the bottom flux increased from the six-optimized parameter scenario (-4.6 mm) to two-parameter scenario (-15.4 mm) in the calibration period, while upward flow increased with increasing number of optimized parameters in validation period (63.3 to 76.9 mm). But these inflows did not meet the crop water requirement (see next section). Huo et al. (2012) reported that the maximum contribution of GWL to crop water requirement occurred when the GWL was less than 100 cm.

Table 2-4. Total duration, number and extent of water stress for different boundary conditions and scenarios (from 1 Mar. to 12 Sep.). Total rainfall and irrigation amount were 398.2 and 64.5 mm in 2012 and 343.3 and 85.4 mm in 2013 respectively. Number between parentheses represents the duration of first water stress event due to light-radiation and temperature limitations.

	Boundary condition	Number of parameters optimized	Number of water stress periods	Total Duration of water stress	Degree of water stress*	Profile bottom flux	Additional required irrigation	Yield reduction
				h		mm		%
Calibration period	Constant head (-140 cm) uncalibrated	0	0	0	≥1	-8.1	0	0
	Free drainage uncalibrated	0	9	1369 (436)	0.20	-310.1	120	28
	Free drainage	2	7	867 (345)	0.37	-167.7	60	18
	Constant head (-120 cm)	2	0	0	≥1	71.9	0	0
	Constant head (-140 cm)	2	7	671 (328)	0.65	-15.4	50	16
	Constant head (-140 cm)	4	4	524 (277)	0.65	-1	50	13
	Constant head (-140 cm)	6	5	540 (276)	0.66	-4.6	45	13
Validation period	Constant head (-135 cm) uncalibrated		0	0	≥1	105.5	0	0
	Free drainage uncalibrated	0	11	1371	0.05	-222.9	120	33
	Free drainage	2	7	1093	0.10	-148.7	70	23
	Constant head (-120 cm)	2	1	20	0. 85	64.4	5	0
	Constant head (-135 cm)	2	5	675	0.65	63.3	30	13
	Constant head (-135 cm)	4	4	598	0.65	76.6	20	11
	Constant head (135 cm)	6	3	579	0.65	76.9	20	11

*Lower degree of water stress shows the more water stress.

Overall, to overcome the water stress effects on crop yield, additional required irrigation should be supplied for different optimization scenarios and boundary conditions. During water stress, yield reduction would be in range of 0 to 33% for different optimization scenarios (Table 2-4). In addition, two- to six-parameter optimizations showed a similar value in yield reduction (16% for two- and 13% for three- to six-parameter in calibration and 13% for two- and 11% for three- to six-parameters to be optimized in validation periods). The maximum yield reduction occurred in the free drainage condition among different boundary conditions and parameter optimization scenarios (see Appendix-Chapter 2, Figure A2-5). Different parameter optimization strategies (two-, three-, four- or six-parameter optimizations) do not affect the calculated water stress as significantly as does the bottom boundary. Therefore, these results

suggest that simultaneous optimization is needed for irrigation management purposes, i.e. optimize/choosing boundary conditions to accurately describe recharge to or from groundwater and, in second order, optimize hydraulic parameters to accurately describe soil-water content variation in the topsoil.

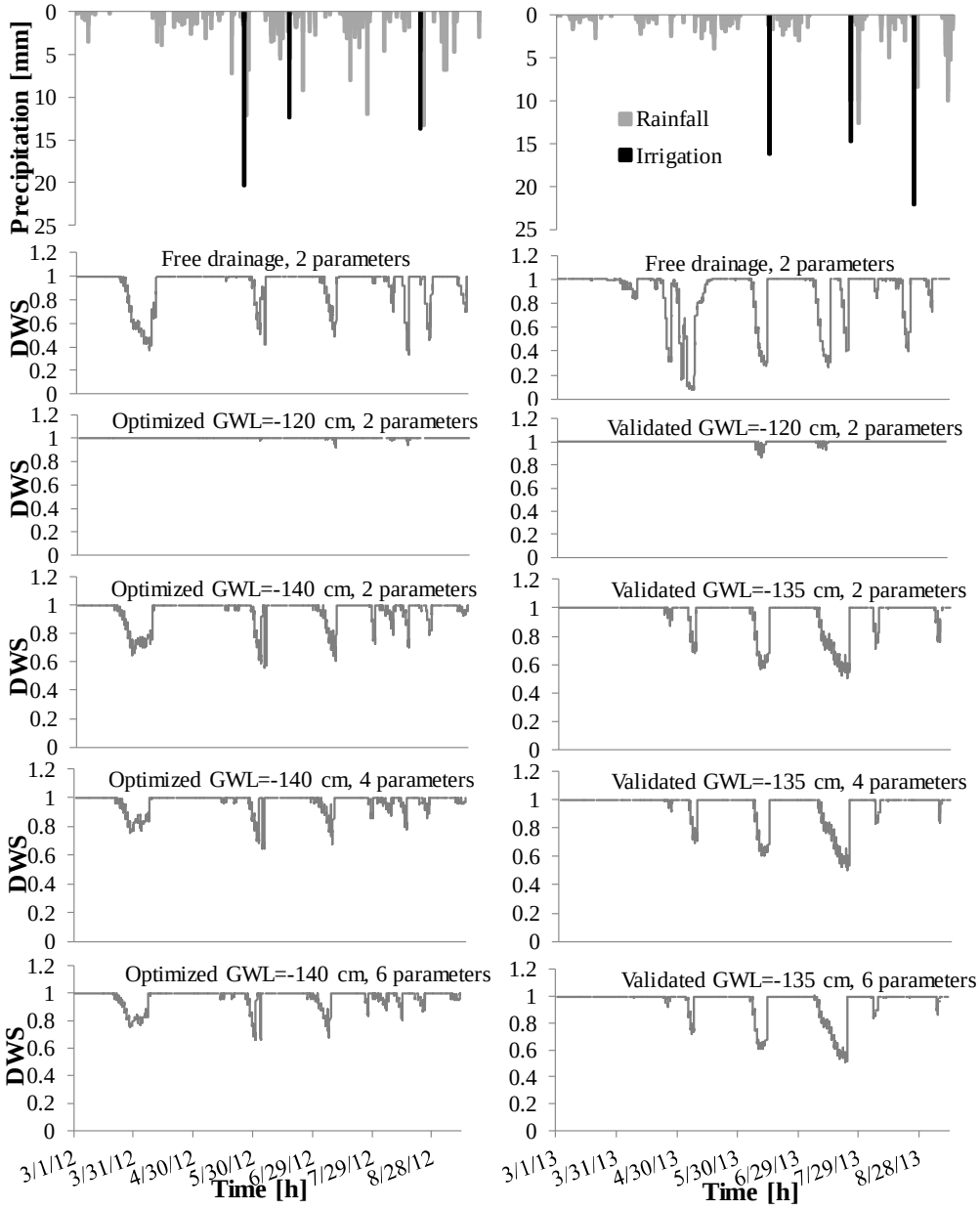

Figure 2-8. Degree of water stress (DWS) at potential reference evapotranspiration in 2012 and 2013 for various scenarios and bottom boundary conditions.

2.5.6 Irrigation scheduling scheme

The simulated results further showed that, to avoid drought stress during summer, a more accurate irrigation schedule would be needed in the drier part of the field. It would be better to supply water in June and July instead of a huge amount in late summer or at an inappropriate time (see Figure 2-8 and 2-9). Results revealed that the actual water supply exceeded crop

demand but did not meet the crop requirement (Figure 2-9 and Table 2-5). Irrigation volume affects soil water fluxes (see Appendix-Chapter 2, Figure A2-7). In the 'no irrigation' scenario for 2012 the upward/inflow fluxes from groundwater were larger than current and guided irrigation scenarios (Figure 2-10). The upward flow of water was not sufficient to meet the crop requirement. For guided irrigation, recharge from groundwater was larger than current irrigation in 2012 and 2013. Which means some part of crop water demand would need to be supplied from groundwater in guided irrigation.

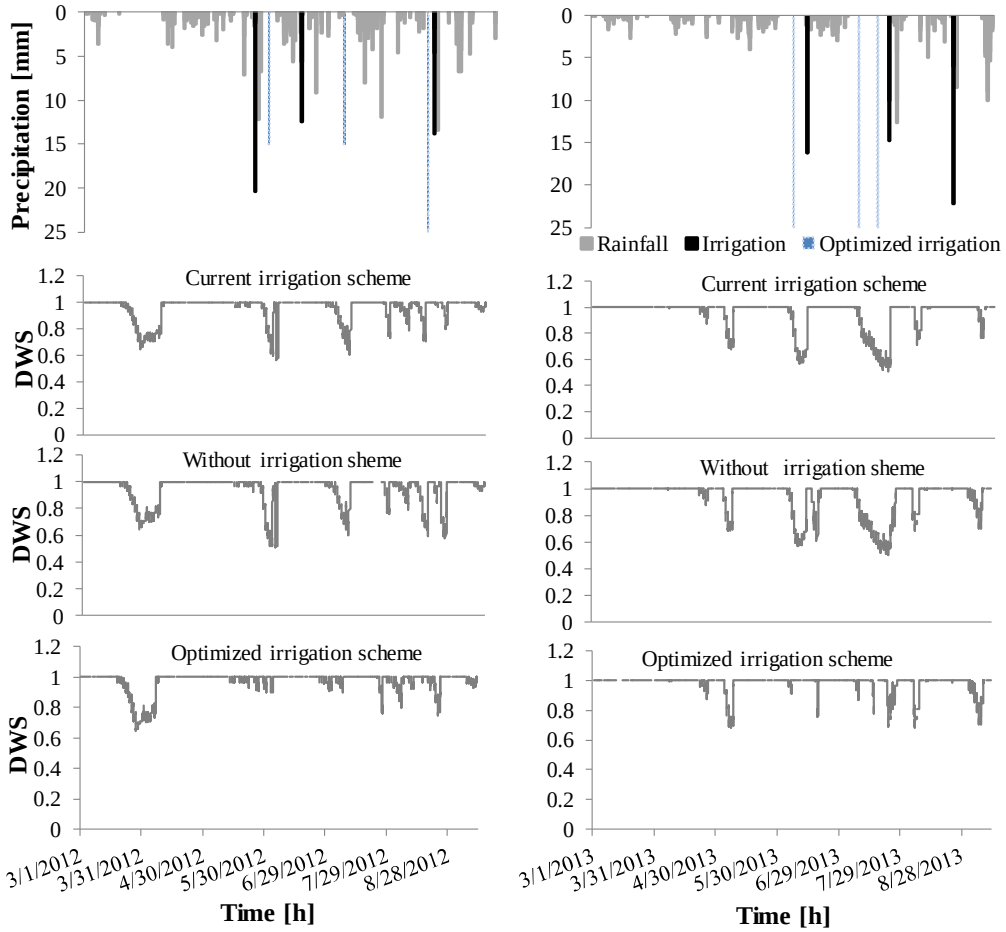

Figure 2-9. Comparison degree of water stress (DWS) between farmer's conventional irrigation (current irrigation), without irrigation and optimized irrigation scheme for calibration and validation periods.

Results show that, despite reducing water supply throughout the growth period by about 22.5% in 2012 and 12% in 2013, yield would have increased about 4.5% in 2012 and 6.5% in 2013 on average (Table 2-5, Figure 2-3), by rescheduling irrigation at the precise time when the crop is exposed to water stress. The number of irrigation events would remain similar to realistic applications (three times in each growing season). At the field scale non-uniform irrigation

distribution (water supply in drier parts with GWL below 120 cm) would be necessary.

Table 2-5. Comparison of optimized irrigation schedule with farmer's conventional irrigation schedule.

Boundary condition	Observed irrigation schedule				Optimized irrigation schedule			Difference
	Time	amount	Yield observed	Yield simulated	Time	amount	Yield simulated	amount
	day	mm	ton ha^{-1}		day	mm	ton ha^{-1}	mm
Calibration period (2012)	20 May	22.5			27 May	15		
	11 June	21			2 July	15		
Constant head (-140 cm) with 2 optimized parameters	13 August	21	10.4	10.9	11 August	20	11.4	14.5
Validation period (2013)	13 June	32.4			6 June	25		
	23 July	24.8			8 July	25		
Constant head (-135 cm) with 2 optimized parameters	23 August	28.2	10.8	11.1	17 July	25	11.8	10.4

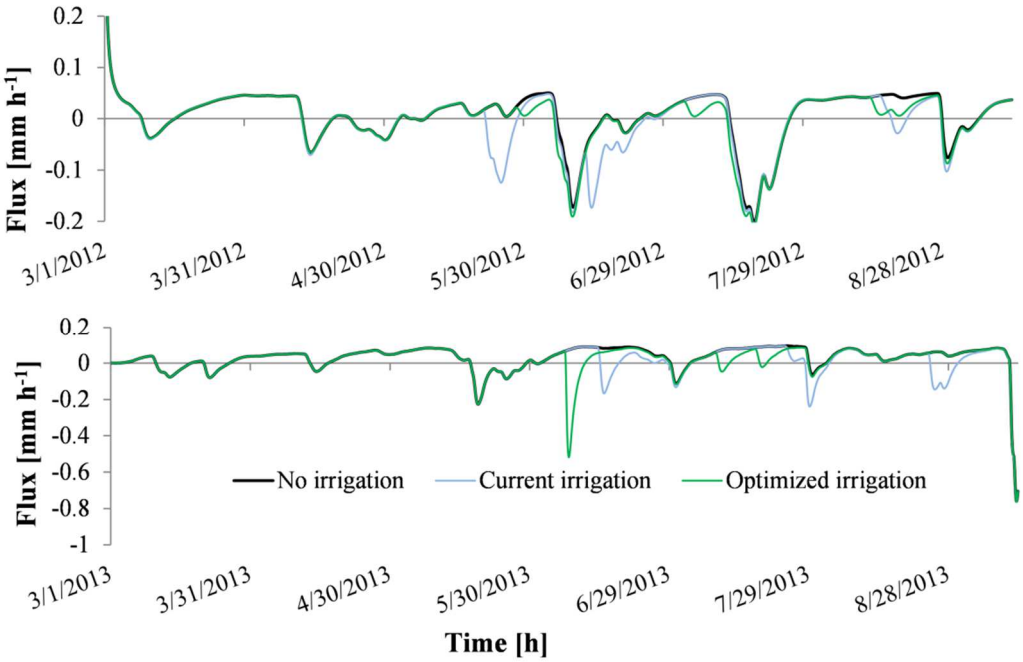

Figure 2-10. Actual flux of farmer's conventional irrigation (current irrigation), without irrigation and optimized irrigation scheme (guided irrigation) for 2012 and 2013 (see also Fig. A 2-5.

2.6 Conclusions

The results of this part of study have demonstrated clearly the profound effect of the position of the groundwater table on the estimated soil-water content and associated water stress in a sandy two-layered soil under grass in a temperate maritime climate. Indeed, field scale

variations in soil-water content can be very large, due to topography and variable depth of the groundwater. Furthermore, the model performance was affected by the spatial variability of hydraulic parameters such as K_s. Results show that the uniform distribution of water using standard gun sprinkler irrigation may not be an efficient approach since at locations with shallow groundwater, the amount of water applied will be excessive as compared to the crop requirements, while in locations with a deeper groundwater table, the crop irrigation requirements will not be met during crop water stress.

The results show that the effect of groundwater level was dominant in soil-water content prediction, at least under conditions similar to those in our study. This reflects the need for accurate determination of the bottom boundary condition, both in space and time. In a subsequent field experiment in an adjacent field, the temporal fluctuations of the groundwater table based on diver (Mini-Diver, Eijkelkamp Agrisearch Equipment, Giesbeek, The Netherlands) measurements in boreholes revealed changes in groundwater depth of about 10 cm between two lower and higher locations (Chapter 4). The changes were smaller than the expected variation due to topography which may well range more than 100 cm even for relatively flat areas. This has important consequences for precision irrigation management and variable water applications at sub-field scale. The use of detailed (cm scale) digital elevation models, geophysical measurement techniques such as electromagnetic induction or ground-penetrating radar as proxies for hydraulic parameters will serve as valuable data sources for hydrological models to calculate variable irrigation requirements within agricultural fields. The parametrization scenarios in the calibration and validation stage of model development should be kept simple in view of the information they generate. We have shown that it is sufficient to estimate limited amount of key parameters for which the temporal variant information of the sensitivity is crucial. Furthermore, that optimization strategies involving multiple parameters do not perform better in view of the optimization of irrigation management. We have shown that a combined modeling approach could increase water use efficiency (12-22.5%) and yield (5-7%) by changing the irrigation scheduling. However, these efficiencies can only be achieved if rainfall is known a priori-while the soil water status could indicate when to irrigate, it would be impossible to know how much to irrigate if the rainfall cannot be accurately predicted. Therefore, the results of the study call for taking into account accurate weather forecast and water content data in irrigation management and precision agriculture. The combination of accurate and spatially distributed field data with appropriate numerical models will make it possible to accurately determine the field-scale irrigation requirements, taking into account

variations in boundary conditions across the field and the spatial variations of model parameters (see Chapters 3 and 5). The information gained in this study with respect to dominant parameters and the effect of boundary conditions at the plot scale (1D) will be scaled up in a 2D approach to the field scale using detailed spatial information on groundwater depth and hydraulic conductivity K_s.

Chapter 3. ***Predicting saturated hydraulic conductivity in a sandy grassland using proximally sensed apparent electrical conductivity***

This chapter is based on the following journal article:

Rezaei, M., Saey, T., Seuntjens, P., Joris, I., Wesley Boënne., Van Meirvenne, M, Cornelis, W. 2016. Predicting saturated hydraulic conductivity in a sandy grassland using proximally sensed apparent electrical conductivity. Journal of Applied Geophysics. 126: 35-41.

3.1 Introduction

Agricultural management requires detailed data at relevant management scales such as the field or the landscape scale. Digital soil property mapping methods and characterization of hydraulic properties at the field scale using proxy data (Brosten et al., 2011; Chaplot et al., 2011; Doolittle and Brevik, 2014; Sudduth et al., 2013) are increasingly being used. Such data in combination with hydraulic properties measured at multiple locations in the field are vital to predict and understand flow, solute and energy fluxes in soil (Vereecken et al., 2007) and needed in various applications. An example is precision irrigation, where accurate information about the spatial variation of field-scale soil hydraulic properties is required (Carroll and Oliver, 2005; Slater, 2007).

Generally, accurate information about the spatial variation of field-scale soil hydraulic properties is required in water management, flow and transport processes (Farzamian et al., 2015), hydrology and hydrogeology (Niwas and Celik, 2012) and irrigation management (Gumiere et al., 2014). Direct measurements of these properties (in the field or laboratory) are not only time-consuming, labor-intensive and expensive, but they also perturb the system. Moreover, a high sampling density (in size and space) is generally required (Jury and Horton, 2004) to obtain an acceptable spatial resolution.

Linking hydraulic properties to apparent electrical conductivity (ECa) measured with electromagnetic induction (EMI) may be a way forward to estimate the spatial distribution of these hydraulic parameters across a field. Such ECa measurements are extensive, less expensive, non-destructive, efficient, reliable and timely (Corwin and Lesch, 2005; Niu et al., 2015; Segal et al., 2008; Sudduth et al., 2005). In addition, in precision agriculture, EMI measured ECa (Hedley et al., 2013) allows to complement the limited density of direct soil samples (Saey et al., 2009b) and assess soil hydraulic properties at higher resolution. Soil ECa is a function of a variety of soil properties including soil-water content, porosity, texture and structure (bulk soil properties), salinity (soil solution properties), cation exchange capacity (CEC), organic matter content, particle shape, size and distribution (solid particle properties), and soil layer thickness and topology (Corwin and Lesch, 2005; Friedman, 2005; Saey et al., 2008; Sudduth et al., 2013). Parameters affecting ECa are similar to those that affect soil physical and hydraulic properties, especially hydraulic conductivity, K (Doussan and Ruy, 2009; Niu et al., 2015; Pulido Moncada et al., 2014; Sudduth et al., 2005). Therefore, ECa can be considered as an indirect indicator of hydraulic properties.

Over the past two decades, a large volume of research has focused on predicting hydraulic properties from basic soil properties to map K_s distribution (Slater, 2007). On the other hand, empirical and semi-empirical relationships were established between ECa and soil properties. Researchers have applied Archie's semi-empirical law (Archie, 1942) to link K and ECa (Huntley, 1986). Both positive and negative significant linear regressions between log ECa and log K were reported (Brosten et al., 2011; Chaplot et al., 2011; Doussan and Ruy, 2009; Morin et al., 2010; Mualem and Friedman, 1991; Purvance and Andricevic, 2000a).

It was shown before that field water content predictions using a hydrological model are very sensitive to saturated hydraulic conductivity, K_s (Gumiere et al., 2014; Verbist et al., 2012). It is also addressed in second chapter of this thesis. In our study site, we concluded that the use of detailed digital elevation models, geophysical measurement techniques such as electromagnetic induction as proxies for hydraulic parameters will serve as valuable data sources for hydrological models to calculate variable irrigation requirements within agricultural fields (see previous chapter). Therefore, a better characterization of the field scale heterogeneity of K_s by using ECa data is very beneficial for precision management purposes. The present study investigates empirical relationships of field ECa data and K_s to predict K_s more effectively and precisely at the field scale. In a first step, we performed a statistical analysis of the soil properties (K_s, ECa, bulk density, texture and organic carbon). We established statistical relationships between co-located K_s, selected soil physical properties and EMI-ECa. These relationships were then evaluated using an independent dataset of K_s. Finally, we estimated the K_s at the locations where the ECa was measured and produced a detailed map of K_s which may be used for irrigation management at the field scale.

3.2 Materials and Methods

3.2.1 Study site description

The study site was located in a sandy agricultural area at the border between Belgium and The Netherlands (central coordinates 51°19′05″ N, 05°10′40″ E). The field site is around 10.5 ha and is partly artificially drained by parallel pipes connected to a ditch in the North-West border of the field (Figure 3-1). The field was planted with grass during the study period 2011-2013. Further information about the study site are given in Chapter 2.

3.2.2 ECa measurements

ECa was measured at 5 m intervals between the measurement lines with a DUALEM-21S sensor (DUALEM, Milton, ON, Canada) on 25 March 2011. In this work, the perpendicular coil configuration data were used, corresponding to depths of exploration near 50 cm ($ECa_{p,50}$) and 100 cm ($ECa_{p,100}$). Details about the applied methodology for measuring ECa with the DUALEM-21S sensor can be found in Saey et al. (2009a, 2011b, 2012). In brief, the DUALEM-21S EMI sensor consists of one transmitter and four receiver coils at 1, 1.1, 2 and 2.1 m spacing from the transmitter coil. The receiver coils at 1 and 2 m from the transmitter are in horizontal coplanar mode and those at 1.1 and 2.1 m are in the perpendicular mode. In this study, all ECa measurements were converted to a reference temperature of 25° C (Slavich and Petterson, 1990).

3.2.3 Sampling strategy and soil sample analysis

Sampling locations for soil investigation were selected by combining design-based, model-based and traditional sampling strategy to account for the maximum variation in soil properties that was suggested by a geophysical survey with the DUALEM-21S sensor (0-100 cm). We decided to use $ECa_{p,100}$ to account for maximum variation in both lateral and vertical directions.

For the design-based sampling strategy, the software package ESAP-RSSD (Lesch, 2006) was applied for a full sampling design with 20 locations where soil cores were taken based on ECa survey data. This tool uses a response-surface sampling design (RSSD), which is proven to be particularly effective to account for the distribution of ECa survey data (Corwin and Lesch, 2005). In this study 20 locations were randomly proposed. Hence, we needed to sample at a few (20) sites across the area in order to develop a prediction model (i.e., an equation which can be used to predict the value(s) of the soil variable(s) from the conductivity survey information). ESAP optimizes our sampling design by selecting sample sites, therefore, two factors (the design factor and the optimum criteria) should be manipulated to get the optimized result. After minimization, the design factor was adjusted to 1.11 and the optimum criteria to 1.29 employing ESAP. A detailed discussion of the application of a design-based sampling strategy using ECa data can be found in Lesch et al. (1995) and Lesch et al. (2000). For the model-based sampling design, the FuzzMe software applying the Fuzzy k-means algorithm (Minasny and McBratney, 2002) was used to classify the ECa field data set. During classification, the fuzziness performance index (FPI), fuzziness exponent (phi), modified partition entropy (MPE), objective function value and number of performance iterations were

minimized to obtain a value of 0.363, 1.9, 0.365, 82.43 and 46 respectively. The ECa data revealed a zonation with three ECa classes crossing the whole field (class A: 0.02 < ECa < 2.949 mS m^{-1}, class B: 2.95 < ECa < 4.629 mS m^{-1}, class C: 4.63 < ECa < 11.96 mS m^{-1}). The suggested 20 locations from the ESAP model covered these classes well, with 7 locations in class A, 6 in class B and 7 in class C. Additionally, eight soil samples were taken along a transect during the growing season in 2011 for validation purposes. Figure 3-1 shows the map of 0-100 cm soil ECa, the 20 soil sampling locations from the ESAP software and eight additional sites on the validation transect.

To determine K_s, and bulk density, ρ_b, two undisturbed soil samples consisting of cores of 5 cm diameter by 5 cm height were taken (100 cm^3 Kopecky rings, Eijkelkamp Agrisearch Equipment, Giesbeek, The Netherlands) at a depth of 20 cm within the Ap horizon at the 28 locations shown on Figure 3-1 within the field during the growing season of 2011 and 2013. The undisturbed samples (primary and replicate soil core samples) were collected at the same depth but at a slightly different location (within maximum 20 cm radius). Saturated hydraulic conductivity was determined using a laboratory permeameter (M1-0902e, Eijkelkamp Agrisearch Equipment, Giesbeek, The Netherlands) maintaining

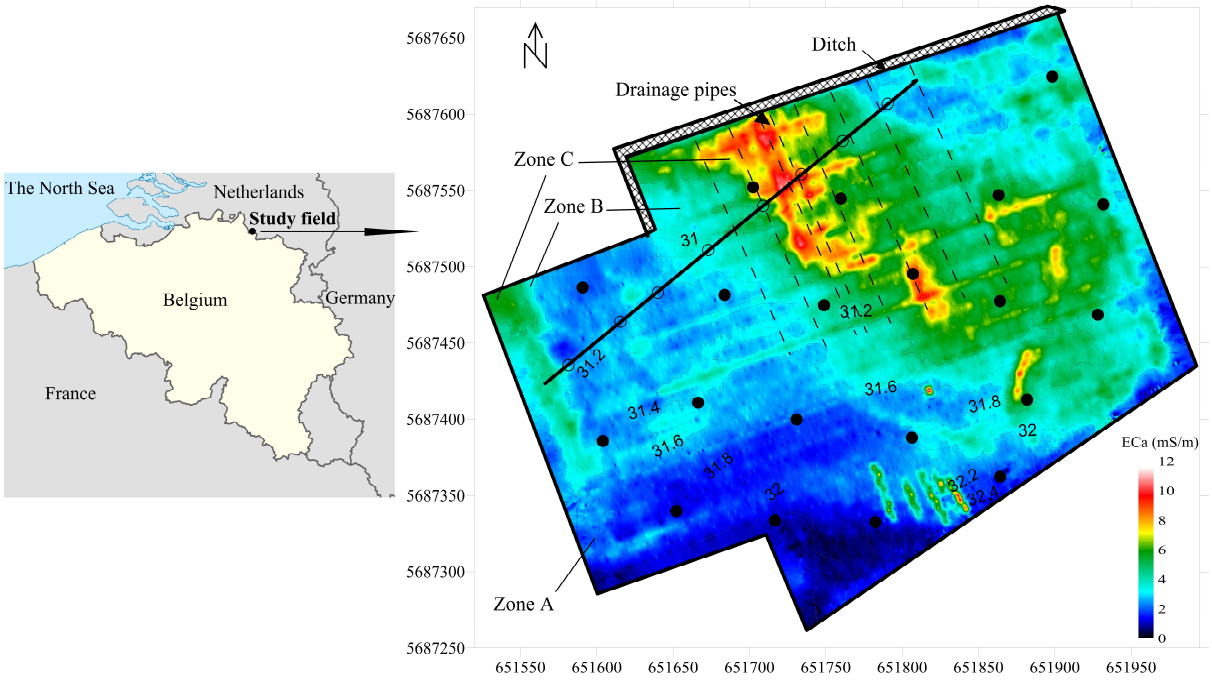

Figure 3-1. Location of the study field and the classified map of 0-100 cm soil ECa with location of the 20 soil sampling locations (black bullets) from the ESAP software (calibration) and the eight additional points along the transect (validation). The 20 locations are well distributed over the FuzzyMe-derived ECa classes, with 7 locations belonging to class A (0.02 < ECa 2.949 mS m-1), 6 locations to class B (2.95 < ECa 4.629 mS m-1), and 7 locations to class C (4.63 < ECa 11.96 mS m-1) with indication of elevation contour intervals (labels in m a.s.l.).

a constant head. Therefore, each core was brought to saturation during 24 h. The weight of each saturated core was measured to support ρ_b determination before each K_s analysis. Subsequently, ρ_b was obtained by drying volumetric soil samples (100 cm^3 Kopecky rings) at 105 °C for 24 h (Grossman and Reinsch, 2002). For final analysis, an arithmetic average of two paired samples of K_s and ρ_b, were calculated.

Additionally, at each location and at the same depth one disturbed sample was collected to measure both soil texture (Gee and Bauder, 1986) and soil organic carbon (Walkley and Black, 1934), followed the procedures explained in Chapter 2.

3.2.4 Statistical and geostatistical analysis

Statistical analyses on K_s, ECa (0-50 and 0-100 cm) and selected physical properties were performed for all soil samples. The mean (m), minimum and maximum (min and max), skewness and standard deviation (SD) of soil properties and ECa surveys were calculated (Table 3-1). The Pearson correlation coefficient was computed between co-located ECa measurements, K_s and selected soil properties. All statistical analyses were performed using IBM SPSS Version 20. The laboratory K_s showed a lognormal distribution ($p<0.05$) according to a Shapiro-Wilk normality distribution test. The geometric mean and standard deviation of K_s were calculated based on the Parkin et al. (1988) recommendation for lognormal distributed populations with a sample size between 4 and 40 (Finney, 1941). The distribution of ECa was neither normal nor lognormal using a Kolmogorov-Smirnov normality distribution test. Therefore, K_s was log-transformed to obtain a normal distribution and the original values of $ECa_{p,50}$ and $ECa_{p,100}$ were used.

The field $ECa_{p,50}$ data were interpolated using ordinary point kriging (OK) to a 0.5 by 0.5 m grid (Saey et al., 2012). The nugget variance (C_0), sill ($C_0 + C_1$), and effective range (a) were 0.31, 3.63 and 281.9 m, respectively, for a spherical variogram model (see the semivariogram in Appendix – Chapter 3). A maximum of 64 neighbors was used within a circular search area with a radius of 20 m. As mentioned previously, K_s was measured at 20 calibration and 8 validation locations. Subsequently, ECa was extracted at these 28 locations from the interpolated 0.5 by 0.5 m grid (OK map) from the center of the corresponding grid cell. Afterwards, a predictive simple linear regression approach between extracted ECa (0-50 cm) and co-located ln K_s values (measured K_s) of 20 locations was applied to explain the spatial variation in K_s. The developed relation was applied to the interpolated kriged ECa map. We chose to only employ the ECa within the top 0-0.5 m soil volume to establish the relationship

with K_s because we assume the hydraulic conductivity of the topsoil layer (20 cm) is mainly related to ECa of the topsoil layers. Moreover, because both $ECa_{p,50}$ and $ECa_{p,100}$ are rather analogue (correlation r = 0.94), there is no added value of including $ECa_{p,100}$ within the regression. Consequently, a detailed K_s map (0.5 by 0.5 m grid) was produced. The predicted K_s values of co-located 8 validation points along the transect (Figure 3-1) were extracted from the modelled K_s map (8 extracted K_s values are co-located with 8 measured validation points). The relation was validated by comparing measured and predicted K_s values of eight locations.

The simple interpolation was performed on measured data for comparison purposes and to show the accuracy of the produced maps. For the interpolation of the 28 K_s data (20 for calibration and 8 for validation), the inverse distance weighting (IDW) was performed (Chaplot et al., 2011; Corwin and Lesch, 2005) with 12 neighbors to a 0.5 by 0.5 m grid using GS+5.1 version of Gamma Design Software (2009). The IDW interpolation method is more accurate than kriging when dealing with low density sample sites (Corwin and Lesch, 2003) such as our case study. The cross validations were used to optimize the estimation condition of K_s interpolation (e.g. optimizing parameter such as neighbors, radius, weighting power, smoothing factor etc.). To evaluate the uncertainty of the map, the validation data (K_s values), as 8 independent observations, were taken at the center of the grid cells of the specific locations of produced map, similar to the procedure mentioned above.

The accuracy and reliability of K_s-ECa relation and the maps were evaluated using the mean estimation error (MEE), root-mean-square errors (RMSE), the coefficient of determination (r^2) and the Nash–Sutcliffe coefficient of model efficiency (C_e). They are calculated as follows:

$$MSE = \frac{\sum_i^n (O_i - S_i)^2}{n} \tag{3-1}$$

$$RMSE = \sqrt{\frac{\sum_i^n (O_i - S_i)^2}{n}} \tag{3-2}$$

$$r^2 = \left(\frac{\sum_{i=1}^n (O_i - \bar{O})(S_i - \bar{S})}{\sqrt{\sum_{i=1}^n (S_i - \bar{S})^2 \sum_{i=1}^n (O_i - \bar{O})^2}}\right)^2 \tag{3-3}$$

$$C_e = 1 - \frac{\sum_{i=1}^n (O_i - S_i)^2}{\sum_{i=1}^n (O_i - \bar{O})^2} \tag{3-4}$$

where O and S are observed and simulated values at time/place i, respectively. The optimal value of the statistics is as close as possible to zero for MEE and RMSE and to one for r^2 and C_e.

3.3 Results and Discussion

3.3.1 Spatial variation of selected soil physical properties, K_s and soil ECa

The summary statistics of selected soil physical properties, K_s and ECa of the field site are given in Table 3-1. The mean values of ECa measured with DUALEM-21S increase with increasing depth of exploration (DOE). The higher electrical conductivity is due to the larger sampled soil volume (Saey et al. 2009a, 2011a) with the subsoil showing higher bulk density by subsoil compaction, and presumably a larger clay and a larger organic carbon content in the soil volume. Increasing the DOE increases the ECa standard deviation (SD) due to the higher differences in absolute values and due to larger soil-water content and clay content variations (Table 3-1). At greater depths (DOE = 0-100 cm), ECa could be affected by fluctuations in groundwater level. ECa gradually increased down-slope, reaching the highest level in the middle of the field (Figure 3-1). The ECa values showed large spatial variation with a coefficient of variation CV of 56 and 54% for 0-50 and 0-100 cm DOE. These CV values are of similar order as those of K_s, clay and OC content (Table 3-1).

The hydraulic parameter K_s exhibited a lognormal distribution ($p<0.05$). This result agrees well with Botors et al. (2009) and Verbist et al. (2013a). K_s values ranged from 0.6 to 9.61 cm h^{-1}, with a geometric mean 3.70 cm h^{-1}. The K_s shows a standard deviation of 3.19 cm^2/h^2 corresponding to a high coefficient of variation CV of 86%. Similar CV values for K_s at the field scale were reported previously by Mallants et al. (1996, 1997) on a sandy loam soil, Iqbal et al. (2005) on alluvial soils, and Jury (1985) on different textural soils. These results confirm the large spatial variability of K_s at the field scale. This could be attributed to the small sampel volume, thus measurement-scale dependent (see Chapter 4).

Table 3-1. Summary statistics of selected topsoil properties across the field site. ρ_b is soil bulk density, OC is organic carbon content, Sand, Silt, Clay are sand, silt and clay content, respectively. K_s is laboratory saturated hydraulic conductivity. ECa is apparent electrical conductivity (at 25 °C), with subscripts p,50 and p,100 denoting ECa of DUALEM-21S 0-50 cm and 0-100 cm perpendicular, respectively. Number between parentheses represents the geometric mean and its standard deviation of *Ks*.

Variable	No. of samples	Min	Max	Mean	SD	CV (%)	Skewness
ρ_b (g cm^{-3})	28	1.43	1.69	1.61	0.06	3.72	-1.13
OC (%)	28	1.06	4.46	2.20	0.59	26.86	1.85
Sand (%)	28	88.1	93.5	90.99	1.31	1.43	-0.07
Silt (%)	28	4.30	9.30	7.27	1.14	15.68	-0.85
Clay (%)	28	1.10	3.60	1.72	0.54	31.39	1.89
K_s (cm h^{-1})	28	0.61	9.61	3.23 (3.70)	2.30 (3.19)	71.21 (86.21)	1.51
$ECa_{p,50}$ (mS m^{-1})	98216	0.06	9.99	2.84	1.59	55.98	0.94
$ECa_{p,100}$ (mS m^{-1})	98442	0.02	10.91	3.44	1.85	53.77	0.73

Soil bulk density, ρ_b, varied between 1.43 and 1.69 g cm^{-3} with an average of 1.61 g cm^{-3}. The average sand, silt and clay content were 91.0±1.3%, 7.3±1.1% and 1.7±0.5%, respectively. Soil organic carbon, OC, ranged between 1.06 and 4.46%. The largest CVs were observed for soil clay content (31%) and OC (27%), whereas those for ρ_b, sand and silt content are rather low (<16%) (Table 3-1).

3.3.2 Relation between selected soil physical properties, K_s and soil ECa

Pearson correlation coefficients between selected physical properties, K_s and ECa and are shown in Table 3-2. Obviously, the most significant correlation was observed between ECa values at different DOEs (r = 0.94). In general, the highest significant negative correlations with ECa are obtained between ln K_s and ECa from both soil volumes (r = -0.83 in both cases). A negative significant relation between log K_s and log ECa was also reported by Purvance and Andricevic (2000a) with 56 samples (r = -0.63) and by Brosten et al. (2011) with 10 observation points (r = -0.62). Morin et al. (2010) reported a negative correlation between log K_s and a normalized ECa for 15 observation points (r = -0.82). The ln K_s is negatively correlated with silt (r = -0.46, P <0.05) and clay (r = -0.38, P <0.05), while a positive significant correlation between ln Ks and sand (r = 0.55, P <0.01) was found. Similar relations were reported by Sobieraj et al. (2001). On the contrary, ECa was negatively and positively correlated with sand (r = -0.54, P <0.05; for $ECa_{p,50}$ and r = -0.49, P <0.05; for $ECa_{p,100}$ and) and silt (r = 0.55, P <0.05; for $ECa_{p,50}$ and r = 0.50, P <0.05; for $ECa_{p,100}$) respectively. An increasing K_s with increasing sand content and decreasing clay content (Chapuis, 2004) leads to a lower ECa (Lesmes and Friedman, 2005; Morin et al., 2010). Moreover, the negative correlation between K_s and ECa can be explained by the fact that highly permeable soils tend to drain and dry out relatively fast. Therefore, these soils have lower ECa as it relates to soil particle size distribution and soil-water content (Lesmes and Friedman, 2005). On the other hand, electrical current is affected by a low conductivity of soil solution in the field and existence and accumulation of humus fibers and clay as was the case for the Podzol in this study. Therefore, both factors lead to a more strongly negative correlation between K_s and ECa. No significant correlation could be detected between ρ_b, OC, and the ECa or K_s values measured from different soil volumes (Table 3-2).

Table 3-2. Pearson correlation coefficient between the selected soil properties. ρ_b is soil bulk density, OC is organic carbon content, Sand, Silt, Clay are sand, silt and clay content, respectively, K_s is laboratory saturated hydraulic conductivity, ECa is apparent electrical conductivity (at 25 °C), with subscripts p,50 and p,100 denoting ECa of DUALEM-21S 0-50 cm and 0-100 cm perpendicular, respectively.

	ρ_b	OC	Sand	Silt	Clay	ln*Ks*	$ECa_{p,50}$	$ECa_{p,100}$
ρ_b	1							
OC	0.17	1						
Sand	-0.3	-0.41*	1					
Silt	0.26	0.46*	-0.91**	1				
Clay	0.02	0.04	-0.52**	0.12	1			
ln*Ks*	-0.35	-0.03	0.55**	-0.46*	-0.38*	1		
$ECa_{p,5}$	0.17	0.27	-0.54*	0.55*	0.16	-0.83**	1	
$ECa_{p,1}$	0.18	0.12	-0.49*	0.50	0.15	-0.83**	0.94**	1

**and * marked correlation significant at $P \leq 0.01$ and $P \leq 0.05$ level respectively.

3.3.3 Estimation of K_s from ECa measurements

A regression analysis between the field ECa data derived for the top 50 cm ($ECa_{p,50}$ collected in 2011) and the 20 ln *Ks* values taken at similar depth within Ap horizon, i.e. 20 cm (sampled in 2013), resulted in the following equation:

$$\ln K_s = -0.398\, ECa_{p.50} + 2.13 \qquad r^2 = 0.694, \qquad SE = 0.439 \qquad (3\text{-}5)$$

where K_s and SE (standard error of estimation), in cm h^{-1} and ECa in mS m^{-1}.

The relatively low SE and large r^2 provides a good estimate of K_s from ECa. The cross plot of co-located ln K_s for the 20 observation points versus ECa with the 95% confidence limits on the prediction is presented in Figure 3-2. The relationship (Figure 3-2) shows nonuniqueness for the lowest ECa and highest K_s values. This can be explained by the fact that only a small ECa range is present. Moreover, the low ECa values approach the noise level of the measurements. The lowest ECa values are unable to capture the variation in high K_s values. In addition, the relationship predicts the K_s with some limits. Local deviations or outliers are either caused by phenomena which could not be gathered by the ECa variations, or by high spatial variation and uncertainties of the K_s measurements (especially in the laboratory which may not represent the field condition).

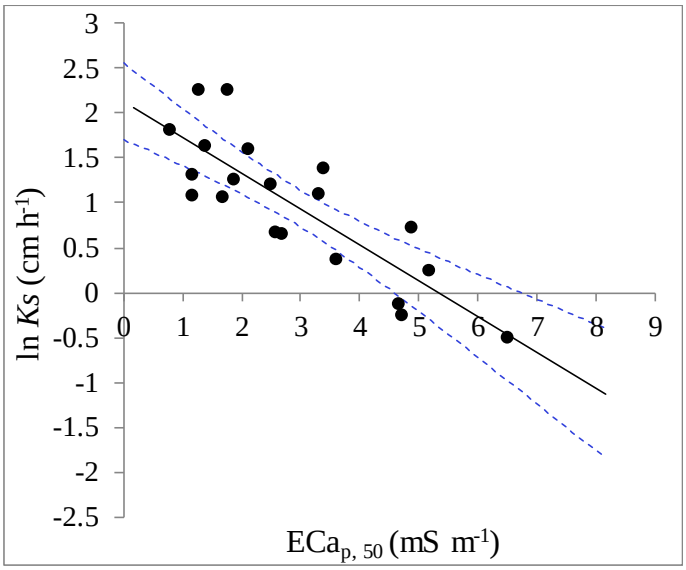

Figure 3-2. The scatter plot of co-located ln K_s for the 20 observation points versus $ECa_{p,50}$. The solid line shows the linear regression. The dashed lines show the 95% confidence limits on the prediction. K_s is laboratory saturated hydraulic conductivity, $ECa_{p,50}$ is apparent electrical conductivity (at 25 °C) measured with a DUALEM-2S EMI sensor over 0-50 cm.

A simple linear site-specific relation between ln K_s and ECa was also reported by Huntley (1986), Purvance and Andricevic (2000b) and Chaplot et al. (2011). The relation between K_s and ECa can be influenced by grain size distribution, pore fluid chemistry, mineralogy (Huntley, 1986) similar to our study (Table 3-2), specific surface area (Slater, 2007), organic matter content, porosity and soil compaction. In fact, there are multiple potential relations between K_s and several soil geophysical properties, which makes an accurate prediction of a single parameter i.e. K_s, from geophysical attributes not straightforward (Corwin and Lesch, 2003). On the other hand, using multiple regression to map a parameter demands more information about independent variables and detailed observations which are not only labor intensive and more expensive but also may increase the uncertainty of predictions due to their interactions and correlations. Therefore, using a linear geophysical relation is an effective approach to characterize K_s at the field scale.

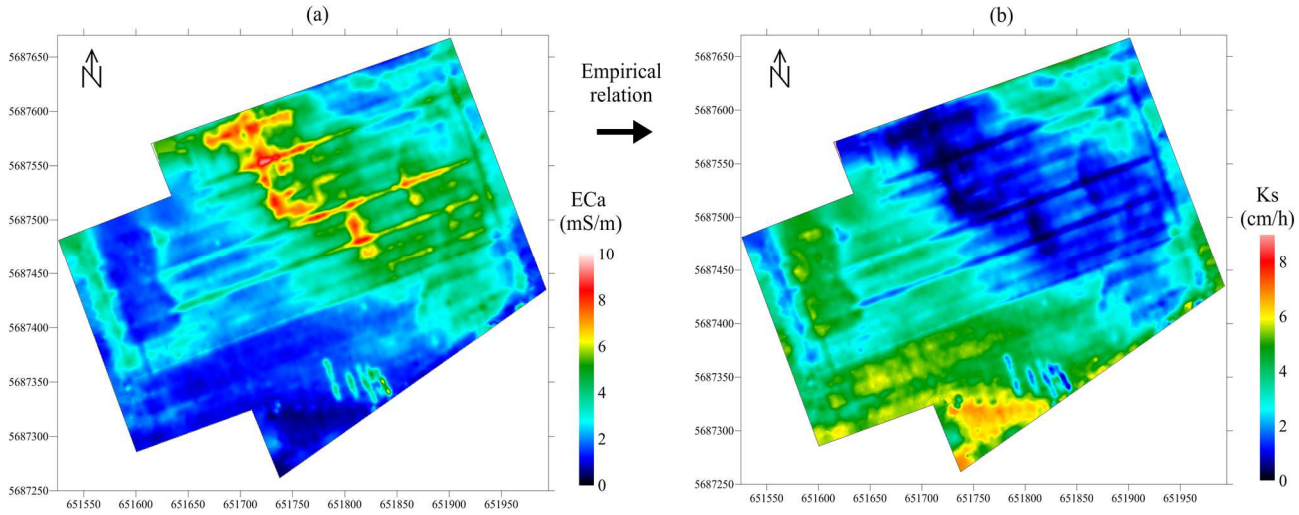

Figure 3-3. Kriged $ECa_{p,50}$ map and estimated K_s from the site-specific empirical (geophysical) relation (Eq. 3-5). K_s is laboratory saturated hydraulic conductivity, $ECa_{p,50}$ is apparent electrical conductivity (at 25 °C) measured with a DUALEM-2S EMI sensor over 0-50 cm.

Linking the developed relation between K_s and ECa with the ECa map (Figure 3-3a) resulted in a high resolution K_s map for the whole field (Figure 3-3b). This K_s map illustrates three distinct zones corresponding to the FuzzMe ECa classes (Figure 3-1). The K_s values measured at eight additional locations versus those predicted from Eq. 3-5 (obtained from the map) are presented in Figure 3-4. The validation indices prove that the modeled K_s map is fairly accurate in predicting the K_s variability across the study site. It should be noted that the accuracy of the estimated K_s values is only valid within the K_s data range used for calibration and validation (broad confidence at 95% confidence interval at the boundaries, Figure 3-4). Moreover, the validation transect has been located within the northern part of the study site, therefore the lowest ECa values (with associated high K_s values) were not covered. We acknowledge that the validation dataset is rather small to draw any meaningful conclusion outside this field. However, the validation transect shows a fairly good spread in ECa values, so we assume the validation observations are representative for estimating the average accuracy of modeled K_s within the field, making it valid within a K_s range from 0.5 to 5.5 cm h^{-1} of K_s.

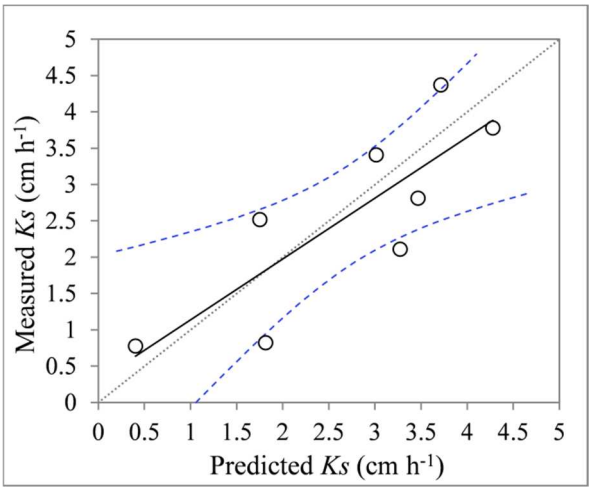

Figure 3-4. Scatterplot of measured vs. predicted K_s (Eq. 3-5), for eight validation points. The dashed lines show the 95% confidence limits on the prediction. K_s is laboratory saturated hydraulic conductivity.

The statistical performance indicators of the relation and its map showed a high r^2 between predicted and measured K_s (0.67), coefficient of model efficiency (C_e = 0.64), and a relatively low RMSE (0.74 cm h^{-1}). This indicates a good accuracy and prediction efficiency of the developed regression model compared to the other reports that addressed in section 3.3.2 (e.g. Brosten et al., 2011; Chaplot et al., 2011; Huntley, 1986; Morin et al., 2010; Purvance and Andricevic, 2000a). Ritter and Munoz-Carpena (2013) considered if the coefficient of model efficiency is <0.65, the model performance is unsatisfactory when using C_e as the only indicator. In addition, the model error is not linearly related with the indicator value, but the value is affected by other factors such as outliers and model bias (Ritter and Munoz-Carpena, 2013). Therefore, a combination of performance indicators is suggested to evaluated the model performance and prediction efficiency. The model slightly over (at high values) and under-estimated (at low values) K_s with a bias of 0.46 cm h^{-1} indicated by the MEE.

Figure 3-5 shows the K_s map of interpolation using the invers distance weighting (IDW). The large bias (2.06) and RMSE (1.06) with a low coefficient of model efficiency (0.25) and a moderate coefficient of determination (0.42) were identical to the value obtained by direct K_s interpolation. The K_s values were strongly overestimated (Figure 3-6). Obviously, results show the developed semi-log relation (Eq. 3-5) between ln K_s and ECa is a better estimator for the prediction of K_s from IDW. To compare and represent the accuracy of the predictions, relative RMSE was computed by dividing RMSE to the standard deviation of the observations (in this case 1.29 cm h^{-1} for eight validation points). As a rule of thumb, if the relative RMSE value is

close to 40%, it is considered as a fairly accurate prediction while if it gets more than 71%, this means the model accounted for less than 50% of variability at the validation points and the prediction is unsatisfactory (Hengl et al., 2004; Saey et al., 2011a). The relative RMSE of the regression model and interpolation of K_s predictions were 57 and 82%, respectively. These results confirmed that the estimation of K_s from the established regression model using the ECa estimator is satisfactory and certainly reasonable for hydrological modeling in the sandy soil of the study site.

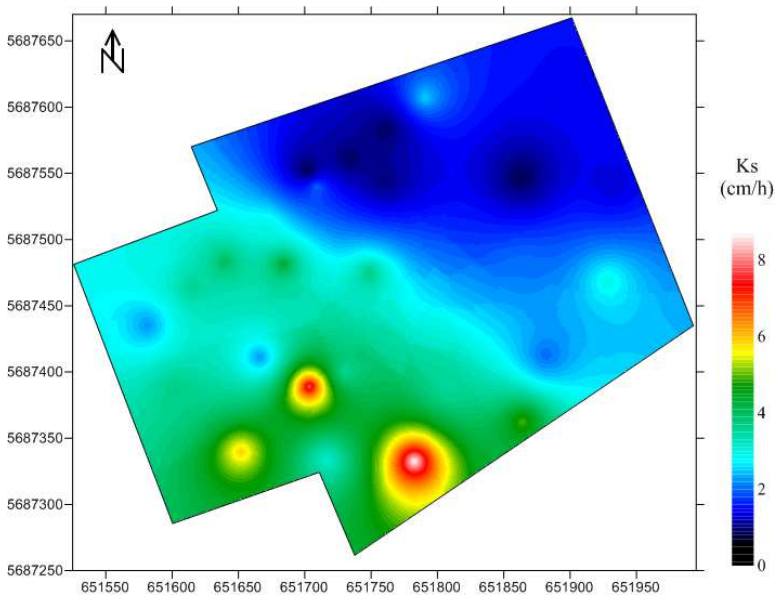

Figure 3-5. The K_s map of interpolation using inverse distance weighting (IDW). K_s is laboratory saturated hydraulic conductivity.

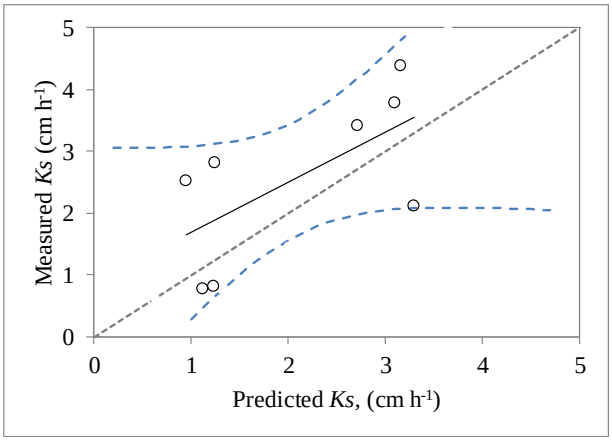

Figure 3-6. Scatterplot of measured vs. predicted (IDW) K_s of eight validation points. The dashed lines show the 95% confidence limits on the prediction. K_s is laboratory saturated hydraulic conductivity, IDW is inverse distance weighing.

3.4 Conclusion

We found good correlations of soil saturated hydraulic conductivity, and some selected physical properties to the ECa data derived by DUALEM-21S sensor measuring over 0-50 cm and 0-100 cm. A simple linear regression approach using high spatial resolution EMI-ECa data, was applied to predict and map K_s over the entire field. In this part of study, the semi-log empirical relation was established and validated to estimate the spatial distribution of K_s using ECa as a proxy. A detailed map of K_s was produced with satisfactory accuracy for hydrological modeling. The utilization of the semi-log empirical relation to produce the detailed map of K_s is an efficient way to predict spatial distribution of water content or water fluxes by hydrological models and to perform crop yield modeling for precision irrigation management purposes.

Chapter 4. ***The relevance of in-situ and laboratory characterization of sandy soil hydraulic properties for soil water simulations***

This chapter is based on a modified published article:

Rezaei, M., Seuntjens, P., Shahidi, R, Joris, I., Wesley Boënne., Al-Barri, B., Cornelis, W. 2016. The relevance of in-situ and laboratory characterization of sandy soil hydraulic properties for soil water simulations. Journal of Hydrology. 534: 251–265.

4.1 Introduction

Field water flow processes can be precisely delineated by using in situ and/or laboratory determined soil hydraulic conductivity functions, *K(h)* and soil water retention curve, *θ(h)*. Proper sets of soil hydraulic properties are indispensable as input for crop and hydrological models which especially use a numerical solution of the Richards' equation (Gandolfi et al., 2006; Radcliffe and Šimůnek, 2010; Wollschlager et al., 2009) to predict water dynamics in field and laboratory situations. A typical example is Hydrus (Šimůnek et al., 2013a). Therefore, comparisons of individual and combined laboratory and in-situ derived hydraulic parameters, and investigations of their spatial variability allow to find appropriate hydraulic parameter sets and enhance our knowledge about the dynamic processes of water flow in the vadose zone. They not only provide information about the uncertainty but also would be helpful in reducing it in simulating the physical processes with various hydrological and crop-based models for precision irrigation management, increasing crop yield and investigating solute and pollutant transport.

Several measurement techniques such as tension disc infiltrometer or constant/falling-head permeameter and sandbox-pressure chambers with soil cores have been developed to determine hydraulic properties in the field and the lab (Dane and Topp, 2002). The most popular methods and benchmarks for evaluating other methods are those that use undisturbed soil cores. The measurements are then carried out under more controlled conditions, and are thus reliable (Fodor et al., 2011) even though they do not necessarily represent field conditions. In that soil core one dimensional flow is imposed and as a result of sampling, preferential flow may be reduced (Jačka et al., 2014) and compaction may have occurred (Reynolds, 2008). The constant/falling head method to determine saturated hydraulic conductivity K_s is inexpensive, simple and convenient (Reynolds et al., 2000), whereas sand boxes-pressure plate methods for soil water retention determination are time consuming and labor intensive (Cornelis et al., 2001). The advantages of laboratory methods for K_s is that it is calculated using Darcy's law in which all the flow conditions are defined exactly, i.e., hydraulic head, one dimensional flow and temperature, and the effects of the entrapped air are minimized (Jačka et al., 2014).

On the other hand, the tension disc infiltrometer is a standard method to measure soil hydraulic conductivity for quasi-steady state and transient flow in the field (Baetens et al., 2009; Latorre et al., 2015; Logsdon and Jaynes, 1993; Reynolds and Elrick, 1991; Verbist et al., 2013b). It is less time consuming and inexpensive, can be easily operated with minimal disturbance of soil

and consistently provides reliable hydraulic properties values (Hu et al., 2009) especially near saturation (Perroux and White, 1988) where soil macrospores are active (Ankeny et al., 1991). Measurements using the tension disc infiltrometer represent the soil matrix (i.e., part of macropores are excluded) and air may be entrapped during the rapid saturation process, thus preventing full saturation of the soil to be obtained. Consequently, hydraulic parameters like water content and hydraulic conductivity at saturation or residual water content, might be underestimated than when using laboratory methods (Fodor et al., 2011). Also under ponding conditions, i.e., at a small positive pressure head and thus including macropores in water transmission, higher K_s values are estimated (Kutílek and Nielsen, 1994), though they are still lower than laboratory values (Reynolds et al., 2000).

Comparison of laboratory and in situ procedures showed different trends for various soil types and field conditions (Ankeny et al., 1991; Evett et al., 1999; Fodor et al., 2011; Hussen and Warrick, 1993; Ramos et al., 2006; Reynolds et al., 2000; Ventrella et al., 2005; Warrick, 1992). Reynolds et al. (2000) encountered very high differences between K_s derived from tension infiltrometer and that from the classical laboratory soil core method, and found very little correlation among the methods used. Overall, the laboratory method mostly provides higher K_s values than field methods (Dušek et al., 2009; Fodor et al., 2011; Jačka et al., 2014; Reynolds et al., 2000), although Ventrella et al. (2005) reported an opposite trend.

Ramos et al. (2006) and Schwartz and Evett (2002) found that the water retention curves obtained by numerical inversion of tension disc experiments closely matched the laboratory measured curves. In contrast, relatively poor agreements were yielded between estimated water retention curves using tension disc numerical inversion and laboratory retention data (Šimůnek et al., 1999; Ventrella et al., 2005). Recently, much research has been dedicated to inversion of tension disc data to soil hydraulic properties, comparing them or not with laboratory derived data (Latorre et al., 2015; Lazarovitch et al., 2007; Rashid et al., 2015; Ventrella et al., 2005; Verbist et al., 2013b), but most of them have not assessed the relevance of different approaches for their applications, e.g., evaluation of hydrological model performance and soil-water dynamics as regards to hydraulic parameter sets derived from different measurement methods.

Therefore, in this chapter we focus on analyzing tension infiltrometer data along the vertical direction within two soil profiles in the field and traditional laboratory-derived data to determine soil hydraulic parameters of a sandy soil. In this study, three calculation procedures

were performed to derive hydraulic parameter sets, i.e., (i) a “quasi-steady state” procedure using Wooding’s equation, (ii) a “transient” procedure using inverse modeling with Richards’ equation, both for tension infiltrometer data and (iii) Darcy’s model in combination with curve fitting using the Mualem-van Genuchten equation for the soil core data from the laboratory. The objectives of this part of study were: i) to compare the results of in situ and laboratory measurements of soil hydraulic properties; and ii) to evaluate the relevance and the influence of differently calculated/estimated hydraulic properties on hydrological model performance with the purpose of finding a proper set of hydraulic parameters to describe water movement in typical Podzol profiles with sand texture in a potato field.

4.2 Material and Methods

4.2.1 Study site and soil profiles description

The study site was located in a sandy agricultural area at the border between Belgium and The Netherlands (with central coordinates 51°18′40″ N, 05°10′04″ E), characterized by a temperate maritime climate with mild winters and cool summers. The farm is almost flat (less than 3% sloping up from NW to SE) and runoff is not considered to be important. The groundwater table fluctuated between 77 and 130 cm below the soil surface depending on the topography. Reel Sprinkler Gun irrigation (type Bauer rainstar E55, Röhren- und Pumpenwerk BAUER Ges.m.b.H., Austria) was used on a 230 m by 600 m field to improve potato growth in the sandy soil during dry periods in summer. The field was irrigated four times throughout the growing season (96 mm). Two locations were selected based on soil topography and agricultural activities, and soil-water content probes and tensiometers were installed (details in next section) for irrigation management purposes. At each location, a soil profile was excavated, analyzed and sampled to characterize soil hydraulic properties. Figure 4-1 shows the elevation map and layout of the field and the location of the soil profiles.

Figure 4-2 shows the soil profile, a typical Podzol (Zcg type, moderately drained sandy soils with a clear B horizon, according to the Belgian soil classification) or Hortic-Ortsteinic Podzol (Arenic) according to WRB (FAO, 2014) consisting of a uniform dark brown layer of sandy soil (Ap/Ah horizon, 0 to 47 cm) with elevated organic matter content, followed by a bright brown to yellowish sand including stones and gravels (Bhsm horizon, 52 to 70 cm). The deeper horizon is light gray sandy soil (C horizon, 70 to 130 cm), including more stones and gravel (max 20%), but having similar hydraulic properties as the Bhsm horizon. The interface between Ah and Bhsm horizon is a compacted and cemented black layer of ~5 cm thickness (Bs

horizon). Maximum potato root density was found at about 4 to 25 cm and decreased from 25 to 40 cm. The properties of the horizons are summarized in Table 4-1.

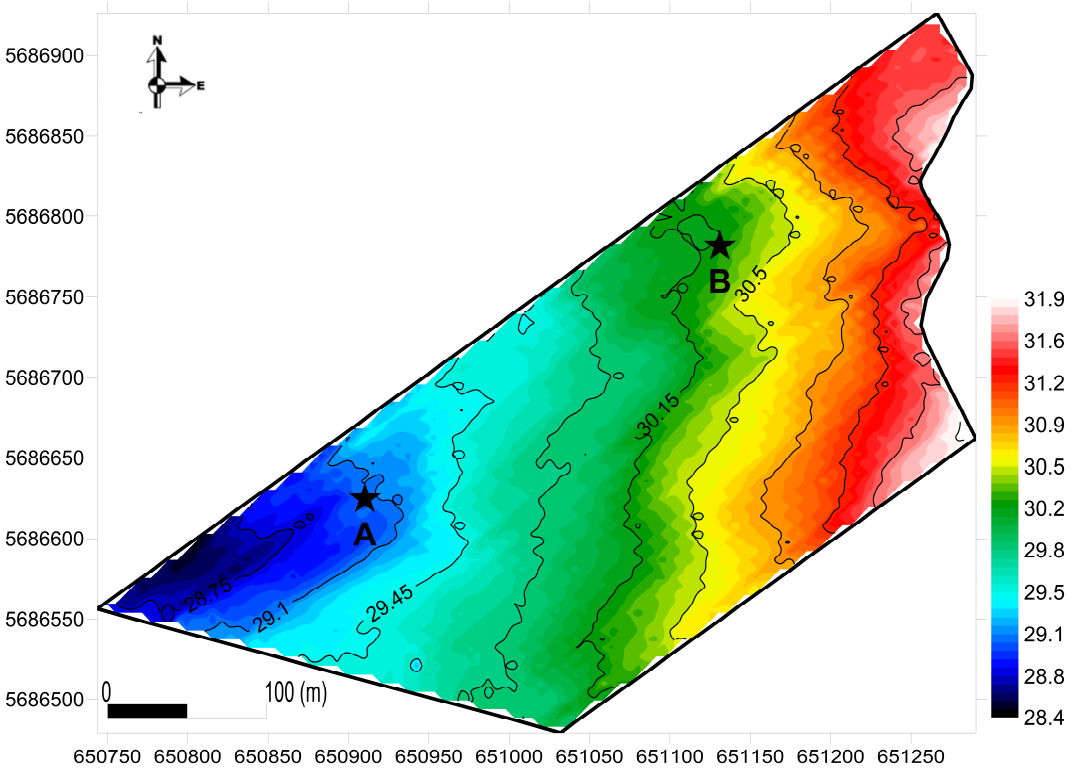

Figure 4-1. The elevation map and field layout with indication of the location of soil profiles A and B.

Table 4-1. Soil properties of two soil profiles, A and B. ρb, ϕ and OC are bulk density, soil porosity and organic carbon, respectively.

Profile	Depth	OC	Sand	Silt	Clay	ρ_b	ϕ
	cm		%			g cm^{-3}	cm^3 cm^{-3}
A	0-10	1.74	93.5	4	2.5	1.356	0.488
	20-30	1.73	93.5	4.1	2.4	1.449	0.453
	47-52	2.75	93.5	4.3	2.2	1.574	0.406
	60-70	0.23	98.2	0.3	1.6	1.677	0.367
	70-90	0.02	99	0.5	0.5	1.706	0.356
B	0-10	2.36	92.7	5.7	1.6	1.352	0.490
	20-30	2.36	92.3	5.9	1.8	1.424	0.463
	47-52	2.58	92.9	5.1	2.1	1.599	0.397
	60-70	0.06	97	2.2	0.9	1.729	0.348

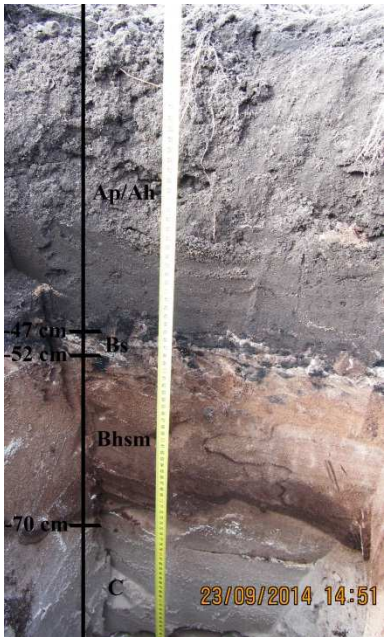

Figure 4-2. A typical Podzol soil profile of the field close to the location of the sensors.

4.2.2 Field Monitoring System

The site was equipped with a weather station (type CM10, Campbell Scientific Inc., Utah, USA) at the border of the field (Appendix Chapter 4, Figure A4-1 and 2). At the lower location A, soil-water content and water potential were recorded (from 12 Apr. until 22 Sep. 2014) using a water content profile probe (type EasyAG50, Sentek Technologies Ltd., Stepney, Australia, accuracy ±0.1%), placed vertically, that measured soil-water content at 10, 20, 30, 40 and 50 cm depths and two tensiometers (type T4e, UMS, Munich, Germany, accuracy ±0.5 kPa), placed horizontally, that measured soil water potential at 10 and 50 cm depths. The weather station and tensiometers were connected to a CR800 data logger (Campbell Scientific Inc., Utah, USA) and the water content profile probe provided the soil-water content wirelessly.

At the higher location B, only soil-water content was recorded using a Dacom soil moisture sensor (Dacom bv, Emmen, The Netherlands), placed vertically, that measured soil-water content at 10, 20, 30, 40, 50 and 60 cm depths. In addition, at each location a Diver (Mini-Diver, Eijkelkamp Agrisearch Equipment, Giesbeek, The Netherlands) was installed in a borehole 2 meters below the soil surface to measure the groundwater fluctuations at each location. Also, a rain gauge was installed at each sensor location to account exact water inlet (rain fed and irrigation), which provided the data wirelessly. All measurements were taken on an hourly basis. The amount of irrigation was derived by subtracting measurements of the rain sensor (i.e. rainfall and irrigation) from those of rain gauges of the field's weather station (i.e. only rainfall).

4.2.3 Field and lab measurements

4.2.3.1 Field measurements

As mentioned previously, at each sensor location (indicated by the star on the map in Figure 4-1), a profile was dug. During the excavation the sensors were removed (i.e., water content profile probe, tensiometer and Diver). The field measurements were carried out using tension disc infiltrometer, TI, model 2825K1 (Soil moisture Equipment Corp, Santa Barbara, CA, USA) with a diameter of 0.20 m that was attached to the Mariotte system of a Guelph permeameter at harvesting time (22 to 24 September 2014). The distance of the infiltration experiments from the water-content profile probe was about 5-50 cm.

Measurements were taken in two replications at the ridge (2 cm), the furrow (20 cm), the Bs horizon (47 cm) and Bhsm to C horizon (60 cm) for both profiles, and C horizon (80 cm) only for location A. For ridge and furrow locations where most structural dynamics were expected, any above plant material was removed carefully by shovel without altering the soil surface to preserve soil properties as much as possible. The soil surface was prepared as flat as possible by shovel and leveled without disturbing the soil structure. Additionally, a 25 cm long Time Domain Reflectometry (TDR) probe with three rods was inserted horizontally at a depth of 2.5 cm directly below the tension disc to measure the water content in a minute time interval. To avoid soil disturbance within the flow domain, firstly the TI was installed at the soil surface, and secondly a small hole was hand dug for inserting the TDR probe. The hole was far enough from the disc to avoid soil disturbance. Then TDR insertion was performed as slow as possible (Figure A4-3). In case of soil disturbance, the installation was repeated. To ensure perfect hydraulic contact between the disc membrane and soil, a fine layer of sand (approximately 2 mm thick) with much higher saturated hydraulic conductivity than the soil under study was placed and leveled as well. Reynolds (2006) found little effects of the contact layer on measured soil hydraulic conductivities. Then, no correction was required for the variable thickness of the contact sand layer at each location. Infiltration tests with four consecutive negative pressure heads of 12, 6, 3 and 0.1 cm were conducted. For each pressure head, flow rates were recorded every minute for at least 15 min or until the infiltration rate of three consecutive time intervals was constant (i.e., when steady state was reached). In addition, disturbed samples were collected before and after the infiltration experiment to determine the initial and final water contents of the soils. The initial water content was determined at a different location (max 10 cm) from where the infiltration took place to avoid disturbance of the soil; however, the final

water content was determined directly under the disc membrane immediately after finishing the last pressure head (-0.1 cm) experiment and the removal of the sand layer.

4.2.3.2 Laboratory measurements

To avoid the effect of seasonal variability, sample collection was carried out together with the field infiltration experiment. In order to minimize the effect of spatial variability, all samples were taken under the disc and/or the least possible area (0.1 m^2). Therefore, at the location of the infiltration experiment, three undisturbed soil samples (100 cm^3 Kopecky rings, of 5 cm height and 5 cm diameter, Eijkelkamp Agrisearch Equipment, Giesbeek, The Netherlands) were taken to determine both the soil saturated hydraulic conductivity, K_{ls}, and the water retention curve, SWRC, $\theta(h)$, and one disturbed sample to measure soil properties such as texture and organic matter, from the Ap to the C horizon.

As mentioned in previous chapters, the SWRC, $\theta(h)$, was determined using the sandbox method (Eijkelkamp Agrisearch Equipment, Giesbeek, The Netherlands) up to a matric head of -100 cm and the standard pressure plate apparatus (Soilmoisture Equipment, Santa Barbara CA, USA) for matric heads equal to or below -200 cm, following the procedure outlined in Cornelis et al. (2005). The K_{ls} was determined using a constant head laboratory permeameter (M1-0902e, Eijkelkamp Agrisearch Equipment, Giesbeek, The Netherlands) just after the first step of SWRC determination, i.e., after using the sandbox, in order to avoid any effect of subsequent measurements. The average hydraulic head was 2.25 cm. Bulk density was obtained by drying volumetric soil samples (100 cm^3) at 105 °C. Soil porosity, ϕ, was calculated from the bulk density and the estimated mean density of soil solid particles i.e., 2.65 Mg m^{-3} (Rühlmann et al., 2006). Particle size distribution of the mineral component was obtained using the pipette method for clay and silt fractions, and the sieving method for sand particles (Gee and Bauder, 1986). The organic matter content was determined by method of Walkley and Black (1934) .

4.2.4 Assessment of hydraulic parameters

4.2.4.1 Steady state flow - Wooding's approach of field measurements

For calculating three dimensional quasi-steady state infiltration rate under the disc infiltrometer, the nonlinear regression method of Logsdon and Jaynes (1993) was used first. This method is fast and it provides stable results from multi-tensions with nonlinear regression based on the Wooding (1968) equation, and does not give any negative values compared to

other methods. The Wooding equation for the unconfined condition of a circular disc can be written as:

$$Q(h) = \pi r^2 K(h) + 4r\lambda\, K(h) \quad (4\text{-}1)$$

where Q is the quasi-steady infiltration rate (L^3T^{-1}), K is unsaturated hydraulic conductivity (LT^{-1}), h is applied head (L), r is the radius of the disc (L) and λ is the macroscopic capillary length (L^{-1}) ($=\alpha_G^{-1}$where α_G is the slope of $K(h)$ function in semi logarithmic form) as defined by Gardner (1958). In this equation water flow is controlled by hydraulic conductivity as influenced by gravity (first term on the right in Eq. 4-1) and soil sorptivity which represents the soil's capillarity (second term on the right in Eq. 4-1). The unsaturated hydraulic can be calculated according to the exponential model of Gardner (1958):

$$K(h) = K_{fs} \exp(\alpha_G h) \quad (4\text{-}2)$$

Logsdon and Jaynes (1993) substituted Gardner's equation (2) in the derivation of Wooding's equation (1):

$$\frac{Q(h)}{\pi r^2} = K_{fs} \exp(\alpha_G h) + \frac{\left(4K_{fs} \exp(\alpha_G\, h)\right)}{\pi \alpha_G r} \quad (4\text{-}3)$$

which contains two unknowns K_{fs} and α_G. With infiltration data for two or more successive pressure heads, the unknown parameters can be calculated using a nonlinear optimization technique by minimizing the sum of square error (SSE), i.e., the squared differences between measured and predicted values of quasi-steady state water fluxes ($q=Q/\pi r^2$):

$$SSE = \sum (q_{measured} - q_{predicted})^2 \quad (4\text{-}4)$$

The hydraulic conductivities and α_G derived using this approach were compared to the inverse estimation and laboratory approaches (methods 2 and 3, see next paragraphs).

4.2.4.2 Transient flow- Inverse solution approach of field measurements

The inverse modeling approach that indirectly estimates the hydraulic properties from transient tension infiltrometer data as described by Šimůnek and van Genuchten (1996) was used. The unknown hydraulic parameters were estimated from cumulative infiltration data with a quasi-three dimensional numerical model in non-swelling, homogeneous, isotropic sandy soil by solving a modified Richards' equation for axisymmetric Darcian flow (Warrick, 1992):

$$\frac{\partial \theta}{\partial t} = \frac{\partial}{\partial z}\left[K(\theta)\left(\frac{\partial h(\theta)}{\partial z} + 1\right)\right] + \frac{1}{r}\frac{\partial}{\partial r}\left(rK(\theta)\frac{\partial h(\theta)}{\partial r}\right) \quad (4\text{-}5)$$

where θ is the volumetric water content ($L^3\ L^{-3}$), t is time (T), r is the radial and z is vertical coordinate taken positive downward (L), K is the hydraulic conductivity ($L\ T^{-1}$) and h is the pressure head (L). This equation can be solved with the following initial and boundary conditions (Šimůnek et al., 2000; Warrick, 1992):

$$\theta(r,z,t) = \theta_i(z)\ or\ h(r,z,t) = h_i(z), \quad t = 0 \quad (4\text{-}6)$$

$$h(r,z,t) = h_0(t)\ , 0 < r < r_0\ , \quad z = 0 \quad (4\text{-}7)$$

$$\frac{\partial h(r,z,t)}{\partial z} = -1\ , r > r_0, \quad z = 0 \quad (4\text{-}8)$$

$$h(r,z,t) = h_i(z), \quad r^2 + z^2 = \infty \quad (4\text{-}9)$$

where $h_0(t)$ is the inlet pressure head (or supply pressure head) at the soil surface, h_i and θ_i are initial pressure head and the initial water content, respectively. To solve the above equations, the finite element code Hydrus-2D/3D (Šimůnek et al., 2008) was applied using the van Genuchten (1980) and Mualem (1976) parametric models for soil water retention, $\theta(h)$, and the hydraulic conductivity function, $K(h)$, respectively (Eqs. 2-1 – 2-4).

Cumulative infiltration rates measured with a tension disc infiltrometer do not provide enough information to estimate more than two MVG soil hydraulic parameters (Šimůnek and van Genuchten, 1996). To obtain a unique solution and at least three unknown parameters (i.e., α, n, and K_{fs}), it is advised to combine multiple-tension cumulative infiltration data with measured values of the initial and final water contents (Šimůnek and van Genuchten, 1997).

The inverse modeling approach was based on minimizing the objective function which expresses the discrepancies between the simulated and observed values, using the Levenberg-Marquardt algorithm (Levenberg, 1944; Marquardt, 1963). The objective function (Φ) can be written as:

$$\Phi(\beta, p_M) = \sum_{j=1}^{M} v_i \sum_{i=1}^{N_j} w_{ij}\left[p_j{}^*(t_i) - p_j(t_i,\beta)\right]^2 \quad (4\text{-}10)$$

where $p_j{}^*(t_i)$ represents specific measurement at time t_i for jth measurement set, p_j (t_i, β) is the model simulation for the vector of optimized parameters β, (i.e., α, n, and Ks), M is the number of different sets of measurements, i.e., cumulative infiltration, pressure head or additional information, N_i represents the number of measurement in a particular measurement set, and v_i and w_{ij} are weights associated with a particular measurement set j or measurement i within set

j, respectively. The weighting coefficients *vj*, which used to minimize differences in weighting between different data types because of different absolute values and numbers of data involved, are given as:

$$v_i = \frac{1}{N_i \sigma_j{}^2} \tag{4-11}$$

As a result, the objective function is the average weighted squared deviation normalized by the measurement variances σ_j^2.

To optimize the objective functions, two scenarios were performed: i) using final soil-water content and cumulative infiltration data with unit weighting (w_{ij}=1, assuming that variances of the errors inside a particular measurement set are all the same and the observation errors of the measurements are unknown), and ii) using soil-water content measured by TDR in one minute intervals and cumulative infiltration data with unit weighting. The initial condition was adjusted by initial measured water content of each experiment. Initial values of θ_s and n, were taken from neural network prediction based on Rosetta software (Schaap et al., 2001) at each measurement location, while K_{fs} and α were taken from Wooding's approach, assuming the Gardner's and van Genuchten's α equivalency at near saturation condition (Rucker et al., 2005).

4.2.4.3 Classical approach of lab measurements

Three soil hydraulic parameters (θ_s, α and n) were determined according to the van Genuchten (1980) and Mualem (1976) conductivity model (MVG model). Their initial parameter values were taken from neural network prediction based on Rosetta software at each measurement location. The parameters of the water retention equation were fitted to the observed data set using RETC, version 6.02 (van Genuchten et al., 1991). The MVG model (Mualem, 1976; van Genuchten, 1980) is given in Chapter 2 (Eqs. 2-1 – 2-4). K_s was determined directly by applying Darcy's law based on measured discharges and preset hydraulic head gradients.

4.2.5 Simulation of water flow

Simulation of root water uptake and water flow, which is assumed to be in the vertical direction in the vadose zone, was carried out for growing season (from 12 Apr until 22 Sep. in 2014) using Hydrus-1D version 4.16 which solves the 1-D Richards' equation (Eq. 2-5). The simulated soil profile in the model extended to 150 cm depth and was divided into three layers: Layer 1 (0 to 47 cm), Layer 2 (47-52) and Layer 3 (52 to 150 cm). The arithmetic average of

hydraulic parameters of the corresponding depths for each three layers was calculated as input value.

To solve Eq. 2-5 (Richards' equation), the MVG soil hydraulic model (Eqs. 2-1 – 2-4) without air entry value and hysteresis was used. The initial pressure head distribution was adjusted using the measured initial pressure head of each observation node (tensiometer data). These point values were then interpolated linearly from the deepest observation node to the groundwater level (h=0, GWL). The pore connectivity parameter of the MVG model was fixed at l=0.5. The upper condition for water flow was an atmospheric boundary condition, based on rainfall and irrigation water supply, measured leaf area index (LAI) and potential evapotranspiration (ET_p) with surface runoff. LAI was measured 11 times during the growing season using ISARIA CROP SENSOR (CLAAS Agrosystems KGaA mbH & Co KG, Harsewinkel, Germany) and was provided by the farmer. ET_p was calculated from the reference evapotranspiration (ET_o) using Eq. 2-10. ET_o was calculated based on the FAO Penman-Monteith equation on an hourly basis (Allen et al., 1998) using weather station data. Crop factors and LAI were scaled to an hourly basis using linear interpolation between two adjacent moments. The Feddes model (Feddes et al., 1978) without solute stress was used for root water uptake. The default potato parameters values provided by Hydrus-1D were used (Taylor and Ashcroft, 1972).

The variable bottom boundary condition (pressure head) was imposed by setting a measured groundwater depth using the Diver water level logger (Mini-Diver, Eijkelkamp Agrisearch Equipment, Giesbeek, The Netherlands). It should be noticed that the spatial fluctuations of the groundwater table were about 10 cm (comparing two location data), which were smaller than the expected variation due to topography with more than 100 cm variation even for relatively flat areas (Figure 4-1). While temporal fluctuations reached up to 35 cm. The model was run applying two different hydraulic parameter sets as input values, i.e. laboratory and field methods. The relevance/effects of these parameter sets on soil-water content and potential predictions were evaluated for two soil profiles.

4.2.6 Statistical analysis

To evaluate and compare the hydraulic parameters derived from the field and laboratory measurements using the three methods, comparisons were performed using the least significant difference (LSD) test at $p \leq 0.05$, to look for significant differences among depths, profiles and

methods. The Pearson correlation coefficient was computed between co-located and specific depth soil hydraulic parameters derived by laboratory and field methods.

The performance of Hydrus-1D in simulating water content from the different hydraulic parameter sets was evaluated with a variety of statistics. The root-mean-square errors (RMSE), the coefficient of determination (r^2), and the Nash–Sutcliffe coefficient of model efficiency (C_e), are applied here to evaluate the difference between observed and modeled data. More information about these criteria are given in Chapter 2 and their formula are presented in Eqs. 2-15 – 2-17.

4.3 Results and Discussion

4.3.1 Hydraulic parameters from lab measurements

As shown in Table 4-1, bulk density increased with depth. The very high bulk density at deeper depth (≥60 cm) is primarily due to the very high sand content, whereas the high bulk density at 47-52 cm depth is due to soil compaction from the use of heavy machinery and cementation due to higher organic carbon content (OC) (Table 4-1), humus and iron accumulations (typical for Podzol) compared to the upper layers (Seuntjens et al., 2001). Note that the higher value of OC at topsoil of profile B (upland) is due to compost application at that location. Table 4-2 presents the hydraulic properties of two soil profiles at location A and B, measured at the laboratory. The mean values of θ_s and α_{vG} decrease with increasing depth in both profiles. The higher topsoil values may be due to soil tillage, higher clay content and lower bulk density (Table 4-1). The values of n and K_{ls} increase with increasing depth as is expected because of increasing sand content with depth. The exception is the Bs horizon (47-52 cm) which shows lower values as compared to upper and deeper depths for reasons as outlined above. The highest sand content, larger fragments of particles such as stones and gravel, lowest clay content, and humus and Fe accumulation (low OC content) in the subsoil (60-80 cm) led to highest K_{ls} values for both profiles. Within two profiles, considerable variations were observed for K_{ls} as compared to other hydraulic parameters. Comparing results showed that profile B (upland) had lower n and K_{ls} than profile A (lowland) particularly at subsoil layers (Table 4-2). Results show almost no differences in soil water retention data of the two profiles in the topsoil, but most differences were observed in the compacted and deeper layers of the profiles (see Figure 4-6). The largest changes in K_{ls} were observed at depth 47 cm compared to upper and deeper layers for both profiles. Comparing hydraulic properties of the two profiles showed significant

differences of K_{ls} values, whereas no significant differences were observed for the other MVG hydraulic parameters.

Table 4-2. Average values of soil hydraulic parameters of two soil profiles, A and B, measured at the laboratory. θ_r, θ_s are residual and saturated water content, respectively; α_{vG} and n are shape parameters for the van Genuchten-Mualem equation. K_{ls} denotes the measured saturated hydraulic conductivity in the laboratory. Samples at 2 cm were taken at the ridge, whereas those at 20 cm depths were from the furrow.

Profile	Depth	θ_r^*	θ_s	α_{vG}	n	K_{ls}
	cm		$cm^3\ cm^{-3}$	cm^{-1}		$cm\ h^{-1}$
A	2	0.053^{ab}	0.525^{a}	0.057^{a}	1.567^{c}	0.881^{c}
	20	0.055^{ab}	0.509^{a}	0.050^{a}	1.584^{c}	10.01^{c}
	47	0.075^{a}	0.403^{b}	0.040^{ab}	1.449^{c}	2.840^{c}
	60	0.03^{b}	0.35^{b}	0.014^{c}	2.213^{b}	34.046^{b}
	80	0.003^{bc}	$0.38.3^{b}$	0.020^{b}	2.885^{a}	60.423^{a}
B	2	0.069^{a}	0.545^{a}	0.072^{a}	1.456^{ab}	1.483^{b}
	20	0.072^{a}	0.530^{a}	0.059^{a}	1.508^{ab}	3.365^{ab}
	47	0.084^{a}	0.367^{b}	0.0245^{b}	1.444^{b}	0.761^{b}
	60	0.013^{b}	0.361^{b}	0.0292^{b}	1.879^{a}	5.752^{a}

* Not estimated (measured at 15000 cm). Means followed by the same letter do not differ across depths (in each profile) by the LSD test at the level of 5% probability.

Overall, statistics show that three horizons with different soil hydraulic properties could be identified, i.e. a top layer (0-47 cm), a compacted/cemented layer (47-52 cm) and a sub layer (52-90 cm) (Table 4-2). Great differences in K_{ls} of various depths were observed for two profiles (-0.2 to 0.8 order of magnitude). K_{ls} of 20 cm depth was approximately five times higher than K_{ls} of the compacted layer (at 47 cm depth) of both profiles. While K_{ls} of compacted layer (47-52 cm) was 12 and 7.5 times lower than that at 60 cm depth for profiles A and B, respectively. These results indicate spatial variability of hydraulic properties in horizontal and vertical dimensions. Indeed, similar to findings of Schwen et al. (2014), we found that the pedogenical horizon boundaries correlated with soil hydraulic properties. However, the horizons may have functional contribution on water flow properties (Finke and Bosma, 1993; Finke et al., 1992). Therefore, we could define three distinct layers for hydrological modeling in the next steps (layer 1: 0-47, layer 2: 47-52 and layer 3: 52-150 cm).

4.3.2 Hydraulic parameters from field measurements

4.3.2.1 Field infiltration experiment

The measured cumulative infiltration is shown in Figure 4-3 as a function of time for each replication and depth of profile A and B. The breaks and slopes in the cumulative infiltration curve are caused by momentary disruption when resupplying the infiltrometer with water and by adjusting the consecutive supply pressure heads (h=-12, -6, -3 and -0.1 cm). Overall, at top

soil (2 cm depth) approximately 0.37 - 0.78 cm water infiltrated in 37 - 45 min at profile A, and 0.38 – 1.03 cm water infiltrated in 38-50 min at profile B. The highest infiltration rates were observed at the highest depths of profile A (1.16 and 3.23 cm in 30 and 40 min respectively) and profile B (2.9 and 3.14 cm in 35 and 36 min respectively). As expected, the lowest infiltration rate was observed within the compacted layer (47 cm depth), with 0.11 cm in 40 min at profile A and 0.17 cm in 38 min at profile B on average.

The infiltration data simulated in the inverse modeling procedure with Hydrus-2D/3D in combination with final water content at the end of the experiments matched well the observed ones (Figure 4-3) enabling to obtain an effective parameter set. In all cases, the model reached convergence on the solution and resulted in low root mean square and mass balance errors values (results not shown). It should be noted that the objective function that incorporated both cumulative infiltration and the TDR-derived soil-water contents (rather than using only final water content as above) performed poorly, and the model did not convergence to a solution in several experiments (more than 60%); therefore, results are not shown and their discussion is beyond the aim of this study.

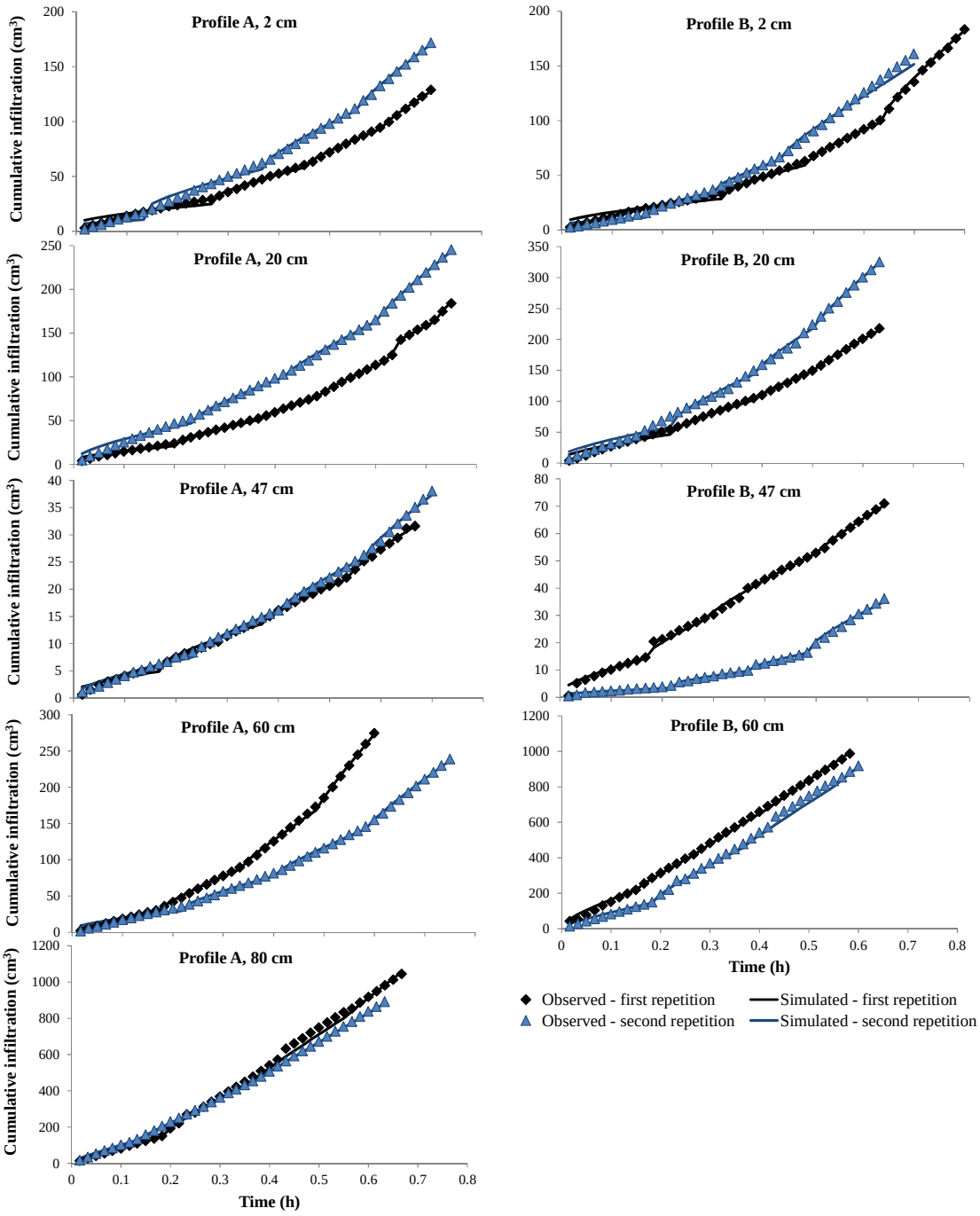

Figure 4-3. Observed cumulative infiltration in the field and corresponding fitted values using Hydrus-2/3D for two replications at different depths of profiles A and B, and at pressure heads of 12, 6, 3 and 0.1 cm.

4.3.2.2 Wooding's solution and inverse optimization

Table 4-3and 4-4 show the average value of initial and optimized hydraulic parameters for tension infiltrometer experiments at two profile locations (A and B) and different depths. As mentioned earlier, the Logsdon and Jaynes (1993) approach was applied to determine the unsaturated and saturated hydraulic conductivity and Gardner's α_G. The values of this approach

were used as initial values in inverse optimization (Table 4-3 and 4-4), allowing also to test the hypothesis about the equivalency of Gardner's α_G and van Genuchten's α_{vG} at near saturation condition, i.e. h≥-20 cm (Rucker et al., 2005). At profile A, the optimized parameter values for K_{fs} were mostly close to or slightly lower than the initial values from Logsdon and Jaynes (1993) approach (Wooding's solution). The largest difference for α and K_{fs} were observed at 47 cm and 2 cm depths, respectively. On the contrary, optimized n values were almost half the initial values for the middle depths, while for the highest and deepest layers they were slightly lower and higher, respectively (Table 4-3).

Table 4-3. Average of initial and optimized values of hydraulic parameters of profile A. θ_i and θ_f are initial and final water content, respectively; the initial value of α and K_{fs} were derived from Wooding's solution, and θ_s and n initial values were estimated from neural network prediction of Hydrus-2D/3D.

Depth	Initial value						Optimized value			
	θ_i	θ_f	θ_s	α_G	n	K_{fs}	θ_s	α_{vG}	n	K_{fs}
cm	$cm^3\,cm^{-3}$		$cm^3\,cm^{-3}$	cm^{-1}		$cm\,h^{-1}$	cm^3cm^{-3}	cm^{-1}		$cm\,h^{-1}$
2	0.130	0.230	0.431	0.102^{a}	2.955	0.559^{bc}	0.219^{a}	0.101^{a}	2.313^{b}	0.281^{bc}
20	0.134	0.237	0.403	0.087^{ab}	3.181	0.546^{bc}	0.225^{a}	0.064^{abc}	1.714^{c}	0.543^{abc}
47	0.181	0.239	0.364	0.124^{a}	3.222	0.101^{c}	0.203^{a}	0.030^{c}	1.352^{c}	0.119^{c}
60	0.075	0.179	0.332	0.123^{a}	3.804	1.194^{ab}	0.164^{a}	0.080^{ab}	1.791^{bc}	1.165^{ab}
80	0.181	0.238	0.323	0.056^{b}	3.978	1.681^{a}	0.232^{a}	0.045^{bc}	4.485^{a}	1.326^{a}

Means followed by the same letter don't differ across depths by the LSD test at the level of 5% probability.

The optimized values for θ_s were completely different from the initial values predicted from the neural network build in in Hydrus-2D/3D (Rosetta Lite v. 1.1, Schaap et al. (1998)) or laboratory θ_s and were close or slightly lower than the final water content at the end of the infiltration experiments (h=-0.1 cm), i.e. θ_f (Table 4-3 and 4-4). However, laboratory measured θ_s and predicted θ_s from the neural network are in good agreement with soil porosity (Table 4-1 and 4-2). After the optimization process, three distinct layers were identified based on hydraulic parameter variations which correlated with pedogenic horizons (similar to laboratory results as discussed in 4.4.1.). The compacted layer (47-52 cm) was significantly different in n, α and K_{fs} compared with deeper depths (60 and 80 cm) and upper depth (2 cm). No significant differences of n, α and K_{fs} between 20 and 47 cm depths were detected. Similar results are observed for profile B. The only difference is that the optimized values for K_{fs} were slightly lower at upper depths (2 and 20 cm) and were slightly higher at deeper depths (47 and 60 cm).

Table 4-4. Average of initial and optimized values of hydraulic parameters of profile B. θ_i and θ_f are initial and final water content, respectively; the initial value of α and K_{fs} were derived from Wooding's solution, and θ_s and n initial values were estimated from neural network prediction of Hydrus-2D/3D.

Depth	Initial value						Optimized value			
	θ_i	θ_f	θ_s	α_G	n	K_{fs}	θ_s	α_{vG}	n	K_{fs}
cm	$cm^3\ cm^{-3}$		$cm^3\ cm^{-3}$	cm^{-1}		$cm\ h^{-1}$	$cm^3\ cm^{-3}$	cm^{-1}		$cm\ h^{-1}$
2	0.158	0.308	0.429	0.152^{a}	2.859	0.713^{a}	0.278^{a}	0.103^{a}	1.634^{bc}	0.611^{b}
20	0.187	0.345	0.408	0.089^{ab}	3.055	0.836^{a}	0.335^{a}	0.061^{b}	2.032^{b}	0.536^{b}
47	0.244	0.285	0.356	0.056^{b}	3.113	0.130^{b}	0.270^{a}	0.046^{b}	1.422^{c}	0.175^{b}
60	0.111	0.201	0.319	0.078^{b}	3.594	0.902^{a}	0.196^{b}	0.036^{b}	3.430^{a}	1.180^{a}

Means followed by the same letter don't differ across depths by the LSD test at the level of 5% probability.

Results indicate no significant differences of θ_r, n, α and K_{fs} values of profiles A and B, whereas significant differences can be observed for θ_s values. Overall, α and K_{fs} values of Wooding's equation were 1.67 and 1.23 times larger than their optimized values using inverse solution, respectively. This result indicates that α_G from using the analytical solution of Wooding's solution may not be equivalent to van Genuchten's α_{vG}, at least for sandy soil. We found Gardner's α_G to be related to van Genuchten's parameters α_{vG} and n as $\alpha_G \approx \alpha_{vG}\ n$, while Ghezzehei et al. (2007) found their relation to be $\alpha_G \approx 1.3\ \alpha_{vG}\ n$ for a broad range of porous media. However, the close correspondence of initial and final estimates of hydraulic parameters (especially K_{fs}) confirms the accuracy of Logsdon and Jaynes' solution of Wooding's equation in sandy soil such as our study field.

4.3.3 Hydraulic conductivity curves

Figure 4-4 shows the average hydraulic conductivity curves obtained by inverse optimization using Hydrus-2/3D and Wooding's solution using the Logsdon and Jaynes (1993) approach from tension disc infiltration data for each depth of profile A and B. Results indicate that the hydraulic conductivity values derived with analytical and numerical solutions deviate. This deviation is most pronounced at upper layers (2 and 20 cm depths) for both profiles (Figure 4-4). This could be due to the loose structure of top layers caused by tillage. Unsaturated hydraulic conductivities obtained from numerical inversion were lower than those from Logsdon and Jaynes' solution of Wooding's equation. This has also been observed by Rashid et al. (2015), because complete steady state conditions were not achieved. In this case, Wooding's solution overestimates the soil hydraulic conductivity (Šimůnek et al., 1999). On the contrary, inverse solution may underestimate soil hydraulic conductivity under incomplete steady state conditions (Table 4-2, 4-3 and 4-4). However, as discussed earlier, both methods

(Wooding and inverse approaches) gave almost similar saturated hydraulic conductivity values and this confirms the usability of inverse optimization using initial values of Wooding's solution in the modeling process.

There were significant differences ($p \leq 0.05$) of K_s values for laboratory and field (optimization and Wooding approaches) measurements between the two profiles and within layers. The graphical comparison of K_s values (q-q plots in Figure 4-5 (left)) suggest differences of laboratory and field methods with similar shapes of measured distributions. Similar to Jačka et al. (2014) results, distinctly lower K_s values were measured using field method. The laboratory measurements yielded much higher values than the field method (two to thirty times from top to subsoil layers). The laboratory saturated hydraulic conductivities were almost two times higher than those derived from the field measurements for 2 cm depth in both profiles, whereas they were 4-6 and 18-30 times higher for profiles B and A, respectively, from top to subsoil layers (Table 4-2, 4-3 and 4-4).

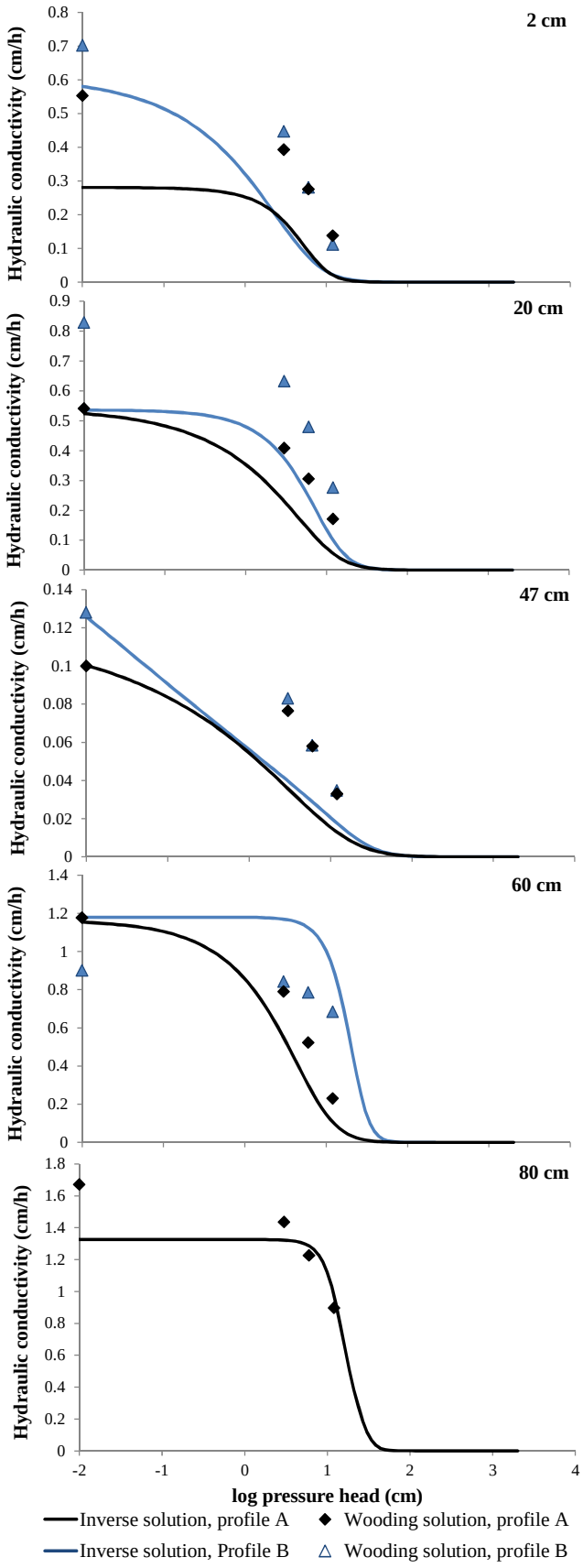

Figure 4-4. The average hydraulic conductivity curves obtained by inverse optimization using Hydrus-2/3D and wooding's solution using Logsdon and Jaynes (1993) approach from tension disc infiltration data at different depths of profiles A and B.

This might not be surprising since K_s is the most difficult parameter to accurately determine in view of tempo-spatial variability and use of small rings (Ramos et al., 2006). Indeed, K_s measured in the laboratory often results in higher values than when measuring it under field conditions, since in that latter case because soil is not fully saturated (even if a positive pressure head on the soil surface is applied and macropores are included). By the way, the tension infiltration experiments never resulted in complete saturation (Šimůnek and van Genuchten, 1996).

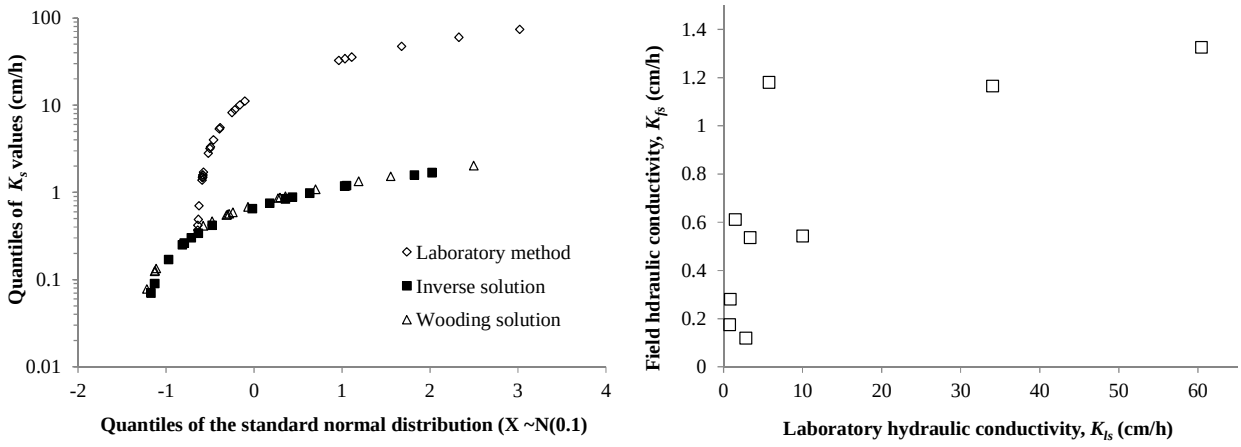

Figure 4-5. The graphical comparison of K_s values of different methods (left), the scatter plot of co-located field K_{fs} values versus laboratory K_{ls} (right).

It has been reported that the ratio of K_s with full saturation to field K_s was equal to 2, and this was attributed to entrapped air (Gupta et al., 1993; Reynolds and Elrick, 1985a). Jačka et al. (2014) found a similar ratio for Podzols. Indeed, estimation of K_s using tension infiltrometer is an indirect procedure and this estimation represents the soil matrix only. On the other hand, because laboratory samples represent a small sampled volume, a large number of replicates is often needed to derive a representative parameter estimation. Lower K_{fs} than K_{ls} values were also reported by Reynolds et al. (2000), who attributed this due to restricted flow through cracks and other preferential flow zones under the disc, thus excluding macropores and only considering matrix flow. They also stressed that this underestimation was not resulting from three-dimensional vs. one-dimensional vertical flow for sandy soil. Higher laboratory K_{ls} values could on the other hand be explained by the impact of elimination of entrapped air. Anyhow, surprisingly a significant correlation was found between K_s values derived from laboratory and field measurements (r = 0.75) (Table 4-5). The relation between pairwise K_s values of both methods presented in Figure 4-5 (right). This confirms that one dimensional flow in the laboratory may be equivalent/correspond to three dimensional flow in the disc

method in the sandy structureless soil without distinct anisotropy of this study. In their study on sandy soils, Reynolds et al. (2000) did not find any significant correlation between lab-determined K_s and that from tension infiltration measurements in the field.

Table 4-5. Pearson correlation coefficient between the hydraulic properties of laboratory measurements and field optimization approach. K_s is saturated hydraulic conductivity; θ_s is saturated water content; α and n are shape parameters for the van Genuchten-Mualem equation.

		Field optimization approach			
		θ_s	α	n	K_s
Laboratory measurement	θ_s	0.59*	0.63*	-0.36	-0.47
	α	0.57	0.55	-0.36	-0.49
	n	-037	-0.18	0.81**	0.84**
	K_s	-0.32	-0.15	0.68**	0.75**

**and * marked correlation significant at $P \leq 0.01$ and $P \leq 0.05$ level respectively.

4.3.4 Water retention curves

The water retention curves estimated from parameter optimization of infiltration data and from the van Genuchten curve fitted to the laboratory data are depicted in Figure 4-6. Statistical analysis showed significant differences of MVG parameters θ_s, n and α_{vG} values between laboratory and field measurements, with parameters derived from both methods being positively correlated (Table 4-5). There was a significant correlation between the slope of the water retention curves, represented by n, estimated from parameter optimization of infiltration data and from the van Genuchten curve fitted to the laboratory data (r = 0.81) (Figure 4-6 and Table 4-5).

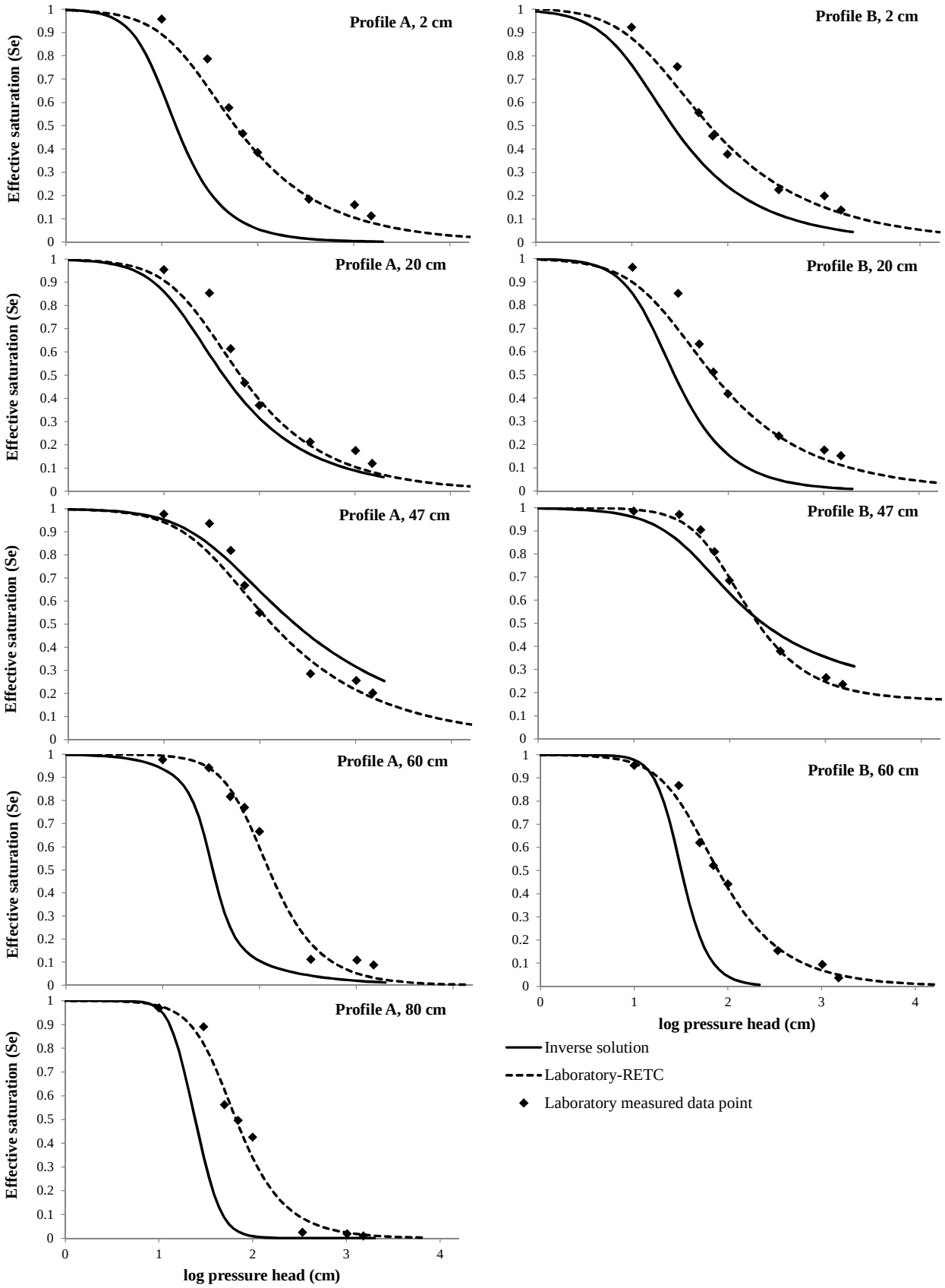

Figure 4-6. The water retention curves estimated from parameter optimization of infiltration data and the RETC curve fitted to the laboratory data at different depths of profiles A and B.

Overall, the retention curves estimated from infiltration measurements were not in good agreement with those estimated from laboratory data. As discussed earlier, results suggest higher saturated water content up to 48% for profile B (upland) as compared to profile A (lowland) (Table 4-2– 4-4). It is definitely related to higher organic carbon observed in profile B (Table 4-1). The saturated water content θ_s estimated from infiltration measurements was close to the final water content θ_f, and θ_f was significantly lower than the laboratory saturated water content (Table 4-2 and 4-3). The underestimation of saturated water content results from the matrix not being fully saturated (the last applied pressure is -0.1 cm and thus not positive) and the tension infiltrometer limitations which are addressed in introduction section. Similar results were reported by Verbist et al. (2009b), Schwartz and Evett (2003), de Vos et al. (1999) and Šimůnek et al. (1998). Šimůnek et al. (1998) reported highly underestimated retention data from an inverse solution compared to laboratory measurements, while a good fit to cumulative infiltration was obtained. They optimized θ_s with a value ~46% less than laboratory measured θ_s. However, a unit weighting coefficient (i.e. $w_{ij} = 1$) was used in the objective function for θ_f (at h=-0.1 cm, i.e. near field effective saturation) and infiltration rates, indicating the high influence of θ_f on water retention curve estimation. Indeed, θ_f was not in agreement with total porosity or laboratory θ_s. Verbist et al. (2009b), Schwartz and Evett (2003) and de Vos et al. (1999) explained the discrepancy by air entrapment during wetting front movement, the presence of flow irregularities, and deviations from equilibrium flow theory (such as gradually increasing water contents even when the infiltration rate and the pressure head reach quasi-steady state). This contrasts with observations of Ramos et al. (2006), who found estimated θ_s being very close to θ_f and laboratory θ_s (using four consecutive supply pressure heads of -15, -6, -3 and 0). Additionally, the deviation of water retention curves estimated from infiltrometer measurements and those from laboratory measurements could be explained by the hysteresis phenomenon. Hysteresis could be present in the retention curves because the infiltration and laboratory experiment represented wetting and drying processes, respectively.

4.3.5 Relevance of hydraulic parameter set on model performance

The Hydrus-1D model was run using the field and laboratory expriments' parameter sets discussed in the previous sections. As discussed, hydraulic properties variations were found in both analyzed soil profiles. Moreover, results suggested three distinct layers (0-47, 47-52 and 52-150 cm depths) based on field observation (pedogenic layers) and experimental results. The performance results (with the different parameters values) under similar upper (rainfall and water supply, ET_o, LAI) and different lower boundary conditions (groundwater depth

variations), show that the model performs almost similarly in soil-water content predictions (with some differences in volumetric water content of on average 5%) for both parameters sets at all observation depths (Figure 4-7).

Comparing the simulation results indicates that the model over and under predicted soil-water content using laboratory and field experiments data sets, respectively, for both profiles at 10 and 20 cm nodes (Figure 4-7). Different parameter sets of laboratory and field experiments resulted in under predicted soil-water content at 30 and 40 cm nodes and over predicted at 50 cm node of profile A (Figure 4-7). In profile B, soil-water content simulations based on the laboratory data set were closer to the observations at 30, 40 and 60 cm nodes compared to those from the field data set (Figure 4-7). The underestimation of hydraulic parameters, especially θ_r, using field methods (inverse modeling approach) could be a possible reason for the under prediction of soil-water content. In addition, due to temporal variation of soil hydraulic properties, e.g. K_s, their value can change during a growing season (Alletto and Coquet, 2009; Bamberg et al., 2011). However, our parameter sets were measured only once at harvesting. As we have tried to reduce the distance between sensor location, and infiltration measurement and sampling (measurement not exactly performed in the same location as sensors are installed ~ 5-50 cm variation), there is also local spatial variability of the soil hydraulic properties. Indeed soil tempo-spatial variability of K_s (even at a pedon scale) caused by local heterogeneity and small sample volume (for both, laboratory and field methods) may be very high (Fodor et al., 2011; Jačka et al., 2014; Lauren et al., 1988). This local spatial variability and time dependence of hydraulic properties during a season could increase the mismatch between observed and simulated soil-water content. To eliminate the effect of local spatial heterogeneity, larger number of samples, especially for K_s estimation, would be needed.

The performance results of the different parameter sets of laboratory and field approaches according to the performance criteria and different boundary conditions are presented in Table 4-6, for both soil-water content and pressure head. Obviously, results indicate that different initial parameter sets influence the simulated soil-water potential and soil-water content differently.

The field experiment data set resulted in lower RSME and higher C_e and r^2 values as compared to that from the laboratory data set at nodes 10 cm for soil-water content and soil-water potential (Table 4-6). Moreover, according to the C_e and RMSE criteria (in Table 4-6, profile A, Node 20cm), the laboratory method yielded slightly better results. However, lower RSME

and higher C_e and r^2 values were achieved using the laboratory data set at 30 to 60 cm nodes for soil-water content, whereas, soil-water potential was predicted less well, especially for the 50 cm node in profile A (Table 4-6).

Table 4-6. Calculated performance criteria describing the correspondence between measured and simulated soil-water content and soil water potential for field and laboratory measured data set at different depths of profiles A and B.

Node (cm)	Profile											
	A						B					
	Field			Lab			Field			Lab		
	RMSE †	**C_e †**	**r^2 †**	**RMSE †**	**C_e †**	**r^2 †**	**RMSE †**	**C_e †**	**r^2 †**	**RMSE †**	**C_e †**	**r^2 †**
water content												
10	0.044	0.11	0.42	0.063	-0.85	0.44	0.052	-3.0	0.38	0.056	-3.55	0.31
20	0.053	-1.06	0.29	0.050	-0.78	0.20	0.046	-3.6	0.26	0.054	-5.33	0.09
30	0.072	-2.87	0.37	0.034	0.10	0.33	0.055	-19.3	0.40	0.037	-7.99	0.17
40	0.070	-4.58	0.27	0.043	-1.13	0.42	0.043	-25.4	0.37	0.024	-7.29	0.49
50	0.051	-3.64	0.39	0.045	-2.65	0.45	0.101	-391.2	0.29	0.062	-144.8	0.55
60							0.156	-121.6	0.38	0.122	-73.1	0.30
water potential												
10	217.7	-0.35	0.16	197.1	-0.10	0.01						
50	99.0	0.05	0.30	156.4	-1.38	0.19						

†RMSE, C_e and r^2 are the root-mean-square deviation (cm and cm^3cm^{-3}), the Nash–Sutcliffe coefficient of efficiency and the coefficient of determination.

Field methods are usually considered more realistic than laboratory methods because of the larger volume of soil involved (as compared with the small size of soil cores, soil disturbance during sampling and short circuit flow through macropores or along core wall in lab methods) and because of continuity in the soil profile versus depth (Ramos et al., 2006). However, estimation of parameters is rather indirect and is based on many assumptions. Indeed, the sampled volume, the flow field and the boundary conditions are not known. In this method, quasi-steady flow is usually reached during a relatively short time of measurement at each small negative pressure head rather than true steady state (part of pores and macropores are excluded) (Fodor et al., 2011). But, the differences in hydraulic properties found in our study do not indicate whether laboratory or field experiments data sets are most successful to predict soil water fluctuations perfectly in a whole soil profile.

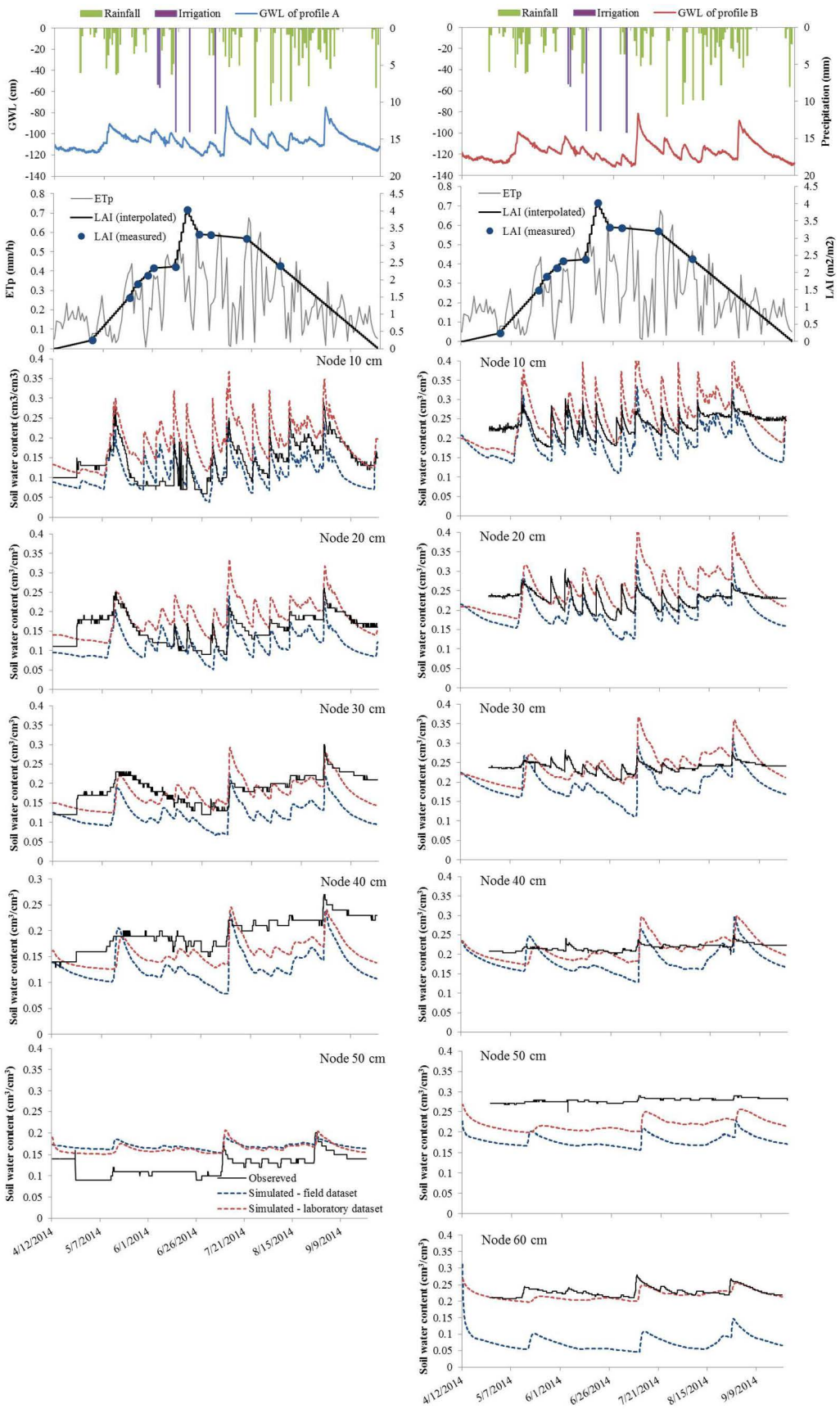

Figure 4-7. Observed and simulated time series of soil-water content with laboratory and field experiments hydraulic parameters sets for profiles A (left) and B (right). GWL is groundwater level (cm), ETp and LAI are potential evapotranspiration and leaf area index respectively.

It should be noted that the model convergences on the solution were slightly faster using the laboratory dataset than when using the field experiment dataset. The presented simulations are based on an input dataset that was not optimized against observed soil-water content or potential values. Calibrating the model using those data, would improve the model performance substantially (see Chapter 2).

4.4 Conclusions

In this chapter, we compared soil hydraulic properties of typical laboratory measurements and field tension infiltration experiments using Wooding's analytical solution and inverse optimization in two soil profiles. Results indicated spatial variability of hydraulic properties in horizontal and vertical dimension. Inverse optimization resulted in excellent matches between observed and fitted infiltration rates in combination with soil-water content at the end of the experiment using Hydrus-2D/3D and resulted in close correspondence of α and K_{fs} with those from Logsdon and Jaynes (1993) solution of Wooding's equation in sandy soil such as our study field. We found the Gardner parameter α_G to be related to the optimized van Genuchten parameters α_{vG} and n as $\alpha_G \approx \alpha_{vG}\, n$.

Laboratory tests yielded 2–30 times higher K_s values from top to subsoil layers than those derived when using field infiltration measurements. Anyhow, significant correlation was found between K_s values from laboratory and field measurements (r = 0.75). We found significant differences in MVG parameters θ_s, n and α values between laboratory and field measurements, with positive correlations being observed between laboratory and field MVG parameters ($r \geq 0.55$). Overall, the estimated retention curves of the inverse solution were not in good agreement with those fitted to laboratory data.

The relevance of the difference in laboratory and field hydraulic parameter sets was evaluated using the hydrological model Hydrus-1D. Results indicated a better simulation performance when using laboratory data set from middle to deeper depths. In the two soil profiles under study, field experiment parameter sets, which were achieved fast and simple (less time consuming and labor intensive), resulted in slightly better soil-water content simulation performance in the topsoil where the plant roots are concentrated, and soil-water potential in the subsoil. Generally, in view of precision agriculture, field measurements and inverse optimization approaches are preferred to determine soil hydraulic properties. But based on the simulation results of the study, it is not possible to judge whether laboratory or field methods

should be preferred. The under estimation of hydraulic parameters especially θ_r using the inverse modeling approach, temporal dynamics and spatial variability of soil hydraulic properties (even at a pedon scale) caused by local heterogeneity and small sample volume (for both, laboratory and field methods) could be possible reasons for poor predictions of soil-water content. However, the reasons behind the deviations should be further unraveled. In Chapter 2 we found that model output, i.e., changes in soil-water content, was mainly affected by the soil saturated hydraulic conductivity K_s and the Mualem-van Genuchten retention curve shape parameters n and α in a field experiment in an adjacent field. On the other hand, results also suggested that to obtain an effective parameter set, not only parameter optimization over long time such as a growing season in combination with independent soil-water content and soil-water potential data is necessary but also a deeper knowledge of the effect of temporal and spatial changes in hydraulic properties is needed to achieve excellent agreement between measured and simulated values. Therefore, further research is required to test the optimization processes.

Chapter 5. ***Quasi 3D modeling of vadose zone soil-water flow for optimizing irrigation strategies: challenges, uncertainties and efficiencies***

5.1 Introduction

Soils are intrinsically heterogeneous, and some heterogeneities, such as those of hydraulic properties control the ability of soil to store and conduct water at the field scale. Additionally, spatial variation of bottom boundary conditions, i.e., groundwater level (GWL), and topography considerably affect soil-water content variability, water flow and root water uptake at the field scale. Efficient techniques to characterize soil physical variability remain the object of scientific pursuit (Teixeira et al., 2014). Moreover, irrigation management strategies aiming at heterogeneous distribution of water under different field conditions and sustainably optimizing soil water conditions on large fields with spatial soil heterogeneity, groundwater and topography variability are needed effectively. However, modern technologies such as those using automated soil probe sensors and tensiometers, can quantify flow processes and soil-water status but only in a limited number of sites, mostly because of labor and cost requirements (Bastiaanssen et al., 2004). As an alternative, advanced numerical modeling for simulating hydrological processes through the vadose zone and understanding the interaction between soil, vegetation, atmospheric forcing and groundwater (Zhu et al., 2012) can be carried out to control soil water status and irrigation in precision agriculture.

Due to the complexity of flow systems, a variety of conceptual simplifications have been made to flow models (Kuznetsov et al., 2012). Such simplifications include e.g. the assumption of water transport in the unsaturated zone as a one-dimensional phenomenon, by considering i) lateral flow and transport as not significant (Sherlock et al., 2002; Tian et al., 2012) unless the capillary fringe is involved (Abit et al., 2008); ii) a simple representation of the bottom boundary condition using a constant or unit-gradient (Carrera-Hernández et al., 2012) or perched saturated layers (Twarakavi et al., 2009); iii) effective homogeneity within and between soil layers (Niswonger and Prudic, 2009) and isotropy of hydraulic properties; iv) the porous matrix as rigid and water density not dependent on solute concentration and temperature (Kuznetsov et al., 2012); and vi) unlike small-scale experiments, similar micro-climate for initial and upper boundary for different parts of the field or region.

In such cases as addressed above, evaluation of the uncertainty and/or sensitivity of the models by performing multiple simulations at different scales or resolutions, investigation of the cost effectiveness of simulation times (pre and post processing), and application of an approach to optimize irrigation management are the challenging issues. However, outputs of field scale water flow simulations depend primarily on uncertainties in model structure, in model input

parameters, in geometry of heterogeneous profiles (layer thicknesses) and in upper and bottom boundary conditions. Recently, a number of studies evaluated the uncertainties of input boundary conditions, profile geometry and input parameter using different methods and algorithms such as the Bayesian methods, Monte Carlo, Fuzzy set theory and an ensemble Kalman filter (Carrera-Hernández et al., 2012; Li et al., 2015; Verbist et al., 2012; Verma et al., 2009; Vrugt et al., 2008; Wöhling and Vrugt, 2008) mostly at a plot scale. Beside these efforts, the challenges still remain between the field scale modeling approaches and practical water irrigation strategies.

From a field to a regional water management perspective, the most important challenge in numerical modeling is to fully model the water flow (unsaturated and saturated flows from the soil surface to groundwater) in a spatially variable context. In addition, generalizing field scale water application based on the results of modeling approach at the plot scale (1D) (i.e., only one spot), is subjected to significant uncertainty. During past decades, a bulk of efforts has been made to develop numerical models, i.e., fully three-dimensional (3D) codes (Arnold et al., 1993; Saxton et al., 1974; Šimůnek et al., 2006b; Therrien et al., 2009; van Dam et al., 1997) and new approaches such as coupling/integrating existing coded modeling concepts (2D or quasi 3D modeling) to simulate water flows in the vadose zone and saturated-unsaturated interactions (Cartwright et al., 2006; Kuznetsov et al., 2012; Refsgaard and Storm, 1995; Twarakavi et al., 2008; Zhu et al., 2012) and in irrigation management (Condon and Maxwell, 2013; Perez et al., 2011; Wu et al., 2015b; Zhu et al., 2012). Despite simplifications and assumptions, they are usually computationally most expensive, particularly 3D tools which are not suitable for modeling large field water problems, as well as in terms of parameterization, uncertainty and sensitivity evaluations (Condon and Maxwell, 2013; Kuznetsov et al., 2012) unless massive parallel computing is used (Coumou et al., 2008). By the way, application of these approaches is complicated and less feasible for applicants (farmers).

It is concluded that the combination of accurate and spatially distributed field data with appropriate numerical models will allow to accurately determine field scale water flow and thus field scale irrigation requirements, taking into account the information gained at the plot scale (1D), variations in boundary conditions across the field and spatial variations of model parameters (Chapter 2). Therefore, it is important to develop an approach that can efficiently simulate field scale water flow. In such case, a quasi 3D modeling approach can be used to apply 1D simulations to cover the field scale (Chapter 2).

To address the challenges discussed above and the need for an integrated water management tool, this chapter focuses on the ability of using a numerical soil hydrological 1D model (coupled with a crop growth model) to predict soil-water content, water stress and crop yield over an entire crop field in a quasi 3D way. This will allow to evaluate the impact of irrigation strategies that account for spatial soil heterogeneity on crop yield at the field scale. In the present study, we simultaneously quantify the uncertainty of model parameters, i.e., hydraulic conductivity, of bottom boundary conditions and of various soil layer depths, and evaluate its effect on soil-water content, soil-water storage and water stress, as well as yield in a sandy grassland. Our approach will illustrate how combined prior information with different resolutions can be used in water flow modeling for managing irrigation more effectively and practically in precision farming. We thus simulated water flow on a large scale field with high resolution characteristics of input factors to i) evaluate the computational efficiency and uncertainty of this modeling approach/framework); and ii) evaluate different irrigation scenarios to find an optimized and cost-effective irrigation scheduling. In this stage the proposed modeling approach is evaluated by implementing different irrigation plans with different resolution allowing to show which resolution of input data is sufficient to optimize irrigation scheduling. Overall, this approach can be a useful decision support tool to help decision makers and applicants in assessing the resolution of data needed for precision agriculture management, in optimizing irrigation scheduling and to address how this results in economic benefits.

5.2 Materials and Methods

5.2.1 Study site description

The study site is located in an agricultural area at the border between Belgium and the Netherlands (with central coordinates 51°19′05″ N, 05°10′40″ E) (Figure 5-1), characterized by a temperate maritime climate with mild winters and cool summers. More information is given in Chapter 2 and 3.

The most common drought that occurs in the study area is precipitation shortage (meteorological drought) in combination with higher than normal temperature (Van Passel et al., 2016), severe wind and lower humidity (atmospheric drought) (Zamani et al., 2015). In Belgium, around early April the average daily evapotranspiration surpasses the average daily precipitation: a deficit can therefore accumulate from April onwards. After September, the precipitation deficit tends to decrease as evapotranspiration reduces and rainfall increases. The

rainfall exceedance probability (%) for the experimental years (April-September, i.e., growing season which constitute the time period during which irrigation takes place) was calculated using RAINBOW software (Raes et al., 2006b) with 31 years (1985-2015) of rainfall data from a nearby station (Eindhoven, The Netherlands) on which a square transformation was carried out to obtain a normal distribution. A probability of exceedance of 20% corresponds to a 'wet' year and of 80% to a 'dry' year. 2012 was a 'wet' year with a probability of exceedance of 5%, while 2013 was close to a 'dry' year with 72% probability of exceedance.

5.2.2 Numerical modeling setup

As discussed earlier, some assumptions are necessary in 1/2/3D modeling. The following assumptions were made in this study; 1) only vertical flow in the vadose zone was considered; 2) the upper boundary conditions are uniform for all locations over the field; and 3) a constant head bottom boundary condition was assumed. The latter is justified for the field study site owing to the presence of the drainage system.

Simulation of root water uptake and water flow was carried out for two growing seasons (from 1 Mar. until 25 Nov. in 2012 and 2013) using Hydrus 1D version 4.16 (Šimůnek et al., 2013b) which solves the 1-D Richards water flow equation (Eq. 2-5). The hydrological model was integrated with the crop growth model LINGRA-N (Wolf, 2012) which can calculate grass growth and yield under potential (i.e. optimal), water limited (i.e. rain fed) and nitrogen limited growing conditions. Details about this model and the coupling procedure can be found in Chapter 2.

The soil profile in the hydrological model extended to 200 cm depth and was divided into two layers. To solve Richards' equation, the van Genuchten-Mualem, MVG (Mualem, 1976; van Genuchten, 1980) soil hydraulic model (Eqs. 2-1 – 2-4) without hysteresis was used. The initial pressure head distribution was interpolated linearly from the node at the groundwater level (h=0, GWL) to the soil surface for each run (head gradient between the soil surface and GWL). The upper boundary condition for water flow was an atmospheric one, i.e., Dirichlet and Neumann (based on rainfall and irrigation water supply, leaf area index, LAI calculated by LINGRA-N and reference evapotranspiration, ET_o) with surface runoff. ET_o was calculated based on the FAO Penman-Monteith equation on an hourly basis (Allen et al., 1998) using local weather station data. The Feddes model (Feddes et al., 1978) without solute stress was used for root water uptake. The default grass parameters values provided by Hydrus-1D were used (Taylor and Ashcroft, 1972).

5.2.3 Model parameterization

5.2.3.1 Hydraulic parameters

Sampling locations for soil characterization were selected by combining a design-based (the ESAP-RSSD software package, (Lesch, 2006)), a model-based (FuzzMe software applying the Fuzzy k-means algorithm, (Minasny and McBratney, 2002)) and a traditional sampling strategy to account for the maximum variation in soil properties that was suggested by a geophysical survey (electromagnetic induction technique, EMI) with a DUALEM-21S sensor (0-100 cm). The comprehensive procedure of this methodology and sampling design is described in Chapter 3. Figure 5-1a shows the apparent soil electrical conductivity (ECa) map produced by the DUALEM-21S, and the 20 soil sampling locations from the ESAP-RSSD software and eight sample locations along a transect according to the traditional approach.

In the same study field and using the Hydrus-1D model at one spot (Chapter 2), we showed that changes in soil-water content are most sensitive to K_s. We also found that calibrating the model by optimizing the key parameter K_s and keeping all other hydraulic parameters constant should suffice for irrigation management purposes. Therefore, in this study the arithmetic average value of SWRC measured at the various sampling locations was used to determine the MVG hydraulic parameters. The K_s value of the second layer was taken from the optimized value derived in Chapter 2, while K_s values of the first layer were taken from relationships established in the same field described in Chapter 3, allowing to predict and upscale laboratory K_s in 0.5 by 0.5 m resolutions over the entire field using proximally sensed ECa (Figure 5-1b). Another study in the same field (Chapter 4) supports this methodology, in that it showed that there is almost no difference in model performance when using field or laboratory determined hydraulic data sets to simulate water flow.

5.2.3.2 Bottom boundary condition and profile geometry

Groundwater and thickness of the first layer at the 28 locations discussed above (Figure 5-1a), were measured on 4 June and 25 October 2013 by augering. The spatial groundwater level distribution was then determined as follows and using Surfer software (Surfer 13, Golden software, LLC). First, the measurements at the 28 locations were converted from level below surface to an absolute groundwater height using detailed (cm scale) digital elevation data, including the water level of the ditch at the border (Figure 5-1). Second, the 28 measurements (expressed as height) were interpolated using ordinary kriging (OK, 0.5 by 0.5 m) over the

field. The interpolated map was then converted to the depth below the surface by subtracting the groundwater height map from the digital elevation map. The same procedure was applied for the distribution of the first layer thickness. Assumptions that were made here are: (i) there are no other layers between layers and in sublayer; (ii) these layers are spatial continuous. The maps of field GWL and first layer thickness are shown in Figure 5-1c and 5-1d respectively.

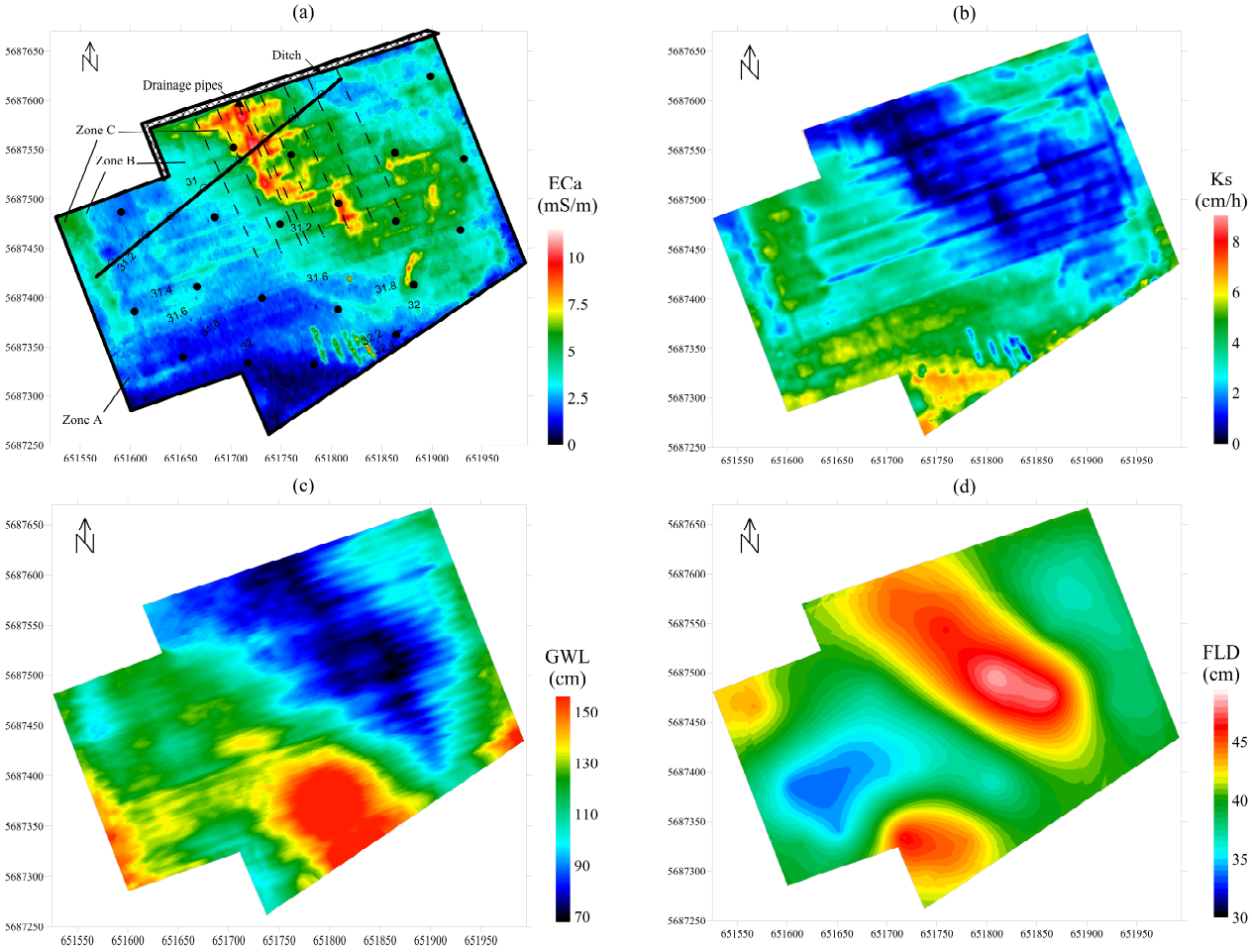

Figure 5-1. Location of the study field and a) the classified map of 0–100 cm soil ECa with indication of the 20 soil sampling locations (black bullets) from the ESAP software, the eight additional points along the transect, and the elevation contour intervals (labels in m a.s.l.); b) estimated saturated hydraulic conductivity, K_s from the site-specific empirical (geophysical) relation (Chapter 3); c) interpolation of groundwater level, GWL and d) first layer depth, FLD.

5.2.4 Model implementation

Instead of running Hydrus-1D in a batch setup using workstation cluster boots parallel computation techniques which would need considerable endeavors in preparing input files for each run and intensive computational efforts, we implemented the Hydrus code into Python™

software (Appendix – Chapetr 5). This allowed to minimize the run time and automatize pre and post processing analysis. This also prevented hampering of model solutions when using high resolution datasets. Several scripts/routines were written to manage the communication between Python™ and the hydrologic tool.

The field is represented as a collection of 1D columns each parameterized using the spatially distributed input parameters and boundary conditions (K_s, GWL, FLD) at various resolutions ranging from 5 x 5 m to 400 x 400 m. Python™ scripts/routines were programmed to automate the calculations, in which, profile geometry, initial and bottom boundary conditions, as well as hydraulic conductivity were generated automatically using the provided datasets for each column run. A computational flowchart is given in Figure 5-2.

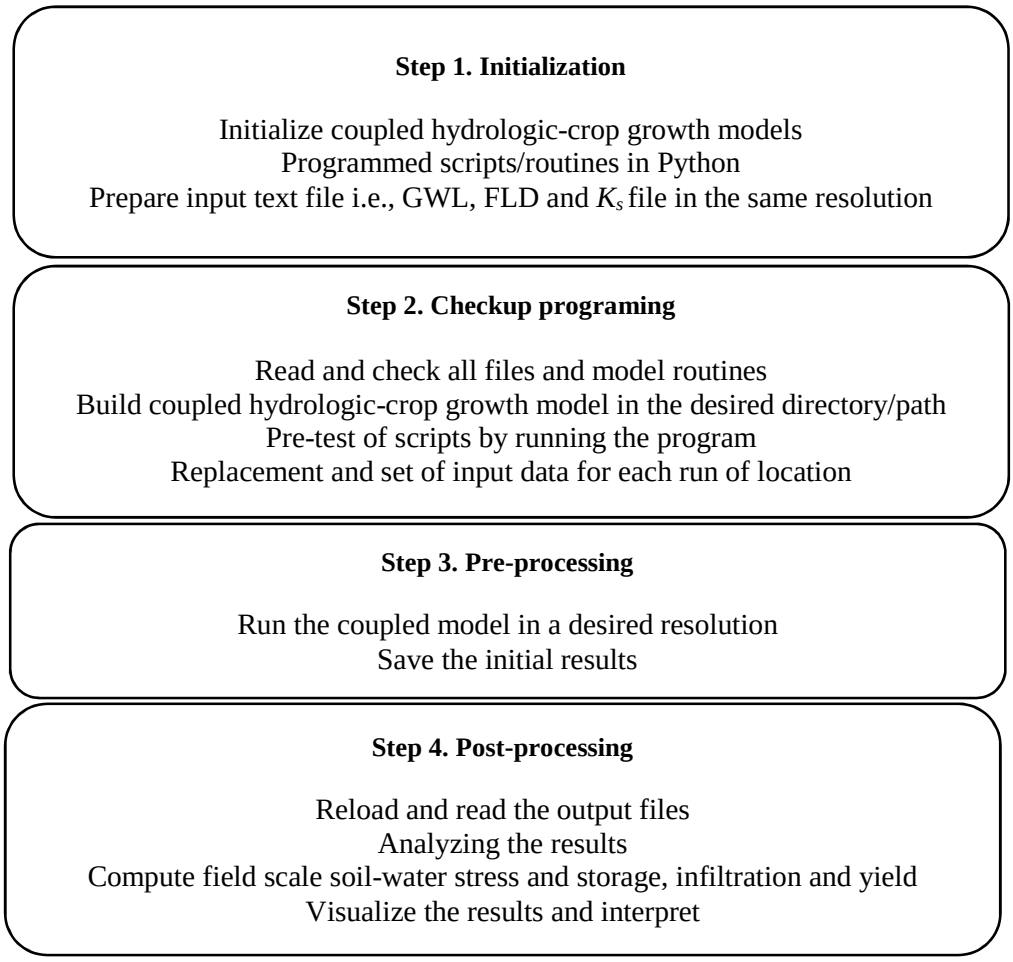

Figure 5-2. Flowchart of the quasi 3D modeling approach, with implementation of the coupled hydrologic-crop growth model in Python™ software.

5.2.5 Model outputs

5.2.5.1 Crop yield

The ratio between actual crop evapotranspiration and potential evapotranspiration was introduced as a water stress factor equal to the crop yield reduction due to water shortage (Doorenbos and Kassam, 1979), which is given in Eq. 2-9. The values are provided by the model and calculation of yield was made using Python™ scripts.

5.2.5.2 Water stress and yield reduction

Feddes' model (Feddes et al., 1978) was used to represent the sink term in Richards' equation (Eq. 2-5), and thus to quantify the potential root water uptake and water stress (Eq. 2-6). By assuming that root water uptake is equal to actual transpiration, the ratio of actual to potential transpiration by root uptake was introduced as a degree of water stress, DWS (Jarvis, 1989) (Eq. 2-8). In optimal and stress free conditions, this ratio should be (close to) unity (>0.90 of maximum reference evapotranspiration).

5.2.5.3 Soil-water storage

The top 20 cm of the soil profiles, where root density is maximum, was taken to calculate soil-water storage (cm) in each run/simulation. To do so, simulated soil-water content at discretization nodes within the top 20 cm were multiplied by the node internal and summed.

5.2.6 Uncertainty and effectiveness of simulations

The resolution of the input data has a great impact on the computational performance of the code (Figure 5-3). To assess the effect of the data resolution on the uncertainty of the water stress and yield predictions and consequently, the irrigation strategy, the tool was run (forward modeling) for several resolutions. Soil columns were constructed with grid cells of 5 x 5 m (4490 runs), 7 x 7 m (2290), 9 x 9 m (1390), 10 x 10 m (1212 runs), 15 x 15 m (499 runs), 20 x 20 m (280 runs), 25 x 25 m (180 runs), 30 x 30 m (130 runs), 35 x 35 m (92 runs), 40 x 40 m (75 runs), 45 x 45 m (55 runs), 50 x 50 m (45 runs), 100 x 100 m (11 runs), 150 x 150 (five runs), 200 x 200 m (three runs), 250 x 250 (two runs), 300 x 300 (two runs), 350 x 350 m (one to two runs) and 400 x 400 m (one run for entire field) with different combinations of their unique conditions, i.e., GWL, FLD, and K_s on a personal computer with a CPU of 2.50 GHz and 8.0 GB RAM. For coarser resolutions, the location of the soil column within its corresponding grid was changed randomly (40 times for the lowest resolution to 5 times for the highest one) in order to have a smooth representation of the field (see Appendix – Chapter 5).

The efficiency of the modeling approach was evaluated by comparing the computational time of pre and post processing. The uncertainty of the simulations, i.e., uncertainty of combinations of different GWL, FLD and K_s of each grid with different resolutions was evaluated by comparing the average and the standard deviation of the water stress, soil-water storage and calculated yield (Eq. 2-8) of each resolution scenario.

In addition, three different resolutions, i.e., 10 x 10 m, 100 x 100 m and 400 x 400 m, were tested in a triggered irrigation scenario (automated irrigation implemented in Hydrus when the pressure at a selected observation depth drops below a specific value, e.g. the upper limit of field capacity (-300 cm), to eliminate water stress, see the next section). The uncertainty of our modeling approach was evaluated with regards to irrigation management purposes as well.

5.2.7 Cost-effective irrigation scenarios

The value of water stress, and the number and the duration of stress periods was considered as an indicator for the performance of the irrigation scheduling (van Dam et al., 2008). After selecting the optimal resolution, four different irrigation scenarios were conducted. They consisted of a) current irrigation, in which all actual water supply and rainfall were taken into account as the upper boundary condition, i.e., model input; b) no irrigation, in which the actual water supply (all irrigation events) was deleted from the model input; c) optimized irrigation or trial and error, in which the actual water supply (all irrigation events) was first deleted from the model input. Subsequently, LAI simulated with the LINGRA-N for optimal conditions (no water stress) was used as a variable in the hydrological model. The hydrological model was then run with the new input variables to calculate water stress without actual water supply, and subsequently, the appropriate (minimum) amount of the required irrigation (using trial and error) was added to the precipitation at the beginning of each water stress period to exclude water stress from the simulations (see Chapter 2 for further information); and d) triggered irrigation, in which all irrigation events were deleted from the input data and then 2.5 cm of water was added automatically by the Hydrus model to retain a pressure head above -300 cm (field capacity hence avoiding any water stress) within 2 hours with a rate of 1.25 cm h^{-1}. At the end, total water supply by the model was calculated.

Crop yield of each run was calculated using Eq. 2-8 to show to what extent different scenarios affect soil-water stress and crop yield. Accordingly, the efficiency and cost-effectiveness (watering amount, and price and yield increase) of different irrigation scheduling scenarios in

combination with different resolutions were calculated and compared. Finally, the best optimal irrigation scenario was selected.

5.3 Results and Discussion

In the calculation procedure, model columns with optimized second layer K_s (Chapter 2), average MVG parameters (Table 5-1), and their unique FLD, GWL and first layer K_s were used. Overall, the quasi 3D flow modeling approach described above and performed in this study differs from the quasi 3D flow modeling procedure presented by Kuznetsov et al. (2012); Perez et al. (2011); Twarakavi et al. (2008); Zhu et al. (2012) in which coupled unsaturated-saturated water flow models (i.e., 1D models-fully 3D models) were applied at the regional and the catchment scale, and from the parallel modeling approach presented by Coumou et al. (2008) in which a 3D model was used to solve fluid flow in complex geologic media. However, it is similar to the approach presented by Joris et al. (2014) in which the Hydrus-1D model was applied to simulate contaminate leaching/transport for the Belgian-Dutch transnational Kempen region (200 x 200 m resolution), though we assessed water flow in the root zone and under the specific conditions of an agricultural field with a dense dataset. It should be noted that model calibration was not an objective of this study since the coupled hydrologic-crop growth model performance was already assessed at the study site against measured soil-water content data (Chapter 2 and 4). Therefore, the model evaluation focused on whether the model, when using a high resolution data set, could reproduce the spatial pattern of water flow in the root zone and consequently water stress, storage and crop yield.

Table 5-1. Average of soil hydraulic properties of two layers of entire field. θr, θs are residual and saturated water content, respectively; α and n are van Genuchten-Mualem shape parameters. K_s is the saturated hydraulic conductivity. GWL is the groundwater level. Number between parentheses represents the coefficient of variation (CV %).

	K_s	θ_r	θ_s	α	n
	cm h^{-1}	cm^3 cm^{-3}		cm^{-1}	
Topsoil	3.94 (78.0)	0.08 (20.9)	0.39 (5.3)	0.017 (39.3)	2.05 (22.8)
Subsoil	2.27 (59.3)	0.05 (59.6)	0.32 (11.94)	0.020 (40.62)	2.52 (27.68)

5.3.1 Computational efficiency of the modeling approach

The computational time (pre and post processing which provided about 200 maps of water stress, water storage and yield at different times) for the various resolution scenarios is shown in Figure 5-3. It ranged from 1.5 s to 9200 s when moving from lower to higher resolutions. The highest resolution scenario (5 x 5 m) showed a computational time of less than 3 hours for the whole 10.5 ha field, which is reasonable for such a dense resolution that provides detailed information on water flow. This efficiency in time performance (in terms of CPU and time consumption of the approach) is indeed significantly larger and less expensive (computational burden) than in previous studies (e.g. Coumou et al., 2008; Kuznetsov et al., 2012; Li et al., 2015; Perez et al., 2011; Wu et al., 2015b; Zhu et al., 2012). The cost of high resolution simulations (below 10 x 10 m; 1950 s) significantly increases with increasing the number of grid cells. At the highest resolution (5 x 5 m), the computational time of the approach was significantly higher (> 400%) as compared to that of the 10 x 10 m resolution. Kuznetsov et al. (2012) reported that computational efficiency (CPU) of a quasi-3D approach (with coupled Hydrus-MODFLOW model) was significantly higher than that of a full-3D model (VFS model). Zhu et al. (2012) compared Hydrus-1D with their coupled unsaturated-saturated model (only for one spot) and reported that the simulation time of the Hydrus-1D was 28 times less than that of the coupled model, while similar outputs, i.e., simulated water content and infiltration were observed for both approaches. The approach developed in this study shows a large effectiveness in that the large number of soil columns does not induce an obvious and relevant flow modeling cost, especially for resolutions below 10 x 10 m. What thus matters only are the expenses (the labor and analysis cost) associated with measuring/determining the input data needed for the spatially explicit input parameters.

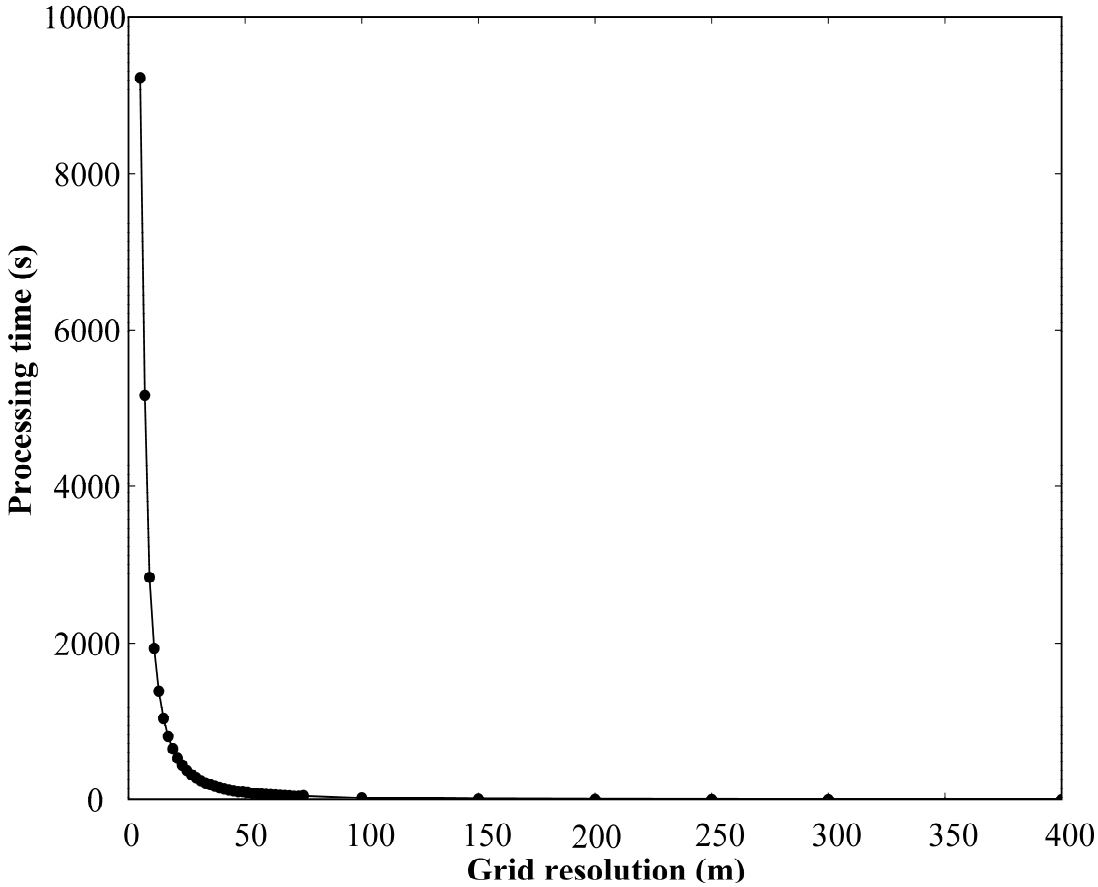

Figure 5-3. Computational pre and post process time of modeling approach for various grid resolutions (5 x 5 m to 400 x 400 m).

Figure 5-4 demonstrates the performance of the approach to represent the simulated soil water status. As expected, the spatial pattern of the predictions agrees well with the spatial distribution of the input variables, GWL, FLD and K_s (Figure 5-1). Comparing the drier and wet zones, the soil-water storage changes drastically due to varying input variables in the root zone (mainly in the top 20 cm). The simulations show a noticeable influence of the GWL as well as FLD and K_s on water stress and storage and consequently crop yield. They also provide new insight on the effectiveness of water management which was considered as satisfactory for the purpose and the scale of the approach.

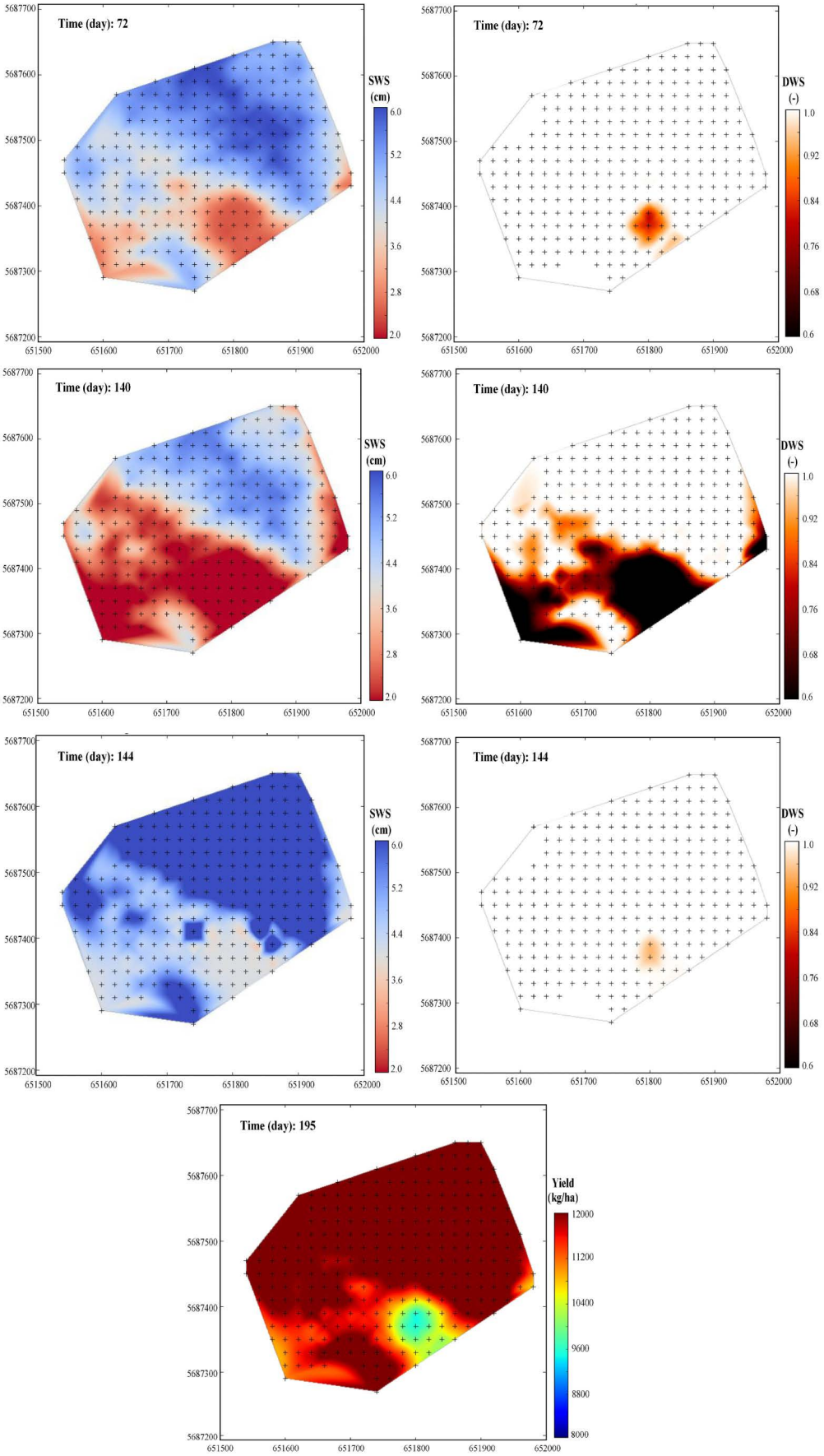

Figure 5-4. Soil-water storage and water stress distribution before (day 72 and 140) and after (day 144) water supply and total yield for current irrigation management (growing season 2013, resolution 20 x 20 m, plus sign shows the grid column locations).

During transient stages the vertical fluxes and consequently soil-water storage and redistribution may vary at different locations, and an insufficient number of soil columns might then cause a deviation in the estimations of the soil-water content at the field scale. Zhu et al. (2012) found no obvious differences in simulations of water flow - vertical flux - with analytical 1D, coupled and full 3D numerical models while taking into account a constant head boundary condition. In comparing 1, 10, 20 and 41 simulation columns along 40 m distance, they also found that the number of soil columns used and how and where these columns were placed, did not matter (although one column overestimated the flux and reduced the accuracy of simulations). In contrast, in our study, the uncertainty in predicted soil-water content was high when lower resolutions were chosen (will be further discussed, Figure 5-5). Lower resolutions lead to both over- and underestimation of soil-water content for drier and wetter zones respectively. Therefore, it seems necessary to have denser column simulations, as can be observed in Figure 5-5, which shows the coefficient of variation (CV) of the soil-water storage, water stress, stressed area and yield simulations for different resolutions (5 x 5 to 400 x 400 m) for the year 2012. It is acknowledged that spatial correlation (via the kriging method as proven by the semivariogram model) exists in the soil characteristics and input parameters. This leads to similar spatial variability (i.e., same CVs) of input parameters for different resolutions. But based on Figure 5-5, the coefficient of variation of the soil-water storage, water stress, stressed area and yield was larger for calculations at lower resolution as compared to the higher resolution in the modeling approach, while their CVs exhibit the same behavior and trend (i.e., fluctuations of CVs) especially for coarser resolutions. Result showed that the CV is high because the standard deviation is high while the average value is the same. The water stressed area shows the largest CV which reaches up to 140% for the lowest resolution. The calculated soil-water storage exhibits a CV of up to 40% depending on the resolution (Figure 5-5). This is not reflected in crop yield and water stress to the same extent, where CVs of only 5-10 % are noted. Crop yield, water stressed area and soil-water storage at various times (and thus various environmental conditions) show relatively larger discrepancies if low resolutions (grid sizes larger than 20 x 20 m) are assigned (Figure 5-5). Increasing the resolution results in a drastic reduction of the uncertainty to less than 1% CV for water stress, soil-water storage and yield (Figure 5-5). Figure 5-6 shows the deviation of simulated water storage, water stress and yield for different locations at 10 x 10 m resolution. It shows that a denser column grid, i.e., higher resolution, can represent the simulated water flow more accurately in the entire domain, which reflects the importance of the resolution on reducing the uncertainty of simulation in this view.

Hence, results showed that the CV values of soil-water storage, water stress and yield did not change significantly for resolutions larger than 10 x 10 m. Since the accuracy of our modeling approach depends on how precisely the input factors are described, assessing the reduction of simulation uncertainty needs more in depth evaluation which is addressed in the next section (irrigation scenarios and their efficiencies).

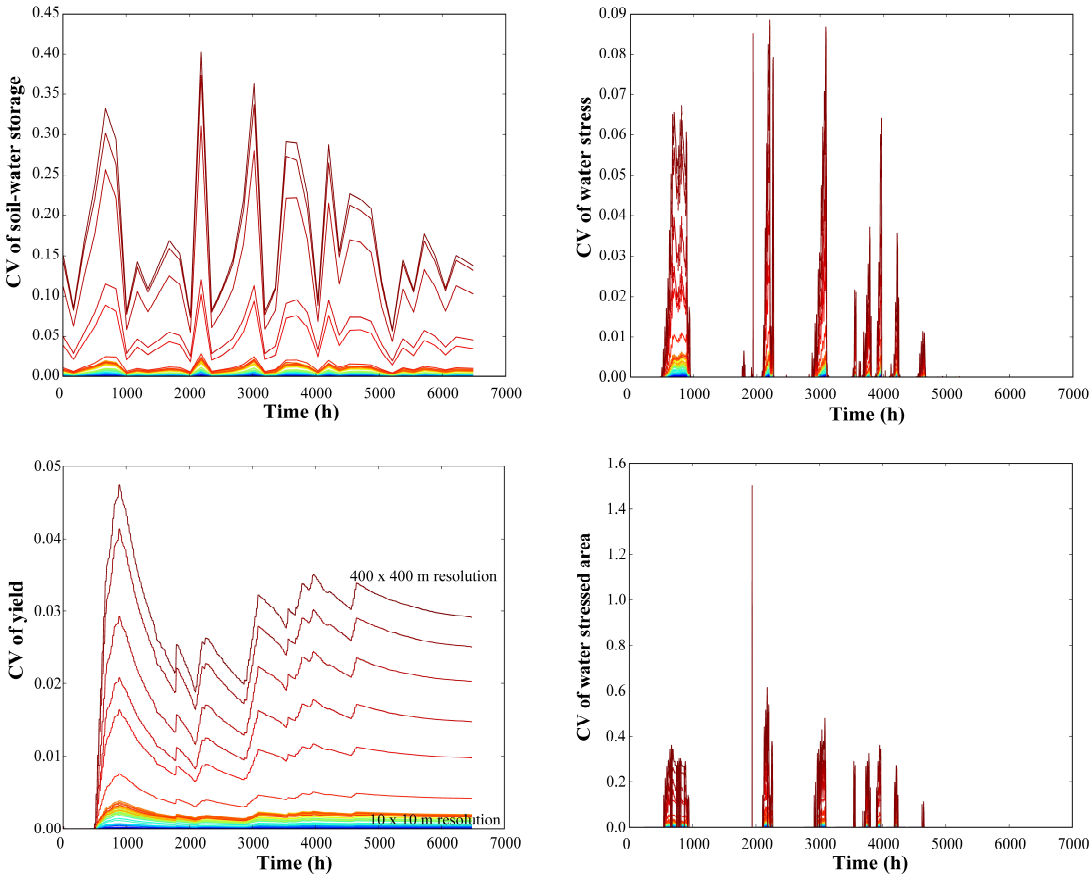

Figure 5-5. The average coefficient of variation (CV) of simulated soil-water storage, water stress, stressed area and yield for different resolutions (5 x 5 m (blue color line) to 400 x 400 m (red color line)) over the growing season 2012 for the entire field.

Our modeling approach provides high resolution predictions and fast performance, which can be easily applied for any smaller or larger area (aggregation level) with shallow groundwater, since with the fairly small thickness of the vadose zone lateral flow was ignored. However, in the deep soil the error could be more pronounced (Hunt et al., 2008; Sheikh and van Loon, 2007) when lateral flow becomes dominant (Zhu et al., 2012). In case of deeper groundwater tables, the approach may not be generalized or specific conditions should be defined. Based on the overall analysis for different resolution scenarios, our approach satisfactorily simulates the spatial pattern of soil water status, water stress and crop yield. This confirms that in predictions of field water status based on single sites or management zones (e.g. some limited sites) plenty of information for the entire field is missed, which might be problematic in view of precision

agriculture and irrigation management (e.g. see Chapter 2). It thus seems that resolutions higher than 10 x 10 m do not increase the information content further, specifically since current irrigation technology such as Reel sprinkler at the particular site cannot go beyond a resolution of 12 x 12 m.

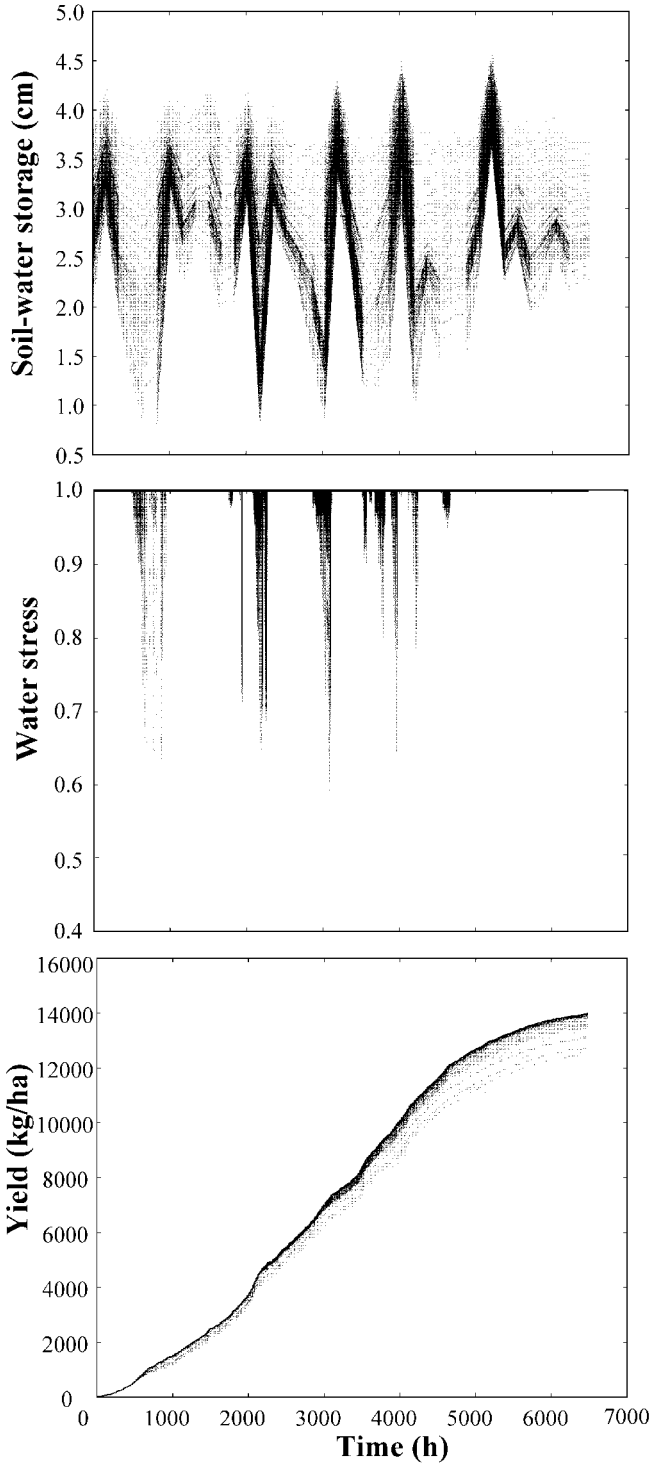

Figure 5-6. The deviation of simulated water storage, water stress and yield for different locations of 10 x 10 m resolution.

5.3.2 Irrigation scenarios

5.3.2.1 No irrigation

As shown in Figure 5-4, there was water shortage and consequently water stress in some parts of the field (with deeper GWL) during the summer period. The water stress could be attributed mostly to the position of the GWL (and thus less water supply by capillary rise from deeper GWL) and lower water holding capacity (linked to first layer thickness and hydraulic parameters) of the root zone at that area (Chapter 2). Additional water supply further eliminates water stress.

Figure 5-7 represents the average of water stressed area and water stress with time for the entire field (1212 columns, i.e, 10 x 10 m resolution) (upper two panels) for non-irrigated conditions for the year 2012 and 2013. According to the results, on average 5 and 13% of the area was under stress in 2012 and 2013, respectively, for the no-irrigation scenario. As shown in the third panel, the time-average soil-water storage was lower and both the stressed area and water stress were larger in those parts of the field with deeper GWL and higher K_s, which should be taken into account in the irrigation strategy. In those parts, crop yield was reduced for both years but most pronounced in 2013 (linked to more water stressed area and water shortage) (Figure 5-7). The differences in hydraulic behaviors, GWL and FLD between the three distinct zones shown in Figure 5-1a, combined with the results of no irrigation scenario (Figure 5-7), justify to adapt the irrigation plan and to find the optimal scenario at different resolutions. According to Figure 5-1a and 5-7, zone C (indicated on the map in Figure 5-1a) exhibits wetter conditions during the growing season and requires less water than zones B and A. When the GWL drops below 120 cm, the crop seems to experience water stress, but for GWL above 100 cm, no irrigation seems to be required. Sufficient water seems then to be provided by capillary rise as to keep the soil-water potential within an extractable range. Huo et al. (2012) also reported larger water content in a soil profile (topsoil/root zone) with a GWL at 120 cm below surface as compared to a GWL at 200 to 300 cm, which was attributed to capillary rise (similar to our results). Consequently, water fluxes through the soil profile were greater for water tables shallower than 120 cm. Results suggest that the overall spatial relationship between input parameters and simulated water storage is linear and it seems that is dominated by the GWL. This suggests that GWL fluctuation over the field should be considered when attempting to optimize irrigation strategies. On the other hand, water (supplied by irrigation or rainfall) drained faster in the dry zones than the wet zones due to differences in K_s. In fact, the wetter

zone showed a lower K_s compared to the drier zone and water tends to stagnate at the surface and within the profile (which was observed during field work), and this zone thus meets most of the crop water demands. Similar findings were reported by Gumiere et al. (2014).

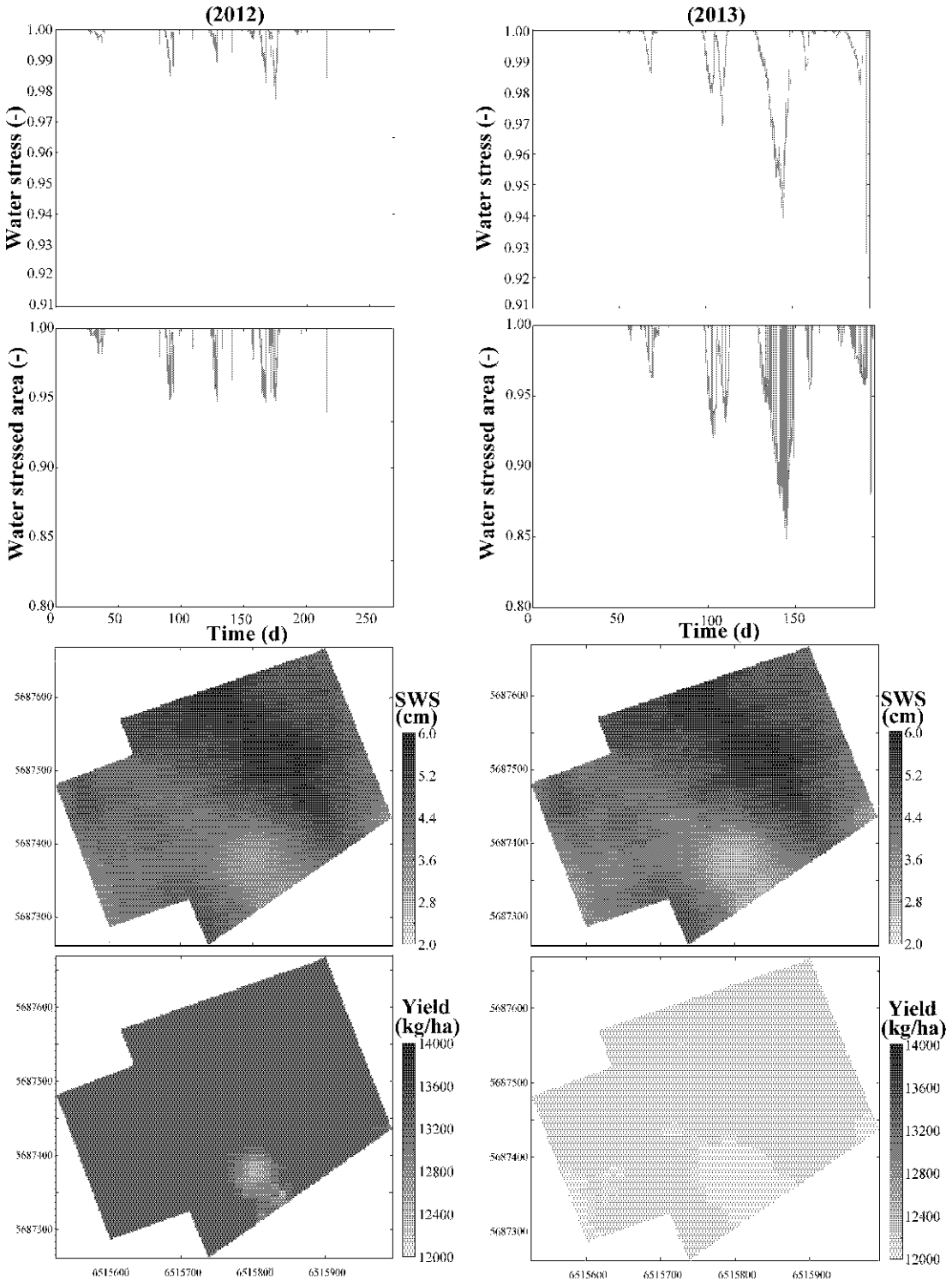

Figure 5-7. Water stressed area, water stress, soil-water storage and yield of no irrigation scenario (resolution 10 x 10 m) for the year 2012 (left) and 2013 (right). Lower degree of water stress shows the more water stress.

5.3.2.2 Current and optimized irrigation

Three types of irrigation scenarios were considered: (1) current irrigation (homogeneous application over the whole field); (2) optimized (trial and error) irrigation scheduling (optimized timing and amount but homogeneous application); and (3) triggered irrigation (this scenario automatically suggests the right time and specified amount of irrigation based on model predictions of soil moisture content in which a plant is exposed to water stress). Figure 5-8 and 5-9 illustrates the effects of different irrigation scenarios on water stress and soil-water storage and eventually crop yield in 2012 and 2013, respectively (resolution: 10 x 10 m). As discussed later, the applied water reduced water-stress and consequently increased yield for both 2012 and 2013. When comparing the optimized and current irrigation scenarios, it is clear that the optimized scenario is remarkably more successful than the current one in reducing water stress and increasing yield, using less water at appropriate time, which means higher water application efficiency (Figure 5-8 and 5-9).

In the current and optimized irrigation scenario (left and middle panels in Figure 5-8 and 5-9), huge amounts of water drain from the vadose zone because irrigation is uniformly distributed over the field and a drainage system is present. Comparing Figure 5-7, 5-8 and 5-9 shows that a significant water surplus (which can be defined as supplied water minus water demand or as supplied water minus soil-water storage) existed in most of the area where a shallow GWL was present and water stress did not occur, in both growing seasons. This also illustrates that soil-water storage was not changed significantly by the supplied water. However, there is variability in soil-water storage which can be attributed to the characteristics of the soil columns (shallower GWL, K_s and FLD). It should be noted that the supplied water, however, significantly reduced the stressed area and water stress (duration and amount) over the field in 2013. Under the current irrigation the stressed area reduced from 5% to 3.5% (2012) and from 13% to 10% (2013). Under optimized irrigation the stressed area further reduced to 3% (2012) and 4% (2013). The modeling approach emphasizes the effect of the irrigation plan under dry and wet year conditions on crop water demand and water stress. Besides soil-water storage, i.e., water status as found by (Kourgialas and Karatzas, 2015), our results confirm that duration of water stress and stressed area are good benchmarks for irrigation management, as their calculations consider crop water requirements, as we showed in Chapter 2. Simulation results also illustrate that under no irrigation and the current irrigation scenario, yield was reduced in

2013 as compared to the 2012 growing season due to metrological drought. Furthermore, crop yield was correlated to water stress and soil-water storage (r=0.93 and r=0.89, respectively).

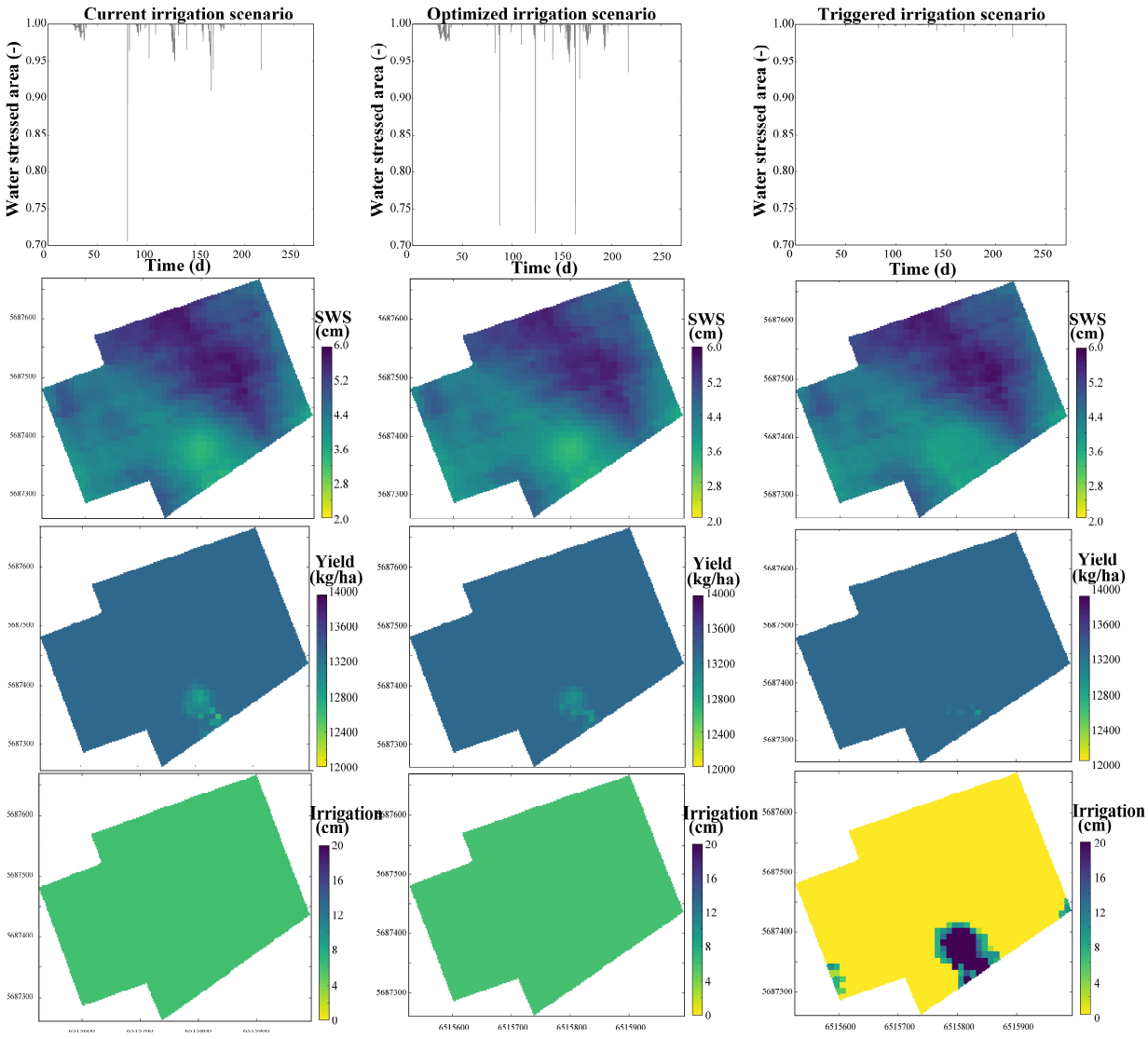

Figure 5-8. Water stressed area, water storage (SWS) and yield of current (left), optimized (middle) and triggered (right) irrigation scenarios with their applied water over the field for 2012 (resolution 10 x10 m).

The results of the spatially explicit approach with high resolution simulation columns agreed well with results derived from one column simulation with the calibrated model (Table 2-5 in Chapter 2, see also Table 5-2). It suggests that if the representative spot on the field is chosen adequately, the results may be generalized for the whole field. As a result, it is enough to calibrate the model (by inverse optimization of K_s) based on limited spots and apply it for a whole domain. This is relevant for the practitioners to select the best location when using one or limited spots for agricultural water management evaluations.

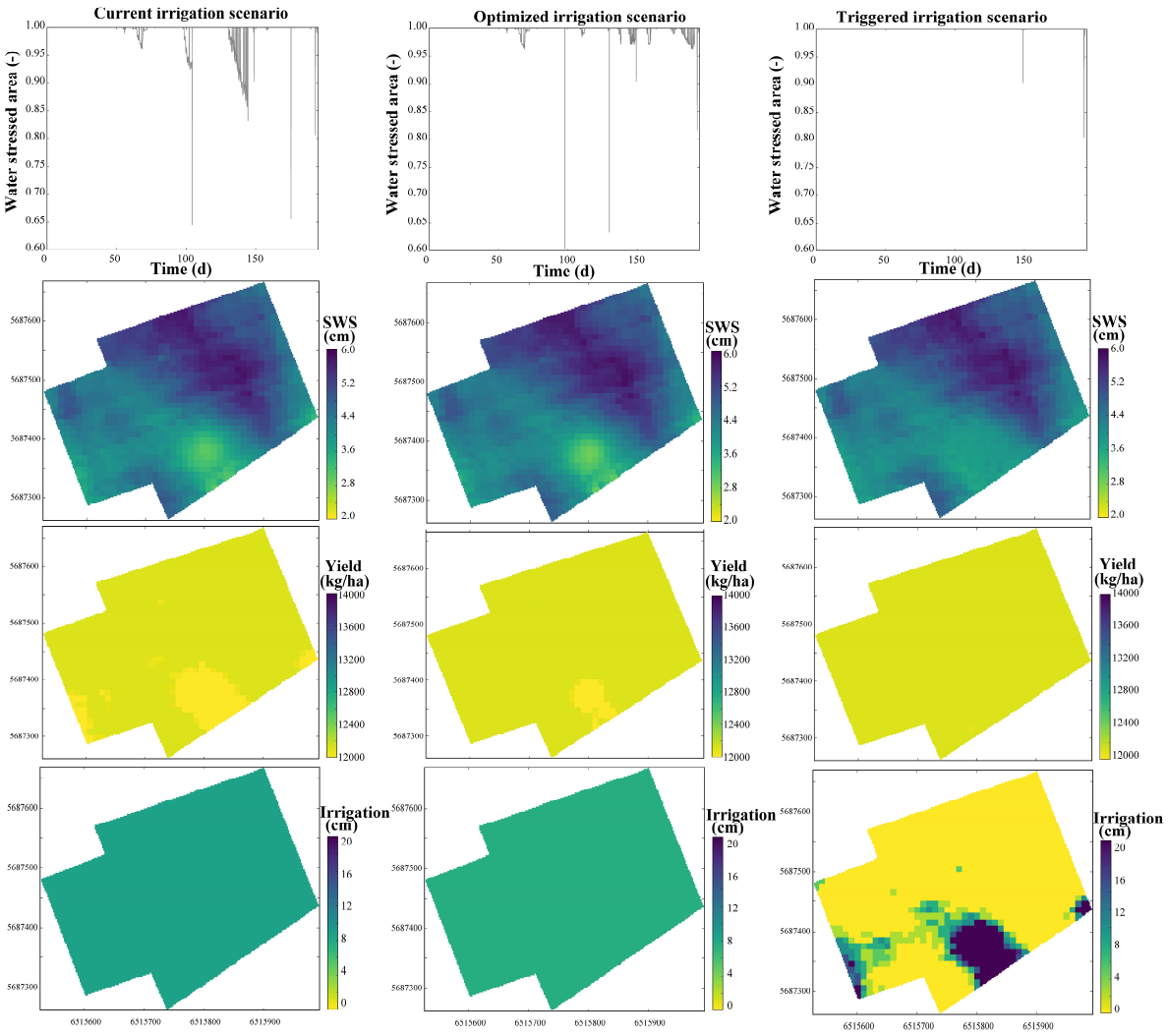

Figure 5-9. Water stressed area, soil-water storage (SWS) and yield of current (left), optimized (middle) and triggered (right) irrigation scenarios with their applied water over the field for 2013 (resolution 10 x 10 m).

5.3.2.3 Triggered irrigation

As the right panels of Figure 5-8 and 5-9, and Table 5-2 demonstrate, the triggered irrigation scenario ensured a significant reduction of the water application for most of the field area (zones A and B, Figure 5-1a) and an increase for most of the dry locations. This results in a yield increase in the dry zones and a continued optimal level in the wet zones. The triggered irrigation scenario eliminated water stress for 2013 and maximally reduced it for 2012, as delivery of water is based on demand and on predefined soil-water pressure at which the plant starts to experience water stress (Figure 5-7, 5-8 and 5-9). The triggered irrigation scenario resulted in optimal crop yield for all locations over the field (see Table 5-2).

Figure 5-8 and 5-9 further show that the model-based triggered irrigation approach would ensure that highest yields are obtained and minimal amount of water is applied, when water is distributed accordingly. Results confirm that many of the water shortages could be mitigated by precision management or by improved infrastructure. This scenario is valid for sprinkler irrigation. The modeling approach is generic and also applicable to other types of irrigation such as drip irrigation. The method (distribution of water supply) still uses actual precipitation and evapotranspiration and does not take into account weather forecast data. It should therefore be acknowledged that performing this approach needs accurate weather forecasting, especially in outdoor farming. Our simulations for different irrigation strategies highlighted that spatial and temporal water demand can be modeled and introduced precisely and efficiently.

5.3.3 Irrigation efficiency and modeling approach

5.3.3.1 Effect of modeling resolution on irrigation uncertainty

As noted previously, the robustness, reliability and effectiveness of the modeling approach and the uncertainty in the simulations were evaluated using different resolutions and various sampling locations generated by the triggered irrigation scheme. Figure 5-10 shows the effect of resolution and sampling design impact on irrigation water management. Obvious differences can be found among the different resolutions and locations. When using a low resolution (100 x 100 m), large uncertainties can be seen in simulation results and consequently in the irrigation plan (Figure 5-10). Changing the locations of calculations shifts the irrigation plan from one zone to another zone. Therefore, the lower resolution barely represents the field scale flow characteristics (columns are too sparse to characterize the flow, therefore an inaccurate area to be irrigated was proposed). It shows that inappropriate locations of modeling may lead to improper irrigation management. In contrast, varying sampling locations (i.e., changing randomly the location of the soil column within its corresponding grid) did not significantly change the irrigation scheme when using a high resolution (10 x 10 m). Additional columns are able to capture the flow process more accurately and precisely.

Figure 5-10. Effects of different resolutions and sampling location on irrigation scheme (resolution: 10 x 10 m and 100 x 100 m with 5 and 10 different sampling locations, respectively, to have a smoother representation).

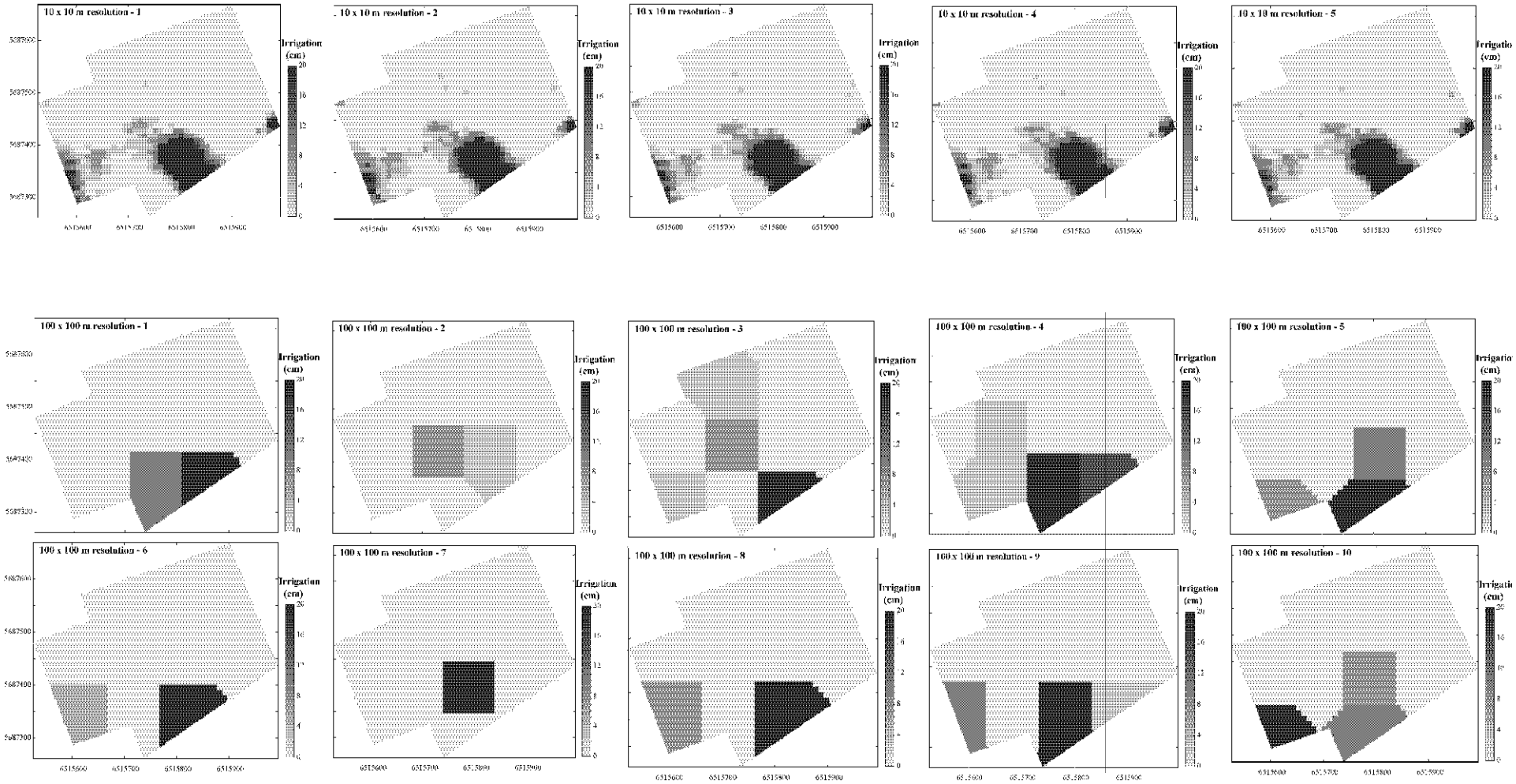

The results thus advocate selecting a 10 x 10 m resolution (as discussed in section 4-3-1) and use the modeling design presented here, and also clearly notify the effective irrigation scheme. Therefore, a dense modeling setup would be recommended for precision agricultural purposes. Results also demonstrate that in evaluating the uncertainty of the approach, not only providing reliable statistics provide a distinctive insight but also, visualization of the results are very helpful for better understanding of this matter.

5.3.3.2 Irrigation cost-effectiveness

Figure 5-11 further shows the difference in simulated water storage, stressed area and yield between the four different irrigation scenarios. According to our results, a proper irrigation plan (triggered irrigation scenario) can be adapted at every location within the modeling domain. Water consumption was reduced with up to 285% as compared to the current irrigation practice (Figure 5-11 and Table 5-2). The triggered irrigation scenario (10 x 10 m resolution) used less water which is beneficial in view of water saving, while it increased yield (non-significant) and decreased the irrigation cost (the operational-maintenance costs) which is important towards economic profitability. As regards average soil-water storage of the top 20 cm, it was increased in this irrigation scenario in the dry year 2013, whereas in the wet year 2012 it was lower than in the current irrigation scheme. However, this would not affect yield and water stress. Results also revealed that optimized/current irrigation strategy (10 x 10 m) required a higher water supply and resulted in less yield compared to triggered irrigation (10 x 10 m resolution).

Table 5-2. Comparing cost-effective irrigation scenarios. Irrigation cost includes operational and water costs.

	2012			2013		
Irrigation scenario	Simulated yield (kg/ha)	Irrigation amount (mm)	Irrigation cost (euro)	Simulated yield (kg/ha)	Irrigation amount (mm)	Irrigation cost (euro)
No	13972	0	0	12056	0	0
current	13987	65	304	12097	85.4	427
optimized	13990	60	300	12143	75	375
Triggered (10x10 m)	14000	11.9	60	12162	29.9	149
Triggered (100x100 m)	13989	14.2	70	12136	33.9	156
Triggered (400x400 m)	13977	47.5	237	12056	-	-

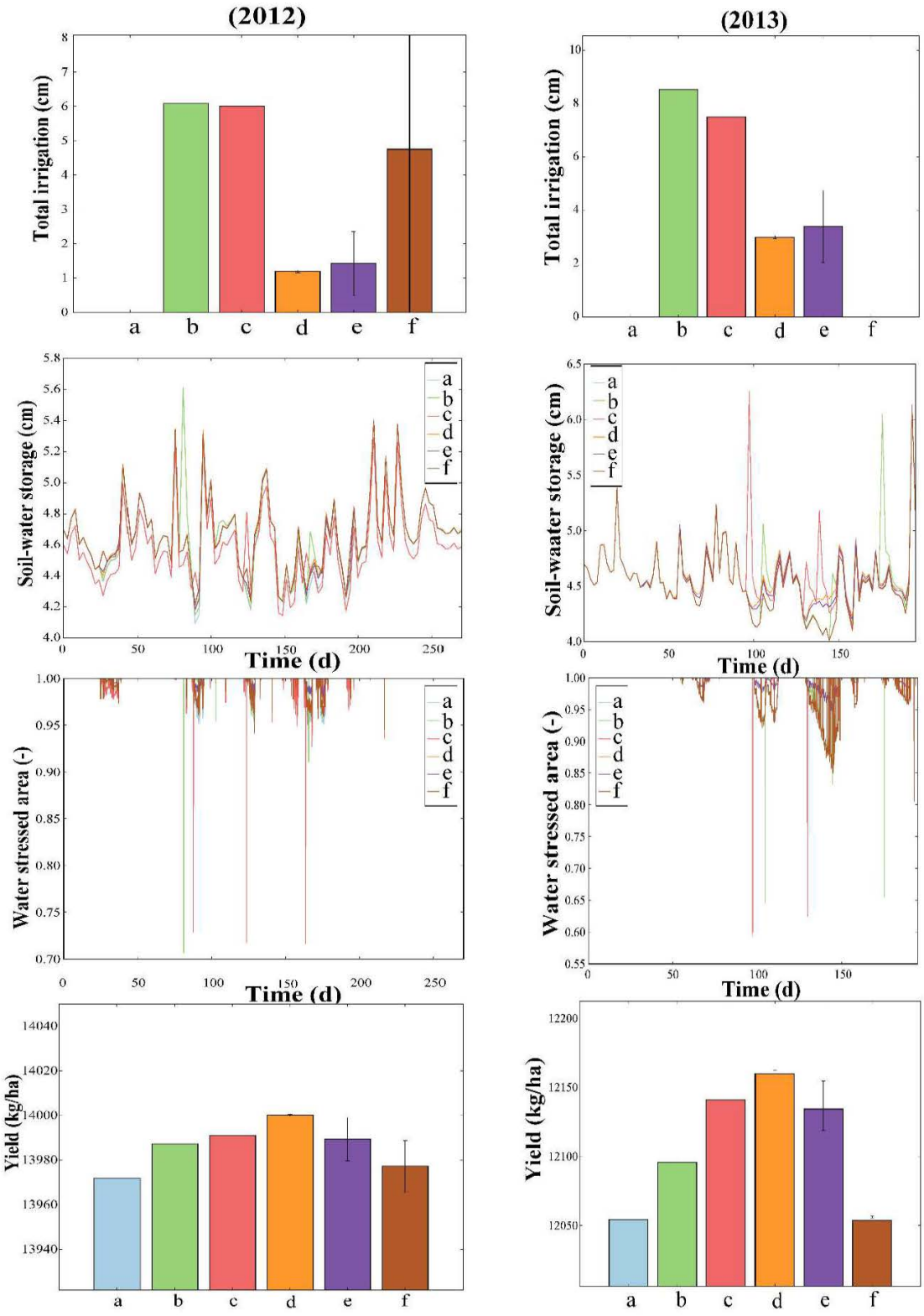

Figure 5-11. Effects of different irrigation scenarios (no- (a), current- (b), optimized- (c), triggered-10 x 10 m (d), triggered-100 x 100 m (e) and triggered-400 x 400 m (f)) with their applied water on yield and the average soil-water storage and water stress with time for 2012 (left) and 2013 (right).

In order to avoid yield reduction, annual total irrigation cost was the most expensive for the low resolution triggered irrigation scenario (resolution 400 x 400m) followed by the moderate resolution current and triggered irrigation scenario (200 x 200 m), the high resolution optimized irrigation scenario (10 x 10 m) and the high resolution triggered irrigation scenario (10 x 10 m) (Table 5-2). This illustrates the large water use efficiency and cost-effectiveness of irrigation planning using triggered irrigation with high resolution (10 x 10 m) by reducing irrigation cost. The best irrigation scheduling (triggered) requires only 124 and 300 m^3/ha in 2012 and 2013, which is 500% and 285% lower than under the current irrigation scenario, respectively. With a cost of 0.5 euro per m^3 of water at the study site at each irrigation event (including operational costs; 125 euro per ha for 25 mm irrigation), this results in a substantial cost reduction. Consequently, the economic benefit on a yearly basis is about 245 and 307 euro/ha for 2012 and 2013, respectively. An interesting result is the potential economic benefit in terms of yield (production) associated with different irrigation scenarios (Table 5-2). The yield deviation between the current and optimized irrigation scenario was 5 and 50 kg/ha for 2012 and 2013, respectively. It means that the efficiency of the optimized scenario was larger in 2013. The maximum yield difference between lower and higher resolutions in the triggered irrigation scenario was 22 and 107 kg/ha in 2012 and 2013, respectively. The yield difference between the high resolution current and triggered irrigation (10 x 10 m) was 13 and 65 kg/ha in 2012 and 2013, respectively. Considering the high resolution triggered irrigation scenario (10 x 10 m), the yield increased by 0.2 and 0.9% compared to the current irrigation regime in 2012 and 2013.

From a profitability point of view, a significant increase in yield cannot be seen. But in a dry year as in 2013, increase in yield was more than in a wetter year as in 2012. The results generated by coarser resolutions (100 x 100 and 400 x 400 m, in Table 5-2) are based on the "best sampling location" scenario (e.g. Figure 5-10, 100 x 100 m resolution- panels 6 and 8). In this example, other sampling locations did not change the yield but increased the irrigation amount (, 100 x 100 m resolution- panels 1-10). As discussed in the previous section, this confirms the importance of selecting the proper resolution as well as the proper strategic sampling location (the best sampling location). For irrigation management purposes at lower spatial resolution, it is important to select the optimal location to characterize a field. For management at higher resolution such as in precision agriculture, the sampling location does not matter that much, and when data are available at high resolution, this high spatial resolution is preferred (i.e., 10 x 10 m). The profitability should be considered as irrigation cost in our

case study. According to Table 5-2, it seems that “no-irrigation” is the best economic option among other scenarios. But the irrigation can be also considered in terms of security and quality of plant production. Nevertheless, yield increase can be more pronounced if the crop is changed to another one like potato. In this study, discussion about the fixed cost and investments is not given and it is beyond the objectives (we used numbers provided by the farmer as a lump sum of investment and fixed costs). The major costs we dealt about are the irrigation expenses (both operation, maintenance and water cost). When reducing irrigation events, duration and the area to be irrigated, the yield remains at the same level as with uniform irrigation (with larger number and amount of water consumption). Therefore, we would emphasis that the benefits are not the yield increase but the reducing other management costs.

Therefore, the final water productivity (economic benefit/water usage) could be high in case of high resolution triggered irrigation scheduling, compared to all other scenarios. It should be noted that we assumed the uncertainty of input factors (hydraulic parameters, FLD and GWL) to be uniform for all irrigation scenarios and different resolutions in this study which can affect the output uncertainty. Indeed, the contribution of GWL fluctuation should be taken into account in water flow simulation and hence, the investigation on this subject is an interesting path for agricultural applications and also future research. The presented approach and performing triggered irrigation seems hence applying variable irrigation distribution can be adopted by changing the speed of the Reel sprinkler and rate of water application in practice.

5.4 Conclusions

We developed an analyzing and visualization setup tool using the same flow model through the whole flow domain. To that end, we integrated Hydrus-1D with Python™ software and ran the tool for the whole field taking into account the spatial variability of input factors. In this modeling setup, the field was modelled as a collection of 1D columns (parallel columns) representing the different field conditions (combination of soil properties, GWL, root zone depth or first layer depth, FLD). Our developed quasi 3D modeling approach was able to reproduce high resolution spatial patterns of water stress, soil-water storage and crop yield more efficiently and effectively which can help to optimize irrigation strategies adequately and practically. The computational time efficiency of each model running strategy (pre and post processing) was calculated and evaluated. Results highlight the reasonable and good performance of the approach. Indeed, results show that higher grid resolutions reduced the uncertainty of the simulations which were affected by GWL, FLD and K_s. The approach allows

to scrutinize how simulations and performance are affected by various hydrological variables and their resolutions. Initial results demonstrate the need for an optimal irrigation strategy with water being supplied to different zones of the field. Four different irrigation scenarios with various resolution were tested to optimize irrigation scheduling with an optimal resolution. This study further illustrates that water consumption can be reduced significantly when taking into account the spatial variability of soil and field conditions. The potential of water saving, and thus cost and potential contamination and solute leaching hazard, essentially stems from reducing the non-beneficial water supply from the current irrigation strategy and/or optimized irrigation based on only limited points and taking into account the shallow groundwater influences particularly (i.e., trial and error (optimized) irrigation scenario).

The study clearly illustrated the benefits of using the modeling approach both in research and application. However, the model cannot precisely predict soil-water content at a specific location unless the model is calibrated and model parameters are optimized (Chapter 2 and 4). Nevertheless, our approach predicted soil water status in a reasonable range and it is promising to fill the gap between modeling and real situations in view of irrigation management. But, it is preferably used to evaluate relative changes in soil-water content in a spatial context, specifically when groundwater level plays a major role in water status simulations (Chapter 2). Indeed, this approach allows to evaluate irrigation strategies, to find the optimal irrigation scheduling to reduce the water consumption up to 300% with respect to common irrigation practice and ensuring water productivity. Therefore, the economic benefit could reach up to 2472 - 2971 Euro for the field on top of a yield increase of ~1%. This modeling approach and methodology could be used as an appropriate tool for water management (pave the path of decision-making) at any scale, with estimating the availability of water at each time and space, and contributing to a cost-effective irrigation program.

Chapter 6. ***General conclusions and future perspectives***

6.1 Introduction

Further improvement of current irrigation strategies with robust and novel irrigation technology is crucial. Advanced monitoring and modeling may promote efficient water utilization and an optimal water supply/distribution to increase food, feed, fiber and fuel production in response to worldwide water scarcity, climate change, growing populations and increasing water demands. This dissertation dealt with precision irrigation planning and agricultural management to achieve an optimal yield with a minimal water use. The main aim of this dissertation was to develop and test methods for optimizing irrigation efficiency using a combination of sensors and process-based soil hydrological models integrated with crop growth models. These methods are not only extremely relevant for arid and semi-arid conditions, but also for the management of intensively used agricultural fields in West- and Southern Europe suffering from summer droughts related to climate change. To address the general aim of study, the focus was put on different aspects of modeling, i.e. model parameterization, sensitivity analysis, calibration and validation, integration of hydrological and crop growth models, irrigation optimization, on providing the required hydraulic input data for field scale modeling, i.e., by estimation methods, field and lab measurements of hydraulic parameters, and on developing a modeling approach for simulating water distribution at the field scale.

6.2 Plot scale modeling

A first step in the thesis was the evaluation of the soil hydrological model that is used in the remainder of the dissertation at the plot scale through modeling one dimensional water flow and redistribution in the soil profile (Chapter 2). Parameterization scenarios for the calibration and validation of the model were tested. The results demonstrated clearly the profound effect of the position of the groundwater table on the estimated soil-water content and associated water stress for a sandy two-layered soil under grass in a temperate maritime climate. Furthermore, field scale variations in soil-water content were found to be very large, due to the spatial variability of hydraulic parameters such as K_s, topography and groundwater level (GWL). The study also provided a suitable procedure to apply the hydrological model in combination with crop growth modeling for irrigation scheduling by the practitioners. This type of modeling setup for precision agricultural management may be extended from the field to a local or regional scale and to different crops from the studied area.

6.2.1 Model concept and boundary conditions

When using hydrological models for irrigation calculations, a sensitivity analysis allows evaluating the appropriate model conceptualization and parameterization together with the appropriate boundary conditions to calculate soil-water stress. In this work, a variety of conceptualizations was carried out to select the appropriate conditions and to identify the associated parameters for a 1D soil profile. The effect of soil layering (Chapter 2) was evaluated by comparing the two layered-soil profile with a homogeneous profile using the effective hydraulic conductivity and the arithmetic average of hydraulic properties based on soil layer thickness. Simulations using the heterogeneous profile with two layers fitted the observed water content data best, which was also confirmed by field observations showing distinct layers.

The results showed that the water content was not sensitive to separating evaporation and transpiration in the reference evapotranspiration (ET_o), which has its own uncertainty in calculating the split between the two. Therefore, ET_o was entered as one of the upper boundary variables for the hydrological model and the leaf area index, LAI was used to take into account crop water uptake. The results clearly showed the great importance of the bottom boundary condition (e.g. free drainage, variable and constant head) in estimating soil-water content and water stress in the soil profile, even for groundwater depths well below 120 cm depth and sandy soils. The effect of the boundary condition may well exceed the impact of the uncertainty on hydraulic parameters in a parameter optimization. This reflects the need for an accurate determination of the bottom boundary condition i.e., GWL, both in space and time (Chapter 2). The tempo-spatial changes of groundwater levels have important consequences for precision irrigation management and variable water applications at sub-field scale. Therefore, the variable bottom boundary condition would be a better option to simulate water content in better agreement with observations. Consequently, groundwater depth fluctuations should be monitored continuously using for example a Diver (Mini-Diver, Eijkelkamp Agrisearch Equipment, Giesbeek, The Netherlands) at different locations in the field (Chapter 4).

Before optimizing hydraulic model parameters, the effect of model conceptualization and of the boundary conditions should therefore be assessed. Accordingly, testing model conceptualizations (with different degrees of complexity) and parameter sensitivity analysis provide insight in the most important aspects in model performance assessment.

6.2.2 Sensitivity analysis

A time-dependent local sensitivity analysis of the hydraulic parameters showed that changes in soil-water content were mainly affected by the soil saturated hydraulic conductivity K_s and the Mualem-van Genuchten retention curve shape parameters n and α (Chapter 2). The fact that the model predictions, especially in the upper part of the soil profile, were extremely sensitive to variations in hydraulic parameters in dry periods. Specifically, for irrigation management which occurs in the dry periods of the year, this is of great importance. To improve the timing of irrigation in these crucial periods, numerical soil models that are used to determine irrigation requirement, need to be well parametrized for α, n and K_s. Determining the initial values (initial-estimates) of these hydraulic parameter is the first step since in the parametrization process, the optimized values are strongly dependent on their initial values and the initial estimates must be reasonably close to their true values. The initial estimations can be taken from various sources: from pedotransfer functions (PTFs) applied to soil basic information, with different datasets depending on available information (Chapter 4). Secondly, they can be determined from laboratory or in situ experiments (Chapter 2 and 4). Thirdly, the initial parameter values can be estimated using field proximally sensed data such as ECa derived by EMI techniques (Chapter 3). The effect of these various sources of basic soil information was tested in this dissertation.

The application of a time variant sensitivity analysis is crucial with respect to parameterization of hydraulic parameters for irrigation management and will be useful in a wide set of conditions, climates and soil types. In the chapters 1 and 2 we elaborated on the drawbacks of a local sensitivity analysis (LSA). LSA is a straightforward methodology, which we consider as an essential step within the modeling workflow to learn about model behavior and to identify key parameters. We found that the selection of a LSA is sufficient since the interest goes specifically to the measured parameter values. However, the results of the LSA of this study cannot be generalized towards other applications, due to the case-specific aspects.

6.2.3 Model parameterization

This study was conducted based on relatively simplified assumptions in modeling approach, in which optimized irrigation scheduling is the main concern. It was found that in optimizing the hydraulic model parameters, the effect of the boundary conditions should be assessed simultaneously and then the appropriate boundary conditions should be chosen in terms of water stress (root water uptake) and soil-water content.

Special attention was given to possible problems of parameter non-uniqueness related to the inverse solution. The parametrization scenarios in the calibration and validation stage of model development were kept simple in view of the information they generate. The scenarios clearly showed that it is sufficient to optimize only a limited number of key parameters (i.e., K_s). Furthermore, it was shown that optimization strategies involving multiple parameters (as result of LSA) do not perform better in view of optimization for irrigation management.

The choice of the calibration period may influence the results of parameter optimization. In our study the observed soil-water content range and dynamics, rainfall intensity and ET_o were similar in the calibration and validation periods (relevant for irrigation management) and a similar model response and performance is expected in other periods. Therefore, selecting a sufficiently long period in a growing season with several drying and wetting events was suggested as good modeling practice.

6.2.4 Optimizing irrigation schemes

The degree of water stress is a good criterion to evaluate irrigation supply scenarios in irrigation management. Soil-water status was converted into water stress and crop yield using a crop growth model. Different optimization scenarios were tested that affected water stress and crop yield. Variations in parameter optimization (two-, three-, four- or six-parameter optimizations) did not affect the calculated water stress and yield reduction as significantly as does the bottom boundary. Therefore, these results again confirm the importance of the optimization of the boundary conditions (to accurately describe recharge to or from groundwater) on top of the hydraulic parameters (to accurately describe soil-water content variation in the topsoil) for irrigation management purposes.

Overall, we would stress that at the field scale non-uniform irrigation distribution (water supply in dryer parts with groundwater level below 120 cm) may be necessary and will result in cost saving for the farmer. Also, timing of the irrigation could be improved by considering actual soil-water status, crop condition and weather forecast using a combined hydrological and crop growth model in irrigation management and precision agriculture. Using soil-water stress as a benchmark, it was shown that a combined modeling approach could increase water use efficiency (12-22.5%) and yield (5-7%) by changing the irrigation scheduling from the current strategy to ‘trial and error’ irrigation optimization at a plot scale study (Chapter 2). Another irrigation scheme which can automate the irrigation scheduling is the triggered irrigation that

is implemented in Hydrus. Using this option, irrigation can be triggered when the pressure head at a selected observation depth drops below a specific value e.g. field capacity, to eliminate soil-water stress. However, high efficiencies can only be achieved if rainfall is known a priori, i.e. while the soil-water status could indicate when to irrigate, it would be impossible to know how much to irrigate if the rainfall cannot be accurately predicted. Therefore, the results of the study call for taking into account accurate weather forecast and water content data in irrigation management and precision agriculture.

6.3 Field scale K_s prediction

To accurately determine the field-scale irrigation requirements, determining the spatial distribution of the most sensitive model parameters (in our case study: K_s) is crucial. Results (Chapter 3) demonstrated the large spatial variability of all studied properties with K_s being the most variable one (CV = 86.21%). Good correlations were found between K_s and ECa data derived by a DUALEM-21S sensor. A semi-log empirical relation was proposed and validated (using an independent dataset of measured K_s) to estimate the spatial distribution of K_s using ECa as a proxy. The statistical performance indicators of the relation and its map demonstrate a high coefficient of determination between predicted and measured K_s (r^2 = 0.67), a high coefficient of model efficiency (C_e = 0.64), and a relatively low root-mean-square estimation error (RMSEE = 0.74 cm h^{-1}). These indicate the good accuracy and prediction efficiency of the developed regression model. Based on the relationship, a detailed map of K_s was produced. This approach offers a promising perspective to facilitate the collection of high resolution data by geophysical surveys and provide more comprehensive information of K_s distribution. The inverse distance weighting (IDW) interpolation method was also tested and compared with the empirical relation. Results showed that the developed semi-log relation between K_s and ECa is a better estimator for the prediction of K_s than IDW interpolation. The relative RMSEE of the regression model and IDW interpolation of K_s predictions were 57 and 82%, respectively. Overall, these results confirm that the estimation of K_s from the established regression model using the ECa estimator is satisfactory and certainly reasonable for hydrological modeling.

6.4 In-situ and laboratory hydraulic parameter sets and model performance

The value of measuring soil hydraulic properties with field (infiltrometry and inverse modeling) and lab methods was assessed (Chapter 4). Results show that both are correlated

(with positive correlations being observed between lab and field MVG parameters (r≥0.55)), though both methods generated significantly different values. Laboratory tests yielded 2–30 times higher K_s values than those derived from field infiltration measurements. Inverse optimization resulted in an excellent match between observed and fitted infiltration rates in combination with soil-water content at the end of the experiment. This method also resulted in close correspondence of α and K_{fs} with those from the Logsdon and Jaynes (1993) solution of the Wooding's equation for the sandy soil in the study field. We found the Gardner parameter α_G to be related to the optimized van Genuchten parameters α_{vG} and n as $\alpha_G \approx \alpha_{vG}\, n$.

The relevance of the difference in lab and field hydraulic parameter sets was evaluated by comparing water content predictions to observations. Results indicated a better performance when using the laboratory data set from middle to deeper depths (i.e., 30 to 60 cm). In the two soil profiles under study, field parameter sets, which were less time consuming and labor intensive to achieve, resulted in slightly better soil-water content simulations in the topsoil (0 to 20 cm) where the plant roots are concentrated, and soil-water potential in the subsoil (50 cm depth). Generally, in view of precision agriculture, field measurements and inverse optimization approaches are preferred to determine soil hydraulic properties. Based on the simulation results of the study, it is not possible to judge whether laboratory or field methods should be preferred.

6.5 Field scale irrigation optimization, quasi 3D approach

The plot scale model was coupled to the 2D maps of groundwater depth, first layer thickness and hydraulic conductivity K_s. Thus, a quasi 3D modeling approach was developed to simulate and visualize high resolution spatial patterns of water flow, water storage, water stress and crop yield over the entire heterogeneous sandy field (Chapter 5).

Evaluating computational performance and time efficiency of the modeling setup (pre and post processing) illustrated good performance and high effectiveness of the approach. Taking into account higher resolution input data for GWL, FLD and K_s, reduced the uncertainty of simulations while, approaches treating the field as a homogeneous unit or dividing the field in a limited number of management zone lose information in view of irrigation management. Results showed that a 10 x 10 m resolution is sufficient, reasonable and fits with current irrigation technology which can be selected in view of modeling approach, precision agriculture and water management strategy. Future developments in irrigation technology can

be assessed using the proposed 3D-modeling approach. This approach provides high resolution predictions and could also be generalized for any area of interest.

We found that the uniform distribution of water using standard gun sprinkler irrigation may not be an efficient approach since at locations with shallow groundwater, the amount of water applied will be excessive as compared to the crop requirements, while in locations with a deeper groundwater table, the crop irrigation requirements will not be met during crop water stress. Therefore, four irrigation scenarios (no, current, optimized (trial and error) and triggered irrigation scenarios) were assessed using a quasi 3D modeling approach to find the optimal and most cost-effective irrigation scheduling. Numerical results showed that optimal irrigation scheduling was obtained by triggered irrigation, using the aforementioned water stress (duration and extension) and stressed area calculations and soil pressure heads resulting in saving up to ~300% irrigation water as compared to the current irrigation regime, while yield was not significantly affected (increase of ~1%). Reducing the water consumption would result in an economic benefit which could reach up to 2472 - 2971 euro for the study area (10.5 ha) on top of yield increase. Overall, it can be stated that the presented approaches and the modeling methodology applied in this study are generic and can be used for a range of crops, soils and topography.

6.6 Future perspective

Further knowledge is required to design and improve spatially distributed irrigation strategies at the field scale. Throughout the different chapters in the manuscript, efforts were made to characterize and model water flow in soils for irrigation optimization. This study proved that the modeling approach we suggested is a feasible solution for precision irrigation management. From the results and conclusions, the following ideas are suggested regarding prospective research:

- The effects of soil layering and boundary conditions on model performance have been taken into account based on the observation and subsequent conceptualization (see Chapters 2 and 4). It would be interesting to know what happens to the model output if the soil profile is divided into several individual layers (model abstraction) with their specific hydraulic parameters and also in such cases with no evidence of pedogenic layers. A kind of model abstraction can show the differences of model conceptualization on the model performance. In this study, specific boundary

conditions for temperate climatological conditions, i.e., shallow groundwater, rainfed and irrigation water supply were considered to affect water fluxes in the subsoil, and the results were limited to the soil type at the study site. Further research is necessary to apply the model to soil water flow and solute transport processes in different soil types especially in arid and semi-arid area with deeper GWL and without rainfall during the growing season.

- Because of the lack of information on GWL fluctuation in time and space (one of the limitation factor in the study), it is suggested to integrate the tool with groundwater models such as MODFLOW. These models provide time series of GWL which can be used in unsaturated zone tools in an iterative approach. This approach can further help to evaluate the effects of variable and constant bottom boundary conditions on water flow and consequently water management strategies.
- In an effort to optimize irrigation management using a combination of hydrological and crop growth models, this study highlighted advantages and limitations to be addressed here and by future work. The integrated model (quasi 3D modeling) performed efficiently in this study and can be regarded as a general tool for irrigation management. However, it is not clear from the current results how the model will perform in more complicated optimization problems e.g., multiobjective optimization at different locations of the field. We found that the Levenberg-Marquardt algorithm is sufficient in our study to calibrate the model for shallow groundwater conditions and to investigate the sensitivity of hydraulic parameters and boundary conditions. However, we did not compare different optimization processes using different algorithms. Future studies may compare different complexity levels of optimization problems (using several algorithms and models). In that case, multiobjective optimization could also be used to evaluate the simultaneous optimization of boundary conditions, hydraulic parameters and other variables especially for deeper GWL.
- As mentioned previously, the study was carried out based on a relatively simplified modeling setup, in which optimized irrigation scheduling was the main concern. More realistic modeling approaches may incorporate other considerations such as water quality, solute and fertilizer leaching (nitrate), etc. so this would warrant a separate study on these matters.
- The research study presents a new modeling approach to optimize full irrigation with an integrated crop growth model, hydrological model and optimization processes.

Hence an optimal irrigation scheduling (full irrigation) was out forward and applied in the study region. However, we suggest to also use the provided framework of this study to examine deficit irrigation strategies.

- The output of downscale climate model can be used as input of hydrological model to evaluate what would be need for future irrigation management. It is also suggested that the tool couple with the downscale regional climate models.
- It is suggested that the approach will be tested for different soils and presence of the slope and other possible conditions regards to different crops.
- A user friendly application (graphical interface) could be developed in which the integrated model implementation in Python^{TM} could be easily and more efficiently used by farmers or applicants.
- Precision irrigation management requires accurate information on spatial variation of field hydraulic properties and in-detail observations. Characterizing field scale soil hydraulic properties can be done by linking them to ECa, which can be measured efficiently and inexpensively, so a spatially dense dataset for describing within-field spatial soil variability could be generated. Further research may attempt to answer the following specific question: how can theoretical and empirical relationships of field ECa data, hydraulic conductivity *K*, and soil water retention data SWR, be applied to predict *K* and SWR more accurately and effectively at the field scale. It can be explored to estimate MVG hydraulic parameters (*K* and SWR) by establishing an in-situ relationship between ECa and hydraulic parameters using empirical and semi-empirical relations such as Archie's first and second laws (1942).
- Results of our study do not confirm whether laboratory or field experiments data sets are most appropriate to predict soil water fluctuations in a complete soil profile, while field experiments are preferred in many studies. On the other hand, results also suggested that parameter optimization is necessary over a longer time such as a full growing season, in combination with independent soil-water content and soil-water potential data, to obtain an effective parameter set. In addition, a deeper knowledge of the effect of temporal and spatial changes in hydraulic properties is needed to achieve better agreement between measured and simulated values. Therefore, further research is required to test the optimization processes in this respect. However, the validity of optimized parameters should always be carefully evaluated because they may merely be a result of modeling rather than reflecting actual realistic soil physical values.

References

Abbasi, F., Feyen, J., van Genuchten, M.T., 2004. Two-dimensional simulation of water flow and solute transport below furrows: model calibration and validation. J Hydrol, 290(1-2): 63-79. DOI:10.1016/j.jhydrol2.003.11.028

Abbasi, F., Jacques, D., Šimůnek, J., Feyen, J., van Genuchten, M.T., 2003a. Inverse estimation of soil hydraulic and solute transport parameters from transient field experiments: Heterogeneous soil. T Asae, 46(4): 1097-1111.

Abbasi, F., Šimůnek, J., Feyen, J., van Genuchten, M.T., Shouse, P.J., 2003b. Simultaneous inverse estimation of soil hydraulic and solute transport parameters from transient field experiments: Homogeneous soil. T Asae, 46(4): 1085-1095.

Abbaspour, K.C., Rouholahnejad, E., Vaghefi, S., Srinivasan, R., Yang, H., Klove, B., 2015. A continental-scale hydrology and water quality model for Europe: Calibration and uncertainty of a high-resolution large-scale SWAT model. J Hydrol, 524: 733-752. DOI:10.1016/j.jhydrol.2015.03.027

Abdu, H., Robinson, D.A., Seyfried, M., Jones, S.B., 2008. Geophysical imaging of watershed subsurface patterns and prediction of soil texture and water holding capacity. Water Resour Res, 44. DOI:DOI:10.1029/2008wr007043

Abedinpour, M., Sarangi, A., Rajput, T.B.S., Singh, M., 2014. Prediction of maize yield under future water availability scenarios using the AquaCrop model. J Agr Sci, 152(4): 558-574. DOI:10.1017/S0021859614000094

Abit, S.M., Amoozegar, A., Vepraskas, M.J., Niewoehner, C.P., 2008. Solute transport in the capillary fringe and shallow groundwater: Field evaluation. Vadose Zone J, 7(3): 890-898. DOI:10.2136/vzj.2007.0102

Abrahamsen, P., Hansen, S., 2000. Daisy: an open soil-crop-atmosphere system model. Environ Modell Softw, 15(3): 313-330. DOI:Doi 10.1016/S1364-8152(00)00003-7

Aggarwal, P.K., Kalra, N., Chander, S., Pathak, H., 2006. InfoCrop: A dynamic simulation model for the assessment of crop yields, losses due to pests, and environmental impact of agro-ecosystems in tropical environments. I. Model description. Agr Syst, 89(1): 1-25. DOI:10.1016/j.agsy.2005.08.001

Akhtar, F., Tischbein, B., Awan, U.K., 2013. Optimizing deficit irrigation scheduling under shallow groundwater conditions in lower reaches of Amu Darya river basin. Water Resour Manag, 27(8): 3165-3178. DOI:10.1007/s11269-013-0341-0

Al-Said, F.A., Ashfaq, M., Al-Barhi, M., Hanjra, M.A., Khan, I.A., 2012. Water Productivity of Vegetables under Modern Irrigation Methods in Oman. Irrig Drain, 61(4): 477-489. DOI:10.1002/ird.1644

Allen, R.G., Pereira, L.S., Raes, D., Smith, M., 1998. Crop evapotranspiration, FAO Irrig. Drain. Paper 56, Rome, Italy.

Alletto, L., Coquet, Y., 2009. Temporal and spatial variability of soil bulk density and near-saturated hydraulic conductivity under two contrasted tillage management systems. Geoderma, 152(1-2): 85-94. DOI:10.1016/j.geoderma.2009.05.023

American Society of Civil Engineers, A.S.C.E., 1993. Criteria for Evaluation of Watershed Models. Journal of Irrigation and Drainage Engineering, 119(3): 429-442. DOI:10.1061/(ASCE)0733-9437(1993)119:3(429)

Amiri, E., Gohari, A.A., Mianabadi, A., 2015. Evaluation of water schemes for peanut, using CSM-CROPGRO-Peanut model. Arch Agron Soil Sci, 61(10): 1439-1453. DOI:10.1080/03650340.2015.1017568

An, Y., Han, S., Wu, X., Cheng, X., Liu, W., 2012. Numerical Simulation and Prediction of High Fluorine Groundwater Transport in Zhangye Basin. In: Wu, J.H., Zhao, M., Wu, B. (Eds.), Intelligent System and Applied Material, Pts 1 and 2. Advanced Materials Research, pp. 36-41. DOI:10.4028/www.scientific.net/AMR.466-467.36

Andersen, D.S., Burns, R.T., Moody, L.B., Helmers, M.J., Horton, R., 2010a. Comparison of the iowa state university effluent limitation guidelines model with the soil-plant-air-water model for evaluating containment basin performance. T Asabe, 53(1): 207-217.

Andersen, D.S., Burns, R.T., Moody, L.B., Helmers, M.J., Horton, R., Pederson, C., 2010b. Use of the soil-plant-air-water model to predict hydraulic performance of vegetative treatment areas controlling open lot runoff. T Asabe, 53(2): 537-543.

Angulo-Jaramillo, R., Vandervaere, J.P., Roulier, S., Thony, J.L., Gaudet, J.P., Vauclin, M., 2000. Field measurement of soil surface hydraulic properties by disc and ring infiltrometers - A review and recent developments. Soil Till Res, 55(1-2): 1-29. DOI:Doi 10.1016/S0167-1987(00)00098-2

Angulo, C., Gaiser, T., Rotter, R.P., Borgesen, C.D., Hlavinka, P., Trnka, M., Ewert, F., 2014. 'Fingerprints' of four crop models as affected by soil input data aggregation. Eur J Agron, 61: 35-48. DOI:10.1016/j.eja.2014.07.005

Ankeny, M.D., Ahmed, M., Kaspar, T.C., Horton, R., 1991. Simple Field Method for Determining Unsaturated Hydraulic Conductivity. Soil Sci Soc Am J, 55(2): 467-470.

Araya, A., Hoogenboom, G., Luedeling, E., Hadgu, K.M., Kisekka, I., Martorano, L.G., 2015. Assessment of maize growth and yield using crop models under present and future climate in southwestern Ethiopia. Agr Forest Meteorol, 214: 252-265. DOI:10.1016/j.agrformet.2015.08.259

Archie, G.E., 1942. The electrical resistivity log as an aid in determining some reservoir characteristics. Transactions of the American Institute of Mining, Metallurgical and Prtrolium Engineers, 146(01): 54-62. DOI:DOI:10.2118/942054-G

Arnold, J.G., Allen, P.M., Bernhardt, G., 1993. A Comprehensive Surface-Groundwater Flow Model. J Hydrol, 142(1-4): 47-69. DOI:Doi 10.1016/0022-1694(93)90004-S

Atkinson, M.D., Kettlewell, P.S., Hollins, P.D., Stephenson, D.B., Hardwick, N.V., 2005. Summer climate mediates UK wheat quality response to winter North Atlantic Oscillation. Agr Forest Meteorol, 130(1-2): 27-37. DOI:10.1016/j.agrformet.2005.02.002

Awan, U., Tischbein, B., Kamalov, P., Martius, C., Hafeez, M., 2012. Modeling Irrigation Scheduling Under Shallow Groundwater Conditions as a Tool for an Integrated Management of Surface and Groundwater Resources. In: Martius, C., Rudenko, I., Lamers, J.P.A., Vlek, P.L.G. (Eds.), Cotton, Water, Salts and Soums. Springer Netherlands, pp. 309-327. DOI:10.1007/978-94-007-1963-7_19

Awan, U.K., Tischbein, B., Martius, C., 2015. Simulating groundwater dynamics using feflow-3d groundwater model under complex irrigation and drainage network of dryland ecosystems of central asia. Irrig Drain, 64(2): 283-296. DOI:10.1002/ird.1897

Baetens, J.M., Verbist, K., Cornelis, W.M., Gabriels, D., Soto, G., 2009. On the influence of coarse fragments on soil water retention. Water Resour Res, 45. DOI:Artn W0740810.1029/2008wr007402

Bakkes, J., Aalbers, L., Biggs, O., Hoff, H., Peterson, G., 2009. Getting into the right lane for 2050: a primer for EU debate, Netherlands Environmental Assessment Agency, Bilthoven.

Baldioli, M. et al., 1994. Expert N, Ein Baukastensystem zur Simulation der Stickstoffdynamik in Boden und Pflanze. Version 1.0, Bodenoekologie, Neuherberg, Germany.

Bamberg, A.L., Cornelis, W.M., Timm, L.C., Gabriels, D., Pauletto, E.A., Pinto, L.F.S., 2011. Temporal changes of soil physical and hydraulic properties in strawberry fields. Soil Use Manage, 27(3): 385-394. DOI:10.1111/j.1475-2743.2011.00355.x

Banedjschafie, S., Bastani, S., Widmoser, P., Mengel, K., 2008. Improvement of water use and N fertilizer efficiency by subsoil irrigation of winter wheat. Eur J Agron, 28(1): 1-7. DOI:http://dx.doi.org/10.1016/j.eja.2007.03.004

Bardossy, A., Li, J., 2008. Geostatistical interpolation using copulas. Water Resour Res, 44(7). DOI:Artn W0741210.1029/2007wr006115

Barrett, P.D., Laidlaw, A.S., Mayne, C.S., 2004. An evaluation of selected perennial ryegrass growth models for development and integration into a pasture management decision support system. J Agr Sci, 142: 327-334. DOI:Doi 10.1017/S0021859604004289

Barrett, P.D., Laidlaw, A.S., Mayne, C.S., 2005. GrazeGro: a European herbage growth model to predict pasture production in perennial ryegrass swards for decision support. Eur J Agron, 23(1): 37-56. DOI:10.1016/j.eja.2004.09.006

Barron, J., Rockstrom, J., Gichuki, F., Hatibu, N., 2003. Dry spell analysis and maize yields for two semi-arid locations in east Africa. Agr Forest Meteorol, 117(1-2): 23-37. DOI:10.1016/S0168-1923(03)00037-6

Bastiaanssen, W.G.M., Allen, R.G., Droogers, P., D'Urso, G., Steduto, P., 2004. Inserting man's irrigation and drainage wisdom into soil water flow models and bringing it back out: how far have we progressed? In: Feddes, R.A., de Rooij, G.H., van Dam, J.C. (Eds.), Unsaturated-zone Modeling: Progress, Challenges and Applications, Wageningen, the Netherland, pp. 263-299.

Bates, B.C., Kundzewicz, Z.W., Wu, S., Palutikof, J.P., 2008. Climate change and water. Technical paper of the Intergovernmental Panel on Climate Change, Geneva, IPCC Secretariat.

Beersma, J.J., Buishand, T.A., 2007. Drought in the Netherlands - Regional frequency analysis versus time series simulation. J Hydrol, 347(3-4): 332-346. DOI:10.1016/j.jhydrol.2007.09.042

Boomiraj, K., Chakrabarti, B., Aggarwal, P.K., Choudhary, R., Chander, S., 2010. Assessing the vulnerability of Indian mustard to climate change. Agr Ecosyst Environ, 138(3-4): 265-273. DOI:10.1016/j.agee.2010.05.010

Bormann, H., 2012. Assessing the soil texture-specific sensitivity of simulated soil moisture to projected climate change by SVAT modelling. Geoderma, 185: 73-83. DOI:10.1016/j.geoderma.2012.03.021

Botors, F.E., Harter, T., Onsoy, Y.S., Tuli, A., Hopmans, J.W., 2009. Spatial Variability of Hydraulic Properties and Sediment Characteristics in a Deep Alluvial Unsaturated Zone. Vadose Zone J, 8(2): 276-289. DOI:10.2136/vzj2008.0087

Botula, Y.-D., Van Ranst, E., Cornelis, W.M., 2014. Pedotransfer functions to predict water retention for soils of the humid tropics: a review. Revista Brasileira de Ciência do Solo, 38: 679-698.

Bouazzama, B., Mailhol, J.C., Xanthoulis, D., Bouaziz, A., Ruelle, P., Belhouchette, H., 2013. Silage Maize Growth Simulation Using Pilote and Cropsyst Model. Irrig Drain, 62(1): 84-96. DOI:10.1002/ird.1715

Bouma, J., 1989. Using Soil Survey Data for Quantitative Land Evaluation. In: Stewart, B.A. (Ed.), Advances in Soil Science. Advances in Soil Science. Springer US, pp. 177-213. DOI:10.1007/978-1-4612-3532-3_4

Bouman, B.A.M., Schapendonk, A.H.C.M., Stol, W., van Kraalingen, D.W.G., 1996. Description of the grassland growth model LINGRA as implemented in CGMS Ispra, Italy.

Brooking, I.R., Jamieson, P.D., Porter, J.R., 1995. The Influence of Daylength on Final Leaf Number in Spring Wheat. Field Crop Res, 41(3): 155-165. DOI:Doi 10.1016/0378-4290(95)00014-H

Brosten, T.R., Day-Lewis, F.D., Schultz, G.M., Curtis, G.P., Lane Jr, J.W., 2011. Inversion of multi-frequency electromagnetic induction data for 3D characterization of hydraulic conductivity. Journal of Applied Geophysics, 73(4): 323-335. DOI:http://dx.doi.org/10.1016/j.jappgeo.2011.02.004

Brouwer, C., Prins, K., Kay, M., Heibloem, M., 1988. Irrigation Water Management: Irrigation Methods, Rome, Italy.

Brown, D.M., , 1969. Heat units for corn in southern Ontario, Ontario Ministry of Agriculture and Food, Factsheet Agdex l1/31, Toronto.

Brown, H.E., Huth, N., Holzworth, D., 2011. A potato model built using the APSIM Plant.NET Framework. 19th International Congress on Modelling and Simulation (Modsim2011): 961-967.

Brun, R., Reichert, P., Kunsch, H.R., 2001. Practical identifiability analysis of large environmental simulation models. Water Resour Res, 37(4): 1015-1030. DOI:Doi 10.1029/2000wr900350

Brunner, P., Simmons, C.T., 2012. HydroGeoSphere: A Fully Integrated, Physically Based Hydrological Model. Ground Water, 50(2): 170-176. DOI:10.1111/j.1745-6584.2011.00882.x

Brutsaert, W., 2005. Hydrology, An Introduction. . Cambrige University Press, Cambridge, United Kingdom.

Bultot, F., Dupriez, G.L., 1976. Conceptual Hydrological Model for an Average-Sized Catchment-Area .1. Concepts and Relationships. J Hydrol, 29(3-4): 251-272. DOI:Doi 10.1016/0022-1694(76)90040-8

Burguete, J., Lacasta, A., Garcia-Navarro, P., 2014. SURCOS: A software tool to simulate irrigation and fertigation in isolated furrows and furrow networks. Comput Electron Agr, 103: 91-103. DOI:10.1016/j.compag.2014.02.004

Burt, C.M., Clemmens, A.J., Bliesner, R., Merriam, J.L., Hardy, L., 2000. Selection of Irrigation Methods for Agriculture. On-Fam Irrigation Committee. American society of civil engineers.

Butkus, D., Konstantinova, M., 2008. Modelling vertical migration of Cs-137 in Lithuanian soils. Journal of Environmental Engineering and Landscape Management, 16(1): 23-29. DOI:10.3846/1648-6897.2008.16.23-29

Butterfield, R.E., Morison, J.I.L., 1992. Modeling the Impact of Climatic Warming on Winter Cereal Development. Agr Forest Meteorol, 62(3-4): 241-261. DOI:Doi 10.1016/0168-1923(92)90017-X

Caldwell, T.G., Wöhling, T., Young, M.H., Boyle, D.P., McDonald, E.V., 2013. Characterizing Disturbed Desert Soils Using Multiobjective Parameter Optimization. Vadose Zone J, 12(1). DOI:10.2136/vzj2012.0083

Camp, C.R., Lamm, F.R., Evans, R.G., Phene, C.J., 2000. Subsurface drip irrigation -Past, present, and future, Phoenix, Az,.

Carrera-Hernández, J.J., Smerdon, B.D., Mendoza, C.A., 2012. Estimating groundwater recharge through unsaturated flow modelling: Sensitivity to boundary conditions and vertical discretization. J Hydrol, 452–453(0): 90-101. DOI:http://dx.doi.org/10.1016/j.jhydrol.2012.05.039

Carrera, J., Alcolea, A., Medina, A., Hidalgo, J., Slooten, L.J., 2005. Inverse problem in hydrogeology. Hydrogeol J, 13(1): 206-222. DOI:10.1007/s10040-004-0404-7

Carrera, J., Neuman, S.P., 1986. Estimation of Aquifer Parameters under Transient and Steady-State Conditions .2. Uniqueness, Stability, and Solution Algorithms. Water Resour Res, 22(2): 211-227. DOI:DOI 10.1029/WR022i002p00211

Carrion, F., Tarjuelo, J.M., Hernandez, D., Moreno, M.A., 2013. Design of microirrigation subunit of minimum cost with proper operation. Irrigation Sci, 31(5): 1199-1211. DOI:10.1007/s00271-013-0399-8

Carroll, Z.L., Oliver, M.A., 2005. Exploring the spatial relations between soil physical properties and apparent electrical conductivity. Geoderma, 128(3-4): 354-374. DOI:DOI:10.1016/j.geoderma.2005.03.008

Cartwright, N., Jessen, O.Z., Nielsen, P., 2006. Application of a coupled ground-surface water flow model to simulate periodic groundwater flow influenced by a sloping boundary, capillarity and vertical flows. Environ Modell Softw, 21(6): 770-778. DOI:http://dx.doi.org/10.1016/j.envsoft.2005.02.005

Castaneda-Vera, A., Leffelaar, P.A., Alvaro-Fuentes, J., Cantero-Martinez, C., Minguez, M.I., 2015. Selecting crop models for decision making in wheat insurance. Eur J Agron, 68: 97-116. DOI:10.1016/j.eja.2015.04.008

Cattivelli, L. et al., 2008. Drought tolerance improvement in crop plants: An integrated view from breeding to genomics. Field Crop Res, 105(1-2): 1-14. DOI:10.1016/j.fcr.2007.07.004

Celia, M.A., Binning, P., 1992. A mass conservative numerical solution for two-phase flow in porous media with application to unsaturated flow. Water Resour Res, 28(10): 2819-2828. DOI:10.1029/92WR01488

Chaplot, V., Jewitt, G., Lorentz, S., 2011. Predicting plot-scale water infiltration using the correlation between soil apparent electrical resistivity and various soil properties. Phys Chem Earth, 36(14-15): 1033-1042. DOI:DOI:10.1016/j.pce.2011.08.017

Chaplot, V., Lorentz, S., Podwojewski, P., Jewitt, G., 2010. Digital mapping of A-horizon thickness using the correlation between various soil properties and soil apparent electrical resistivity. Geoderma, 157(3-4): 154-164. DOI:DOI: 10.1016/j.geoderma.2010.04.006

Chapuis, R.P., 2004. Predicting the saturated hydraulic conductivity of sand and gravel using effective diameter and void ratio. Can Geotech J, 41(5): 787-795. DOI:DOI: 10.1139/T04-022

Chopart, J.L., Mezino, M., Aure, F., Le Mezo, L., Mete, M., Vauclin, M., 2007. OSIRI: A simple decision-making tool for monitoring irrigation of small farms in heterogeneous environments. Agr Water Manage, 87(2): 128-138. DOI:10.1016/j.agwat.2006.06.023

Ciais, P. et al., 2005. Europe-wide reduction in primary productivity caused by the heat and drought in 2003. Nature, 437(7058): 529-533. DOI:10.1038/nature03972

Condon, L.E., Maxwell, R.M., 2013. Implementation of a linear optimization water allocation algorithm into a fully integrated physical hydrology model. Adv Water Resour, 60: 135-147. DOI:10.1016/j.advwatres.2013.07.012

Cong, R.H., Wang, X.J., Xu, M.G., Ogle, S.M., Parton, W.J., 2014. Evaluation of the CENTURY Model Using Long-Term Fertilization Trials under Corn-Wheat Cropping Systems in the Typical Croplands of China. Plos One, 9(4). DOI:ARTN e9514210.1371/journal.pone.0095142

Conrad, Y., Fohrer, N., 2009. A test of CoupModel for assessing the nitrogen leaching in grassland systems with two different fertilization levels. J Plant Nutr Soil Sc, 172(6): 745-756. DOI:10.1002/jpln.200800264

Cooke, R.A., Mostaghimi, S., Campbell, J.B., 1993. Assessment of Methods for Interpolating Steady-State Infiltrability. T Asae, 36(5): 1333-1341.

Coppola, A., Basile, A., Comegna, A., Lamaddalena, N., 2009. Monte Carlo analysis of field water flow comparing uni- and bimodal effective hydraulic parameters for structured soil. J Contam Hydrol, 104(1–4): 153-165. DOI:http://dx.doi.org/10.1016/j.jconhyd.2008.09.007

Cornelis, W.M., Khlosi, M., Hartmann, R., Van Meirvenne, M., De Vos, B., 2005. Comparison of unimodal analytical expressions for the soil-water retention curve. Soil Sci Soc Am J, 69(6): 1902-1911. DOI:10.2136/sssaj2004.0238

Cornelis, W.M., Ronsyn, J., Van Meirvenne, M., Hartmann, R., 2001. Evaluation of pedotransfer functions for predicting the soil moisture retention curve. Soil Sci Soc Am J, 65(3): 638-648.

Corwin, D., Lesch, S., 2003. Application of soil electrical conductivity to precision agriculture. Agronomy Journal, 95(3): 455-471. DOI:DOI: 10.2134/agronj2003.4550

Corwin, D.L., Lesch, S.M., 2005. Characterizing soil spatial variability with apparent soil electrical conductivity I. Survey protocols. Comput Electron Agr, 46(1-3): 103-133. DOI:10.1016/j.compag.2004.11.002

Cosentini, R.M., Della Vecchia, G., Foti, S., Musso, G., 2012. Estimation of the hydraulic parameters of unsaturated samples by electrical resistivity tomography. Geotechnique, 62(7): 583-594. DOI:DOI: 10.1680/geot.10.P.066

Coumou, D., Matthai, S., Geiger, S., Driesner, T., 2008. A parallel FE-FV scheme to solve fluid flow in complex geologic media. Computers & Geosciences, 34(12): 1697-1707. DOI:10.1016/j.cageo.2007.11.010

Crawford, N.H., Burges, J.S., 1966. Digital simulation in hydrology stanford watershed model, Department Civil Engineering, Stanford university, USA.

Cresswell, H.P., Coquet, Y., Bruand, A., McKenzie, N.J., 2006. The transferability of Australian pedotransfer functions for predicting water retention characteristics of French soils. Soil Use Manage, 22(1): 62-70. DOI:10.1111/j.1475-2743.2006.00001.x

Dafflon, B., Irving, J., Holliger, K., 2009. Use of high-resolution geophysical data to characterize heterogeneous aquifers: Influence of data integration method on hydrological predictions. Water Resour Res, 45. DOI:Artn W0940710.1029/2008wr007646

Dane, J.H., Hruska, S., 1983. In-Situ Determination of Soil Hydraulic Properties during Drainage1. Soil Sci Soc Am J, 47(4). DOI:10.2136/sssaj1983.03615995004700040001x

Dane, J.H., Topp, G.C.e., 2002. Methods of soil analysis. Part 4. Physical methods. SSSA Book Ser. 5, SSSA, Madison, WI.

Danierhan, S., Abudu, S., Donghai, G., 2013. Coupled GSI-SVAT Model with Groundwater-Surface Water Interaction in the Riparian Zone of Tarim River. Journal of Hydrologic Engineering, 18(10): 1211-1218. DOI:10.1061/(asce)he.1943-5584.0000732

Darouich, H.M., Pedras, C.M.G., Goncalves, J.M., Pereira, L.S., 2014. Drip vs. surface irrigation: A comparison focussing on water saving and economic returns using multicriteria analysis applied to cotton. Biosyst Eng, 122: 74-90. DOI:10.1016/j.biosystemseng.2014.03.010

De Pauw, D., 2005. Optimal Experimental Design for Calibration of Bioprocess Models: a Validated Software Toolbox, Ghent university, Ghent, Belgium, 246 pp. DOI:1854/4975

de Vos, J.A., Šimůnek, J., Raats, P.A.C., Feddes, R.A., 1999. Identification of the hydraulic properties of a layered silt loam. In: al., M.T.v.G.e. (Ed.), Characterization and measurement of the hydraulic properties of unsaturated porous media. University of California, Riverside, USA, pp. 783-798.

Devia, G.K., Ganasri, B.P., Dwarakish, G.S., 2015. A Review on Hydrological Models. Aquatic Procedia, 4: 1001-1007. DOI:http://dx.doi.org/10.1016/j.aqpro.2015.02.126

Diersch, H.J.G., Kolditz, O., 1998. Coupled groundwater flow and transport: 2. Thermohaline and 3D convection systems. Adv Water Resour, 21(5): 401-425. DOI:Doi 10.1016/S0309-1708(97)00003-1

Dirksen, C., Kool, J.B., Koorevaar, P., Genuchten, M.T., 1993. HYSWASOR — Simulation Model of Hysteretic Water and Solute Transport in the Root Zone. In: Russo, D., Dagan, G. (Eds.), Water Flow and Solute Transport in Soils. Advanced Series in Agricultural Sciences. Springer Berlin Heidelberg, pp. 99-122. DOI:10.1007/978-3-642-77947-3_8

Dogrul, E.C., 2007. Integrated Water Flow Model (IWFM v3.0). User's manual Hydrology Development Unit, Modeling Support Branch California.

Dogrul, E.C., Kadir, T.N., Chung, F.I., 2011. Root Zone Moisture Routing and Water Demand Calculations in the Context of Integrated Hydrology. J Irrig Drain E-Asce, 137(6): 359-366. DOI:10.1061/(Asce)Ir.1943-4774.0000306

Donatelli, M., Stockle, C., Ceotto, E., Rinaldi, M., 1997. Evaluation of CropSyst for cropping systems at two locations of northern and southern Italy. Eur J Agron, 6(1-2): 35-45. DOI:Doi 10.1016/S1161-0301(96)02029-1

Doolittle, J.A., Brevik, E.C., 2014. The use of electromagnetic induction techniques in soils studies. Geoderma, 223: 33-45. DOI:10.1016/j.geoderma2014.01.027

Doorenbos, J., Kassam, A.H., 1979. Yield response to water, FAO Irrigation and Drainage Paper No. 33, Rome, Italy.

Doussan, C., Ruy, S., 2009. Prediction of unsaturated soil hydraulic conductivity with electrical conductivity. Water Resour Res, 45. DOI:DOI:10.1029/2008wr007309

Dowman, C.E.V., Ferre, T.P.A., Hoffmann, J.P., Rucker, D.F., Callegary, J.B., 2003. Quantifying Ephemeral Streambed Infiltration from Downhole Temperature Measurements Collected Before and After Streamflow. Vadose Zone J, 2(4): 595-601.

Dušek, J., Dohnal, M., Vogel, T., 2009. Numerical analysis of ponded infiltration experiment under different experimental conditions. Soil Water Res, 4: S22-S27.

Ebrahim, A., 2008. Evaluation of the Rice Growth Model ORYZA2000 Under Water Management. . Asian Journal of Plant Sciences, 7: 291-297.

Ebrahimian, H., Noory, H., 2015. Modeling paddy field subsurface drainage using HYDRUS-2D. Paddy and Water Environment, 13(4): 477-485. DOI:10.1007/s10333-014-0465-8

Eitzinger, J. et al., 2013. Sensitivities of crop models to extreme weather conditions during flowering period demonstrated for maize and winter wheat in Austria. J Agr Sci, 151(6): 813-835. DOI:10.1017/S0021859612000779

Elmaloglou, S., Malamos, N., 2003. A method to estimate soil-water movement under a trickle surface line source, with water extraction by roots. Irrig Drain, 52(3): 273-284. DOI:10.1002/ird.097

Elsen, F., Bries, J., Vandendriessche, H., Geypens, M., 1995. Watervoorziening en kunstmatige beregening In: Bries J., Vandendriessche H., Geypens M., 1995 Bemesting en beregening van aardappelen in functie van opbrengst en kwaliteit., Brussels, Belgium.

English, M., 1990. Deficit irrigation. I: Analytical framework. Journal of Irrigation and Drainage Engineering, 116: 399-412.

English, M., Raja, S.N., 1996. Perspectives on deficit irrigation. Agr Water Manage, 32(1): 1-14. DOI:Doi 10.1016/S0378-3774(96)01255-3

Evett, S.R., Heng, L.K., Moutonnet, P., Nguyen, M.L., 2008. Field estimation of soil water content: A practical guide to methods, instrumentation and sensor technology. IAEA-TCS-30, Vienna, Austria.

Evett, S.R., Peters, F.H., Jones, O.R., Unger, P.W., 1999. Soil hydraulic conductivity and retention curves from tension infiltrometer and laboratory data In: van Genuchten, M.T., Leij, F.J., Wu, L. (Eds.), Characterization and Measurement of the Hydraulic Properties of Unsaturated Porous Media: Part I. U.S. Salinity Laboratory USDA-ARS, pp. 541–551.

Falkenmark, M., 1997. Society's interaction with the water cycle: A conceptual framework for a more holistic approach. Hydrolog Sci J, 42(4): 451-466. DOI:Doi 10.1080/02626669709492046

Fang, Q., Ma, L., Yu, Q., Ahuja, L.R., Malone, R.W., Hoogenboom, G., 2010. Irrigation strategies to improve the water use efficiency of wheat-maize double cropping systems in North China Plain. Agr Water Manage, 97(8): 1165-1174. DOI:10.1016/j.agwat.2009.02.012

FAO, 2011. Climate change, water and food security. By Turra H., Burke, J, and Faurès, J. M., Food and agrriculture organization of the united nation Rome, Italy.

FAO, 2012a. Coping with water scarcity. An action framework for agriculture and food security, Rome, Italy.

FAO, 2012b. Crop yield response to water. by Steduto, P. Hsiao, T. C. Raes, D. and Fereres, El. . Food and Agriculture Organization of the United Nations Rome, Rome, Italy.

FAO, 2013. Climate Smart Agriculture Sourcebook. , Rome, Italy. DOI:978-92-5-107720-7

FAO, 2014. World reference base for soil resources 2014. World soil resources reports, 106. FAO, Rome, Italy, 191 pp.

FAO, 2015. Hot Issues:Water Scarcity. Available online at: http://www.fao.org/nr/water/issues/scarcity.html (verified 8 October 2015).

Farzamian, M., Santos, F.A.M., Khalil, M.A., 2015. Application of EM38 and ERT methods in estimation of saturated hydraulic conductivity in unsaturated soil. Journal of Applied Geophysics, 112: 175-189. DOI:10.1016/j.jappgeo.2014.11.016

Feddes, R.A., Kowalik, P.J., Zaradny, H., 1978. Simulation of field water use and crop yield. Simul. Monogr. Pudoc, Wageningen, The Netherlands, 189 pp.

Feddes, R.A., Roats, P.A.C., 2004. Parameterizing the soil-water-plant root system. Unsaturated-Zone Modeling: Progress, Challenges and Applications, 6, 95-141 pp.

Fekete, B.M., Vörösmarty, C.J., Grabs, W., 1999. Global, Composite Runoff Fields Based on Observed River Discharge and Simulated Water Balances. 22, Koblenz, Germany.

Fekete, B.M., Wisser, D., Kroeze, C., Mayorga, E., Bouwman, L., Wollheim, W.M., Vörösmarty, C., 2010. Millennium Ecosystem Assessment scenario drivers (1970–2050): Climate and hydrological alterations. Global Biogeochemical Cycles, 24(4): n/a-n/a. DOI:10.1029/2009GB003593

Feng, L., Mailhol, J.C., Rey, H., Griffon, S., Auclair, D., De Reffye, P., 2014. Comparing an empirical crop model with a functional structural plant model to account for individual variability. Eur J Agron, 53: 16-27. DOI:10.1016/j.eja.2013.11.005

Fereres, E., Orgaz, F., Gonzalez-Dugo, V., 2011. Reflections on food security under water scarcity. Journal of experimental botany. DOI:10.1093/jxb/err165

Fernández-Gálvez, J., Simmonds, L.P., Barahona, E., 2006. Estimating detailed soil water profile records from point measurements. European Journal of Soil Science, 57(5): 708-718. DOI:10.1111/j.1365-2389.2005.00761.x

Finke, P.A., 2012. On digital soil assessment with models and the Pedometrics agenda. Geoderma, 171: 3-15. DOI:10.1016/j.geoderma.2011.01.001

Finke, P.A., Bosma, W.J.P., 1993. Obtaining Basic Simulation Data for a Heterogeneous Field with Stratified Marine Soils. Hydrol Process, 7(1): 63-75. DOI:DOI 10.1002/hyp.3360070107

Finke, P.A., Bouma, J., Stein, A., 1992. Measuring Field Variability of Disturbed Soils for Simulation Purposes. Soil Sci Soc Am J, 56(1): 187-192.

Finke, P.A., Hutson, J.L., 2008. Modelling soil genesis in calcareous loess. Geoderma, 145(3-4): 462-479. DOI:10.1016/j.geoderma.2008.01.017

Finney, D.J., 1941. On the distribution of a variate whose logarithm is normally distributed. Suppl. J. R. Stat. Soc, 7: 155-161.

Fischer, B.M.C., Mul, M.L., Savenije, H.H.G., 2013. Determining spatial variability of dry spells: a Markov-based method, applied to the Makanya catchment, Tanzania. Hydrol Earth Syst Sc, 17(6): 2161-2170. DOI:10.5194/hess-17-2161-2013

Fodor, N., Sandor, R., Orfanus, T., Lichner, L., Rajkai, K., 2011. Evaluation method dependency of measured saturated hydraulic conductivity. Geoderma, 165(1): 60-68. DOI:DOI 10.1016/j.geoderma.2011.07.004

Forkel, M., Migliavacca, M., Thonicke, K., Reichstein, M., Schaphoff, S., Weber, U., Carvalhais, N., 2015. Codominant water control on global interannual variability and trends in land surface phenology and greenness. Global Change Biol, 21(9): 3414-3435. DOI:10.1111/gcb.12950

Frame, J., Laidlow, A., 2011. Improved grassland management. Crowood Press, Ipswich, UK.

Franke, A.C., Haverkort, A.J., Steyn, J.M., 2013. Climate Change and Potato Production in Contrasting South African Agro-Ecosystems 2. Assessing Risks and Opportunities of Adaptation Strategies. Potato Res, 56(1): 51-66. DOI:10.1007/s11540-013-9229-x

Frederiksen, H.D., Allen, R.G., 2011. A common basis for analysis, evaluation and comparison of offstream water uses. Water Int, 36(3): 266-282. DOI:10.1080/02508060.2011.580449

Friedman, S.P., 2005. Soil properties influencing apparent electrical conductivity: a review. Comput Electron Agr, 46(1-3): 45-70. DOI:DOI: 10.1016/j.compag.2004.11.001

Friedman, S.P., Seaton, N.A., 1998. Critical path analysis of the relationship between permeability and electrical conductivity of three-dimensional pore networks. Water Resour Res, 34(7): 1703-1710. DOI:DOI: 10.1029/98wr00939

Gaiser, T. et al., 2013. Modeling biopore effects on root growth and biomass production on soils with pronounced sub-soil clay accumulation. Ecol Model, 256: 6-15. DOI:10.1016/j.ecolmodel.2013.02.016

Gandolfi, C., Facchi, A., Maggi, D., 2006. Comparison of 1D models of water flow in unsaturated soils. Environ Modell Softw, 21(12): 1759-1764. DOI:10.1016/j.envsoft.2006.04.004

Gao, L.Z., Jin, Z.Q., Huang, Y., Zhang, L.Z., 1992. Rice Clock Model - a Computer-Model to Simulate Rice Development. Agr Forest Meteorol, 60(1-2): 1-16. DOI:Doi 10.1016/0168-1923(92)90071-B

Garcia-Vila, M., Fereres, E., Mateos, L., Orgaz, F., Steduto, P., 2009. Deficit Irrigation Optimization of Cotton with AquaCrop. Agron J, 101(3): 477-487. DOI:10.2134/agronj2008.0179s

Gardner, W.R., 1958. Some steady-state solution of the unsaturated moisture flow equation with application to evaporation from a water table. Soil Sci, 85(4): 228-232. DOI:10.1097/00010694-195804000-00006

Gayler, S., Wang, E., Priesack, E., Schaaf, T., Maidl, F.X., 2002. Modeling biomass growth, N-uptake and phenological development of potato crop. Geoderma, 105(3-4): 367-383. DOI:Doi 10.1016/S0016-7061(01)00113-6

Gee, G.W., Bauder, J.W., 1986. Particle-size analysis. In: Klute, A. (Ed.), Methods of soil analysis, Part 1, 2nd edn. Soil Science Society of America, Madison, pp. 383-411.

Geerts, S., Raes, D., 2009. Deficit irrigation as an on-farm strategy to maximize crop water productivity in dry areas. Agr Water Manage, 96(9): 1275-1284. DOI:10.1016/j.agwat.2009.04.009

Geerts, S., Raes, D., Garcia, M., 2010. Using AquaCrop to derive deficit irrigation schedules. Agr Water Manage, 98(1): 213-216. DOI:10.1016/j.agwat.2010.07.003

George, B.A., Shende, S.A., Raghuwanshi, N.S., 2000. Development and testing of an irrigation scheduling model. Agr Water Manage, 46(2): 121-136. DOI:Doi 10.1016/S0378-3774(00)00083-4

Ghezzehei, T.A., Kneafsey, T.J., Su, G.W., 2007. Correspondence of the Gardner and van Genuchten–Mualem relative permeability function parameters. Water Resour Res, 43(10): n/a-n/a. DOI:10.1029/2006WR005339

Gobin, A., 2010. Modelling climate impacts on crop yields in Belgium. Clim Res, 44(1): 55-68. DOI:10.3354/cr00925

Gobin, A., 2012. Impact of heat and drought stress on arable crop production in Belgium. Nat Hazard Earth Sys, 12(6): 1911-1922. DOI:10.5194/nhess-12-1911-2012

Gong, J., Wang, K., Kellomaki, S., Zhang, C., Martikainen, P.J., Shurpali, N., 2012. Modeling water table changes in boreal peatlands of Finland under changing climate conditions. Ecol Model, 244: 65-78. DOI:10.1016/j.ecolmodel.2012.06.031

Gongalves, J.M., Pereira, L.S., Fang, S.X., Dong, B., 2007. Modelling and multicriteria analysis of water saving scenarios for an irrigation district in the upper Yellow River basin. Agr Water Manage, 94(1-3): 93-108. DOI:10.1016/j.agwat.2007.08.011

Gonzalez, M.G. et al., 2015. Modelling soil water dynamics of full and deficit drip irrigated maize cultivated under a rain shelter. Biosyst Eng, 132: 1-18. DOI:10.1016/j.biosystemseng.2015.02.001

Gooley, L., Huang, J., Page, D., Triantafilis, J., 2014. Digital soil mapping of available water content using proximal and remotely sensed data. Soil Use Manage, 30(1): 139-151. DOI:DOI: 10.1111/Sum.12094

Greenwood, D.J., Zhang, K., Hilton, H.W., Thompson, A.J., 2010. Opportunities for improving irrigation efficiency with quantitative models, soil water sensors and wireless technology. J Agr Sci, 148: 1-16. DOI:10.1017/S0021859609990487

Grossman, R.B., Reinsch, T.G., 2002. Bulk density and linear extensibility. In: Dane, J.H., Topp, G. C. (Ed.), Methods of soil analysis: part 4: Physical methods. Soil Science Society of America book series, Soil Science Society of America Inc. Madison, Wisconsin, USA, pp. 201–228.

Gumiere, S.J., Lafond, J.A., Hallema, D.W., Périard, Y., Caron, J., Gallichand, J., 2014. Mapping soil hydraulic conductivity and matric potential for water management of cranberry: Characterisation and spatial interpolation methods. Biosystems Engineering, 128: 29-40. DOI:http://dx.doi.org/10.1016/j.biosystemseng.2014.09.002

Gupta, R.K., Rudra, R.P., Dickinson, W.T., Patni, N.K., Wall, G.J., 1993. Comparison of saturated hydraulic conductivity measured by various field methods. Trans. ASAE, 36(1): 51-55.

Gupta, S.C., Larson, W.E., 1979. Estimating Soil-Water Retention Characteristics from Particle-Size Distribution, Organic-Matter Percent, and Bulk-Density. Water Resour Res, 15(6): 1633-1635. DOI:DOI 10.1029/WR015i006p01633

Gwenzi, W., Hinz, C., Holmes, K., Phillips, I.R., Mullins, I.J., 2011. Field-scale spatial variability of saturated hydraulic conductivity on a recently constructed artificial ecosystem. Geoderma, 166(1): 43-56. DOI:10.1016/j.geoderma.2011.06.010

Hack-ten Broeke, M.J.D., 2001. Irrigation management for optimizing crop production and nitrate leaching on grassland. Agr Water Manage, 49(2): 97-114. DOI:Doi 10.1016/S0378-3774(00)00141-4

Haddeland, I., Lettenmaier, D.P., Skaugen, T., 2006. Effects of irrigation on the water and energy balances of the Colorado and Mekong river basins. J Hydrol, 324(1-4): 210-223. DOI:10.1016/j.jhydrol.2005.09.028

Hall, J.M., 2001. How well does your model fit the data? J. Hydroinform 3: 49–55.

Hanasaki, N. et al., 2013. A global water scarcity assessment under Shared Socio-economic Pathways - Part 1: Water use. Hydrol Earth Syst Sc, 17(7): 2375-2391. DOI:10.5194/hess-17-2375-2013

Hanson, B., Schwankl, L., Orloff, S., Sanden, B., 2011. Sprinkle Irrigation of Row and Field Crops, University of California, Agricultural and Natural Resources, Publication 3527, Richmond, CA.

Harter, T., Yeh, T.C.J., 1998. Flow in unsaturated random porous media, nonlinear numerical analysis and comparison to analytical stochastic models. Adv Water Resour, 22(3): 257-272. DOI:Doi 10.1016/S0309-1708(98)00010-4

Hasegawa, H., Bryant, D.C., Denison, R.F., 2000. Testing CERES model predictions of crop growth and N dynamics, in cropping systems with leguminous green manures in a Mediterranean climate. Field Crop Res, 67(3): 239-255. DOI:Doi 10.1016/S0378-4290(00)00099-X

Hashemian, M., Ryu, D., Crow, W.T., Kustas, W.P., 2015. Improving root-zone soil moisture estimations using dynamic root growth and crop phenology. Adv Water Resour, 86: 170-183. DOI:10.1016/j.advwatres.2015.10.001

Hassan, S.M.T., Lubczynski, M.W., Niswonger, R.G., Su, Z., 2014. Surface-groundwater interactions in hard rocks in Sardon Catchment of western Spain: An integrated modeling approach. J Hydrol, 517: 390-410. DOI:10.1016/j.jhydrol.2014.05.026

Healy, R.W., 2008. Simulating water, solute, and heat transport in the subsurface with the VS2DI software package. Vadose Zone J, 7(2): 632-639. DOI:10.2136/vzj2007.0075

Healy, R.W., Essaid, H.I., 2012. VS2DI: MODEL USE, CALIBRATION, AND VALIDATION. T Asabe, 55(4): 1249-1260.

Hedley, C.B., Roudier, P., Yule, I.J., Ekanayake, J., Bradbury, S., 2013. Soil water status and water table depth modelling using electromagnetic surveys for precision irrigation scheduling. Geoderma, 199: 22-29. DOI:DOI: 10.1016/j.geoderma.2012.07.018

Hengl, T., Heuvelink, G.B.M., Stein, A., 2004. A generic framework for spatial prediction of soil variables based on regression-kriging. Geoderma, 120(1-2): 75-93. DOI:DOI: 10.1016/j.geoderma.2003.08.018

Herbst, M., Diekkruger, B., Vereecken, H., 2006. Geostatistical co-regionalization of soil hydraulic properties in a micro-scale catchment using terrain attributes. Geoderma, 132(1-2): 206-221. DOI:10.1016/j.geoderma.2005.05.008

Hijmans, R.J., Condori, B., Carrillo, R., Kropff, M.J., 2003. A quantitative and constraint-specific method to assess the potential impact of new agricultural technology: the case of frost resistant potato for the Altiplano (Peru and Bolivia). Agr Syst, 76(3): 895-911. DOI:10.1016/S0308-521x(02)00081-1

Hlavinka, P. et al., 2014. Modelling of yields and soil nitrogen dynamics for crop rotations by HERMES under different climate and soil conditions in the Czech Republic. J Agr Sci, 152(2): 188-204. DOI:10.1017/S0021859612001001

Hoffmann, F., Beinhauer, R., Dadoun, F., 1993. Soil-Temperature Model for Ceres and Similar Crop Models. J Agron Crop Sci, 170(1): 56-65. DOI:DOI 10.1111/j.1439-037X.1993.tb01056.x

Homaee, M., 2004. Modelling the sink term under variable water stress. Water-Saving Agriculture and Sustainable Use of Water and Land Resources, Vols 1 and 2, Proceedings, 364-369 pp.

Homaee, M., Dirksen, C., Feddes, R.A., 2002. Simulation of root water uptake I. Non-uniform transient salinity using different macroscopic reduction functions. Agr Water Manage, 57(2): 89-109. DOI:10.1016/s0378-3774(02)00072-0

Homaee, M., Feddes, R.A., 1999. Root water uptake under non-uniform transient salinity and water stress. Modelling of Transport Processes in Soils: At Various Scales in Time and Space, 416-427 pp.

Hoogenboom, G., Jones, J.W., Boote, K.J., 1992. Modeling the growth, development and yield of grain legumes usingSOYGRO, PNUTGRO and BEANGRO: a review.

Hooijer, A.A., van der Wal, T., 1994. CGMS version 3.1, user manual, DLO Winand Staring Centre, Wageningen.

Hopmans, J.W., Šimůnek, J., Romano, N., Durner, W., 2002. Simultaneous determination of water transmission and retention properties. Inverse Methods. In: Dane, J.H., Topp, G.C. (Eds.), Method of soil analysis. Part 4. Physical methods. Soil Science Society of America Book Series, Madison, USA, pp. 963-1008.

Horta, A., Pereira, M.J., Goncalves, M., Ramos, T., Soares, A., 2014. Spatial modelling of soil hydraulic properties integrating different supports. J Hydrol, 511: 1-9. DOI:10.1016/j.jhydrol.2014.01.027

Hu, W., Shao, M.G., Wang, Q.J., Fan, J., Horton, R., 2009. Temporal changes of soil hydraulic properties under different land uses. Geoderma, 149(3-4): 355-366. DOI:DOI 10.1016/j.geoderma.2008.12.016

Hunt, R.J., Prudic, D.E., Walker, J.F., Anderson, M.P., 2008. Importance of unsaturated zone flow for simulating recharge in a humid climate. Ground Water, 46(4): 551-560. DOI:10.1111/j.1745-6584.2007.00427.x

Huntley, D., 1986. Relations between permeability and electrical resistivity in granular aquifers. Ground Water, 24(4): 466-474. DOI:DOI:10.1111/j.1745-6584.1986.tb01025.x

Huo, Z., Feng, S., Dai, X., Zheng, Y., Wang, Y., 2012. Simulation of hydrology following various volumes of irrigation to soil with different depths to the water table. Soil Use and Management, 28(2): 229-239. DOI:10.1111/j.1475-2743.2012.00393.x

Hupet, F., Lambot, S., Javaux, M., Vanclooster, M., 2002. On the identification of macroscopic root water uptake parameters from soil water content observations. Water Resour Res, 38(12). DOI:10.1029/2002wr001556

Hussen, A.A., Warrick, A.W., 1993. Alternative Analyses of Hydraulic Data from Disc Tension Infiltrometers. Water Resour Res, 29(12): 4103-4108. DOI:Doi 10.1029/93wr02404

Hutchings, N.J. et al., 2012. A model for simulating the timelines of field operations at a European scale for use in complex dynamic models. Biogeosciences, 9(11): 4487-4496. DOI:10.5194/bg-9-4487-2012

Huygen, J., 1992. SWACROP2, a quasi-two-dimensional crop growth & soil water flow simulation model. User's guide. , WAU, Department of Water Resources, DLO Winand Staring Centre, Wageningen.

Iman, R.L., Helton, J.C., 1988. An Investigation of Uncertainty and Sensitivity Analysis Techniques for Computer-Models. Risk Anal, 8(1): 71-90. DOI:DOI 10.1111/j.1539-6924.1988.tb01155.x

Iñiguez, V., Morales, O., Cisneros, F., Bauwens, W., Wyseure, G., 2015. Analysis of the drought resilience of Andosols on southern Ecuadorian Andean páramos. Hydrol. Earth Syst. Sci. Discuss, 12: 11449–11484. DOI:10.5194/hessd-12-11449-2015

Iñiguez, V., Morales, O., Cisneros, F., Bauwens, W., Wyseure, G., 2016. Analysis of the drought recovery of Andosols on southern Ecuadorian Andean páramos. Hydrol. Earth Syst. Sci., 20(6): 2421-2435. DOI:10.5194/hess-20-2421-2016

IPCC, 2007. Climate Change, Cambridge, UK

IPCC, 2012. Managing the Risks of Extreme Events and Disasters to Advance Climate Change Adaptation. Cambridge University Press, Cambridge, UK.

IPCC, 2013a. Climate change 2013: the physical science basis. Contribution of Working Group I to the Fifth Assessment Report of the Intergovernmental Panel on Climate Change, Cambridge, UK: Cambridge University Press.

IPCC, 2013b. Summary for Policymakers, Cambridge, UK and New York, NY.

Iqbal, J., Thomasson, J.A., Jenkins, J.N., Owens, P.R., Whisler, F.D., 2005. Spatial variability analysis of soil physical properties of alluvial soils. Soil Sci Soc Am J, 69(4): 1338-1350. DOI:DOI 10.2136/sssaj2004.0154

Jabro, J.D., Evans, R.G., Kim, Y., Iversen, W.M., 2009. Estimating in situ soil-water retention and field water capacity in two contrasting soil textures. Irrigation Sci, 27(3): 223-229. DOI:10.1007/s00271-008-0137-9

Jačka, L., Pavlásek, J., Kuráž, V., Pech, P., 2014. A comparison of three measuring methods for estimating the saturated hydraulic conductivity in the shallow subsurface layer of mountain podzols. Geoderma, 219–220(0): 82-88. DOI:http://dx.doi.org/10.1016/j.geoderma.2013.12.027

Jacques, D., Smith, C., Simunek, J., Smiles, D., 2012. Inverse optimization of hydraulic, solute transport, and cation exchange parameters using HP1 and UCODE to simulate cation exchange. J Contam Hydrol, 142: 109-125. DOI:10.1016/j.jconhyd.2012.03.008

Jagermeyr, J., Gerten, D., Heinke, J., Schaphoff, S., Kummu, M., Lucht, W., 2015. Water savings potentials of irrigation systems: global simulation of processes and linkages. Hydrol Earth Syst Sc, 19(7): 3073-3091. DOI:10.5194/hess-19-3073-2015

Jajarmizadeh, M., Harun, S., Salarpour, M., 2012. A Review on Theoretical Consideration and Types of Models in Hydrology. Journal of Environmental Science and Technology, 5: 249-261.

Jame, Y.W., Cutforth, H.W., 1996. Crop growth models for decision support systems. Can J Plant Sci, 76(1): 9-19.

Jamieson, P.D., Porter, J.R., Goudriaan, J., Ritchie, J.T., van Keulen, H., Stol, W., 1998. A comparison of the models AFRCWHEAT2, CERES-wheat, Sirius, SUCROS2 and SWHEAT with measurements from wheat grown under drought. Field Crop Res, 55(1-2): 23-44. DOI:Doi 10.1016/S0378-4290(97)00060-9

Jansson, P.E., Karlberg, L., 2001. Coupled Heat and Mass Transfer Model for Soil-Plant-Atmosphere Systems, Department of Civil and Environmental Engineering, Royal Institute of Technology, Stockholm.

Jarvis, N.J., 1989. A simple empirical model of root water uptake. J Hydrol, 107(1–4): 57-72. DOI:http://dx.doi.org/10.1016/0022-1694(89)90050-4

Jarvis, N.J., Larsson, M.H., 1998. The MACRO model (Version 4.1). Technical description, Department of Soil Sciences, Swedish University of Agricultural Sciences, Uppsala.

Jonard, F., Weihermuller, L., Schwank, M., Jadoon, K.Z., Vereecken, H., Lambot, S., 2015. Estimation of Hydraulic Properties of a Sandy Soil Using Ground-Based Active and Passive Microwave Remote Sensing. Ieee T Geosci Remote, 53(6): 3095-3109. DOI:10.1109/Tgrs.2014.2368831

Jones, C.A., Kiniry, J.R., 1986. CERES-Maize: A Simulation Model of Maize Growth and Development, College Station, Texas.

Jones, H.G., 2004. Irrigation scheduling: advantages and pitfalls of plant-based methods. Journal of experimental botany, 55(407): 2427-2436. DOI:10.1093/jxb/erh213

Joris, I., Bronders, J., van der Grift, B., Seuntjens, P., 2014. Model-based Scenario Analysis of the Impact of Remediation Measures on Metal Leaching from Soils Contaminated by Historic Smelter Emissions. J Environ Qual, 43(3): 859-868. DOI:10.2134/jeq2013.07.0287

Jury, W., Horton, R., 2004. Soil Physics. John Wiley & Sons, New York.

Jury, W.A., 1985. Spatial variability of soil physical parameters in solute migration: A critical literature review, Electrical Power Research Institute, Riverside, Palo Alto, CA.

Kandelous, M.M., Kamai, T., Vrugt, J.A., Šimůnek, J., Hanson, B., Hopmans, J., 2012. Evaluation of subsurface drip irrigation design and management parameters for alfalfa. Agr Water Manage, 109: 81-93. DOI:http://dx.doi.org/10.1016/j.agwat.2012.02.009

Karlberg, L., Ben-Gal, A., Jansson, P.E., Shani, U., 2006. Modelling transpiration and growth in salinity-stressed tomato under different climatic conditions. Ecol Model, 190(1-2): 15-40. DOI:10.1016/j.ecolmodel.2005.04.015

Keating, B.A. et al., 2003. An overview of APSIM, a model designed for farming systems simulation. Eur J Agron, 18(3-4): 267-288. DOI:10.1016/S1161-0301(02)00108-9

Kelishadi, H., Mosaddeghi, M.R., Hajabbasi, M.A., Ayoubi, S., 2014. Near-saturated soil hydraulic properties as influenced by land use management systems in Koohrang region of central Zagros, Iran. Geoderma, 213: 426-434. DOI:10.1016/j.geoderma.2013.08.008

Kelleners, T.J., Soppe, R.W.O., Ayars, J.E., Simunek, J., Skaggs, T.H., 2005. Inverse analysis of upward water flow in a groundwater table lysimeter. Vadose Zone J, 4(3): 558-572. DOI:10.2136/Vzj2004.0118

Keller, J., Bliesner, R.D., 1990. Sprinkle and Trickle Irrigation, Van Nostrand Reinhold, Chapman and Hall: New York.

Khlosi, M., Cornelis, W.M., Douaik, A., van Genuchten, M.T., Gabriels, D., 2008. Performance Evaluation of Models That Describe the Soil Water Retention Curve between Saturation and Oven Dryness. Vadose Zone J, 7(1): 87-96. DOI:10.2136/vzj2007.0099

Kleijnen, J.P.C., Vanham, G., Rotmans, J., 1992. Techniques for sensitivity analysis of simulation-models - a case-study of the co2 greenhouse-effect. Simulation, 58(6): 410-417. DOI:10.1177/003754979205800610

Kloss, S., Grundmann, J., Seidel, S.J., Werisch, S., Truemmner, J., Schmidhalter, U., Schuetze, N., 2014. Investigation of deficit irrigation strategies combining SVAT-modeling, optimization and experiments. Environ Earth Sci, 72(12): 4901-4915. DOI:10.1007/s12665-014-3463-7

Kloss, S., Pushpalatha, R., Kamoyo, K.J., Schutze, N., 2012. Evaluation of Crop Models for Simulating and Optimizing Deficit Irrigation Systems in Arid and Semi-arid Countries Under Climate Variability. Water Resour Manag, 26(4): 997-1014. DOI:10.1007/s11269-011-9906-y

Klute, A., 1986. Methods of soil analysis, part 1, physical and mineralogical methods (2nd edition) 1986, . American Society of Agronomy, Agronomy Monographs 9, Madison, Wisconsin.

Kooman, P.L., Haverkort, A.J., 1995. Modelling development and growth of the potato crop influenced by temperature and daylength: LINTUL-POTATO. Curr Iss Prod Ecol, 3: 41-59.

Kourgialas, N.N., Karatzas, G.P., 2015. A modeling approach for agricultural water management in citrus orchards: cost-effective irrigation scheduling and agrochemical transport simulation. Environ Monit Assess, 187(7): 462. DOI:10.1007/s10661-015-4655-7

Krause, P., Boyle, D.P., Bäse, F., 2005. Comparison of different efficiency criteria for hydrological model assessment. Adv. Geosci., 5: 89-97. DOI:10.5194/adgeo-5-89-2005

Krysanova, V., Muller-Wohlfeil, D.I., Becker, A., 1998. Development and test of a spatially distributed hydrological water quality model for mesoscale watersheds. Ecol Model, 106(2-3): 261-289. DOI:Doi 10.1016/S0304-3800(97)00204-4

Kulasekera, P.B., Parkin, G.W., 2011. Influence of the shape of inter-horizon boundary and size of soil tongues on preferential flow under shallow groundwater conditions: A simulation study. Canadian Journal of Soil Science, 91(2): 211-221. DOI:10.4141/cjss10079

Kuo, S.F., Ho, S.S., Liu, C.W., 2006. Estimation irrigation water requirements with derived crop coefficients for upland and paddy crops in ChiaNan Irrigation Association, Taiwan. Agr Water Manage, 82(3): 433-451. DOI:10.1016/j.agwat.2005.08.002

Kutílek, M., Nielsen, D.R., 1994. Soil Hydrology. Catena Verlag, Cremlingen-Destedt, Germany.

Kuznetsov, M., Yakirevich, A., Pachepsky, Y.A., Sorek, S., Weisbrod, N., 2012. Quasi 3D modeling of water flow in vadose zone and groundwater. J Hydrol, 450: 140-149. DOI:10.1016/j.jhydrol.2012.05.025

Lamm, F.R., Trooien, T.P., 2003. Subsurface drip irrigation for corn production: a review of 10 years of research in Kansas. Irrigation Sci, 22(3-4): 195-200. DOI:10.1007/s00271-003-0085-3

Langerwisch, F., Rost, S., Poulter, B., Zimmermann-Timm, H., Cramer, W., 2008. Assessing carbon dynamics in amazonia with the Dynamic Global Vegetation Model LPJmL - discharge evaluation. Int Ver Theor Angew, 30: 455-458.

Latorre, G.B., Peña, S.C., Lassabatere, L., Angulo-Jaramillo, R., Moret-Fernández, D., 2015. Estimate of soil hydraulic properties from disc infiltrometer three-dimensional infiltration curve. Numerical analysis and field application. Journal of Hydrology, 527: 1-12.

Lauren, J.G., Wagenet, R.J., Bouma, J., Wosten, J.H.M., 1988. Variability of Saturated Hydraulic Conductivity in a Glossaquic Hapludalf with Macropores. Soil Sci, 145(1): 20-28. DOI:Doi 10.1097/00010694-198801000-00003

Laurila, H.A., 1995. Modelling the effects of elevated CO2 and temperature on Swedish and German spring wheat varieties with CERES-wheat and AFRC-wheat crop models. J Biogeogr, 22(4-5): 591-595. DOI:Doi 10.2307/2845959

Lazarovitch, N., Ben-Gal, A., Šimůnek, J., Shani, U., 2007. Uniqueness of Soil Hydraulic Parameters Determined by a Combined Wooding Inverse Approach. Soil Sci Soc Am J, 71(3): 860-865. DOI:10.2136/sssaj2005.0420

Lebourgeois, V., Chopart, J.L., Begue, A., Le Mezo, L., 2010. Towards using a thermal infrared index combined with water balance modelling to monitor sugarcane irrigation in a tropical environment. Agr Water Manage, 97(1): 75-82. DOI:10.1016/j.agwat.2009.08.013

Lee, J.E., 2015. Effects of Irrigation Reservoirs and Groundwater Withdrawals on Streamflow for the Anseongcheon Upper Watershed. Journal of the Korean Society of Civil Engineers, 35(4): 835-844. DOI:10.12652/Ksce.2015.35.4.0835

Lesch, S.M., 2006. ESAP Software Suite: XP-Release Version 2.35, USDA-ARS George E. Brown Jr. Salinity Laboratory, Riverside, CA, USA.

Lesch, S.M., Rhoades, J.D., Corwin, D.L., 2000. The ESAP-95 version 2.01R user manual and tutorial guide. Research Report No. 146, USDA-ARS, George E. Brown, Jr.,Salinity Laboratory, Riverside, California.

Lesch, S.M., Strauss, D.J., Rhoades, J.D., 1995. Spatial Prediction of Soil Salinity Using Electromagnetic Induction Techniques: 2. An Efficient Spatial Sampling Algorithm Suitable for Multiple Linear Regression Model Identification and Estimation. Water Resour Res, 31(2): 387-398. DOI:10.1029/94WR02180

Lesmes, D., Friedman, S., 2005. Relationships between the Electrical and Hydrogeological Properties of Rocks and Soils. In: Rubin, Y., Hubbard, S. (Eds.), Hydrogeophysics. Water Science and Technology Library. Springer Netherlands, pp. 87-128. DOI:10.1007/1-4020-3102-5_4

Levenberg, K., 1944. A method for the solution of certain problems in least squares. Quart. Appl. Math, 2: 164-168.

Li, N., McLaughlin, D., Kinzelbach, W., Li, W.P., Dong, X.G., 2015. Using an ensemble smoother to evaluate parameter uncertainty of an integrated hydrological model of Yanqi basin. J Hydrol, 529: 146-158. DOI:10.1016/j.jhydrol.2015.07.024

Li, Q., Unger, A.J.A., Sudicky, E.A., Kassenaar, D., Wexler, E.J., Shikaze, S., 2008. Simulating the multi-seasonal response of a large-scale watershed with a 3D physically-based hydrologic model. J Hydrol, 357(3-4): 317-336. DOI:10.1016/j.jhydrol.2008.05.024

Li, X.P., Zhang, J.B., Liu, J.T., Liu, J.L., Zhu, A.N., Lv, F., Zhang, C.Z., 2011. A modified checkbook irrigation method based on GIS-coupled model for regional irrigation scheduling. Irrigation Sci, 29(2): 115-126. DOI:10.1007/s00271-010-0221-9

Li, Y., Kinzelbach, W., Zhou, J., Cheng, G.D., Li, X., 2012. Modelling irrigated maize with a combination of coupled-model simulation and uncertainty analysis, in the northwest of China. Hydrol Earth Syst Sc, 16(5): 1465-1480. DOI:10.5194/hess-16-1465-2012

Li, Y., Zhou, J., Kinzelbach, W., Cheng, G., Li, X., Zhao, W., 2013. Coupling a SVAT heat and water flow model, a stomatal-photosynthesis model and a crop growth model to simulate energy, water and carbon fluxes in an irrigated maize ecosystem. Agr Forest Meteorol, 176: 10-24. DOI:10.1016/j.agrformet.2013.03.004

Liang, X., Lettenmaier, D.P., Wood, E.F., Burges, S.J., 1994. A Simple Hydrologically Based Model of Land-Surface Water and Energy Fluxes for General-Circulation Models. J Geophys Res-Atmos, 99(D7): 14415-14428. DOI:Doi 10.1029/94jd00483

Liu, L., Cui, Y., Luo, Y., 2013. Integrated Modeling of Conjunctive Water Use in a Canal-Well Irrigation District in the Lower Yellow River Basin, China. Journal of Irrigation and Drainage Engineering, 139(9): 775-784. DOI:10.1061/(asce)ir.1943-4774.0000620

Liu, Y., Shang, S.-h., Mao, X.-m., 2012. TIDAL EFFECTS ON GROUNDWATER DYNAMICS IN COASTAL AQUIFER UNDER DIFFERENT BEACH SLOPES. Journal of Hydrodynamics, 24(1): 97-106. DOI:10.1016/s1001-6058(11)60223-0

Logsdon, S.D., Jaynes, D.B., 1993. Methodology for Determining Hydraulic Conductivity with Tension Infiltrometers. Soil Sci Soc Am J, 57(6): 1426-1431.

Loosvelt, L., 2013. Assessment of uncertainty in land surface characterization and implications for spatially distributed hydrological modelling, Ghent University, Ghent, Belgium, 295 pp.

Loukas, A., Tzabiras, J., Spiliotopoulos, M., Kokkinos, K., Fafoutis, C., Mylopoulos, N., 2015. Development of a district information system for water management planning and strategic decision making. Proc Spie, 9535. DOI:Artn 95351l10.1117/12.2193892

Luo, X.P., Xia, J., Yang, H., 2015. Modeling water requirements of major crops and their responses to climate change in the North China Plain. Environ Earth Sci, 74(4): 3531-3541. DOI:10.1007/s12665-015-4400-0

Luo, Y., Sophocleous, M., 2011. Two-way coupling of unsaturated-saturated flow by integrating the SWAT and MODFLOW models with application in an irrigation district in arid region of West China. Journal of Arid Land, 3(3): 164-173. DOI:10.3724/sp.j.1227.2011.00164

Luquet, D., Vidal, A., Smith, M., Dauzat, J., 2005. 'More crop per drop': how to make it acceptable for farmers? Agr Water Manage, 76(2): 108-119. DOI:http://dx.doi.org/10.1016/j.agwat.2005.01.011

Maharjan, G.R. et al., 2016. Assessing the effectiveness of split fertilization and cover crop cultivation in order to conserve soil and water resources and improve crop productivity. Agr Water Manage, 163: 305-318. DOI:10.1016/j.agwat.2015.10.005

Mailhol, J.C., Olufayo, A.A., Ruelle, P., 1997. Sorghum and sunflower evapotranspiration and yield from simulated leaf area index. Agr Water Manage, 35(1-2): 167-182. DOI:Doi 10.1016/S0378-3774(97)00029-2

Mailhol, J.C., Ruelle, P., Revol, P., 1996. PILOTE: Un modele operationnel pour deceler l'apparition du stress hydrique Workshop on Crop-Water-Environment Models, 16th International Congress on Irrigation and Drainage (ICID-CIID). 47th International Executive Council Meeting, Cairo International Conference Centre Cairo, Egypt, pp. 209-222.

Mailhol, J.C., Ruelle, P., Walser, S., Schutze, N., Dejean, C., 2011. Analysis of AET and yield predictions under surface and buried drip irrigation systems using the Crop Model PILOTE and Hydrus-2D. Agr Water Manage, 98(6): 1033-1044. DOI:10.1016/j.agwat.2011.01.014

Malekpour, M., Babazadeh, H., 2011. Simulation of Yield Decline as a Result of Water Stress Using BUDGET Model International Journal of Agricultural Science and Research, 2(3): 39-47.

Mallants, D., Mohanty, B.P., Jacques, D., Feyen, J., 1996. Spatial variability of hydraulic properties in a multi-layered soil profile. Soil Science, 161(3): 167-181. DOI:DOI: 10.1097/00010694-199603000-00003

Mallants, D., Mohanty, B.P., Vervoort, A., Feyen, J., 1997. Spatial analysis of saturated hydraulic conductivity in a soil with macropores. Soil Technol, 10(2): 115-131. DOI:DOI: 10.1016/S0933-3630(96)00093-1

Maracchi, G., Sirotenko, O., Bindi, M., 2005. Impacts of present and future climate variability on agriculture and forestry in the temperate regions: Europe. Climatic Change, 70(1-2): 117-135. DOI:DOI 10.1007/s10584-005-5939-7

Markstrom, S.L., Niswonger, R.G., Regan, R.S., Prudic, D.E., Barlow, P.M., 2008. GSFLOW-Coupled Ground-water and Surface-water FLOW model based on the integration of the Precipitation-Runoff Modeling System (PRMS) and the Modular Ground-Water Flow Model (MODFLOW-2005), U.S. Geological Survey Techniques and Methods 6-D1.

Marquardt, D.W., 1963. An algorithm for least-squares estimation of nonlinear parameters. SIAM J. Appl. Math., 11(2): 431-441.

Marshall, A., 2015. AHDB Potatoes business report for Northern Europe. Euro-Potato 30 October 2015.

Matthews, R., Wassmann, R., 2003. Modelling the impacts of climate change and methane emission reductions on rice production: a review. Eur J Agron, 19(4): 573-598. DOI:10.1016/S1161-0301(03)00005-4

Mawer, C., Knight, R., Kitanidis, P.K., 2015. Relating relative hydraulic and electrical conductivity in the unsaturated zone. Water Resour Res, 51(1): 599-618. DOI:10.1002/2014wr015658

McCown, R.L., Hammer, G.L., Hargreaves, J.N.G., Holzworth, D.P., Freebairn, D.M., 1996. APSIM: A novel software system for model development, model testing and simulation in agricultural systems research. Agr Syst, 50(3): 255-271. DOI:Doi 10.1016/0308-521x(94)00055-V

McDonald, M.G., Harbaugh, A.W., 1983. A modular three-dimensional finite-difference ground-water flow model, Open-File Report 83-875. U.S. Geological Survey.

Merdun, H., Quisenberry, V.L., 2005. Evaluation of MACRO model by short-term water and solute transport simulation in Maury silt loam soil. Plant Soil Environ, 51(3): 110-123.

Mertens, J., Madsen, H., Kristensen, M., Jacques, D., Feyen, J., 2005. Sensitivity of soil parameters in unsaturated zone modelling and the relation between effective, laboratory and in situ estimates. Hydrol Process, 19(8): 1611-1633. DOI:10.1002/hyp.5591

Mertens, J., Stenger, R., Barkle, G.F., 2006. Multiobjective inverse modeling for soil parameter estimation and model verification. Vadose Zone J, 5(3): 917-933. DOI:10.2136/Vzj2005.0117

Miháliková, M., Başkan, O., Dengiz, O., 2015. Capability of different interpolation models and pedotransfer functions to estimate soil hydraulic properties in Büyükçay Watershed. Environmental Earth Sciences, 74(3): 2425-2437. DOI:10.1007/s12665-015-4246-5

Miller, N.L., Dale, L.L., Brush, C.F., Vicuna, S.D., Kadir, T.N., Dogrul, E.C., Chung, F.I., 2009. Drought Resilience of the California Central Valley Surface-Ground-Water-Conveyance System1. JAWRA Journal of the American Water Resources Association, 45(4): 857-866. DOI:10.1111/j.1752-1688.2009.00329.x

Minasny, B., McBratney, A.B., 2002. FuzME version 3.0, Australian Centre for Precision Agriculture, The University of Sydney, Australia.

Minasny, B., Whelan, B.M., Triantafilis, J., McBratney, A.B., 2013. Pedometrics Research in the Vadose Zone-Review and Perspectives. Vadose Zone J, 12(4). DOI:10.2136/vzj2012.0141

Mirus, B.B., Perkins, K.S., Nimmo, J.R., Singha, K., 2009. Hydrologic Characterization of Desert Soils with Varying Degrees of Pedogenesis: 2. Inverse Modeling for Effective Properties. Vadose Zone J, 8(2): 496-509. DOI:10.2136/vzj2008.0051

Mishra, S.K., Shekh, A.M., Pandey, V., Yadav, S.B., Patel, H.R., 2015. Sensitivity analysis of four wheat cultivars to varying photoperiod and temperature at different phenological stages using WOFOST model. J Agrometeorol, 17(1): 74-79.

Mohanty, B.P., 2013. Soil Hydraulic Property Estimation Using Remote Sensing: A Review. Vadose Zone J, 12(4). DOI:10.2136/vzj2013.06.0100

Mohanty, B.P., Cosh, M., Lakshmi, V., Montzka, C., 2013. Remote sensing for vadose zone hydrology: A synthesis from the vantage point. Vadose Zone J, 12(3): 1-6. DOI:10.2136/vzj2013.07.0128

Molden, D., Oweis, T., Steduto, P., Bindraban, P., Hanjra, M.A., Kijne, J., 2010. Improving agricultural water productivity: Between optimism and caution. Agr Water Manage, 97(4): 528-535. DOI:10.1016/j.agwat.2009.03.023

Mora, D.E., Campozano, L., Cisneros, F., Wyseure, G., Willems, P., 2014. Climate changes of hydrometeorological and hydrological extremes in the Paute basin, Ecuadorean Andes. Hydrol. Earth Syst. Sci., 18(2): 631-648. DOI:10.5194/hess-18-631-2014

Moreno, A., Ramos, T.B., Goncalves, M.C., Pereira, L.S., 2014. Estimating Soil Hydraulic Properties from Limited Data to Improve Irrigation Management in Agricultural Soils of Santiago Island, Cape Verde. Irrig Drain, 63(3): 405-415. DOI:10.1002/ird.1810

Morgan, K.T., Parsons, L.R., Wheaton, T.A., 2001. Comparison of laboratory- and field-derived soil water retention curves for a fine sand soil using tensiometric, resistance and capacitance methods. Plant Soil, 234(2): 153-157. DOI:Doi 10.1023/A:1017915114685

Morin, R.H., LeBlanc, D.R., Troutman, B.M., 2010. The Influence of topology on hydraulic conductivity in a sand-and-gravel aquifer. Ground Water, 48(2): 181-190. DOI:DOI: 10.1111/j.1745-6584.2009.00646.x

Morris, M.D., 1991. Factorial Sampling Plans for Preliminary Computational Experiments. Technometrics, 33(2): 161-174. DOI:Doi 10.2307/1269043

Mualem, Y., 1976. New model for predicting hydraulic conductivity of unsaturated porous-media. Water Resour Res, 12(3): 513-522. DOI:10.1029/Wr012i003p00513

Mualem, Y., Friedman, S.P., 1991. Theoretical prediction of electrical-conductivity in saturated and unsaturated soil. Water Resour Res, 27(10): 2771-2777. DOI:DOI: 10.1029/91wr01095

Murthy, V.R.K., 2004. Crop growth modeling and its applications in agricultural meteorology. satellite remote sensing and GIS applications in agricultural meteorology. Ed. Sivakumar, MV K: 235-261.

Napoli, M., Orlandini, S., Grifoni, D., Zanchi, C.A., 2013. Modeling Soil and Nutrient Runoff Yields from an Italian Vineyard Using Swat. T Asabe, 56(6): 1397-1406.

Nasta, P., Vrugt, J.A., Romano, N., 2013. Prediction of the saturated hydraulic conductivity from Brooks and Corey's water retention parameters. Water Resour Res, 49(5): 2918-2925.

Nendel, C. et al., 2011. The MONICA model: Testing predictability for crop growth, soil moisture and nitrogen dynamics. Ecol Model, 222(9): 1614-1625. DOI:10.1016/j.ecolmodel.2011.02.018

Neuman, S.P., Feddes, R.A., Bresler, E., 1974. Finite element simulation on flow in saturated-unsaturated soils considering water uptake by plants, Institute of Technology, Haifa, Israel.

Neuman, S.P., Wierenga, P.J., 2003. A comprehensive strategy of hydrogeologic modeling and uncertainty analysis for nuclear facilities and sites. Division of Systems Analysis and Regulatory Effectiveness, Office of Nuclear Regulatory Research, U.S. Nuclear Regulatory Commission, Washington, DC.

Nguyen, P.M., De Pue, J., Le, K.V., Cornelis, W., 2015. Impact of regression methods on improved effects of soil structure on soil water retention estimates. J Hydrol, 525: 598-606. DOI:10.1016/j.jhydrol.2015.04.014

Nijssen, B., Schnur, R., Lettenmaier, D.P., 2001. Global retrospective estimation of soil moisture using the variable infiltration capacity land surface model, 1980-93. J Climate, 14(8): 1790-1808. DOI:Doi 10.1175/1520-0442(2001)014<1790:Greosm>2.0.Co;2

Nimmo, J.R., Perkins, K.S., Schmidt, K.M., Miller, D.M., Stock, J.D., Singha, K., 2009. Hydrologic Characterization of Desert Soils with Varying Degrees of Pedogenesis: 1. Field Experiments Evaluating Plant-Relevant Soil Water Behavior. Vadose Zone J, 8(2): 480-495. DOI:10.2136/vzj2008.0052

Niswonger, R.G., Prudic, D.E., 2009. Comment on "Evaluating Interactions between Groundwater and Vadose Zone Using the HYDRUS-Based Flow Package for MODFLOW" by Navin Kumar C. Twarakavi, Jirka Simunek, and Sophia Seo. Vadose Zone J, 8(3): 818-819. DOI:10.2136/vzj2008.0155

Niu, Q.F., Fratta, D., Wang, Y.H., 2015. The use of electrical conductivity measurements in the prediction of hydraulic conductivity of unsaturated soils. J Hydrol, 522: 475-487. DOI:10.1016/j.jhydrol.2014.12.055

Niwas, S., Celik, M., 2012. Equation estimation of porosity and hydraulic conductivity of Ruhrtal aquifer in Germany using near surface geophysics. Journal of Applied Geophysics, 84: 77-85. DOI:http://dx.doi.org/10.1016/j.jappgeo.2012.06.001

Noilhan, J., Planton, S., 1989. A Simple Parameterization of Land Surface Processes for Meteorological Models. Mon Weather Rev, 117(3): 536-549. DOI:Doi 10.1175/1520-0493(1989)117<0536:Aspols>2.0.Co;2

Norris, I.B., 1982. Soil-Moisture and Growth of Contrasting Varieties of Lolium, Dactylis and Festuca Species. Grass Forage Sci, 37(4): 273-283. DOI:DOI 10.1111/j.1365-2494.1982.tb01607.x

Nosetto, M.D., Jobbagy, E.G., Brizuela, A.B., Jackson, R.B., 2012. The hydrologic consequences of land cover change in central Argentina. Agr Ecosyst Environ, 154: 2-11. DOI:10.1016/j.agee.2011.01.008

O'Leary, G.J. et al., 2015. Response of wheat growth, grain yield and water use to elevated CO2 under a Free-Air CO2 Enrichment (FACE) experiment and modelling in a semi-arid environment. Global Change Biol, 21(7): 2670-2686. DOI:10.1111/gcb.12830

O'Neill, C.J., Humphreys, E., Louis, J., Katupitiya, A., 2008. Maize productivity in southern New South Wales under furrow and pressurised irrigation. Aust J Exp Agr, 48(3): 285-295. DOI:10.1071/Ea06093

Oki, T., Kanae, S., 2006. Global hydrological cycles and world water resources. Science, 313(5790): 1068-1072. DOI:10.1126/science.1128845

Olesen, J.E., Bindi, M., 2002. Consequences of climate change for European agricultural productivity, land use and policy. Eur J Agron, 16(4): 239-262. DOI:10.1016/S1161-0301(02)00004-7

Olesen, J.E. et al., 2011. Impacts and adaptation of European crop production systems to climate change. Eur J Agron, 34(2): 96-112. DOI:10.1016/j.eja.2010.11.003

Ostovari, Y., Asgari, K., Cornelis, W., 2015. Performance Evaluation of Pedotransfer Functions to Predict Field Capacity and Permanent Wilting Point Using UNSODA and HYPRES Datasets. Arid Land Research and Management, 29(4): 383-398. DOI:10.1080/15324982.2015.1029649

Pardossi, A. et al., 2009. Root zone sensors for irrigation management in intensive agriculture. Sensors-Basel, 9(4): 2809-2835. DOI:10.3390/S90402809

Parkin, T.B., Meisinger, J.J., Chester, S.T., Starr, J.L., Robinson, J.A., 1988. Evaluation of Statistical Estimation Methods for Lognormally Distributed Variables. Soil Sci Soc Am J, 52(2): 323-329.

Partington, D., Werner, A.D., Brunner, P., Simmons, C.T., Dandy, G.C., Maier, H.R., 2009. Using a fully coupled surface water - groundwater model to quantify streamflow components. 18th World Imacs Congress and Modsim09 International Congress on Modelling and Simulation: Interfacing Modelling and Simulation with Mathematical and Computational Sciences: 3102-3108.

Parton, W.J., McKoewn, B., Kirchner, V., Ojima, D., 1992. User Manual for the CENTURY model.

Paudyal, G.N., Dasgupta, A., 1990. Irrigation Planning by Multilevel Optimization. J Irrig Drain E-Asce, 116(2): 273-291. DOI:Doi 10.1061/(Asce)0733-9437(1990)116:2(273)

PC-Agrar., 1994. Handbuch zum Stickstoffsimulationsmodell "Hermes" Manual, PC-Agrar Informations- und Beratungsdienst,.

Peeters, A., 2010. Country Pasture/Forage Resource Profiles. Belgium, Food and Agriculture Organization of the United Nations, Rome, Italy.

Peltonen-Sainio, P., Jauhiainen, L., Palosuo, T., Hakala, K., Ruosteenoja, K., 2015. Rainfed crop production challenges under European high-latitude conditions. Reg Environ Change: 1-13. DOI:10.1007/s10113-015-0875-1

Peltonen-Sainio, P. et al., 2010. Coincidence of variation in yield and climate in Europe. Agr Ecosyst Environ, 139(4): 483-489. DOI:10.1016/j.agee.2010.09.006

Penning de Vries, F.W.T., Jansen, D.M., H.F.M., t.B., Bakema, A., 1989. Simulation of Ecophysiological Process of Growth in Several Annual Crops. 271.

Pereira, L.S., Oweis, T., Zairi, A., 2002. Irrigation management under water scarcity. Agr Water Manage, 57(3): 175-206. DOI:10.1016/S0378-3774(02)00075-6

Pereira, L.S., Paredes, P., Cholpankulov, E.D., Inchenkova, O.P., Teodoro, P.R., Horst, M.G., 2009. Irrigation scheduling strategies for cotton to cope with water scarcity in the Fergana Valley, Central Asia. Agr Water Manage, 96(5): 723-735. DOI:10.1016/j.agwat.2008.10.013

Pereira, L.S., Paredes, P., Rodrigues, G.C., Neves, M., 2016. Modeling malt barley water use and evapotranspiration partitioning in two contrasting rainfall years. Assessing AquaCrop and SIMDualKc models (vol 159, pg 239, 2015). Agr Water Manage, 163: 408-408. DOI:10.1016/j.agwat.2015.08.017

Perez, A.J., Abrahao, R., Causape, J., Cirpka, O.A., Burger, C.M., 2011. Simulating the transition of a semi-arid rainfed catchment towards irrigation agriculture. J Hydrol, 409(3-4): 663-681. DOI:10.1016/j.jhydrol.2011.08.061

Perkins, S.P., Sophocleous, M., 1999. Development of a comprehensive watershed model applied to study stream yield under drought conditions. Ground Water, 37(3): 418-426. DOI:10.1111/j.1745-6584.1999.tb01121.x

Perroux, K.M., White, I., 1988. Designs for Disk Permeameters. Soil Sci Soc Am J, 52(5): 1205-1215.

Perry, C., Steduto, P., Allen, R.G., Burt, C.M., 2009. Increasing productivity in irrigated agriculture: Agronomic constraints and hydrological realities. Agr Water Manage, 96(11): 1517-1524. DOI:10.1016/j.agwat.2009.05.005

Pinthong, P., Clemente, R.S., 2014. Simulation of Surface/Subsurface Transport of Water and Solutes Under Different Agro-ecological Conditions and Practices. International Conference on Water Resource and Environmental Protection Wrep 2014: 121-130.

Place, R.E., Brown, D.M., 1987. Modeling Corn Yields from Soil-Moisture Estimates - Description, Sensitivity Analysis and Validation. Agr Forest Meteorol, 41(1-2): 31-56. DOI:Doi 10.1016/0168-1923(87)90068-2

Plauborg, F. et al., 2010. Modelling of root ABA synthesis, stomatal conductance, transpiration and potato production under water saving irrigation regimes. Agr Water Manage, 98(3): 425-439. DOI:10.1016/j.agwat.2010.10.006

Potopová, V., Boroneanţ, C., Boincean, B., Soukup, J., 2015. Impact of agricultural drought on main crop yields in the Republic of Moldova. International Journal of Climatology: n/a-n/a. DOI:10.1002/joc.4481

Priesack, E., Gayler, S., Hartmann, H.P., 2007. The impact of crop growth sub-model choice on simulated water and nitrogen balances. Modelling Water and Nutrient Dynamics in Soil-Crop Systems: 183-195. DOI:Doi 10.1007/978-1-4020-4479-3_13

Pulido Moncada, M., Gabriels, D., Cornelis, W.M., 2014. Data-driven analysis of soil quality indicators using limited data. Geoderma, 235–236(0): 271-278. DOI:http://dx.doi.org/10.1016/j.geoderma.2014.07.014

Purvance, D.T., Andricevic, R., 2000a. Geoelectric characterization of the hydraulic conductivity field and its spatial structure at variable scales. Water Resour Res, 36(10): 2915-2924. DOI:DOI: 10.1029/2000wr900187

Purvance, D.T., Andricevic, R., 2000b. On the electrical-hydraulic conductivity correlation in aquifers. Water Resour Res, 36(10): 2905-2913. DOI:DOI: 10.1029/2000wr900165

Qiu, R.J., Du, T.S., Kang, S.Z., Chen, R.Q., Wu, L.S., 2015. Assessing the SIMDualKc model for estimating evapotranspiration of hot pepper grown in a solar greenhouse in Northwest China. Agr Syst, 138: 1-9. DOI:10.1016/j.agsy.2015.05.001

Quiring, S.M., Legates, D.R., 2008. Application of CERES-Maize for within-season prediction of rainfed corn yields in Delaware, USA. Agr Forest Meteorol, 148(6-7): 964-975. DOI:10.1016/j.agrformet.2008.01.009

Radcliffe, D.E., Šimůnek, J., 2010. Soil Physics with HYDRUS: Modeling and Applications. CRC Press. Taylor & Francis group.

Raes, D., 2002. BUDGET - a soil water and salt balance model. Reference manual, K.U.Leuven, Department Land Management, Leuven, Belgium.

Raes, D., Geerts, S., Kipkorir, E., Wellens, J., Sahli, A., 2006a. Simulation of yield decline as a result of water stress with a robust soil water balance model. Agr Water Manage, 81(3): 335-357. DOI:10.1016/j.agwat.2005.04.006

Raes, D., Steduto, P., Hsiao, T.C., Fereres, E., 2009. AquaCrop-The FAO Crop Model to Simulate Yield Response to Water: II. Main Algorithms and Software Description. Agron J, 101(3): 438-447. DOI:10.2134/agronj2008.0140s

Raes, D., Willems, P., Gbaguidi, F., 2006b. RAINBOW – A software package for hydrometeorological frequency analysis and testing the homogeneity of historical data sets, Proceedings of the 4th International Workshop on Sustainable Management of Marginal Drylands. 4th International Workshop on Sustainable Management of Marginal Drylands, Islamabad, Pakistan, 27-31 January, 2006, 41-55.

Raman, H., Mohan, S., Rangacharya, N.C.V., 1992. Decision Support for Crop Planning during Droughts. J Irrig Drain E-Asce, 118(2): 229-241. DOI:Doi 10.1061/(Asce)0733-9437(1992)118:2(229)

Ramos, T.B., Goncalves, M.C., Martins, J.C., van Genuchten, M.T., Pires, F.P., 2006. Estimation of soil hydraulic properties from numerical inversion of tension disk infiltrometer data. Vadose Zone J, 5(2): 684-696. DOI:Doi 10.2136/Vzj2005.0076

Rao, A.S., Saxton, K.E., 1995. ANALYSIS OF SOIL-WATER AND WATER-STRESS FOR PEARL-MILLET IN AN INDIAN ARID REGION USING THE SPAW MODEL. Journal of Arid Environments, 29(2): 155-167. DOI:10.1016/s0140-1963(05)80086-2

Rashid, N.S.A., Askari, M., Tanaka, T., Simunek, J., van Genuchten, M.T., 2015. Inverse estimation of soil hydraulic properties under oil palm trees. Geoderma, 241–242(0): 306-312. DOI:http://dx.doi.org/10.1016/j.geoderma.2014.12.003

Raul, S.K., Panda, S.N., Inamdar, P.M., 2012. Sectoral Conjunctive Use Planning for Optimal Cropping under Hydrological Uncertainty. J Irrig Drain E-Asce, 138(2): 145-155. DOI:10.1061/(Asce)Ir.1943-4774.0000393

Refsgaard, J.C., Storm, B., 1995. MIKE SHE. In: Singh, V.P. (Ed.), Computer Models of Watershed Hydrology. Water Resources Publications, Colorado, USA, pp. 809-846.

Reidsma, P., Ewert, F., Lansink, A.O., Leemans, R., 2009. Vulnerability and adaptation of European farmers: a multi-level analysis of yield and income responses to climate variability. Reg Environ Change, 9(1): 25-40. DOI:10.1007/s10113-008-0059-3

Reidsma, P., Ewert, F., Lansink, A.O., Leemans, R., 2010. Adaptation to climate change and climate variability in European agriculture: The importance of farm level responses. Eur J Agron, 32(1): 91-102. DOI:10.1016/j.eja.2009.06.003

Ren, J., Yang, Y., Hu, X., 2012. Application of GIS and FEFLOW in Forecasting Groundwater Flow Field of Minqin Basin. In: Yang, Q., Zhu, L.H., He, J.J., Yan, Z.F., Ren, R. (Eds.), Advances in Civil Engineering and Architecture Innovation, Pts 1-6. Advanced Materials Research, pp. 2128-2131. DOI:10.4028/www.scientific.net/AMR.368-373.2128

Reynolds, W.D., 2006. Tension infiltrometer measurements: Implications of pressure head offset due to contact sand. Vadose Zone J, 5(4): 1287-1292. DOI:DOI 10.2136/vzj2006.0098c

Reynolds, W.D., 2008. , 2008. Saturated hydraulic properties: laboratory methods. In: Carter, M.R., Gregorich, E.G. (Eds.), Soil Sampling and Methods of Analysis. CRC Press Taylor & Francis, Boca Raton, USA, pp. 1013-1024.

Reynolds, W.D., Bowman, B.T., Brunke, R.R., Drury, C.F., Tan, C.S., 2000. Comparison of tension infiltrometer, pressure infiltrometer, and soil core estimates of saturated hydraulic conductivity. Soil Sci Soc Am J, 64(2): 478-484.

Reynolds, W.D., Elrick, D.E., 1985a. In situ measurement of field saturated hydraulic conductivity, sorptivity and the alpha parameter using the Guelph permeameter. Soil Sci., 140: 292-301.

Reynolds, W.D., Elrick, D.E., 1985b. Insitu Measurement of Field-Saturated Hydraulic Conductivity, Sorptivity, and the Alpha-Parameter Using the Guelph Permeameter. Soil Sci, 140(4): 292-302.

Reynolds, W.D., Elrick, D.E., 1991. Determination of Hydraulic Conductivity Using a Tension Infiltrometer. Soil Sci Soc Am J, 55(3): 633-639.

Rezaei, E.E., Siebert, S., Ewert, F., 2015. Impact of data resolution on heat and drought stress simulated for winter wheat in Germany. Eur J Agron, 65: 69-82. DOI:10.1016/j.eja.2015.02.003

Rezaei, M., Saey, T., Seuntjens, P., Joris, I., Boenne, W., Van Meirvenne, M., Cornelis, W., 2016a. Predicting saturated hydraulic conductivity in a sandy grassland using proximally sensed apparent electrical conductivity. Journal of Applied Geophysics, 126: 35-41.

Rezaei, M., Seuntjens, P., Joris, I., Boënne, W., Van Hoey, S., Campling, P., Cornelis, W.M., 2016b. Sensitivity of water stress in a two-layered sandy grassland soil to variations in groundwater depth and soil hydraulic parameters. Hydrol. Earth Syst. Sci., 20(1): 487-503. DOI:10.5194/hess-20-487-2016

Rezaei, M., Seuntjens, P., Shahidi, R., Joris, I., Boënne, W., Al-Barri, B., Cornelis, W., 2016c. The relevance of in-situ and laboratory characterization of sandy soil hydraulic properties for soil

water simulations. J Hydrol, 534: 251-265. DOI:http://dx.doi.org/10.1016/j.jhydrol.2015.12.062

Richards, L.A., 1931. Capillary conduction of liqids through porous mediums. Journal of Applied Physics, 1(5): 318-333. DOI:10.1063/1.1745010

Ritter, A., Hupet, F., Muñoz-Carpena, R., Lambot, S., Vanclooster, M., 2003. Using inverse methods for estimating soil hydraulic properties from field data as an alternative to direct methods. Agr Water Manage, 59(2): 77-96. DOI:http://dx.doi.org/10.1016/S0378-3774(02)00160-9

Ritter, A., Munoz-Carpena, R., 2013. Performance evaluation of hydrological models: Statistical significance for reducing subjectivity in goodness-of-fit assessments. J Hydrol, 480: 33-45. DOI:10.1016/j.jhydrol.2012.12.004

Rocha, D., Abbasi, F., Feyen, J., 2006. Sensitivity analysis of soil hydraulic properties on subsurface water flow in furrows. J Irrig Drain E-Asce, 132(4): 418-424. DOI:10.1061/(Asce)0733-9437(2006)132:4(418)

Rodrigues, G.C., Pereira, L.S., 2009. Assessing economic impacts of deficit irrigation as related to water productivity and water costs. Biosyst Eng, 103(4): 536-551. DOI:10.1016/j.biosystemseng.2009.05.002

Romano, N., 1993. Use of an Inverse Method and Geostatistics to Estimate Soil Hydraulic Conductivity for Spatial Variability Analysis. Geoderma, 60(1-4): 169-186. DOI:Doi 10.1016/0016-7061(93)90025-G

Ronayne, M.J., Houghton, T.B., Stednick, J.D., 2012. Field characterization of hydraulic conductivity in a heterogeneous alpine glacial till. J Hydrol, 458: 103-109. DOI:10.1016/j.jhydrol.2012.06.036

Rosa, R.D., Paredes, P., Rodrigues, G.C., Alves, I., Fernando, R.M., Pereira, L.S., Allen, R.G., 2012. Implementing the dual crop coefficient approach in interactive software. 1. Background and computational strategy. Agr Water Manage, 103: 8-24. DOI:10.1016/j.agwat.2011.10.013

Rosenbom, A.E., Therrien, R., Refsgaard, J.C., Jensen, K.H., Ernstsen, V., Klint, K.E.S., 2009. Numerical analysis of water and solute transport in variably-saturated fractured clayey till. J Contam Hydrol, 104(1-4): 137-152. DOI:10.1016/j.jconhyd.2008.09.001

Rossi, G., Benedini, M., Tsakiris, G., Giakoumakis, S., 1992. On regional drought estimation and analysis. Water Resour Manag, 6(4): 249-277. DOI:10.1007/BF00872280

Rotter, R.P. et al., 2012. Simulation of spring barley yield in different climatic zones of Northern and Central Europe: A comparison of nine crop models. Field Crop Res, 133: 23-36. DOI:10.1016/j.fcr.2012.03.016

Rucker, D.F., Warrick, A.W., Ferre, T.P.A., 2005. Parameter equivalence for the Gardner and van Genuchten soil hydraulic conductivity functions for steady vertical flow with inclusions. Adv Water Resour, 28(7): 689-699. DOI:10.1016/j.advwatres.2005.01.004

Rühlmann, J., Körschens, M., Graefe, J., 2006. A new approach to calculate the particle density of soils considering properties of the soil organic matter and the mineral matrix. Geoderma, 130(3–4): 272-283. DOI:http://dx.doi.org/10.1016/j.geoderma.2005.01.024

Russo, D., Bresler, E., Shani, U., Parker, J.C., 1991. Analyses of infiltration events in relation to determining soil hydraulic properties by inverse problem methodology. Water Resour Res, 27(6): 1361-1373. DOI:10.1029/90WR02776

Sadeghi, M., Jones, S.B., 2012. Scaled solutions to coupled soil-water flow and solute transport during the redistribution process. Vadose Zone J, 11, no. 2(4). DOI:10.2136/Vzj2012.0023

Saey, T. et al., 2012. Electrical conductivity depth modelling with a multireceiver EMI sensor for prospecting archaeological features. Archaeol Prospect, 19(1): 21-30. DOI:DOI: 10.1002/Arp.425

Saey, T., Simpson, D., Vermeersch, H., Cockx, L., Van Meirvenne, M., 2009a. Comparing the EM38DD and DUALEM-21S Sensors for Depth-to-Clay Mapping. Soil Sci Soc Am J, 73(1): 7-12. DOI:DOI: 10.2136/sssaj2008.0079

Saey, T., Simpson, D., Vitharana, U.W.A., Vermeersch, H., Vermang, J., Van Meirvenne, M., 2008. Reconstructing the paleotopography beneath the loess cover with the aid of an

electromagnetic induction sensor. CATENA, 74(1): 58-64. DOI:http://dx.doi.org/10.1016/j.catena.2008.03.007

Saey, T., Van Meirvenne, M., De Smedt, P., Cockx, L., Meerschman, E., Islam, M.M., Meeuws, F., 2011a. Mapping depth-to-clay using fitted multiple depth response curves of a proximal EMI sensor. Geoderma, 162(1-2): 151-158. DOI:DOI: 10.1016/j.geoderma.2011.01.015

Saey, T. et al., 2011b. Combining multiple signals of an electromagnetic induction sensor to prospect land for metal objects. Near Surf Geophys, 9(4): 309-317. DOI:DOI: 10.3997/1873-0604.2010070

Saey, T., Van Meirvenne, M., Vermeersch, H., Ameloot, N., Cockx, L., 2009b. A pedotransfer function to evaluate the soil profile textural heterogeneity using proximally sensed apparent electrical conductivity. Geoderma, 150(3-4): 389-395. DOI:DOI:10.1016/j.geoderma.2009.02.024

Salemi, H., Soom, M.A.M., Lee, T.S., Mousavi, S.F., Ganji, A., KamilYusoff, M., 2011. Application of AquaCrop model in deficit irrigation management of Winter wheat in arid region. Afr J Agr Res, 6(10): 2204-2215.

Saltelli, A. et al., 2008. Global sensitivity analysis. The Primer. John Wiley & Sons, West Sussex, England.

Sanaee-Jahromi, S., Feyen, J., Wyseure, G., Javan, M., 2001. Approach to the Evaluation of Undependable Delivery of Water in Irrigation Schemes. Irrigation and Drainage Systems, 15(3): 197-213. DOI:10.1023/a:1012674714229

Santanello, J.A., Peters-Lidard, C.D., Garcia, M.E., Mocko, D.M., Tischler, M.A., Moran, M.S., Thoma, D.P., 2007. Using remotely-sensed estimates of soil moisture to infer soil texture and hydraulic properties across a semi-arid watershed. Remote Sens Environ, 110(1): 79-97. DOI:10.1016/j.rse.2007.02.007

Satchithanantham, S., Krahn, V., Sri Ranjan, R., Sager, S., 2014. Shallow groundwater uptake and irrigation water redistribution within the potato root zone. Agr Water Manage, 132: 101-110.

Saxton, K.E., Johnson, H.P., Shaw, R.H., 1974. Modeling evapo-transpiration and soil moisture. Transactions of American Society of Agricultural Engineers, 17: 673-677.

Saxton, K.E., Porter, M.A., McMahon, T.A., 1992. CLIMATIC IMPACTS ON DRYLAND WINTER-WHEAT YIELDS BY DAILY SOILWATER AND CROP STRESS SIMULATIONS. Agr Forest Meteorol, 58(3-4): 177-192. DOI:10.1016/0168-1923(92)90060-h

Schaap, M.G., Leij, F.J., van Genuchten, M.T., 1998. Neural network analysis for hierarchical prediction of soil hydraulic properties. Soil Sci Soc Am J, 62(4): 847-855.

Schaap, M.G., Leij, F.J., van Genuchten, M.T., 2001. Rosetta: a computer program for estimating soil hydraulic parameters with hierarchical pedotransfer functions. Journal of Hydrology, 251(3–4): 163-176. DOI:http://dx.doi.org/10.1016/S0022-1694(01)00466-8

Schaible, G.D., Marcel, P.A., 2012. Water Conservation in Irrigated Agriculture: Trends and Challenges in the Face of Emerging Demands, United States.

Schapendonk, A.H.C.M., Stol, W., van Kraalingen, D.W.G., Bouman, B.A.M., 1998. LINGRA, a sink/sourced model to simulate grassland productivity in Europe. European J. of Agronomy 9: 87-100.

Scheibe, T.D., Chien, Y.J., 2003. An evaluation of conditioning data for solute transport prediction. Ground Water, 41(2): 128-141. DOI:DOI 10.1111/j.1745-6584.2003.tb02577.x

Scherberg, J., Baker, T., Selker, J.S., Henry, R., 2014. Design of Managed Aquifer Recharge for Agricultural and Ecological Water Supply Assessed Through Numerical Modeling. Water Resour Manag, 28(14): 4971-4984. DOI:10.1007/s11269-014-0780-2

Schewe, J. et al., 2014. Multimodel assessment of water scarcity under climate change. Proceedings of the National Academy of Sciences of the United States of America, 111(9): 3245-3250. DOI:10.1073/pnas.1222460110

Schindler, U., Durner, W., von Unold, G., Müller, L., 2010. Evaporation Method for Measuring Unsaturated Hydraulic Properties of Soils: Extending the Measurement Range Soil Sci Soc Am J, 74(4). DOI:10.2136/sssaj2008.0358

Schmugge, T., 2013. Estimating Near-Surface Soil Hydraulic Properties with Microwave Remote Sensing, Assessment of Non-Point Source Pollution in the Vadose Zone. American Geophysical Union, pp. 217-222. DOI:10.1029/GM108p0217

Schneider, S., Jacques, D., Mallants, D., 2013. Inverse modelling with a genetic algorithm to derive hydraulic properties of a multi-layered forest soil. Soil Res, 51(5): 372-389. DOI:10.1071/Sr13144

Schnorbus, M., Alila, Y., 2004a. Forest harvesting impacts on the peak flow regime in the Columbia Mountains of southeastern British Columbia: An investigation using long-term numerical modeling. Water Resour Res, 40(5). DOI:10.1029/2003wr002918

Schnorbus, M., Alila, Y., 2004b. Generation of an hourly meteorological time series for an alpine basin in British Columbia for use in numerical hydrologic modeling. J Hydrometeorol, 5(5): 862-882. DOI:10.1175/1525-7541(2004)005<0862:goahmt>2.0.co;2

Scholberg, J.M.S., Boote, K.J., Jones, J.W., McNeal, B.L., 1997. Adaptation of the CROPGRO model to simulate the growth of field-grown tomato. Syst Appr S, 6: 135-151.

Schulz, W.H., Lidke, D.J., Godt, J.W., 2008. Modeling the spatial distribution of landslide-prone colluvium and shallow groundwater on hillslopes of Seattle, WA. Earth Surface Processes and Landforms, 33(1): 123-141. DOI:10.1002/esp.1535

Schütze, N., Schmitz, G., 2010. OCCASION: New planning tool for optimal climate change adaption strategies in irrigation. Journal of Irrigation and Drainage Engineering, 136(12): 836-846. DOI:10.1061/(ASCE)IR.1943-4774.0000266

Schwartz, R.C., Evett, S.R., 2002. Estimating hydraulic properties of a fine-textured soil using a disc infiltrometer. Soil Sci Soc Am J, 66(5): 1409-1423.

Schwartz, R.C., Evett, S.R., 2003. Conjunctive Use of Tension Infiltrometry and Time-Domain Reflectometry for Inverse Estimation of Soil Hydraulic Properties. Vadose Zone J, 2(4): 530-538.

Schwen, A., Zimmermann, M., Bodner, G., 2014. Vertical variations of soil hydraulic properties within two soil profiles and its relevance for soil water simulations. Journal of Hydrology, 516: 169-181. DOI:10.1016/j.jhydrol.2014.01.042

Segal, E., Bradford, S.A., Shouse, P., Lazarovitch, N., Corwin, D., 2008. Integration of Hard and Soft Data to Characterize Field-Scale Hydraulic Properties for Flow and Transport Studies Vadose Zone J., 7(3): 878-889. DOI:DOI:10.2136/vzj2007.0090

Semenov, M.A., 2009. Impacts of climate change on wheat in England and Wales. J R Soc Interface, 6(33): 343-350. DOI:10.1098/rsif.2008.0285

Seuntjens, P., 2002. Field-scale cadmium transport in a heterogeneous layered soil. Water Air Soil Poll, 140(1-4): 401-423. DOI:10.1023/A:1020147610743

Seuntjens, P., Mallants, D., Toride, N., Cornelis, C., Geuzens, P., 2001. Grid lysimeter study of steady state chloride transport in two Spodosol types using TDR and wick samplers. J Contam Hydrol, 51(1-2): 13-39. DOI:10.1016/S0169-7722(01)00120-6

Shang, S.H., Mao, X.M., 2006. Application of a simulation based optimization model for winter wheat irrigation scheduling in North China. Agr Water Manage, 85(3): 314-322. DOI:10.1016/j.agwat.2006.05.015

Sheikh, V., van Loon, E.E., 2007. Comparing performance and parameterization of a one-dimensional unsaturated zone model across scales. Vadose Zone J, 6(3): 638-650. DOI:10.2136/vzj2006.0077

Sherlock, M.D., McDonnell, J.J., Curry, D.S., Zumbuhl, A.T., 2002. Physical controls on septic leachate movement in the vadose zone at the hillslope scale, Putnam County, New York, USA. Hydrol Process, 16(13): 2559-2575. DOI:10.1002/hyp.1048

Shin, Y., Mohanty, B.P., Ines, A.V.M., 2013. Estimating Effective Soil Hydraulic Properties Using Spatially Distributed Soil Moisture and Evapotranspiration. Vadose Zone J, 12(3). DOI:10.2136/vzj2012.0094

Shukla, S., Steinemann, A.C., Lettenmaier, D.P., 2011. Drought Monitoring for Washington State: Indicators and Applications. J Hydrometeorol, 12(1): 66-83. DOI:10.1175/2010jhm1307.1

Siebert, S., Burke, J., Faures, J.M., Frenken, K., Hoogeveen, J., Doll, P., Portmann, F.T., 2010. Groundwater use for irrigation - a global inventory. Hydrol Earth Syst Sc, 14(10): 1863-1880. DOI:10.5194/hess-14-1863-2010

Siebert, S., Döll, P., 2010. Quantifying blue and green virtual water contents in global crop production as well as potential production losses without irrigation. J Hydrol, 384(3–4): 198-217. DOI:http://dx.doi.org/10.1016/j.jhydrol.2009.07.031

Siebert, S., Henrich, V., Frenken, K., Burke, J., 2013. Global Map of Irrigation Areas version 5, Rheinische Friedrich-Wilhelms-University, Bonn, Germany / Food and Agriculture Organization of the United Nations, Rome, Italy.

Siimes, K., Kamari, J., 2003. A review of available pesticide leaching models: Selection of models for simulation of herbicide fate in Finnish sugar beet cultivation. Boreal Environ Res, 8(1): 31-51.

Simons, G.W.H., Bastiaanssen, W.G.M., Immerzeel, W.W., 2015. Water reuse in river basins with multiple users: A literature review. J Hydrol, 522: 558-571. DOI:http://dx.doi.org/10.1016/j.jhydrol.2015.01.016

Šimůnek, J., Hopmans, J.W., 2002. Parameter optimization and nonlinear fitting, Method of soil analysis. Part 4. Physical methods (Dane, J.H., and Topp, G.C. Eds.). Soil Science Society of America Book Series, pp. 139-157.

Šimůnek, J., Šejna, M., Saito, H., Sakai, M., van Genuchten, M.T., 2013a. The Hydrus-1D software package for simulating the movement of water, heat, and multiple solutes in variably saturated media, version 4.16, HYDRUS software series 3 Department of Environmental Sciences, University of California Riverside, Riverside, California, USA.

Šimůnek, J., Šejna, M., Saito, H., Sakai, M., van Genuchten, M.T., 2013b. The Hydrus-1D software package for simulating the movement of water, heat, and multiple solutes in variably saturated media, version 4.16, HYDRUS software series 3 Department of Environmental Sciences, University of California Riverside, Riverside, California, USA.

Šimůnek, J., Šejna, M., van Genuchten, M.T., 2006a. The HYDRUS Software Package for Simulating Two- and Three-Dimensional Movement of Water, Heat, and Multiple Solutes in Variably-Saturated Media, User Manual, Version 1.0, PC Progress, Prague, Czech Republic.

Šimůnek, J., van Genuchten, M.T., 1996. Estimating unsaturated soil hydraulic properties from tension disc infiltrometer data by numerical inversion. Water Resour Res, 32(9): 2683-2696. DOI:Doi 10.1029/96wr01525

Šimůnek, J., van Genuchten, M.T., 1997. Estimating unsaturated soil hydraulic properties from multiple tension disc infiltrometer data. Soil Sci, 162(6): 383-398. DOI:Doi 10.1097/00010694-199706000-00001

Šimůnek, J., van Genuchten, M.T., Gribb, M.M., Hopmans, J.W., 1998. Parameter estimation of unsaturated soil hydraulic properties from transient flow processes1. Soil and Tillage Research, 47(1–2): 27-36. DOI:http://dx.doi.org/10.1016/S0167-1987(98)00069-5

Šimůnek, J., van Genuchten, M.T., Sejna, M., 2000. The DISC computer software for analyzing tension disc infiltrometer data by parameter estimation. Version 1.0, U.S. Salinity Laboratory, Riverside, California.

Šimůnek, J., van Genuchten, M.T., Sejna, M., 2008. Development and applications of the HYDRUS and STANMOD software packages and related codes. Vadose Zone J, 7(2): 587-600. DOI:Doi 10.2136/Vzj2007.0077

Šimůnek, J., van Genuchten, M.T., Sejna, M., 2012. Hydrus: Model use, calibration, and validation. T Asabe, 55(4): 1261-1274.

Šimůnek, J., van Genuchten, M.T., Šejna, M., 2006b. The HYDRUS Software Package for Simulating Two- and Three-Dimensional Movement of Water, Heat, and Multiple Solutes in Variably-Saturated Media, Technical Manual, Version 1.0, PC Progress, Prague, Czech Republic

Šimůnek, J., Vogel, T., van Genuchten, M.T., 1994. The SWMS-2D Code for Simulating Water Flow and Solute Transport in Two-Dimensional Variably Saturated Media. Version 1.21. 132, USDA-ARS U.S. Salinity Laboratory, Riverside, California.

Šimůnek, J., Wendroth, O., van Genuchten, M.T., 1999. Estimating unsaturated soil hydraulic properties from laboratory tension disc infiltrometer experiments. Water Resour Res, 35(10): 2965-2979. DOI:10.1029/1999WR900179

Sitch, S. et al., 2003. Evaluation of ecosystem dynamics, plant geography and terrestrial carbon cycling in the LPJ dynamic global vegetation model. Global Change Biol, 9(2): 161-185. DOI:DOI 10.1046/j.1365-2486.2003.00569.x

Skaggs, T.H., Shouse, P.J., Poss, J.A., 2006. Irrigating forage crops with saline waters: 2. Modeling root uptake and drainage. Vadose Zone J, 5(3): 824-837. DOI:10.2136/Vzj2005.0120

Skoien, J.O., Bloschl, G., 2006. Scale effects in estimating the variogram and implications for soil hydrology. Vadose Zone J, 5(1): 153-167. DOI:10.2136/vzj2005.0069

Slater, L., 2007. Near surface electrical characterization of hydraulic conductivity: from petrophysical properties to aquifer geometries—A Review. Surv Geophys, 28(2-3): 169-197. DOI:DOI: 10.1007/s10712-007-9022-y

Slavich, P., Petterson, G., 1990. Estimating average rootzone salinity from electromagnetic induction (EM-38) measurements. Soil Research, 28(3): 453-463. DOI:http://dx.doi.org/10.1071/SR9900453

Smith, M., 1991. CROPWAT: a computer program for irrigation planning and management. , FAO Land and Water Development Division, FAO, Rome.

Sobieraj, J.A., Elsenbeer, H., Vertessy, R.A., 2001. Pedotransfer functions for estimating saturated hydraulic conductivity: implications for modeling storm flow generation. J Hydrol, 251(3-4): 202-220. DOI:DOI: 10.1016/S0022-1694(01)00469-3

Sobol, I.M., 1993. Sensitivity estimates for nonlinear mathematical models. Mathematical Modeling and Computation, 1(4): 407-414.

Spear, R.C., Hornberger, G.M., 1980. Eutrophication in peel inlet—II. Identification of critical uncertainties via generalized sensitivity analysis. Water Res, 14(1): 43-49. DOI:http://dx.doi.org/10.1016/0043-1354(80)90040-8

Specka, X., Nendel, C., Wieland, R., 2015. Analysing the parameter sensitivity of the agro-ecosystem model MONICA for different crops. Eur J Agron, 71: 73-87. DOI:10.1016/j.eja.2015.08.004

Spitters, C.J.T., 1988. An analysis of variation in yield among potato cultivars in terms of light absorption, light utilization and dry matter partitioning. International Society for Horticultural Science (ISHS), Leuven, Belgium, pp. 71-84. DOI:10.17660/ActaHortic.1988.214.5

Spitters, C.J.T., 1990. Crop growth models: Their usefulness and limitations. International Society for Horticultural Science (ISHS), Leuven, Belgium, pp. 349-368. DOI:10.17660/ActaHortic.1990.267.42

Spitters, C.J.T., van Keulen, H., van Kraalingen, D.W.G., 1989. A simple and universal crop growth simulator: SUCROS87. In: Rabbinge, R., Ward, S.A., van Laar, H.H. (Eds.), Simulation and systems management in crop protection, Wageningen, the Netherlands, pp. 147-181.

St'astna, M., Trnka, M., Kren, J., Dubrovsky, M., Zalud, Z., 2002. Evaluation of the CERES models in different production regions of the Czech Republic. Rost Vyroba, 48(3): 125-132.

Steffens, K., Larsbo, M., Moeys, J., Kjellstrom, E., Jarvis, N., Lewan, E., 2014. Modelling pesticide leaching under climate change: parameter vs. climate input uncertainty. Hydrol Earth Syst Sc, 18(2): 479-491. DOI:10.5194/hess-18-479-2014

Sternberg, T., 2011. Regional drought has a global impact. Nature, 472(7342): 169-169.

Stewart, B.A., Nielsen, D.R., 1990. Irrigation of Agricultural Crops. Agronomy No. 30, Madison, WI: ASA CSSA SSSA.

Stockle, C.O., Donatelli, M., Nelson, R., 2003. CropSyst, a cropping systems simulation model. Eur J Agron, 18(3-4): 289-307. DOI:10.1016/S1161-0301(02)00109-0

Stockle, C.O., Martin, S.A., Campbell, G.S., 1994. Cropsyst, a Cropping Systems Simulation-Model - Water Nitrogen Budgets and Crop Yield. Agr Syst, 46(3): 335-359. DOI:Doi 10.1016/0308-521x(94)90006-2

Stratonovitch, P., Storkey, J., Semenov, A.A., 2012. A process-based approach to modelling impacts of climate change on the damage niche of an agricultural weed. Global Change Biol, 18(6): 2071-2080. DOI:10.1111/j.1365-2486.2012.02650.x

Sudduth, K.A. et al., 2005. Relating apparent electrical conductivity to soil properties across the north-central USA. Comput Electron Agr, 46(1-3): 263-283. DOI:DOI: 10.1016/j.compag.2004.11.010

Sudduth, K.A., Myers, D.B., Kitchen, N.R., Drummond, S.T., 2013. Modeling soil electrical conductivity-depth relationships with data from proximal and penetrating ECa sensors. Geoderma, 199: 12-21. DOI:DOI: 10.1016/j.geoderma.2012.10.006

Sulzbacher, H. et al., 2012. Numerical modelling of climate change impacts on freshwater lenses on the North Sea Island of Borkum using hydrological and geophysical methods. Hydrol Earth Syst Sc, 16(10): 3621-3643. DOI:10.5194/hess-16-3621-2012

Sun, D., Zhao, C., Wei, H., Peng, D., 2011. Simulation of the relationship between land use and groundwater level in Tailan River basin, Xinjiang, China. Quaternary International, 244(2): 254-263. DOI:10.1016/j.quaint.2010.08.017

Sun, H.Y., Liu, C.M., Zhang, X.Y., Shen, Y.J., Zhang, Y.Q., 2006. Effects of irrigation on water balance, yield and WUE of winter wheat in the North China Plain. Agr Water Manage, 85(1-2): 211-218. DOI:10.1016/j.agwat.2006.04.008

Switzman, H., Coulibaly, P., Adeel, Z., 2015. Modeling the impacts of dryland agricultural reclamation on groundwater resources in Northern Egypt using sparse data. J Hydrol, 520: 420-438. DOI:10.1016/j.jhydrol.2014.10.064

Tafteh, A., Sepaskhah, A.R., 2012. Application of HYDRUS-1D model for simulating water and nitrate leaching from continuous and alternate furrow irrigated rapeseed and maize fields. Agr Water Manage, 113: 19-29. DOI:10.1016/j.agwat.2012.06.011

Tavakoli, A.R., Moghadam, M.M., Sepaskhah, A.R., 2016. Evaluation of the aquacrop model for barley production under deficit irrigation and rainfed condition in Iran (vol 161, pg 136, 2015). Agr Water Manage, 163: 409-409. DOI:10.1016/j.agwat.2015.08.016

Taylor, S.T., Ashcroft, G.L., 1972. Physical edaphology: The physics of irrigated and nonirrigated soils W.H. Freeman, San Francisco, CA.

Technow, F., Messina, C.D., Totir, L.R., Cooper, M., 2015. Integrating Crop Growth Models with Whole Genome Prediction through Approximate Bayesian Computation. Plos One, 10(6). DOI:10.1371/journal.pone.0130855

Teixeira, J.L., Pereira, L.S., 1992. ISAREG, an irrigation scheduling model. ICID Bulletin, 41(2): 29-48.

Teixeira, W.G., Ceddia, M.B., Ottoni, M.V., Donnagema, G.K., 2014. Application of Soil Physics in Environmental Analyses. Springer, Springer International Publishing Switzerland. DOI:10.1007/978-3-319-06013-2

Therrien, R., R.G. McLaren, E.A. Sudicky, and S.M. Panday, fully-integrated, S.A.t.-d.n.m.d., Groundwater, s.a.s.f.o.a.s.t.U.s.g., Simula, 2009. HydroGeoSphere: A three-dimensional numerical model describing fully-integrated subsurface and surface flow and solute transport: User's guide, Groundwater Simulations Group, Waterloo, ON, Canada.

Thorp, K.R., Hunsaker, D.J., French, A.N., Bautista, E., Bronson, K.F., 2015. Integrating geospatial data and cropping system simulation within a geographic information system to analyze spatial seed cotton yield, water use, and irrigation requirements. Precis Agric, 16(5): 532-557. DOI:10.1007/s11119-015-9393-x

Thyer, M., Beckers, J., Spittlehouse, D., Alila, Y., Winkler, R., 2004. Diagnosing a distributed hydrologic model for two high-elevation forested catchments based on detailed stand- and basin-scale data. Water Resour Res, 40(1). DOI:10.1029/2003wr002414

Tian, W., Li, X., Cheng, G.D., Wang, X.S., Hu, B.X., 2012. Coupling a groundwater model with a land surface model to improve water and energy cycle simulation. Hydrol Earth Syst Sc, 16(12): 4707-4723. DOI:10.5194/hess-16-4707-2012

Tian, Y., Zheng, Y., Wu, B., Wu, X., Liu, J., Zheng, C., 2015a. Modeling surface water-groundwater interaction in arid and semi-arid regions with intensive agriculture. Environ Modell Softw, 63: 170-184. DOI:10.1016/j.envsoft.2014.10.011

Tian, Y., Zheng, Y., Zheng, C., 2016. Development of a visualization tool for integrated surface water-groundwater modeling. Computers & Geosciences, 86: 1-14. DOI:10.1016/j.cageo.2015.09.019

Tian, Y. et al., 2015b. Exploring scale-dependent ecohydrological responses in a large endorheic river basin through integrated surface water-groundwater modeling. Water Resour Res, 51(6): 4065-4085. DOI:10.1002/2015wr016881

Todini, E., 2007. Hydrological catchment modelling: past, present and future. Hydrol Earth Syst Sc, 11(1): 468-482.

Toksoz, S., Kirkham, D., 1971. Steady drainage of layered soils. 1. theory. Journal of the Irrigation and Drainage Division: 1-18.

Trenberth, K.E., Dai, A.G., van der Schrier, G., Jones, P.D., Barichivich, J., Briffa, K.R., Sheffield, J., 2014. Global warming and changes in drought. Nat Clim Change, 4(1): 17-22. DOI:10.1038/Nclimate2067

Tsarouchi, G.M., Buytaert, W., Mijic, A., 2014. Coupling a land-surface model with a crop growth model to improve ET flux estimations in the Upper Ganges basin, India. Hydrol Earth Syst Sc, 18(10): 4223-4238. DOI:10.5194/hess-18-4223-2014

Tsuji, G.T., Uehara, G., Salas, S., 1994. DSSAT v3.0, University of Hawaii, Honolulu, Hawaii.

Twarakavi, N.K.C., Simunek, J., Seo, S., 2009. Reply to "Comment on 'Evaluating Interactions between Groundwater and Vadose Zone Using the HYDRUS-based Flow Package for MODFLOW'" by Navin Kumar C. Twarakavi, Jirka Simunek, and Sophia Seo. Vadose Zone J, 8(3): 820-821. DOI:10.2136/vzj2008.0004L

Twarakavi, N.K.C., Šimůnek, J., Seo, S., 2008. Evaluating Interactions between Groundwater and Vadose Zone Using the HYDRUS-Based Flow Package for MODFLOW. Vadose Zone J, 7(2): 757-768. DOI:10.2136/vzj2007.0082

UNEP, 2012. UNEP year book, Emerging issues in our global environment. United Nations Environment Programme, Nairobi, Kenya.

UNEP, 2014. UNEP year book, Emerging issues in our global environment. United Nations Environment Programme, Nairobi, Kenya.

Utset, A., Ruiz, M.E., Garcia, J., Feddes, R.A., 2000. A SWACROP-based potato root water-uptake function as determined under tropical conditions. Potato Res, 43(1): 19-29. DOI:Doi 10.1007/Bf02358510

Valverde, P., Serralheiro, R., de Carvalho, M., Maia, R., Oliveira, B., Ramos, V., 2015. Climate change impacts on irrigated agriculture in the Guadiana river basin (Portugal). Agr Water Manage, 152: 17-30. DOI:10.1016/j.agwat.2014.12.012

van Dam, J.C., Groenendijk, P., Hendriks, R.F.A., Kroes, J.G., 2008. Advances of Modeling Water Flow in Variably Saturated Soils with SWAP Vadose Zone J, 7(2): 640-653. DOI:10.2136/vzj2007.0060

van Dam, J.C., Huygen, J., Wesseling, J.G., 1997. Theory of SWAP version 2.0: simulation of water flow, solute transport and plant growth in the Soil- Water-Atmosphere-Plant environment. 71, DLO Winand Staring Centre, Wageningen. Report / Wageningen Agricultural University, Department Water Resources.

van Diepen, C.A., Wolf, J., Vankeulen, H., Rappoldt, C., 1989. Wofost - a Simulation-Model of Crop Production. Soil Use and Management, 5(1): 16-24.

van Genuchten, M.T., 1980. A closed-form equation for predicting the hydraulic conductivity of unsaturated soils. Soil Sci Soc Am J, 44(5): 892-898.

van Genuchten, M.T., Leij, F.J., Yates, S.R., 1991. The RETC code for quantifying the hydraulic functions of unsaturated soils, version 1.0, USDA, ARS, Riverside, California. .

van Genuchten, M.T., Naveira-Cotta, C., Skaggs, T.H., Raoof, A., Pontedeiro, E.M., 2014. The Use of Numerical Flow and Transport Models in Environmental Analyses. In: Teixeira, W.G., Ceddia, M.B., Ottoni, M.V., Donnagema, G.K. (Eds.), Application of Soil Physics in Environmental Analyses. Springer, Springer International Publishing Switzerland, pp. 349-376.

van Genuchten, M.T., Simunek, J., Leij, F.J., Toride, N., Sejna, M., 2012. Stanmod: Model use, calibration, and validation. T Asabe, 55(4): 1353-1366.

Van Keulen, H., Wolf, J., 1986. Modelling of agricultural production: weather, soils and crops. Pudoc, Wageningen. Simulation Monographs.

van Oijen, M., 1992. Evaluation of Breeding Strategies for Resistance and Tolerance to Late Blight in Potato by Means of Simulation. Neth J Plant Pathol, 98(1): 3-11.

Van Passel, S., Massetti, E., Mendelsohn, R., 2016. A Ricardian Analysis of the Impact of Climate Change on European Agriculture. Environmental and Resource Economics: 1-36. DOI:10.1007/s10640-016-0001-y

VanShaar, J.R., Haddeland, I., Lettenmaier, D.P., 2002. Effects of land-cover changes on the hydrological response of interior Columbia River basin forested catchments. Hydrol Process, 16(13): 2499-2520. DOI:10.1002/hyp.1017

Vazifedoust, M., van Dam, J.C., Feddes, R.A., Feizi, M., 2008. Increasing water productivity of irrigated crops under limited water supply at field scale. Agr Water Manage, 95(2): 89-102. DOI:10.1016/j.agwat.2007.09.007

Ventrella, D., Losavio, N., Vonella, A.V., Leij, F.J., 2005. Estimating hydraulic conductivity of a fine-textured soil using tension infiltrometry. Geoderma, 124(3–4): 267-277. DOI:http://dx.doi.org/10.1016/j.geoderma.2004.05.005

Verbist, K., Baetens, J., Cornelis, W.M., Gabriels, D., Torres, C., Soto, G., 2009a. Hydraulic Conductivity as Influenced by Stoniness in Degraded Drylands of Chile. Soil Sci Soc Am J, 73(2): 471-484. DOI:10.2136/sssaj2008.0066

Verbist, K., Cornelis, W.M., Gabriels, D., Alaerts, K., Soto, G., 2009b. Using an inverse modelling approach to evaluate the water retention in a simple water harvesting technique. Hydrol. Earth Syst. Sci., 13(10): 1979-1992. DOI:10.5194/hess-13-1979-2009

Verbist, K., Torfs, S., Cornelis, W.M., Oyarzun, R., Soto, G., Gabriels, D., 2010. Comparison of Single- and Double-Ring Infiltrometer Methods on Stony Soils. Vadose Zone J, 9(2): 462-475. DOI:Doi 10.2136/Vzj2009.0058

Verbist, K.M.J., Cornelis, W.M., Torfs, S., Gabriels, D., 2013a. Comparing methods to determine hydraulic conductivities on stony soils. Soil Sci. Soc. Am. J., 77(1): 25-42. DOI:10.2136/sssaj2012.0025

Verbist, K.M.J., Cornelis, W.M., Torfs, S., Gabriels, D., 2013b. Comparing Methods to Determine Hydraulic Conductivities on Stony Soils. Soil Sci Soc Am J, 77(1): 25-42. DOI:DOI 10.2136/sssaj2012.0025

Verbist, K.M.J., Pierreux, S., Cornelis, W.M., McLaren, R., Gabriels, D., 2012. Parameterizing a coupled surface-subsurface three-dimensional soil hydrological model to evaluate the efficiency of a runoff water harvesting technique. Vadose Zone J, 11(4). DOI:DOI: 10.2136/Vzj2011.0141

Vereecken, H., Kasteel, R., Vanderborght, J., Harter, T., 2007. Upscaling hydraulic properties and soil water flow processes in heterogeneous soils: A review. Vadose Zone J, 6(1): 1-28. DOI:DOI: 10.2136/Vzj2006.0055

Vereecken, H., Weynants, M., Javaux, M., Pachepsky, Y., Schaap, M.G., van Genuchten, M.T., 2010. Using Pedotransfer Functions to Estimate the van Genuchten-Mualem Soil Hydraulic Properties: A Review. Vadose Zone J, 9(4): 795-820. DOI:10.2136/vzj2010.0045

Verma, P., Singh, P., George, K.V., Singh, H.V., Devotta, S., Singh, R.N., 2009. Uncertainty analysis of transport of water and pesticide in an unsaturated layered soil profile using fuzzy set theory. Appl Math Model, 33(2): 770-782. DOI:10.1016/j.apm.2007.12.004

Voltz, M., Goulard, M., 1994. Spatial Interpolation of Soil-Moisture Retention Curves. Geoderma, 62(1-3): 109-123. DOI:Doi 10.1016/0016-7061(94)90031-0

Vorosmarty, C.J., Willmott, C.J., Choudhury, B.J., Schloss, A.L., Stearns, T.K., Robeson, S.M., Dorman, T.J., 1996. Analyzing the discharge regime of a large tropical river through remote sensing, ground-based climatic data, and modeling. Water Resour Res, 32(10): 3137-3150. DOI:10.1029/96wr01333

Vrugt, J.A., Schoups, G., Hopmans, J.W., Young, C., Wallender, W.W., Harter, T., Bouten, W., 2004. Inverse modeling of large-scale spatially distributed vadose zone properties using global optimization. Water Resour Res, 40(6). DOI:Artn W0650310.1029/2003wr002706

Vrugt, J.A., Stauffer, P.H., Wohling, T., Robinson, B.A., Vesselinov, V.V., 2008. Inverse modeling of subsurface flow and transport properties: A review with new developments. Vadose Zone J, 7(2): 843-864. DOI:10.2136/Vzj2007.0078

Vrugt, J.A., van Wijk, M.T., Hopmans, J.W., Simunek, J., 2001. One-, two-, and three-dimensional root water uptake functions for transient modeling. Water Resour Res, 37(10): 2457-2470. DOI:10.1029/2000wr000027

Waichler, S.R., Wigmosta, M.S., 2003. Development of hourly meteorological values from daily data and significance to hydrological modeling at H.J. Andrews experimental forest. J Hydrometeorol, 4(2): 251-263. DOI:10.1175/1525-7541(2003)4<251:dohmvf>2.0.co;2

Walkley, A., Black, I.A., 1934. An examination of the Degtjareff method for determining soil organic matter, and a proposed modification of the chromic acid titration method. Soil Science 37: 29-38.

Wang, E. et al., 2002. Development of a generic crop model template in the cropping system model APSIM. Eur J Agron, 18(1-2): 121-140. DOI:10.1016/S1161-0301(02)00100-4

Wang, J.H. et al., 2011. The coupled routing and excess storage (CREST) distributed hydrological model. Hydrolog Sci J, 56(1): 84-98. DOI:10.1080/02626667.2010.543087

Wang, N., Wang, J., Wang, E.L., Yu, Q., Shi, Y., He, D., 2015a. Increased uncertainty in simulated maize phenology with more frequent supra-optimal temperature under climate warming. Eur J Agron, 71: 19-33. DOI:10.1016/j.eja.2015.08.005

Wang, X., Huang, G., Yang, J., Huang, Q., Liu, H., Yu, L., 2015b. An assessment of irrigation practices: Sprinkler irrigation of winter wheat in the North China Plain. Agr Water Manage, 159: 197-208. DOI:10.1016/j.agwat.2015.06.011

Warrick, A.W., 1992. Models for Disk Infiltrometers. Water Resour Res, 28(5): 1319-1327. DOI:Doi 10.1029/92wr00149

Wegehenkel, M., Beyrich, F., 2014. Modelling hourly evapotranspiration and soil water content at the grass-covered boundary-layer field site Falkenberg, Germany. Hydrolog Sci J, 59(2): 376-394. DOI:10.1080/02626667.2013.835488

Weir, A.H., Bragg, P.L., Porter, J.R., Rayner, J.H., 1984. A Winter-Wheat Crop Simulation-Model without Water or Nutrient Limitations. J Agr Sci, 102(Apr): 371-382.

Weynants, M., Vereecken, H., Javaux, M., 2009. Revisiting Vereecken pedotransfer functions: Introducing a closed-form hydraulic model. Vadose Zone J, 8(1): 86-95. DOI:DOI: 10.2136/vzj2008.0062

Whitaker, A., Alila, Y., Beckers, J., Toews, D., 2003. Application of the distributed hydrology soil vegetation model to redfish creek, British columbia: model evaluation using internal catchment data. Hydrol Process, 17(2): 199-224. DOI:10.1002/hyp.1119

Wigmosta, M.S., Vail, L.W., Lettenmaier, D.P., 1994. A Distributed Hydrology-Vegetation Model for Complex Terrain. Water Resour Res, 30(6): 1665-1679. DOI:Doi 10.1029/94wr00436

Wildenschild, D., Roberts, J.J., Carlberg, E.D., 2000. On the relationship between microstructure and electrical and hydraulic properties of sand-clay mixtures. Geophys Res Lett, 27(19): 3085-3088. DOI:DOI: 10.1029/2000gl011553

Williams, J.R., Dyke, P.T., Jones, C.A., 1983. EPIC: a model for assessing the effects of erosion on soil productivity. In Analysis of Ecological Systems: State-of-the-Art in Ecological Modeling. , Elsevier, Amsterdam, pp.

Wöhling, T., Geiges, A., Nowak, W., Gayler, S., Hogy, P., Wizemann, H.D., 2013. Towards optimizing experiments for maximum-confidence model selection between different soil-plant models. Procedia Environ Sci, 19: 514-523. DOI:10.1016/j.proenv.2013.06.058

Wöhling, T., Schütze, N., Heinrich, B., Šimůnek, J., Barkle, G.F., 2009. Three-dimensional modeling of multiple automated equilibrium tension lysimeters to measure vadose zone fluxes. Vadose Zone J, 8(4): 1051-1063. DOI:10.2136/vzj2009.0040

Wöhling, T., Vrugt, J.A., 2008. Combining multiobjective optimization and Bayesian model averaging to calibrate forecast ensembles of soil hydraulic models. Water Resour Res, 44(12). DOI:10.1029/2008wr007154

Wöhling, T., Vrugt, J.A., 2011. Multiresponse multilayer vadose zone model calibration using Markov chain Monte Carlo simulation and field water retention data. Water Resour Res, 47. DOI:10.1029/2010wr009265

Wöhling, T., Vrugt, J.A., Barkle, G.F., 2008. Comparison of three multiobjective optimization algorithms for inverse modeling of vadose zone hydraulic properties. Soil Sci Soc Am J, 72(2): 305-319. DOI:10.2136/sssaj2007.0176

Wolf, J., 2012. LINGRA-N a grassland model for potential, water limited and N limited conditions (FORTRAN), Wageningen University, Wageningen, The Netherlands.

Wollschlager, U., Pfaff, T., Roth, K., 2009. Field-scale apparent hydraulic parameterisation obtained from TDR time series and inverse modelling. Hydrol Earth Syst Sc, 13(10): 1953-1966.

Wooding, R.A., 1968. Steady Infiltration from a Shallow Circular Pond. Water Resour Res, 4(6): 1259-&. DOI:Doi 10.1029/Wr004i006p01259

Wosten, J.H.M., Lilly, A., Nemes, A., Le Bas, C., 1999. Development and use of a database of hydraulic properties of European soils. Geoderma, 90(3-4): 169-185. DOI:Doi 10.1016/S0016-7061(98)00132-3

Wu, B., Zheng, Y., Wu, X., Tian, Y., Han, F., Liu, J., Zheng, C., 2015a. Optimizing water resources management in large river basins with integrated surface water-groundwater modeling: A surrogate-based approach. Water Resour Res, 51(4): 2153-2173. DOI:10.1002/2014wr016653

Wu, B., Zheng, Y., Wu, X., Tian, Y., Han, F., Liu, J., Zheng, C.M., 2015b. Optimizing water resources management in large river basins with integrated surface water-groundwater modeling: A surrogate-based approach. Water Resour Res, 51(4): 2153-2173. DOI:10.1002/2014wr016653

WWDR, 2015. The United Nations world water development report 2015, water for a sustainable world, Paris.

Wyseure, G., Chou, P.-Y., 2010. Short-term groundwater fluxes in the hyporheic zone as a consequence of changing river stages; numerical simulation by HYDRUS 2D/3D, EGU2010 location:. European Geosciences Union, Vienna date: 2-7 May 2010.

Xu, X., Huang, G., Zhan, H., Qu, Z., Huang, Q., 2012. Integration of SWAP and MODFLOW-2000 for modeling groundwater dynamics in shallow water table areas. J Hydrol, 412: 170-181. DOI:10.1016/j.jhydrol.2011.07.002

Xue, X.W. et al., 2013. Statistical and hydrological evaluation of TRMM-based Multi-satellite Precipitation Analysis over the Wangchu Basin of Bhutan: Are the latest satellite precipitation products 3B42V7 ready for use in ungauged basins? J Hydrol, 499: 91-99. DOI:10.1016/j.jhydrol.2013.06.042

Zadeh, K.S., Shirmohammadi, A., Montas, H.J., Felton, G., 2007. Evaluation of infiltration models in contaminated landscape. J Environ Sci Heal A, 42(7): 983-988. DOI:10.1080/10934520701373000

Zamani, S., Gobin, A., Van de Vyver, H., Gerlo, J., 2015. Atmospheric drought in Belgium – statistical analysis of precipitation deficit. International Journal of Climatology: n/a-n/a. DOI:10.1002/joc.4536

Zaradny, H., Feddes, R.A., 1979. Calculation of Non-Steady Flow Towards a Drain in Saturated-Unsaturated Soil by Finite-Elements. Agr Water Manage, 2(1): 37-53. DOI:Doi 10.1016/0378-3774(79)90012-X

Zhang, Z.F., 2015. Field Soil Water Retention of the Prototype Hanford Barrier and Its Variability with Space and Time. Vadose Zone J, 14(8). DOI:10.2136/vzj2015.01.0011

Zhao, G., Webber, H., Hoffmann, H., Wolf, J., Siebert, S., Ewert, F., 2015. The implication of irrigation in climate change impact assessment: a European-wide study. Global Change Biol, 21(11): 4031-4048. DOI:10.1111/gcb.13008

Zheng, G., Gao, L., Xue, X., 2000. Study on the simulation model for maize phenology. Jiangsu J. Agric. Sci: 15-21.

Zhou, J., Cheng, G.D., Li, X., Hu, B.X., Wang, G.X., 2012. Numerical Modeling of Wheat Irrigation using Coupled HYDRUS and WOFOST Models. Soil Sci Soc Am J, 76(2): 648-662. DOI:DOI 10.2136/sssaj2010.0467

Zhu, Y., Shi, L., Yang, J., Wu, J., Mao, D., 2013. Coupling methodology and application of a fully integrated model for contaminant transport in the subsurface system. J Hydrol, 501: 56-72. DOI:10.1016/j.jhydrol.2013.07.038

Zhu, Y., Shi, L.S., Lin, L., Yang, J.Z., Ye, M., 2012. A fully coupled numerical modeling for regional unsaturated-saturated water flow. J Hydrol, 475: 188-203. DOI:10.1016/j.jhydrol.2012.09.048

Zwart, S.J., Bastiaanssen, W.G.M., 2004. Review of measured crop water productivity values for irrigated wheat, rice, cotton and maize. Agr Water Manage, 69(2): 115-133. DOI:10.1016/j.agwat.2004.04.007

Appendices

Appendix - Chapter 2.

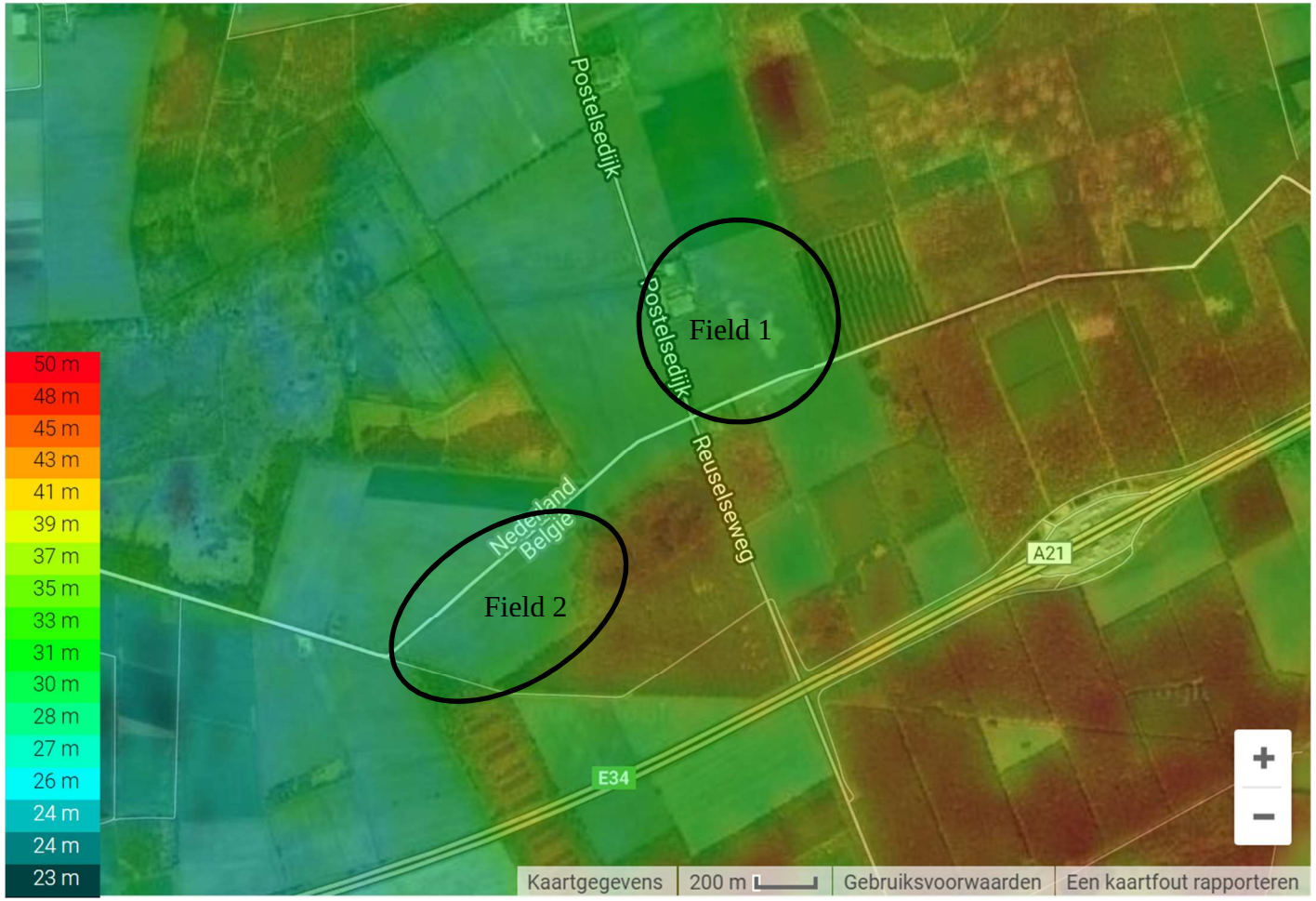

Figure. A2. 1. A topographic map of the study sites area.

The scripts for local SA programmed in Python™ software linking to Hydrus-1D (Definitions and example).

```
'''
Hydrus Parameter file adaptor:
    This modules changes a specific parameter of the Hydrus input file
    and runs the model with the adapted parameter files.
    Specifically created for the 1D columns model of the project,
    but easy to adapt to other model configurations
Project: PhD Meisam Rezaei
Author: Van Hoey Stijn

TODO:
    Hydrus Routine
        -OK input: change water parameter and rerun hydrus
        -OK output: read the output file and prepare for plot, save,...
    Local sensitivity:
        -OK define parameter-adjustment step
        -OK sensitivity calculation function in for loop (all pars and all
outputs)
        -OK plots in time (4 output plots, all pars in one plot)
    Globale sensitivity:
        - Sample MonteCarlo
        - decide the output variable
        - run model
        - visual sensitivity with scatter plots
        - calculate SRC's
import os
import sys
import time
import subprocess
import pandas as pd
import numpy as np
import matplotlib.pyplot as plt
import matplotlib.gridspec as gridspec
#-------------------------------------------------------------------------
# INPUT/OUTPUT ROUTINES
#-------------------------------------------------------------------------
def replaceInputWater(path_to_dir, newvalue, parname='Ks', layer=1):
    The Hydrus input file Selector.in always puts the water flow in BLOCK B
    The parameters values are given for each profile layer under the
parameter
    name. As such, this definition search for the parameter and layer and
    changes the par.
    Parameters
    -----------
    path_to_dir:
        Directory with the Hydrus-input and output files in
    newvalue:
        New parameter value to be used, %.9f value
    parname:
        The name of the parameter as is appears in the file
    layer:
        The layer where the parameter need to be changed
    '''
    try:

os.rename(os.path.join(path_to_dir,'Selector.in'),os.path.join(path_to_dir,
'Selector_old.in'))
```

```
    except:
        os.remove(os.path.join(path_to_dir,'Selector_old.in'))

os.rename(os.path.join(path_to_dir,'Selector.in'),os.path.join(path_to_dir,
'Selector_old.in'))

    fin = open(os.path.join(path_to_dir,'Selector_old.in'),'r')
    fout = open(os.path.join(path_to_dir,'Selector_new.in'),'wt')
    fintext = fin.readlines()
    #Get line with par headers assuming Ks is always a parameter
    #using the parameter is not possible, since eg 'n' woul give errors
    parstartline = fintext.index([x for x in fintext if 'Ks' in x][0])
    #Get index (column) of the parameter
    parcolumn = fintext[parstartline].split().index(parname)

    #adapting the lines after it
    adaptline = parstartline + layer
    parline = fintext[adaptline].split()
    parline[parcolumn] = '%.9f' % newvalue
    #we assume the floats are printed in eigth characters '%8s'
    parline_new = ['%18s'%i for i in parline]
    fintext[adaptline] = ''.join(parline_new)+'\n'
    fout.writelines(fintext)

    fin.close()
    fout.close()

os.rename(os.path.join(path_to_dir,'Selector_new.in'),os.path.join(path_to_
dir,'Selector.in'))
def runHydrus(guessed_runtime=8,
path_to_dir='D:\\Python_sensitivity\\1Dmodel2',install_dir="C:\\Program
Files (x86)\\PC-Progress\\Hydrus-1D 4.xx"):
    '''
    Run the Hydrus model from within Python

    Parameters
    ------------
    guessed_runtime:
        runtime of the model, in seconds (take some seconds more)
    path_to_dir:
        path to the working directory with input/output of Hydrus
    install_dir:
        path to the installation directory of the Hydrus software
    '''
#    cdtorun='"C:\\Program Files\\PC-Progress\\Hydrus-1D
4.xx\\H1D_CALC.EXE"  D:\\Projecten\\2013_Meisam\\1D_model'
    cdtorun=os.path.join(install_dir,'H1D_CALC.EXE')+' '+path_to_dir
    print cdtorun
    proc = subprocess.Popen(cdtorun)
#    proc = subprocess.call(cdtorun)
#    proc = subprocess.Popen(cdtorun, stderr=subprocess.PIPE,
stdout=subprocess.PIPE)
    time.sleep(guessed_runtime) #time nothing is happening to let model run
    proc.terminate()
    #WINDOWS ONLY: ADAPT FOR LINUX:
#    subprocess.Popen("taskkill /F /T /PID %i"%proc.pid , shell=True)
    #control if sleep was long enough
    #all files with the .out extension need to have 'end' in the last line
    #except of the balance, which has the runtime
    #When doing multiple runs, the calculation time of the first will be
reused if this one was too short
```

```
    files_in_dir = os.listdir(path_to_dir)
    for file_in_dir in files_in_dir:
        if file_in_dir[-4:]=='.out':
            f=open(os.path.join(path_to_dir,file_in_dir))
            f.seek(-100, os.SEEK_END) #100 should be enough for the purpose
here
            line = f.readlines()[-1]
            if file_in_dir ==  'Balance.out':
                print line
            else:
                if line <> 'end\n':
                    print 'The sleep time was not long enough to perform
the entire simulation. The file',file_in_dir,'has not the entire simulation
period written.'
            f.close()


def
filter_on_timestep(infile='Obs_Node.out',outfile='Obs_Node_filtered.out',
nnodes=5):
    '''
    Reads the node file and deletes the not-measurement timesteps
    control the presence oif every timestep
    '''
    #calculate columns with data
    cols =nnodes*3+1

    fin = open(infile)
    fout = open(outfile, 'wt')
    for line in fin.readlines():
        if not len(line.split())==cols: #copy the none-data rows
            fout.write(line)
        elif line.split()[0] =='time': #copy the data header row
            fout.write(line)
            ftaker=True
        else:
            if ftaker==True: #Always take first line/timestep up
                fout.write(line)
                old = float(line.split()[0])
                ftaker=False
            if line.split()[0][-4:]=='0000': #only take timesteps with
measurements
                new= float(line.split()[0])
                if not abs(old-new) == 1.0:
                    print 'Filtering on
timestep',line.split()[0],'failed.', abs(old-new), 'hour is considered as
timestep'
                fout.write(line)
                old = new
    fin.close()
    fout.close()
def readoutput_to_dataframe(filename='Obs_Node_filtered.out',
startdate='3/1/2012 00:00', enddate='6/13/2012 03:00', variable='theta',
nnodes=5):
    '''
    Reads data from file and puts it in a pandas dataframe to plot,
handle,...
    Always considerd 5 nodes measured, hourly frequency and 12 header lines

    Parameters
    ------------
```

```
    filename:
        Name of the file with the outputs of the model
    startdate:
        Hour of the first output
    enddate:
        Hour of the last output
    variable:
        string of theta, h or flux, representing moisture, head or flux
    Notes
    ------
    #start-date=1march 2012, 00u
    #end-date=13jun 2012, 3u

    We do the date-managing with pandas here, since scikits outdated
    '''
    if nnodes==5:
        if variable == 'theta':
            cols = (2,5,8,11,14)
        elif variable == 'h':
            cols = (1,4,7,10,13)
        elif variable == 'flux':
            cols = (3,6,9,12,15)
        else:
            raise Exception('Variable must be theta, flux or h')
    elif nnodes==4:
        if variable == 'theta':
            cols = (2,5,8,11)
        elif variable == 'h':
            cols = (1,4,7,10)
        elif variable == 'flux':
            cols = (3,6,9,12)
        else:
            raise Exception('Variable must be theta, flux or h')

    outarray = np.loadtxt(filename, skiprows=11, usecols=cols,
comments='end')
    rng = pd.date_range(start=startdate, end=enddate, freq='H')
    if nnodes==4:
        df = pd.DataFrame(outarray, index=rng, columns=['Node 10','Node
20','Node 30','Node 40'])
    elif nnodes==5:
        df = pd.DataFrame(outarray, index=rng, columns=['Node 10','Node
20','Node 30','Node 40','Node 50'])
    return df
def read_current_value():
    '''
    instead of giving a value, just read the original value from the
current selector.in
    TODO
    '''
    pass
def check_for_error(path_to_model):
    '''
    Check in model directory for error messages
    '''
    files_in_dir = os.listdir(path_to_model)
    if 'Error.msg' in files_in_dir:
        raise Exception('ATTENTION: ERROR in model run!')
def create_default_selector(path_to_model):
    '''
    To make sure, the default parameters are always used before the
```

```
    sensitivity indices are calculated.

    #original values
    #   thr     ths    Alfa      n         Ks       l
    #      0     0.4   0.015     2.4       2.18     0.5
    #      0    0.35  0.0196     2.5      2.271     0.5

    TODO: adapt to make generic
    '''
    parnames=['thr','ths','Alfa','n','Ks','l']
    parlayer1=[0.0,0.4,0.015,2.4,2.187,0.5]
    parlayer2=[0.0,0.35,0.0196,2.5, 2.271,0.5]
    ide=0
    for par in parnames:
        replaceInputWater(path_to_model, parlayer1[ide],
parname=parnames[ide], layer=1)
        replaceInputWater(path_to_model, parlayer2[ide],
parname=parnames[ide], layer=2)
        ide+=1
#-------------------------------------------------------------------------
#  LOCAL SENSITIVITY ANALYSIS
#-------------------------------------------------------------------------
#Central relative sensitivity (CRS), as calculated in CierkensK
#1/ run model 2/ run with perturbation minus 3/ run with perturbation plus
#4/ compare both visually 5/ calculates sensitvitiy (normalised stuff) for
each timestep
#original values
#   thr     ths    Alfa      n         Ks       l
#      0     0.364   0.01452     2.4693       2.187     0.5
 #      0    0.3764 0.06227     2.537      2.271     0.5
#Preliminar tests for perturbation factor
#-------------------------------------
##smaller perturbation factors not feasible with current output writing
profile
##0.01 should be better, but the output accuracy is not fine
enough!##perturbation_factor = 0.1
#path_to_model = 'D:\\Projecten\\2013_Meisam\\1D_model'
#dename = 'Alfa'
#depar = 0.01965
#llayer=2
#create_default_selector(path_to_model)
#run model with par
#replaceInputWater(path_to_model, depar, parname=dename, layer=llayer)
#runHydrus(guessed_runtime=8)
#filter_on_timestep(infile='1D_model\Obs_Node.out',outfile='1D_model\Obs_No
de_filtered1.out')
#df_Ks1 =
readoutput_to_dataframe(filename='1D_model\Obs_Node_filtered1.out',
startdate='5/4/2011 13:00', enddate='9/2/2011 11:00', variable='theta')
#run model with par + pert
#replaceInputWater(path_to_model, depar + perturbation_factor*depar,
parname=dename, layer=llayer)
#runHydrus(guessed_runtime=8)
#filter_on_timestep(infile='1D_model\Obs_Node.out',outfile='1D_model\Obs_No
de_filtered2.out')
#df_Ks1_plus =
readoutput_to_dataframe(filename='1D_model\Obs_Node_filtered2.out',
startdate='5/4/2011 13:00', enddate='9/2/2011 11:00', variable='theta')
#run model with par - pert
#replaceInputWater(path_to_model, depar - perturbation_factor*depar,
parname=dename, layer=llayer)
```

```
#runHydrus(guessed_runtime=8)
#filter_on_timestep(infile='1D_model\Obs_Node.out',outfile='1D_model\Obs_No
de_filtered3.out')
#df_Ks1_min =
readoutput_to_dataframe(filename='1D_model\Obs_Node_filtered3.out',
startdate='5/4/2011 13:00', enddate='9/2/2011 11:00', variable='theta')
##output creating of the testenvironment
##tt1 = df_Ks1_min - df_Ks1
##tt2 = df_Ks1_plus - df_Ks1
##tt1.columns = ['minus 10', 'minus 20','minus 30','minus 40','minus 50']
##tt2.columns = ['plus 10', 'plus 20','plus 30','plus 40','plus 50']
##tt = tt1.join(tt2)
##tt.plot(subplots=True, figsize=(16, 8))
#
#plt.figure()
#plt.plot(df_Ks1_plus['Node 10']-df_Ks1['Node 10'])
#plt.plot(df_Ks1['Node 10']-df_Ks1_min['Node 10'])
#dp_plus = df_Ks1_plus['Node 10']-df_Ks1['Node 10']
#dp_min = df_Ks1['Node 10']-df_Ks1_min['Node 10']
#plt.plot((dp_plus+dp_min)/2.)
#plt.plot(dp_min-dp_plus)
#-------------------------------------
#Sensitivity calcluations
#-------------------------------------
def calculate_sens(path_to_model, parameter_value, perturbation_factor =
0.01, parameter_name='Ks', parameter_layer=1,
                   startdate='3/1/2011 00:00', enddate='6/13/2012 03:00',
variable = 'theta', guessed_runtime=8,
                   nnodes=5):
    '''
    run model two (or three) times and get outputs to calculate the
sensitivity indices
    one parameter changes, all the rest stays the same; all outputs are
plotted

    make class from it to avoid the startdate/endddate arguments... TODO!
    '''
    #Make default parameter file before starting analysis
    create_default_selector(path_to_model)

    #run model with parameter value-> depreciated
#    replaceInputWater(path_to_model, parameter_value,
parname=parameter_name, layer=parameter_layer)
#    runHydrus(guessed_runtime=guessed_runtime)
filter_on_timestep(infile=os.path.join(path_to_model,'Obs_Node.out'),outfil
e=os.path.join(path_to_model,'Obs_Node_filtered1.out'))
#    df_par =
readoutput_to_dataframe(filename=os.path.join(path_to_model,'Obs_Node_filte
red1.out'), startdate=startdate, enddate=enddate, variable=variable)
    #run model with parameter value plus perturbation
    replaceInputWater(path_to_model, parameter_value +
perturbation_factor*parameter_value, parname=parameter_name,
layer=parameter_layer)
    runHydrus(guessed_runtime=guessed_runtime)

filter_on_timestep(infile=os.path.join(path_to_model,'Obs_Node.out'),outfil
e=os.path.join(path_to_model,'Obs_Node_filtered2.out'), nnodes=nnodes)
    df_par_plus =
readoutput_to_dataframe(filename=os.path.join(path_to_model,'Obs_Node_filte
red2.out'), startdate=startdate, enddate=enddate, variable=variable,
nnodes=nnodes)
```

```
    #run model with parameter value minus perturbation
    replaceInputWater(path_to_model, parameter_value -
perturbation_factor*parameter_value, parname=parameter_name,
layer=parameter_layer)
    runHydrus(guessed_runtime=guessed_runtime)

filter_on_timestep(infile=os.path.join(path_to_model,'Obs_Node.out'),outfil
e=os.path.join(path_to_model,'Obs_Node_filtered3.out'), nnodes=nnodes)
    df_par_min =
readoutput_to_dataframe(filename=os.path.join(path_to_model,'Obs_Node_filte
red3.out'), startdate=startdate, enddate=enddate, variable=variable,
nnodes=nnodes)
    #calculate sensitivity for this parameter, all outputs
    average_out = (df_par_plus+df_par_min)/2.
    #sensitivity indices:
    CAS = (df_par_plus-df_par_min)/(2.*perturbation_factor*parameter_value)
#dy/dp
    CPRS = CAS*parameter_value
    CTRS = CAS*parameter_value/average_out #or average_out  -> run less!
    #check for error files:
    check_for_error(path_to_model)
    return CAS, CPRS, CTRS, average_out, df_par_plus, df_par_min
#sensitivity for all pars in the two layers
def local_sensitivity(path_to_model,parnames, parvalues,
                      perturbation_factor = 0.1, nnodes=5,
startdate='3/1/2011 00:00',
                      enddate='6/13/2012 03:00',  guessed_runtime=8):
    Fo all parameters and all layers, do sensitivity
    plot CAS and CRS for all parameters
    TODO: save outputs for later evaluations and checkup for global
sensitvity testing
    TODO: choose output types to save to file
    '''
    #thr is assumed to be zero, sp not included
    #    parnames=['ths','Alfa','n','Ks','l']
    #    parlayer1=[0.4,0.015,2.4,2.18,0.5]
    #    parlayer2=[0.35,0.01965,2.5, 2.271,0.5]
    #    parvalues=([0.4,0.015,2.4,2.18,0.5],[0.35,0.01965,2.5, 2.271,0.5])
    #TODO: control the tuple construction
    layers = len(par_values) #length of the tuple defines the number of
layers
    ide=0
    for par in parnames: #for every parameter
        print 'Running the model for sensitivity calculation of parameter
',par
        for lay in range(layers):
            worklayer=lay+1
            print 'currently changing in layer ',str(worklayer)
            #calcluate for first layer
            CAS, CPRS, CTRS, outputs, df_par_plus, df_par_min =
calculate_sens(path_to_model, parvalues[lay][ide], parameter_name=par,

parameter_layer=worklayer,

perturbation_factor = perturbation_factor,

nnodes=nnodes,

startdate=startdate, enddate=enddate,  guessed_runtime=guessed_runtime)
            #Save outputs of CPRS in files without dates
            CPRS.to_csv('CPRS_l'+str(worklayer)+'_'+par+'.txt',index=False)
```

```
            CAS.to_csv('CPRS_l'+str(worklayer)+'_'+par+'.txt',index=False)
            CTRS.to_csv('CTRS_l'+str(worklayer)+'_'+par+'.txt',index=False)
        ide+=1
def plot_sensitivity(par='Ks', senstype="CTRS", nnodes=5):
    '''
    Plot the outputs
    '''
# read Rain data
    rain = pd.read_csv('1DModel2\\rain.csv', index_col=0, names=['rain'],
parse_dates=True,
                       dayfirst=True)
    #read the CPRS outputs
    CPRS1 = pd.read_csv(senstype+'_l1_'+par+'.txt')
    CPRS1.index=rain.index
    CPRS1_rain=rain.join(CPRS1)
    CPRS2 = pd.read_csv(senstype+'_l2_'+par+'.txt')
    CPRS2.index=rain.index
    CPRS2_rain=rain.join(CPRS2)
    #PLOT THE CPRS-outputs-----------------------------------------
    f = plt.figure(figsize=(16, 8))
    gs = gridspec.GridSpec(3, 1,height_ratios=[1,3,3])

#    ax1 = plt.subplot(gs[0])
#    ax2 = plt.subplot(gs[1])
#    ax3 = plt.subplot(gs[2])
    plt.subplots_adjust(hspace=0.08)

    ax1 = f.add_subplot(gs[0])
    ax2 = f.add_subplot(gs[1], sharex=ax1)
    ax3 = f.add_subplot(gs[2], sharex=ax1)

#    rain in ax1
#  CPRS1_rain['rain'].plot(kind='bar',style='black',ax=ax1,
xticks=[],yticks=[10,20,30,40])
    CPRS1_rain['rain'].plot(style='black',ax=ax1,
xticks=[])#,yticks=[10,20,30,40])
    ax1.set_ylabel(r'rain (mm)')

    #parchange of layer 1 in ax2
    CPRS1_rain['Node 10'].plot(ax=ax2,style='b', xticks=[])
    CPRS1_rain['Node 20'].plot(ax=ax2,style='g', xticks=[])
    CPRS1_rain['Node 30'].plot(ax=ax2,style='r', xticks=[])
    CPRS1_rain['Node 40'].plot(ax=ax2,style='y', xticks=[])
    if nnodes==5:
        CPRS1_rain['Node 50'].plot(ax=ax2,style='purple', xticks=[])
    ax2.set_ylabel(r' '+senstype+' - '+par+'$_1$')
    #parchange of layer 2 in ax3
    CPRS2_rain['Node 10'].plot(ax=ax3,style='b')
    CPRS2_rain['Node 20'].plot(ax=ax3,style='g')
    CPRS2_rain['Node 30'].plot(ax=ax3,style='r')
    CPRS2_rain['Node 40'].plot(ax=ax3,style='y')
    if nnodes==5:
        CPRS2_rain['Node 50'].plot(ax=ax3,style='purple')
    ax3.set_ylabel(r' '+senstype+' - '+par+'$_2$')
    # Shink current axis's height by 10% on the bottom
    box = ax3.get_position()
    ax3.set_position([box.x0, box.y0 + box.height * 0.1,
                      box.width, box.height * 0.9])
    # Put a legend below current axis
    ax3.legend(loc='lower center', bbox_to_anchor=(0.5, -0.35),
              fancybox=False, shadow=False, ncol=5)
```

```
#    ax1.xaxis.set_visible(False)
#    ax2.xaxis.set_visible(False)
    for tl in ax1.get_xticklabels():
            tl.set_visible(False)
    for tl in ax2.get_xticklabels():
            tl.set_visible(False)
    plt.savefig('CPRS_newversion'+par+'.pdf')
def quickplot(df,nnodes=5):
    """
    Test for docu;entation
    """
    f=plt.figure(figsize=(16,8))
    gs = gridspec.GridSpec(2, 1,height_ratios=[1,3])
    plt.subplots_adjust(hspace=0.08)
    ax1 = f.add_subplot(gs[0])
    ax2 = f.add_subplot(gs[1], sharex=ax1)
    rain.plot(ax=ax1,style='k', xticks=[])
    df['Node 10'].plot(ax=ax2,style='b')
    df['Node 20'].plot(ax=ax2,style='g')
    df['Node 30'].plot(ax=ax2,style='r')
    df['Node 40'].plot(ax=ax2,style='y')
    if nnodes==5:
        df['Node 50'].plot(ax=ax2,style='purple')
    # Shink current axis's height by 10% on the bottom
    box = ax2.get_position()
    ax2.set_position([box.x0, box.y0 + box.height * 0.1,
                      box.width, box.height * 0.9])
    # Put a legend below current axis
    ax2.legend(loc='lower center', bbox_to_anchor=(0.5, -0.25),
              fancybox=False, shadow=False, ncol=5)
#-------------------------------------------------------------------------
#TUTORIAL HOW TO USE THE MODEL RUNNING
#-------------------------------------------------------------------------
###Put the defqult parameters
#path_to_model='D:\\Python_sensitivity\\1Dmodel2'
##create_default_selector(path_to_model)
###replace a parameter
#replaceInputWater(path_to_model, 3., parname='Ks', layer=1)
###run the model
#runHydrus(guessed_runtime=4, path_to_dir=
'D:\\Python_sensitivity\\1Dmodel2',install_dir="C:\\Program Files
(x86)\\PC-Progress\\Hydrus-1D 4.xx")
####prepare the filtered output file
#filter_on_timestep(infile='1Dmodel2\Obs_Node.out',outfile='1Dmodel2\Obs_No
de_filtered.out', nnodes=4)
####read output in dataframe
#df = readoutput_to_dataframe(filename='1Dmodel2\Obs_Node_filtered.out',
startdate='3/1/2012 00:00', enddate='6/13/2012 03:00', variable='theta',
nnodes=4)
####plot the outputs in graph
##df.plot(subplots=True, figsize=(16, 8), yticks=[0.0,0.2,0.4])
##get the rain from the data
#rain = pd.read_csv('D:\\Python_sensitivity\\1Dmodel2\\rain.csv',
index_col=0, names=['rain'], parse_dates=True, dayfirst=True)
#quickplot(df,nnodes=4)
#TUTORIAL SENSITIVTY
#-----------------------------------------------
#path_to_model='D:\\Python_sensitivity\\1Dmodel2'
```

```
#CAS, CPRS, CTRS, average_out, df_par_plus, df_par_min =
calculate_sens(path_to_model, 22.2, perturbation_factor = 0.1,
parameter_name='Ks', parameter_layer=1,
#                   startdate='5/4/2011 13:00', enddate='9/2/2011 11:00',
variable = 'theta', guessed_runtime=8)
#bf=CTRS
#f=plt.figure(figsize=(16,8))
#gs = gridspec.GridSpec(2, 1,height_ratios=[1,3])
#plt.subplots_adjust(hspace=0.08)
#ax1 = f.add_subplot(gs[0])
#ax2 = f.add_subplot(gs[1], sharex=ax1)
#rain.plot(ax=ax1,style='k', xticks=[])
#bf['Node 10'].plot(ax=ax2,style='b')
#bf['Node 20'].plot(ax=ax2,style='g')
#bf['Node 30'].plot(ax=ax2,style='r')
#bf['Node 40'].plot(ax=ax2,style='y')
#bf['Node 50'].plot(ax=ax2,style='purple')
## Shink current axis's height by 10% on the bottom
#box = ax2.get_position()
#ax2.set_position([box.x0, box.y0 + box.height * 0.1,
#                 box.width, box.height * 0.9])
## Put a legend below current axis
#ax2.legend(loc='lower center', bbox_to_anchor=(0.5, -0.25),
#          fancybox=False, shadow=False, ncol=5)
####DO SENSITIVITY FOR ALL
#par_names=['ths','Alfa','n','Ks','l']
par_names=['Ks', 'Alfa', 'n', 'ths', 'l']
#par_names=['Ks']
#par_values=([2.18],[2.271])
par_values=([2.18, 0.015, 2.4, 0.4, 0.5],[2.271, 0.0196, 2.271, 0.35, 0.5])
local_sensitivity(path_to_model,par_names, par_values, nnodes=4,
guessed_runtime=2, startdate='3/1/2012 00:00',
                    enddate='6/13/2012 03:00')
plot_sensitivity(par='Ks', senstype="CTRS", nnodes=4)
plot_sensitivity(par='Alfa', senstype="CTRS", nnodes=4)
plot_sensitivity(par='n', senstype="CTRS", nnodes=4)
plot_sensitivity(par='ths', senstype="CTRS", nnodes=4)
plot_sensitivity(par='l', senstype="CTRS", nnodes=4)
plot_sensitivity(par='Ks', senstype="CPRS", nnodes=4)
plot_sensitivity(par='Alfa', senstype="CPRS", nnodes=4)
plot_sensitivity(par='n', senstype="CPRS", nnodes=4)
plot_sensitivity(par='ths', senstype="CPRS", nnodes=4)
plot_sensitivity(par='l', senstype="CPRS", nnodes=4)
```

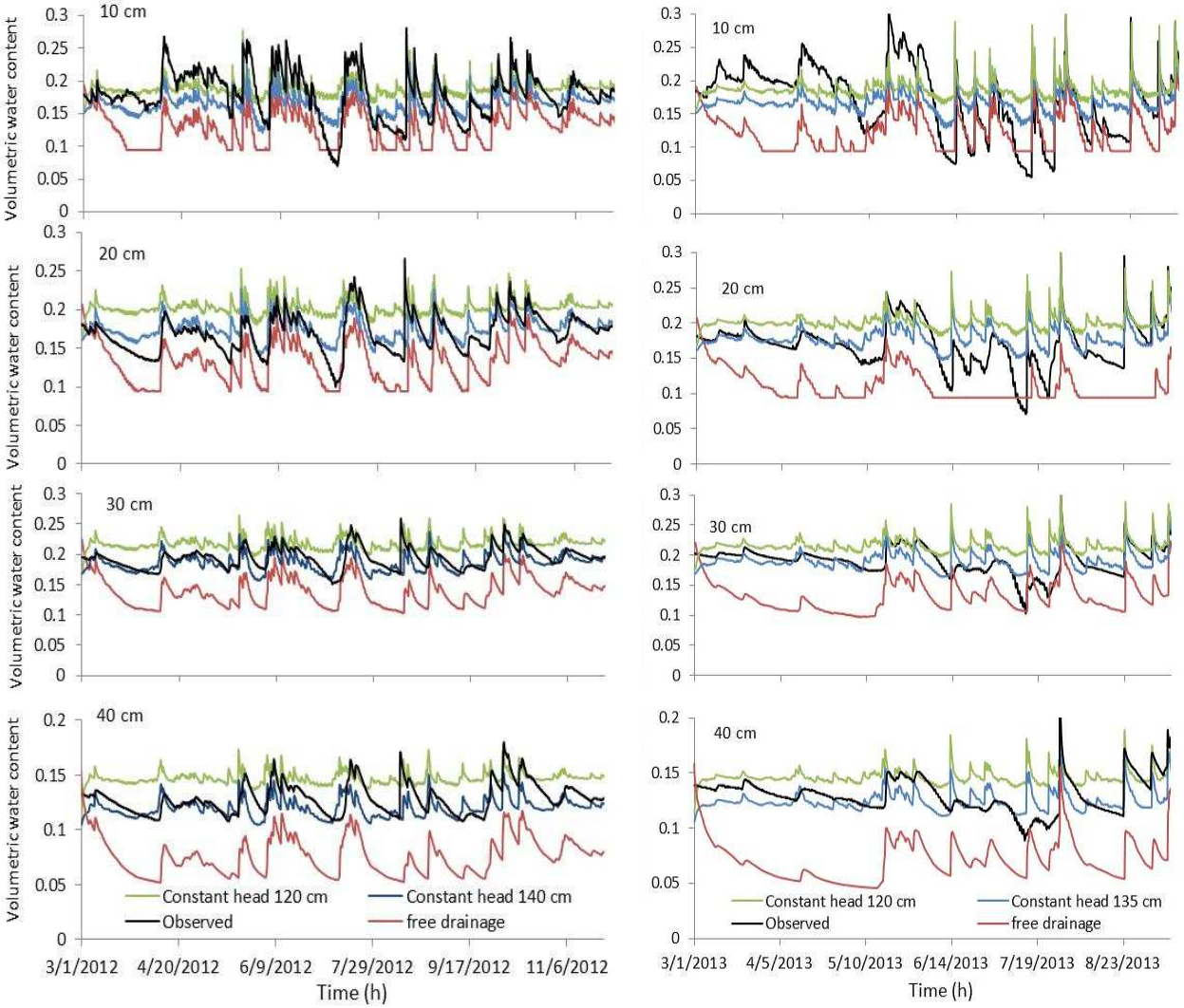

Figure A2-2. Effects of homogeneous and heterogeneous of free drainage and different constant head conditions on water content estimation for 2012.

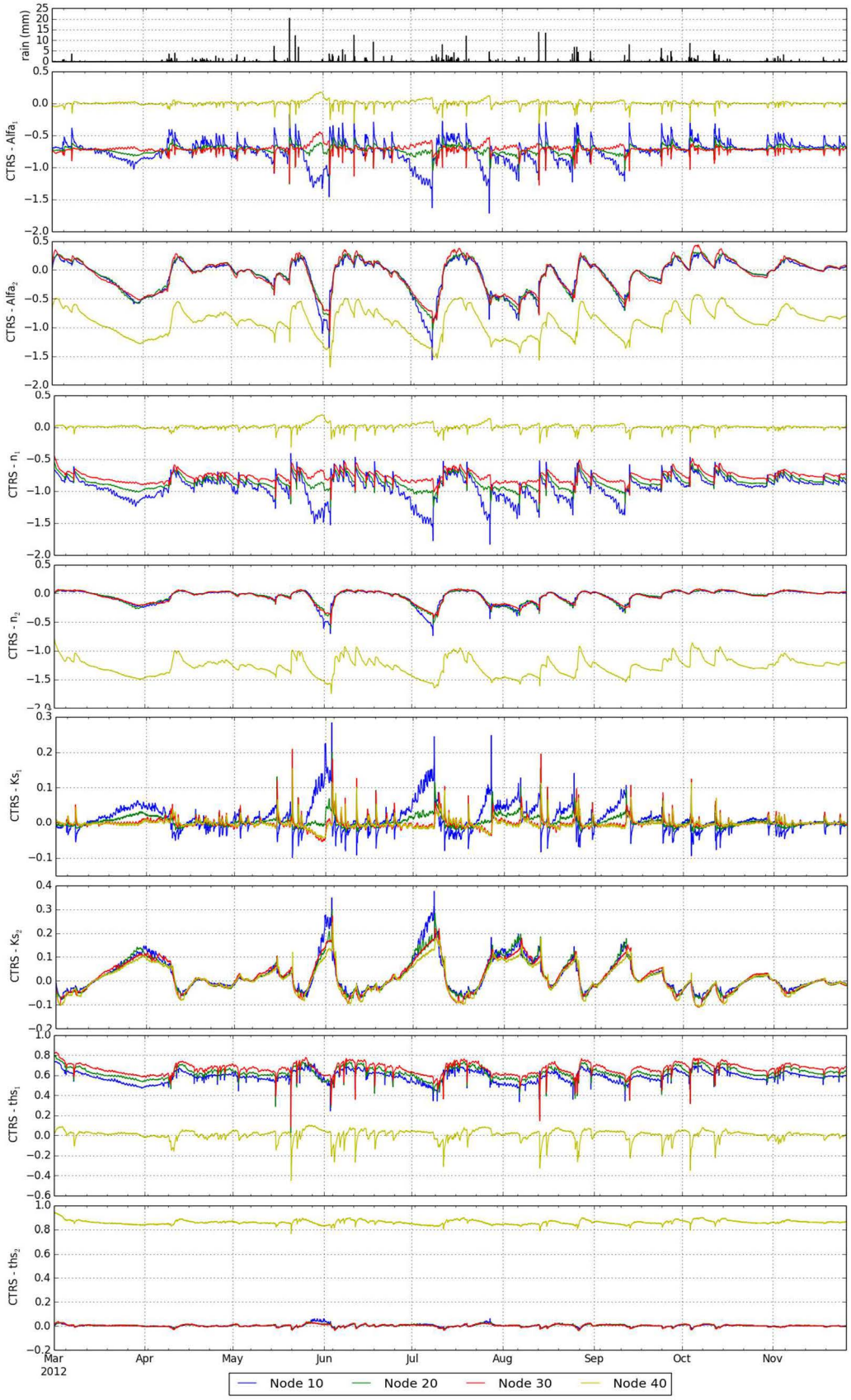

Figure. A2-3. Parameter sensitivity as a function of time (constant head) in 2012. The numbers 1 and 2 correspond to the first and second layer.

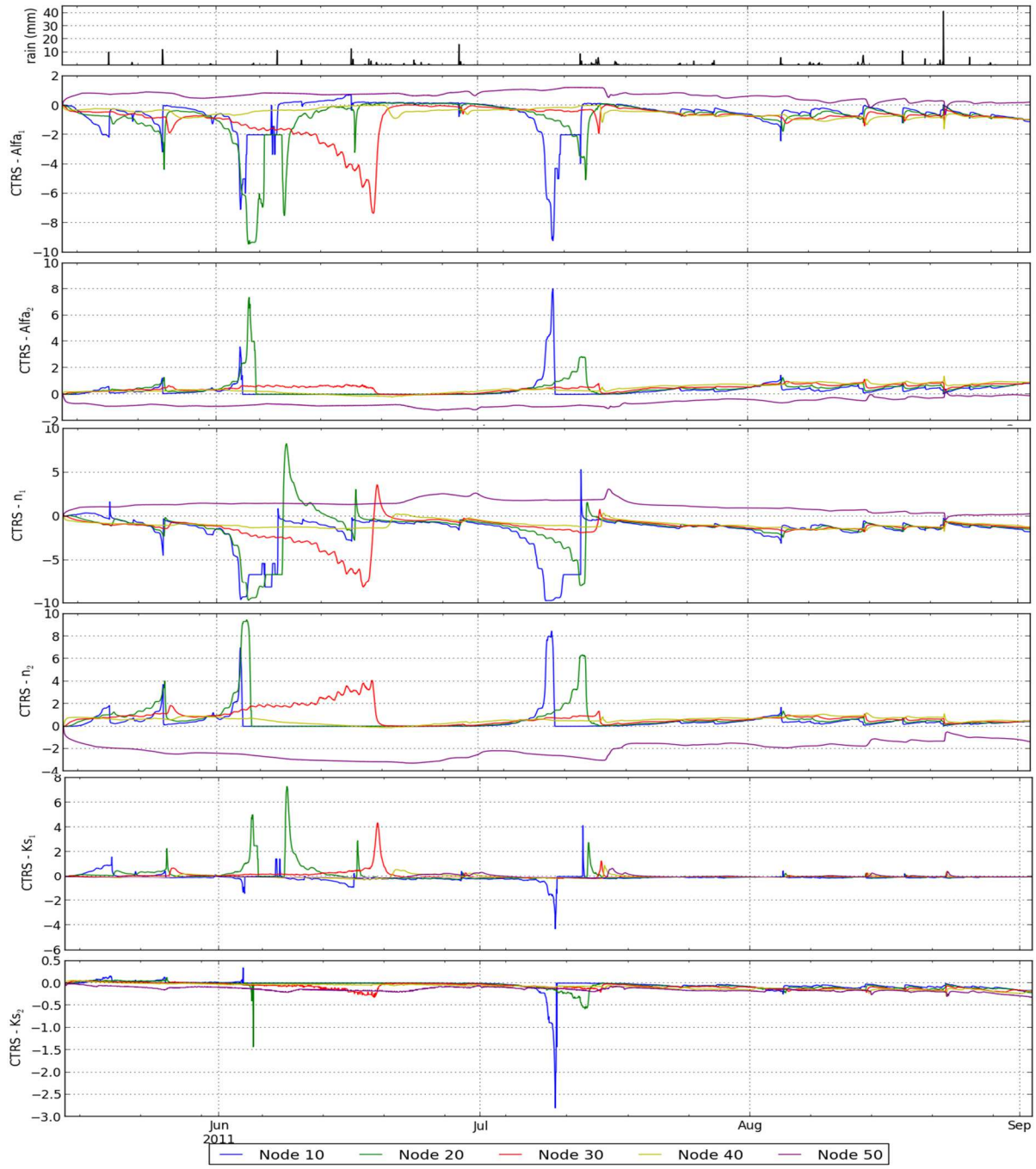

Figure. A2-4. Parameter sensitivity as a function of time (free drainage) in 2011. The numbers 1 and 2 correspond to the first and second layer.

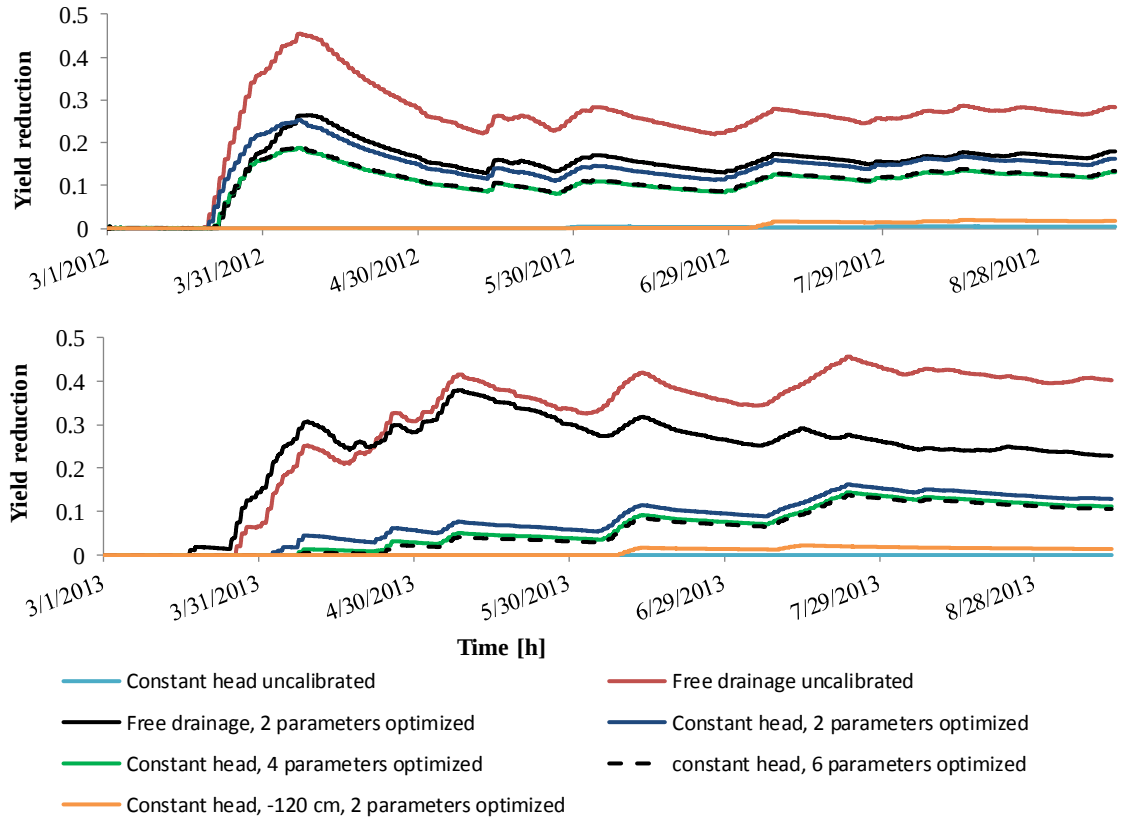

Figure A2-5. Yield reduction of various scenarios and bottom boundary conditions in 2012 and 2013 (Eq. 2-9).

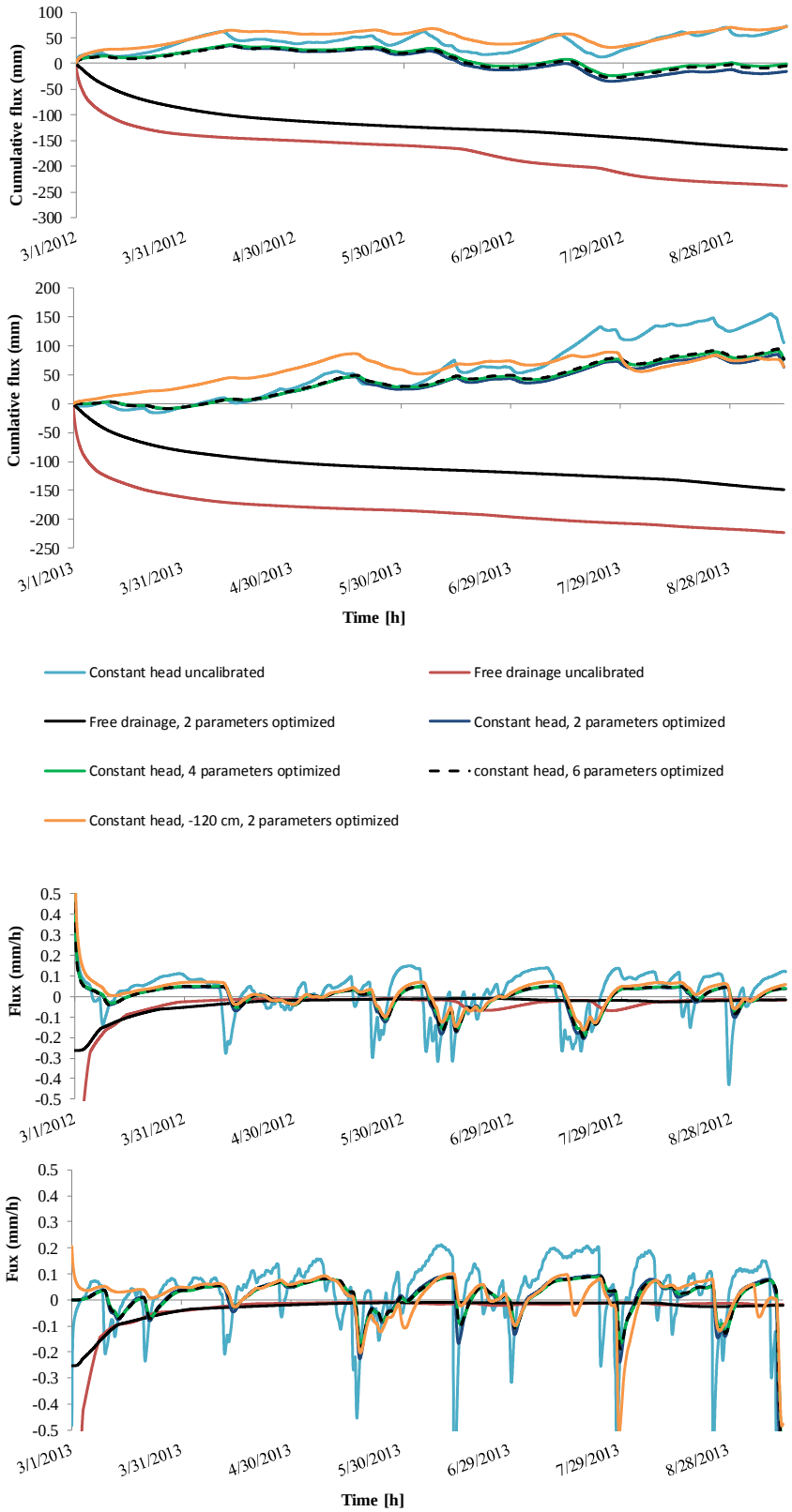

Figure A2-6. Cumulative fluxes of different boundary condition and parameter scenarios for calibration and validation periods (top), Actual fluxes of different boundary condition and parameter scenarios for calibration and validation periods (bottom).

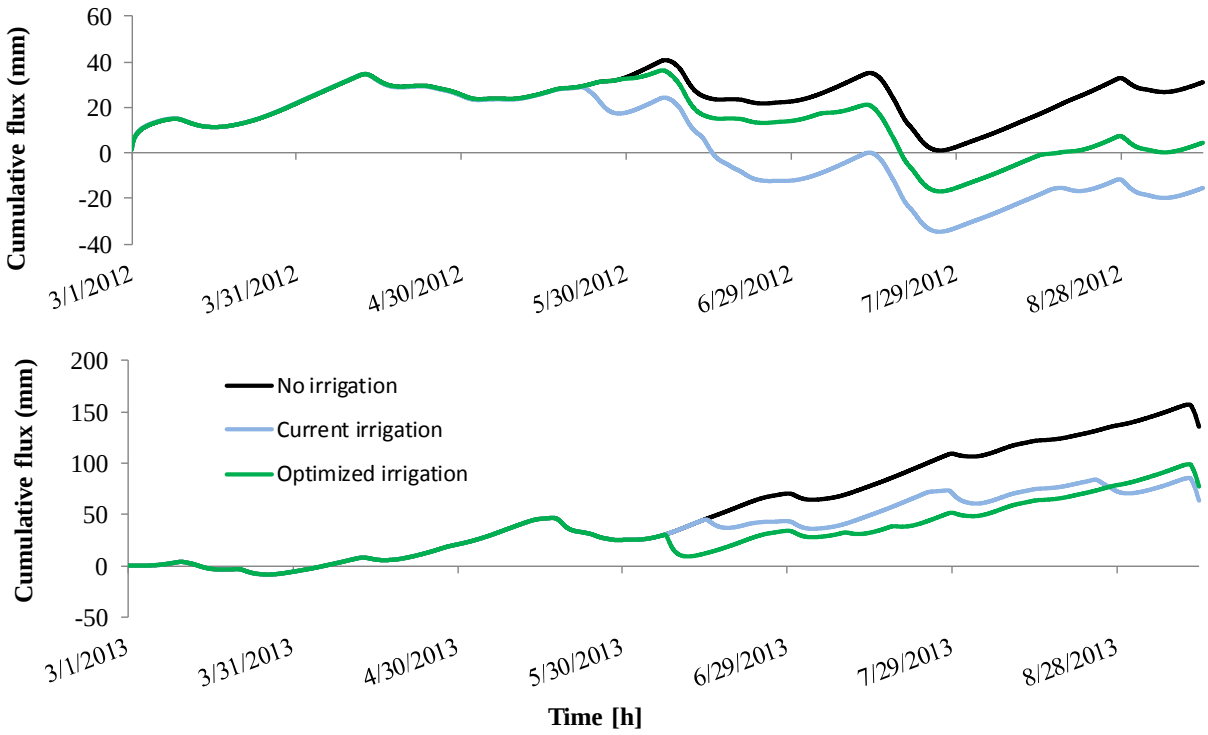

Figure A2-7. Cumulative flux of farmer's conventional irrigation (current irrigation), without irrigation and optimized irrigation scheme (guided irrigation) for calibration and validation periods.

Appendix-Chapter 3.

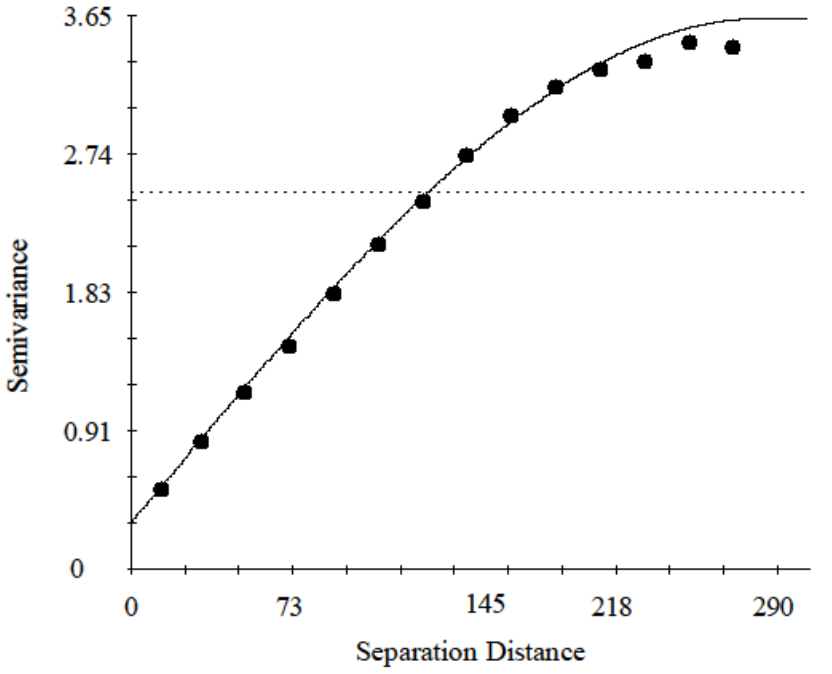

Spherical model (Co = 0.310; Co + C = 3.630; Ao = 281.90; r^2 = 0.989;RSS = 0.094)

Figure A3-1. Semivariogram of soil electrical conductivity, ECa, (DOE of 0-50 cm).

Appendix-Chapter 4. Photos of location of sensors and field hydraulic conductivity measurements.

Figure A4-1. Local weather station and installed sensors in the field.

Figure A4-2. Sensors location at late growing season and the tensiometer which was installed the interface of layers (right)..

Figure A4-3. Field hydraulic conductivity measurement at different depths.

Appendix-Chapter 5. The scripts for quasi 3D modeling approach programmed in Python™ software linking to Hydrus-1D (Definitions and example). The scripts are based on SA scripts (Appendix-Chapter 1)

Run Hydrus in Batch

```
@author: Jan De Pue,
#==============================================================================
# Run Hydrus in Batch
#==============================================================================
import os
import sys
import numpy
import pylab
import shutil
import distutils.dir_util as dir_util
import linecache
import glob
from matplotlib.path import Path
import matplotlib.patches as patches
from scipy.interpolate import griddata
import time
from Hydrus_Funky import *
from matplotlib.backends.backend_pdf import PdfPages
figlist=[]
#figsize=[10,8]
figsize=[20,16]
dpi=None
pylab.ioff()
font = {'family' : 'monospace',
        'size'   : 11}
pylab.rc('font', **font)
HydrusPath="C:\\Program Files (x86)\\PC-Progress\\Hydrus-1D 4.xx"  #
RefProjectPath="C:\\HydrusProjects\\Quasi3D_ResolutionTest\\quasitest2012triggered
_NoInverse"
OutputPath="C:\\HydrusProjects\\Quasi3D_ResolutionTest\\Output"
FinalOutputPath='Z:\\shares\\bw12\\OG
Bodemfysica\\WorkInProgress\\Quasi3D_ResolutionTest'
#==============================================================================
# Get Input Data
#==============================================================================
print('Open Input')
InputFilename_FL="C:\HydrusProjects\Quasi3D_ResolutionTest\FL_50cm.txt"
# PATH TO KS & GWT INPUT DATA
InputFilename_GWT="C:\HydrusProjects\Quasi3D_ResolutionTest\GWL_50cm.txt" # PATH
TO KS & GWT INPUT DATA
InputFilename_KS="C:\HydrusProjects\Quasi3D_ResolutionTest\KSAT_50cm.txt" # PATH
TO KS & GWT INPUT DATA
InputFilename_Irrigation="Z:\\shares\\bw12\\OG
Bodemfysica\\WorkInProgress\\Quasi3D_ResolutionTest\\Hydrus_Meisam_BatchSampleGrid
Run_quasitest2012triggered_NoInverse_2.npz" # PATH TO KS & GWT INPUT DATA
FL_Source=numpy.genfromtxt(InputFilename_FL,delimiter='\t',skip_header=1)
nI=FL_Source.shape[0]
X_FL=FL_Source[:,0]
Y_FL=FL_Source[:,1]
FL=FL_Source[:,2] # cm

KS_Source=numpy.genfromtxt(InputFilename_KS,delimiter='\t',skip_header=1)
nI=KS_Source.shape[0]
X_KS=KS_Source[:,0]
Y_KS=KS_Source[:,1]
KS=KS_Source[:,2] # cm
GWT_Source=numpy.genfromtxt(InputFilename_GWT,delimiter='\t',skip_header=1)
nI=GWT_Source.shape[0]
```

```
X_GWT=GWT_Source[:,0]
Y_GWT=GWT_Source[:,1]
GWT=GWT_Source[:,2]*100 # cm
#========================================================================
# Run Hydrus
#========================================================================
Resolution_All=numpy.array([10.,])
nR=Resolution_All.size
Hull=[[651634.0,5687522.0],[651617,5687567],[651617,5687571],[651901,5687667.5],[6
51993,5687435.5],[651738,5687261.1],[651711,5687324],[651601,5687285.5],[651526,56
87481.5],[651634.0,5687522.0]]
hull_path = Path(Hull)
Storage_All=[]
Stress_All=[]
StressArea_All=[]
Yield_All=[]
SampleData_All=[]
ProcessingTime_All=[]
Irrigation_All=[]
for iR in range(nR):
#for iR in [20,]:
    Storage_Sample=[]
    Stress_Sample=[]
    StressArea_Sample=[]
    Yield_Sample=[]
    SampleData_Sample=[]
    ProcessingTime_Sample=[]
    Irrigation_Sample=[]
#    nS=nS_L[iR]
    if 'triggered' in RefProjectPath:
        Savez=numpy.load(InputFilename_Irrigation)
        SampleData_Sample=Savez['SampleData_Sample']
        IrrigationData_Full=Savez['Irrigation']
        nS=IrrigationData_Full.shape[0]
    else:
        nS=1
    for iS in range(nS):
        print('%s/%s - %s/%s'%(iR,nR,iS,nS))
        print('Subsample Grid : Resolution = %s m'%(Resolution_All[iR]))

        nI=0
        while nI<1:
FL_RandomSample=SubSampleGrid_random(FL_Source,Resolution_All[iR],Hull_Coordinates
=Hull)
            nI=numpy.size(FL_RandomSample)
        X_RandomSample=FL_RandomSample[:,0]
        Y_RandomSample=FL_RandomSample[:,1]
        FL_RandomSample=FL_RandomSample[:,2]
        KS_RandomSample = griddata((X_KS,Y_KS), KS, (X_RandomSample,
Y_RandomSample), method='nearest')
        GWT_RandomSample = griddata((X_GWT,Y_GWT), GWT, (X_RandomSample,
Y_RandomSample), method='nearest')
        if 'triggered' in RefProjectPath:
            X_Irrigation=SampleData_Sample[iS][:,0]
            Y_Irrigation=SampleData_Sample[iS][:,1]
            IrrigationID=numpy.arange(X_Irrigation.size).astype(int)
            IrrigationData=IrrigationData_Full[iS]
            TotalIrrigationVolume=[]
            nIrr=Y_Irrigation.size
            for iIrr in range(nIrr):
                IrrrigationData_iIrr=numpy.array(IrrigationData[iIrr])
                if IrrrigationData_iIrr.size>0:
TotalIrrigationVolume.append(IrrrigationData_iIrr[:,4].sum())
                else:
                    TotalIrrigationVolume.append(0.0)
            TotalIrrigationVolume=numpy.array(TotalIrrigationVolume)
```

```
            IrrigationID_RandomSample = griddata((X_Irrigation,Y_Irrigation),
IrrigationID, (X_RandomSample, Y_RandomSample), method='nearest')
            ## Irrigation map
            IrrMapRes=2.0
IrrigationPlotX=numpy.arange(numpy.array(Hull)[:,0].min(),numpy.array(Hull)[:,0].m
ax()+IrrMapRes,IrrMapRes)

IrrigationPlotY=numpy.arange(numpy.array(Hull)[:,1].min(),numpy.array(Hull)[:,1].m
ax()+IrrMapRes,IrrMapRes)
            IrrigationPlotGrid=numpy.meshgrid(IrrigationPlotX,IrrigationPlotY)
            IrrigationPlotGrid_Volume = griddata((X_Irrigation,Y_Irrigation),
TotalIrrigationVolume, (IrrigationPlotGrid[0], IrrigationPlotGrid[1]),
method='nearest')
            hull_path = Path(Hull)

Hull_check=hull_path.contains_points(numpy.array([IrrigationPlotGrid[0].flatten(),
IrrigationPlotGrid[1].flatten()]).transpose())
            IrrigationPlotGrid_Volume=IrrigationPlotGrid_Volume.flatten()
            IrrigationPlotGrid_Volume[~Hull_check]=numpy.nan

IrrigationPlotGrid_Volume=numpy.reshape(IrrigationPlotGrid_Volume,IrrigationPlotGr
id[0].shape)
            fig=pylab.figure(figsize=figsize)
            ax=fig.add_subplot(111)
            extent=[IrrigationPlotX[0],IrrigationPlotX[-1],IrrigationPlotY[-
1],IrrigationPlotY[0]]
im=ax.imshow(IrrigationPlotGrid_Volume,interpolation='nearest',cmap='viridis_r',vm
in=0,vmax=50,extent=extent)
            ax.plot(X_Irrigation,Y_Irrigation,'wo')
            ax.set_aspect('equal')
            ax.invert_yaxis()
            fig.colorbar(im)
            pylab.show()
        nI=X_RandomSample.size
        print('Walk The Grid')
        Storage_Temp=[]
        Stress_Temp=[]
        Yield_Temp=[]
        Irrig_Temp=[]
        tic = time.clock()
        for iI in range(nI):
            print('\t%s/%s'%(iI,nI))
            RunCorrect=0
            while RunCorrect==0:
                print('\tReplace')
                # Copy Original project
                Postfix='_Temp'
                ReplaceProjectPath=RefProjectPath+Postfix
                time.sleep(0.1)
#                shutil.rmtree(ReplaceProjectPath)
                dir_util.copy_tree(RefProjectPath,ReplaceProjectPath)
                shutil.copy(RefProjectPath+'.h1d',ReplaceProjectPath+'.h1d')
                time.sleep(0.1)

                Ks_replacement=KS_RandomSample[iI]
                GWT_replacement=GWT_RandomSample[iI]
                FL_replacement=FL_RandomSample[iI]
                # Modify Selector.in
                SelectorPath=os.path.join(RefProjectPath,'SELECTOR.IN')
                fID=open(SelectorPath,'r')
                SelectorOriginal=fID.read()
                fID.close()
                OriginalLine="   thr     ths    Alfa      n         Ks       l\n
0.082   0.385   0.017    2.05      1.199     0.5 \n   0.05    0.32    0.02    2.52
2.27     0.5 \n"
```

```
                ReplaceLine="   thr     ths    Alfa      n         Ks       l\n
0.082   0.385   0.017    2.05      %s     0.5 \n   0.05    0.32    0.02    2.52
2.27     0.5 \n"%Ks_replacement
                SelectorReplace=SelectorOriginal.replace(OriginalLine,ReplaceLine)
                if ReplaceLine not in SelectorReplace:
                    print('WARNING: KS REPLACEMENT UNSUCCESSFUL')
ReplaceSelectorPath=os.path.join(ReplaceProjectPath,'SELECTOR.IN')
                fID=open(ReplaceSelectorPath,'r+')
                fID.seek(0)
                fID.write(SelectorReplace)
                fID.truncate()
                fID.close()
                # Modify Profile.dat
                ProfilePath=os.path.join(RefProjectPath,'PROFILE.DAT')

ProfileData=numpy.genfromtxt(ProfilePath,skip_header=5,skip_footer=2)
                nZ=ProfileData.shape[0]
                    # Replace GWT
                ProfileData[:,2]=-ProfileData[:,1]-GWT_replacement
                    # Change layer depth
                ProfileData[ProfileData[:,1] >= -FL_replacement,3]=1
                ProfileData[ProfileData[:,1] < -FL_replacement,3]=2
                formatline=' %3.0d %7.7e %7.7e %3.0d %3.0d %7.7e %7.7e %7.7e
%7.7e\n'
                ReplaceProfilePath=os.path.join(ReplaceProjectPath,'PROFILE.DAT')
                fID=open(ProfilePath,'r')
                fIDreplace=open(ReplaceProfilePath,'w')
                nH=5
                nF=2
                for iH in range(nH):
                    fIDreplace.write(fID.readline())
                fID.close()
                for iZ in range(nZ):
                    fIDreplace.write(formatline%tuple(ProfileData[iZ,:]))
                for iF in range(1+nH+nZ,1+nH+nZ+nF):
                    fIDreplace.write(linecache.getline(ProfilePath,iF))
                fIDreplace.close()
                # Irrigation
                if 'triggered' in RefProjectPath:
                    Irrigation_ReplacementID=IrrigationID_RandomSample[iI]
IrrigationData_Replacement=IrrigationData[Irrigation_ReplacementID]
                    if len(IrrigationData_Replacement)>0:
IrrigationData_Replacement=numpy.array(IrrigationData_Replacement)
IrrigationData_Replacement_TSTART=IrrigationData_Replacement[:,2]
IrrigationData_Replacement_TEND=IrrigationData_Replacement[:,3]
IrrigationData_Replacement_FLUX=IrrigationData_Replacement[:,4]/(IrrigationData_Re
placement_TEND-IrrigationData_Replacement_TSTART)
 AtmosphPath=os.path.join(RefProjectPath,'ATMOSPH.IN')
ReplaceAtmosphPath=os.path.join(ReplaceProjectPath,'ATMOSPH.IN')
AtmosphData=numpy.genfromtxt(AtmosphPath,skip_header=11,skip_footer=1)
                        nT=AtmosphData.shape[0]
                        AtmosphData_T=AtmosphData[:,0]
                        AtmosphData_P=AtmosphData[:,1]
                        fID=open(AtmosphPath,'r')
                        fIDreplace=open(ReplaceAtmosphPath,'w')
                        nH=11
                        nF=5
                        formatline='          %s           %s %s        %s      %s
%s           %s           %s \n'
                        for iH in range(nH):
                            fIDreplace.write(fID.readline())
                        iIrr=0
                        if IrrigationData_Replacement_TSTART[0]<AtmosphData_T[0]:
                            DoIrrigation=1
                        else:
                            DoIrrigation=0
                        for iT in range(nT):
```

```
                            T=AtmosphData_T[iT]
                            if DoIrrigation == 1:
                                skipstring=fID.readline()
fIDreplace.write(formatline%(AtmosphData[iT,0],
AtmosphData[iT,1]+IrrigationData_Replacement_FLUX[iIrr],
AtmosphData[iT,2],
AtmosphData[iT,3],
AtmosphData[iT,4],
AtmosphData[iT,5],
AtmosphData[iT,6],
AtmosphData[iT,7])) ## LET ME THINK
                            else:
                                fIDreplace.write(fID.readline())
                            if T>=IrrigationData_Replacement_TSTART[iIrr]:
                                DoIrrigation=1
                            if T>=IrrigationData_Replacement_TEND[iIrr]:
                                DoIrrigation=0
                                if iIrr<IrrigationData_Replacement_TEND.size-1:
                                    iIrr+=1
                        for iF in range(nF):
                            fIDreplace.write(fID.readline())
                        fIDreplace.close()
                print('\tRun')
                runHydrus(ReplaceProjectPath,HydrusPath, guessed_runtime=-1)
NodInfOutName=os.path.join(ReplaceProjectPath,'Nod_Inf.out')
NodInf_T,NodInf_Data,NodInf_Header=ReadNodInfOut(NodInfOutName)

                nNT=NodInf_T.size
#                 if nNT == 39:
                if nNT == 101:
#                 if nNT == 79:
                    RunCorrect = 1
                else :
                    print('Hydrus Malfunction: Retry')
                    time.sleep(2)
            Storage_zTop=0 # cm
            Storage_zBottom=-20 # cm

            NodInfOutName=os.path.join(ReplaceProjectPath,'Nod_Inf.out')
            NodInf_T,NodInf_Data,NodInf_Header=ReadNodInfOut(NodInfOutName)

            nNT=NodInf_T.size
            Storage_SubTemp=numpy.zeros(nNT)
            for iNT in range(nNT):
                NodInf_StorageLayer_NodeDepth=NodInf_Data[iNT][:,1]

NodInf_StorageLayer_NodeDepth=NodInf_StorageLayer_NodeDepth[(NodInf_StorageLayer_N
odeDepth>=Storage_zBottom) & (NodInf_StorageLayer_NodeDepth<=Storage_zTop)]

NodInf_StorageLayer_NodeDepthHalfway=numpy.concatenate(([NodInf_StorageLayer_NodeD
epth[0],],(NodInf_StorageLayer_NodeDepth[:-
1]+NodInf_StorageLayer_NodeDepth[1:])/2,[NodInf_StorageLayer_NodeDepth[-1],]))

NodInf_StorageLayer_NodeWidth=NodInf_StorageLayer_NodeDepthHalfway[:-1]-
NodInf_StorageLayer_NodeDepthHalfway[1:]
                NodInf_StorageLayer_VWC=NodInf_Data[iNT][:,3]

NodInf_StorageLayer_VWC=NodInf_StorageLayer_VWC[(NodInf_Data[iNT][:,1]>=Storage_zB
ottom) & (NodInf_Data[iNT][:,1]<=Storage_zTop)]


Storage_SubTemp[iNT]=numpy.sum(NodInf_StorageLayer_VWC*NodInf_StorageLayer_NodeWid
th)

            Storage_Temp.append(Storage_SubTemp)
```

```
            # Stress

            TLevelOutName=os.path.join(ReplaceProjectPath,'T_Level.out')
            TlevelData,TLevel_Header=ReadTLevelOut(TLevelOutName)
            Stress=TlevelData[:,4]/TlevelData[:,2]
            Stress_Temp.append(Stress)

            # Yield
            Yield=(12160*((TlevelData[:,9])+(TlevelData[:,18]))/52.4)
            Yield_Temp.append(Yield)

            # Irrigation
            IrrigOutName=os.path.join(ReplaceProjectPath,'Irrig.out')
            IrrigationHappened=os.path.isfile(IrrigOutName)
            if IrrigationHappened:
IrrigMeta,IrrigMeta_Header,IrrigData,IrrigData_Header=ReadIrrigOut(IrrigOutName)
                Irrig_Temp.append(IrrigData)
        toc = time.clock()
        print('Collect Output')
        ProcessingTime=toc - tic
        fig=pylab.figure(figsize=figsize)
        ax=fig.add_subplot(111)
        patch = patches.PathPatch(hull_path, facecolor='w', lw=2)
        ax.add_patch(patch)
ax.plot(X_RandomSample,Y_RandomSample,'o',mec='r',mew=2,mfc='None',label='Sample')
        ax.set_aspect('equal')
        ax.set_xlabel('X (m)')
        ax.set_ylabel('Y (m)')
        ax.set_title('Sample Locations')
        figlist.append(fig)
        Storage_Sample.append(numpy.array(Storage_Temp).mean(axis=0))
        Stress_Sample.append(numpy.array(Stress_Temp).mean(axis=0))
        StressLevel=0.95
StressArea_Sample.append((numpy.array(Stress_Temp)<StressLevel).mean(axis=0))
        Yield_Sample.append(numpy.array(Yield_Temp).mean(axis=0))
SampleData_Sample.append(numpy.array([X_RandomSample,Y_RandomSample,FL_RandomSampl
e,KS_RandomSample,GWT_RandomSample]).transpose())
        ProcessingTime_Sample.append(ProcessingTime)
        Irrigation_Sample.append(Irrig_Temp)
    Storage_All.append(Storage_Sample)
    Stress_All.append(Stress_Sample)
    StressArea_All.append(StressArea_Sample)
    Yield_All.append(Yield_Sample)
    SampleData_All.append(SampleData_Sample)
    ProcessingTime_All.append(ProcessingTime_Sample)
    Irrigation_All.append(Irrigation_Sample)
    basename=os.path.basename(sys.argv[0])[:-3]
    postfix=os.path.basename(RefProjectPath)
    savename='%s_%s_%s'%(basename,postfix,iR)
    savename=os.path.join(FinalOutputPath,savename)
numpy.savez(savename,Storage_Sample=Storage_Sample,Stress_Sample=Stress_Sample,Str
essArea_Sample=StressArea_Sample,Yield_Sample=Yield_Sample,SampleData_Sample=Sampl
eData_Sample,ProcessingTime_Sample=ProcessingTime_Sample,Resolution=Resolution_All
[iR],NodInf_T=NodInf_T,Tlevel_T=TlevelData[:,0],Irrigation=Irrigation_Sample)
    ## PDF
    pdfname=savename+'.pdf'
    pp = PdfPages(pdfname)
    for fig in figlist:
        pp.savefig(fig)

    pp.close()
    figlist = []
```

Output of run Hydrus in batch

```
#========================================================================
# Read Hydrus output files
#========================================================================
import os
import sys
import numpy
import pylab
import shutil
import distutils.dir_util as dir_util
import linecache
import glob
import StringIO
from Hydrus_Funky import *
from matplotlib.backends.backend_pdf import PdfPages
figlist=[]
figsize=[10,8]
#figsize=[20,10]
dpi=None
pylab.ioff()
font = {'family' : 'monospace',
        'size'   : 11}
pylab.rc('font', **font)
HydrusPath="D:\\quasirun"  # INSTALLATION FOLDER HYDRUS
RefProjectPath="D:\\quasitest" # PROJECT FOLDER
OutputPath="D:\\batchrun\\Output2" # OUTPUT FOLDER (CREATE NEW IF NESCESSARY)
#========================================================================
# Input
#========================================================================
InputFilename="D:Quasi3D_FL_280.txt" # PATH TO KS & GWT INPUT DATA
InputData=numpy.genfromtxt(InputFilename,delimiter='\t',skip_header=1)
nI=InputData.shape[0]
X_In=InputData[:,0]
Y_In=InputData[:,1]
GWT_In=InputData[:,2]*100 # cm
Ks_In=InputData[:,3] # cm/h
FL_In=InputData[:,4] # cm
ID_In=numpy.arange(nI)
#========================================================================
# Find files
#========================================================================
print('Find')
OutputList=glob.glob(OutputPath+'\\*Obs_Node.out')
OutputList.sort()
nF=len(OutputList)
ObsNode_All=[]
for iF in range(nF):
    filename=OutputList[iF]
    ObsNode_ID=int(os.path.basename(filename).split('_')[0])
    ObsNode_Nodes,ObsNode_t,ObsNode_L=ReadObsNodeOut(filename)
    ObsNode_All.append([ObsNode_ID,ObsNode_Nodes,ObsNode_t,ObsNode_L])
OutputList=glob.glob(OutputPath+'\\*Nod_Inf.out')
OutputList.sort()
nF=len(OutputList)
NodInf_All=[]
for iF in range(nF):
    filename=OutputList[iF]
    NodInf_ID=int(os.path.basename(filename).split('_')[0])
    NodInf_T,NodInf_Data = ReadNodInfOut(filename)
    NodInf_All.append([NodInf_ID,NodInf_T,NodInf_Data])
OutputList=glob.glob(OutputPath+'\\*A_Level.out')
OutputList.sort()
nF=len(OutputList)
ALevel_All=[]
for iF in range(nF):
    filename=OutputList[iF]
```

```
    ALevel_ID=int(os.path.basename(filename).split('_')[0])
    ALevel_Data=ReadALevelOut(filename)
    ALevel_All.append([ALevel_ID,ALevel_Data])
## T_Level.out
OutputList=glob.glob(OutputPath+'\\*T_Level.out')
OutputList.sort()
nF=len(OutputList)
TLevel_All=[]
for iF in range(nF):
    filename=OutputList[iF]
    TLevel_ID=int(os.path.basename(filename).split('_')[0])
    TLevel_Data=numpy.genfromtxt(filename,skip_header=9,skip_footer=1)
    TLevel_All.append([TLevel_ID,TLevel_Data])
#=========================================================================
# Extract specific data for analysis
#=========================================================================
ID=numpy.zeros(nF)
X=numpy.zeros(nF)
Y=numpy.zeros(nF)
TLevel_T_All=[]
TLevel_RootStress_All=[]
Storage_zTop=0
Storage_zBottom=-20
NodInf_StorageLayer=[]
for iF in range(nF):
    ID[iF]=ID_In[iF]
    X[iF]=X_In[ID_In==ID[iF]]
    Y[iF]=Y_In[ID_In==ID[iF]]
    TLevel_ID=numpy.array(map(lambda x: x[0], TLevel_All))
    iTLevel=numpy.where(TLevel_ID==ID_In[iF])[0]
    TLevel_T_All.append(TLevel_All[iTLevel][1][:,0])
TLevel_RootStress_All.append(TLevel_All[iTLevel][1][:,4]/TLevel_All[iTLevel][1][:,
2])
    NodInf_ID=numpy.array(map(lambda x: x[0], NodInf_All))
    iNodInf=numpy.where(NodInf_ID==ID_In[iF])[0]
    NodInf_StorageLayer_T=NodInf_All[iNodInf][1]
    nNT=NodInf_StorageLayer_T.size
    NodInf_StorageLayer_Temp=numpy.zeros(nNT)
    for iNT in range(nNT):
        NodInf_StorageLayer_NodeDepth=NodInf_All[iNodInf][2][iNT][:,1]
NodInf_StorageLayer_NodeDepth=NodInf_StorageLayer_NodeDepth[(NodInf_StorageLayer_N
odeDepth>=Storage_zBottom) & (NodInf_StorageLayer_NodeDepth<=Storage_zTop)]

NodInf_StorageLayer_NodeDepthHalfway=numpy.concatenate(([NodInf_StorageLayer_NodeD
epth[0],],(NodInf_StorageLayer_NodeDepth[:-
1]+NodInf_StorageLayer_NodeDepth[1:])/2,[NodInf_StorageLayer_NodeDepth[-1],]))
NodInf_StorageLayer_NodeWidth=NodInf_StorageLayer_NodeDepthHalfway[:-1]-
NodInf_StorageLayer_NodeDepthHalfway[1:]
        NodInf_StorageLayer_VWC=NodInf_All[iNodInf][2][iNT][:,3]
NodInf_StorageLayer_VWC=NodInf_StorageLayer_VWC[(NodInf_StorageLayer_NodeDepth>=St
orage_zBottom) & (NodInf_StorageLayer_NodeDepth<=Storage_zTop)]
NodInf_StorageLayer_Temp[iNT]=numpy.sum(NodInf_StorageLayer_VWC*NodInf_StorageLaye
r_NodeWidth)
    NodInf_StorageLayer.append(NodInf_StorageLayer_Temp)
NodInf_StorageLayer=numpy.array(NodInf_StorageLayer)
printT_Tlevel=numpy.arange(0,6480,7*24)
printT_Tlevel=numpy.append(printT_Tlevel,6480)
nPT_Tlevel=printT_Tlevel.size
TLevel_RootStress=numpy.zeros((nF,nPT_Tlevel))
for iF in range(nF):
    for iPT in range(nPT_Tlevel):
        iPT_T=numpy.argmin((TLevel_T_All-printT_Tlevel[iPT])**2)
        TLevel_RootStress[iF,iPT]=TLevel_RootStress_All[iF][iPT_T]
#=========================================================================
# Plot
#=========================================================================
print('Plot')
```

```
cm=pylab.get_cmap('Paired')
fig=pylab.figure(figsize=figsize,dpi=dpi)
ax=fig.add_subplot(111)
sc=ax.scatter(X_In,Y_In,40,GWT_In,lw=0)
ax.set_title('GWT')
ax.axis('equal')
fig.colorbar(sc)
figlist.append(fig)
fig=pylab.figure(figsize=figsize,dpi=dpi)
ax=fig.add_subplot(111)
sc=ax.scatter(X_In,Y_In,40,Ks_In,lw=0)
ax.set_title('Ks')
ax.axis('equal')
fig.colorbar(sc)
figlist.append(fig)
fig=pylab.figure(figsize=figsize,dpi=dpi)
ax=fig.add_subplot(111)
sc=ax.scatter(X_In,Y_In,40,FL_In,lw=0)
ax.set_title('Top Layer Thickness')
ax.axis('equal')
fig.colorbar(sc)
figlist.append(fig)
vmn=0.9
vmx=1
cmap='gist_heat'
for iPT in range(nPT_Tlevel):
    fig=pylab.figure(figsize=figsize,dpi=dpi)
    ax=fig.add_subplot(111)
sc=ax.scatter(X,Y,50,TLevel_RootStress[:,iPT],vmin=vmn,vmax=vmx,cmap=cmap,edgecolo
rs='0.2')
    ax.set_title('Soil Water Stress | T = %s d'%(printT_Tlevel[iPT]/24))
    ax.axis('equal')
    fig.colorbar(sc)
    figlist.append(fig)
fig=pylab.figure(figsize=figsize,dpi=dpi)
ax=fig.add_subplot(111)
for iF in range(nF):
    ID=TLevel_All[iF][0]
    color=cm(1.*ID/nF)
    Tp=TLevel_T_All[iF]
    Yp=TLevel_RootStress_All[iF]
    ax.plot(Tp,Yp,color=color,label=ID)
ax.set_title('Soil Water Stress')
ax.set_ylabel('Soil Water Stress ')
ax.set_xlabel('Time (h)')
ax.legend()
figlist.append(fig)
vmn=2
vmx=6
cmap='coolwarm_r'
for iNT in range(nNT):
    fig=pylab.figure(figsize=figsize,dpi=dpi)
    ax=fig.add_subplot(111)
sc=ax.scatter(X,Y,50,NodInf_StorageLayer[:,iNT],vmin=vmn,vmax=vmx,cmap=cmap,edgeco
lors='0.2')
    ax.set_title('Storage between %s cm and %s cm | T = %5.0d
d'%(Storage_zTop,Storage_zBottom,NodInf_StorageLayer_T[iNT]/24))
    ax.axis('equal')
    fig.colorbar(sc)
    figlist.append(fig)
fig=pylab.figure(figsize=figsize,dpi=dpi)
ax=fig.add_subplot(111)
for iF in range(nF):
    ID=TLevel_All[iF][0]
    color=cm(1.*ID/nF)
    Tp=NodInf_StorageLayer_T
    Yp=NodInf_StorageLayer[iF]
```

```
    ax.plot(Tp,Yp,color=color,label=ID)
ax.set_title('Storage between %s cm and %s cm'%(Storage_zTop,Storage_zBottom))
ax.set_ylim(0,10)
ax.set_ylabel('Storage')
ax.set_xlabel('Time (h)')
ax.legend()
figlist.append(fig)
#================================================================================
# Save
#================================================================================
print('Save')
import sys
basename=os.path.basename(sys.argv[0])[:-3]
## PDF
directory='D:\\batchrun\\Output2'
pdfname=os.path.join(directory, basename+'.pdf')
pp = PdfPages(pdfname)
for fig in figlist:
    pp.savefig(fig)
pp.close()
pylab.show()
```

Hydrus -Funky

```
#================================================================================
# Hydrus related Functions- RUN HYDRUS
#================================================================================
def runHydrus(path_to_dir,install_dir="C:\\Program Files (x86)\\PC-
Progress\\Hydrus-1D 4.xx", guessed_runtime=8):
    Author: Van Hoey Stijn
    Run the Hydrus model from within Python
    Parameters
    guessed_runtime:  runtime of the model, in seconds (take some seconds more)
    path_to_dir:      path to the working directory with input/output of Hydrus
    install_dir:       path to the installation directory of the Hydrus software
    import os
    import subprocess
    import time
    cdtorun=os.path.join(install_dir,'H1D_CALC.EXE')+' '+path_to_dir
    print(cdtorun)
    proc = subprocess.Popen(cdtorun)
    time.sleep(guessed_runtime)    proc.terminate()
    files_in_dir = os.listdir(path_to_dir)
    for file_in_dir in files_in_dir:
        if file_in_dir[-4:]=='.out':
            f=open(os.path.join(path_to_dir,file_in_dir))
            f.seek(-100, os.SEEK_END)            line = f.readlines()[-1]
            if file_in_dir ==  'Balance.out':
                print(line)
            elif file_in_dir ==  'Fit.out':
                print(line)
            else:
                if line <> 'end\n':
                    print('The sleep time was not long enough to perform the
entire simulation. The file',file_in_dir,'has not the entire simulation period
written.')
            f.close()
    check_for_error(path_to_dir)
def check_for_error(path_to_model):
    Author: Van Hoey Stijn
    Check in model directory for error messages
    import os
    files_in_dir = os.listdir(path_to_model)
    if 'Error.msg' in files_in_dir:
```

```
        raise Exception('ATTENTION: ERROR in model run!')
#==========================================================================
# I/O
#==========================================================================
def ReadObsNodeOut(ObsOutName):
    read Obs_Node.out:
    h, theta, Flux versus time
    import numpy
    import linecache
    Sim=numpy.genfromtxt(ObsOutName,skip_header=11,skip_footer=1)
    sh=Sim.shape
    nNodes_sim=(sh[1]-1)/3
    ObsNode_Nodes=numpy.array(linecache.getline(ObsOutName,9).replace('
','').replace('\n','').replace('Node(','').split(')')[:-1]).astype('int')
    ObsNode_L=[]
    ObsNode_t=Sim[:,0]
    for iN in range(nNodes_sim):
        ObsNode_L.append(Sim[:,iN*3+1:(iN+1)*3+1])
    return ObsNode_Nodes,ObsNode_t,ObsNode_L
def ReadNodInfOut(NodInfOutName):
    read Obs_Node.out:
    0 Node
    1 Depth
    2 Head
    3 Moisture
    4 K
    5 C
    6 Flux
    7 Sink
    8 Kappa
    9 v/KsTop
    10 Temp
    import numpy
    import StringIO
    fID=open(NodInfOutName)
    for i in xrange(6):
        skipheader=fID.readline()
    NodInf=fID.read()
    fID.close()
    NodInf=NodInf.replace('\nend\n','').replace('\n\n Node      Depth      Head
Moisture     K      C     Flux    Sink      Kappa   v/KsTop   Temp\n       [L]
[L]    [-]     [L/T]   [1/L]    [L/T]     [1/T]     [-]   [-]
[C]\n\n','').split('\n Time:')[1:]
    nP=len(NodInf)
    NodInf_T=[]
    NodInf_Data=[]
    for iP in range(nP):
        Buffer=StringIO.StringIO(NodInf[iP])
        NodInf_T.append(Buffer.readline())
        NodInf_Data.append(numpy.genfromtxt(Buffer))
    NodInf_T=numpy.array(NodInf_T).astype('float')
    return NodInf_T,NodInf_Data
def ReadALevelOut(ALevelOutName):
    read A_Level.out:
    0 Time
    1 sum(rTop)
    2 sum(rRoot)
    3 sum(vTop)
    4 sum(vRoot)
    5 sum(vBot)
    6 hTop
    7 hRoot
    8 hBot
    9 A-level
    import numpy
ALevel_Data=numpy.genfromtxt(ALevelOutName,delimiter=[12,14,14,14,14,14,11,11,11,8
],skip_header=5,skip_footer=1)
```

```
    return ALevel_Data
def ReadTLevelOut(TLevelOutName):
    read T_Level.out:
    0 Time
    1 rTop
    2 rRoot
    3 vTop
    4 vRoot
    5 vBot
    6 sum(rTop)
    7 sum(rRoot)
    8 sum(vTop)
    9 sum(vRoot)
    10 sum(vBot)
    11 hTop
    12 hRoot
    13 hBot
    14 RunOff
    15 sum(RunOff)
    16 Volume
    17 sum(Infil)
    18 sum(Evap)
    19 TLevel
    20 Cum(WTrans)
    21 SnowLayer
    import numpy
TLevel_Data=numpy.genfromtxt(TLevelOutName,skip_header=9,skip_footer=1)
    return TLevel_Data
```

Irrigation scenarios/maping the quasi 3D-Resolution results

```
#===============================================================================
# Open Quasi3D Resolution Results
#===============================================================================
import os
import sys
import numpy
import pylab
import fnmatch
from matplotlib.backends.backend_pdf import PdfPages
figlist=[]
figsize=[10,8]
#figsize=[20,10]
dpi=None
pylab.ioff()
font = {'family' : 'monospace',
        'size'   : 11}
pylab.rc('font', **font)
#===============================================================================
# Open
#===============================================================================
print('Open')
path='/home/supersoil/Documents/Jan/Data/Hydrus/Quasi3D_Resolution'
FiltString='Hydrus_Meisam_BatchSampleGridRun'
filelist = []
for root, dirnames, filenames in os.walk(path):
  for filename in fnmatch.filter(filenames, FiltString+'*.npz'):
      if 'FirstRun' not in root:
          filelist.append(os.path.join(root, filename))
nF=len(filelist)
Storage_Mean=[]
Storage_Std=[]
Stress_Mean=[]
Stress_Std=[]
StressArea_Mean=[]
```

```
StressArea_Std=[]
Yield_Mean=[]
Yield_Std=[]
ProcessingTime=[]
Resolution=[]
for iF in range(nF):
    filename=filelist[iF]
    Savez=numpy.load(filename)

    Storage_Sample=Savez['Storage_Sample']
    Stress_Sample=Savez['Stress_Sample']
    StressArea_Sample=1-Savez['StressArea_Sample']
    Yield_Sample=Savez['Yield_Sample']
    SampleData_Sample=Savez['SampleData_Sample']
    ProcessingTime_Sample=Savez['ProcessingTime_Sample']
    Resolution_Sample=Savez['Resolution']
    NodInf_T=Savez['NodInf_T']
    Tlevel_T=Savez['Tlevel_T']
    nS = ProcessingTime_Sample.size
#    fig=pylab.figure(figsize=figsize,dpi=dpi)
    Storage_Mean.append(Storage_Sample.mean(axis=0))
    Storage_Std.append(Storage_Sample.std(axis=0))
    Stress_Mean.append(numpy.nanmean(Stress_Sample,axis=0))
    Stress_Std.append(numpy.nanstd(Stress_Sample,axis=0))
    StressArea_Mean.append(numpy.nanmean(StressArea_Sample,axis=0))
    StressArea_Std.append(numpy.nanstd(StressArea_Sample,axis=0))
    Yield_Mean.append(Yield_Sample.mean(axis=0))
    Yield_Std.append(Yield_Sample.std(axis=0))
    ProcessingTime.append(ProcessingTime_Sample.mean())
    Resolution.append(Resolution_Sample)
    pylab.close('all')
[Storage_Mean,Storage_Std,Stress_Mean,Stress_Std,StressArea_Mean,StressArea_Std,Yi
eld_Mean,Yield_Std,ProcessingTime,Resolution]=map(lambda x :
numpy.array(x),[Storage_Mean,Storage_Std,Stress_Mean,Stress_Std,StressArea_Mean,St
ressArea_Std,Yield_Mean,Yield_Std,ProcessingTime,Resolution])
Res_Sort=numpy.argsort(Resolution)
[Storage_Mean,Storage_Std,Stress_Mean,Stress_Std,StressArea_Mean,StressArea_Std,Yi
eld_Mean,Yield_Std,ProcessingTime,Resolution]=map(lambda x :
x[Res_Sort],[Storage_Mean,Storage_Std,Stress_Mean,Stress_Std,StressArea_Mean,Stres
sArea_Std,Yield_Mean,Yield_Std,ProcessingTime,Resolution])
Storage_CVmean=numpy.mean(Storage_Std/Storage_Mean,axis=1)
Stress_CVmean=numpy.nanmean(Stress_Std/Stress_Mean,axis=1)
StressArea_CVmean=numpy.nanmean(StressArea_Std/StressArea_Mean,axis=1)
Yield_CVmean=numpy.mean(Yield_Std/Yield_Mean,axis=1)
#============================================================================
# Plot
#============================================================================
print('Plot')
cm=pylab.get_cmap('jet')
fig=pylab.figure(figsize=figsize,dpi=dpi)
ax=fig.add_subplot(111)
ax.plot(Resolution,ProcessingTime,'ko-',alpha=1)
ax.set_xlabel('Resolution')
ax.set_ylabel('Processing Time (s)')
ax.set_title('Processing Time')
figlist.append(fig)
Filt=[Resolution>0,Resolution<50]
nFi=len(Filt)
for iFi in range(nFi):
    nF=numpy.sum(Filt[iFi])
    ## Time Series CV/STD
    fig=pylab.figure(figsize=figsize,dpi=dpi)
    ax=fig.add_subplot(111)
    for iF in range(nF):
        color=cm(iF/(nF-0.999))
ax.plot(NodInf_T,Storage_Std[Filt[iFi],:][iF,:]/Storage_Mean[iF,:],'-
',color=color,alpha=1)
```

```
    ax.set_xlabel('Time')
    ax.set_ylabel('Storage')
    ax.set_title('Storage')
    figlist.append(fig)
    fig=pylab.figure(figsize=figsize,dpi=dpi)
    ax=fig.add_subplot(111)
    for iF in range(nF):
        color=cm(iF/(nF-0.999))
ax.plot(Tlevel_T,Stress_Std[Filt[iFi],:][iF,:]/Stress_Mean[Filt[iFi],:][iF,:],'-
',color=color,alpha=1)
    ax.set_xlabel('Time')
    ax.set_ylabel('Stress')
    ax.set_title('Stress')
    figlist.append(fig)
    fig=pylab.figure(figsize=figsize,dpi=dpi)
    ax=fig.add_subplot(111)
    for iF in range(nF):
        color=cm(iF/(nF-0.999))
ax.plot(Tlevel_T,StressArea_Std[Filt[iFi],:][iF,:]/StressArea_Mean[Filt[iFi],:][iF
,:],'-',color=color,alpha=1)
    ax.set_xlabel('Time')
    ax.set_ylabel('StressArea')
    ax.set_title('StressArea')
    figlist.append(fig)
    fig=pylab.figure(figsize=figsize,dpi=dpi)
    ax=fig.add_subplot(111)
    for iF in range(nF):
        color=cm(iF/(nF-0.999))
ax.plot(Tlevel_T,Yield_Std[Filt[iFi],:][iF,:]/Yield_Mean[Filt[iFi],:][iF,:],'-
',color=color,alpha=1)
    ax.set_xlabel('Time')
    ax.set_ylabel('Yield')
    ax.set_title('Yield')
    figlist.append(fig)
    ## Time Series MEAN +-STD
    fig=pylab.figure(figsize=figsize,dpi=dpi)
    ax=fig.add_subplot(111)
    for iF in range(nF):
        color=cm(iF/(nF-0.999))
        ax.plot(NodInf_T,Storage_Mean[iF,:],'-',color='k',alpha=0.1)
ax.plot(NodInf_T,Storage_Mean[iF,:]+Storage_Std[Filt[iFi],:][iF,:],'-
',color=color,alpha=1)
        ax.plot(NodInf_T,Storage_Mean[iF,:]-Storage_Std[Filt[iFi],:][iF,:],'-
',color=color,alpha=1)
    ax.set_xlabel('Time')
    ax.set_ylabel('Storage')
    ax.set_title('Storage')
    figlist.append(fig)
    fig=pylab.figure(figsize=figsize,dpi=dpi)
    ax=fig.add_subplot(111)
    for iF in range(nF):
        color=cm(iF/(nF-0.999))
        ax.plot(Tlevel_T,Stress_Mean[iF,:],'-',color='k',alpha=0.1)
ax.plot(Tlevel_T,Stress_Mean[Filt[iFi],:][iF,:]+Stress_Std[Filt[iFi],:][iF,:],'-
',color=color,alpha=1)
        ax.plot(Tlevel_T,Stress_Mean[Filt[iFi],:][iF,:]-
Stress_Std[Filt[iFi],:][iF,:],'-',color=color,alpha=1)
    ax.set_xlabel('Time')
    ax.set_ylabel('Stress')
    ax.set_title('Stress')
    figlist.append(fig)
    fig=pylab.figure(figsize=figsize,dpi=dpi)
    ax=fig.add_subplot(111)
    for iF in range(nF):
        color=cm(iF/(nF-0.999))
        ax.plot(Tlevel_T,StressArea_Mean[iF,:],'-',color='k',alpha=0.1)
```

```
ax.plot(Tlevel_T,StressArea_Mean[Filt[iFi],:][iF,:]+StressArea_Std[Filt[iFi],:][iF
,:],'-',color=color,alpha=1)
        ax.plot(Tlevel_T,StressArea_Mean[Filt[iFi],:][iF,:]-
StressArea_Std[Filt[iFi],:][iF,:],'-',color=color,alpha=1)
    ax.set_xlabel('Time')
    ax.set_ylabel('StressArea')
    ax.set_title('StressArea')
    figlist.append(fig)
    fig=pylab.figure(figsize=figsize,dpi=dpi)
    ax=fig.add_subplot(111)
    for iF in range(nF):
        color=cm(iF/(nF-0.999))
        ax.plot(Tlevel_T,Yield_Mean[iF,:],'-',color='k',alpha=0.1)
ax.plot(Tlevel_T,Yield_Mean[Filt[iFi],:][iF,:]+Yield_Std[Filt[iFi],:][iF,:],'-
',color=color,alpha=1)
        ax.plot(Tlevel_T,Yield_Mean[Filt[iFi],:][iF,:]-
Yield_Std[Filt[iFi],:][iF,:],'-',color=color,alpha=1)
    ax.set_xlabel('Time')
    ax.set_ylabel('Yield')
    ax.set_title('Yield')
    figlist.append(fig)
    ##  RESOLUTION
    fig=pylab.figure(figsize=figsize,dpi=dpi)
    ax=fig.add_subplot(111)
    ax.plot(Resolution[Filt[iFi]],Storage_CVmean[Filt[iFi]],'b-',alpha=1)
    ax.set_xlabel('Resolution')
    ax.set_ylabel('Storage')
    ax.set_title('Storage')
    figlist.append(fig)
    fig=pylab.figure(figsize=figsize,dpi=dpi)
    ax=fig.add_subplot(111)
    ax.plot(Resolution[Filt[iFi]],Stress_CVmean[Filt[iFi]],'r-',alpha=1)
    ax.set_xlabel('Resolution')
    ax.set_ylabel('Stress')
    ax.set_title('Stress')
    figlist.append(fig)
    fig=pylab.figure(figsize=figsize,dpi=dpi)
    ax=fig.add_subplot(111)
    ax.plot(Resolution[Filt[iFi]],StressArea_CVmean[Filt[iFi]],'r-',alpha=1)
    ax.set_xlabel('Resolution')
    ax.set_ylabel('Stress')
    ax.set_title('Stress')
    figlist.append(fig)
    fig=pylab.figure(figsize=figsize,dpi=dpi)
    ax=fig.add_subplot(111)
    ax.plot(Resolution[Filt[iFi]],Yield_CVmean[Filt[iFi]],'g-',alpha=1)
    ax.set_xlabel('Resolution')
    ax.set_ylabel('Yield')
    ax.set_title('Yield')
    figlist.append(fig)
#================================================================================
# Save
#================================================================================
print('Save')
basename=os.path.basename(sys.argv[0])[:-3]
directory=path
pdfname=os.path.join(directory, basename+'0.pdf')
pp = PdfPages(pdfname)
for fig in figlist:
    pp.savefig(fig)
pp.close()
#pylab.show()
os.startfile(pdfname)
```

Appendix-Chapter 5-2. An example of sampling location (resolution 30 x 30 m).

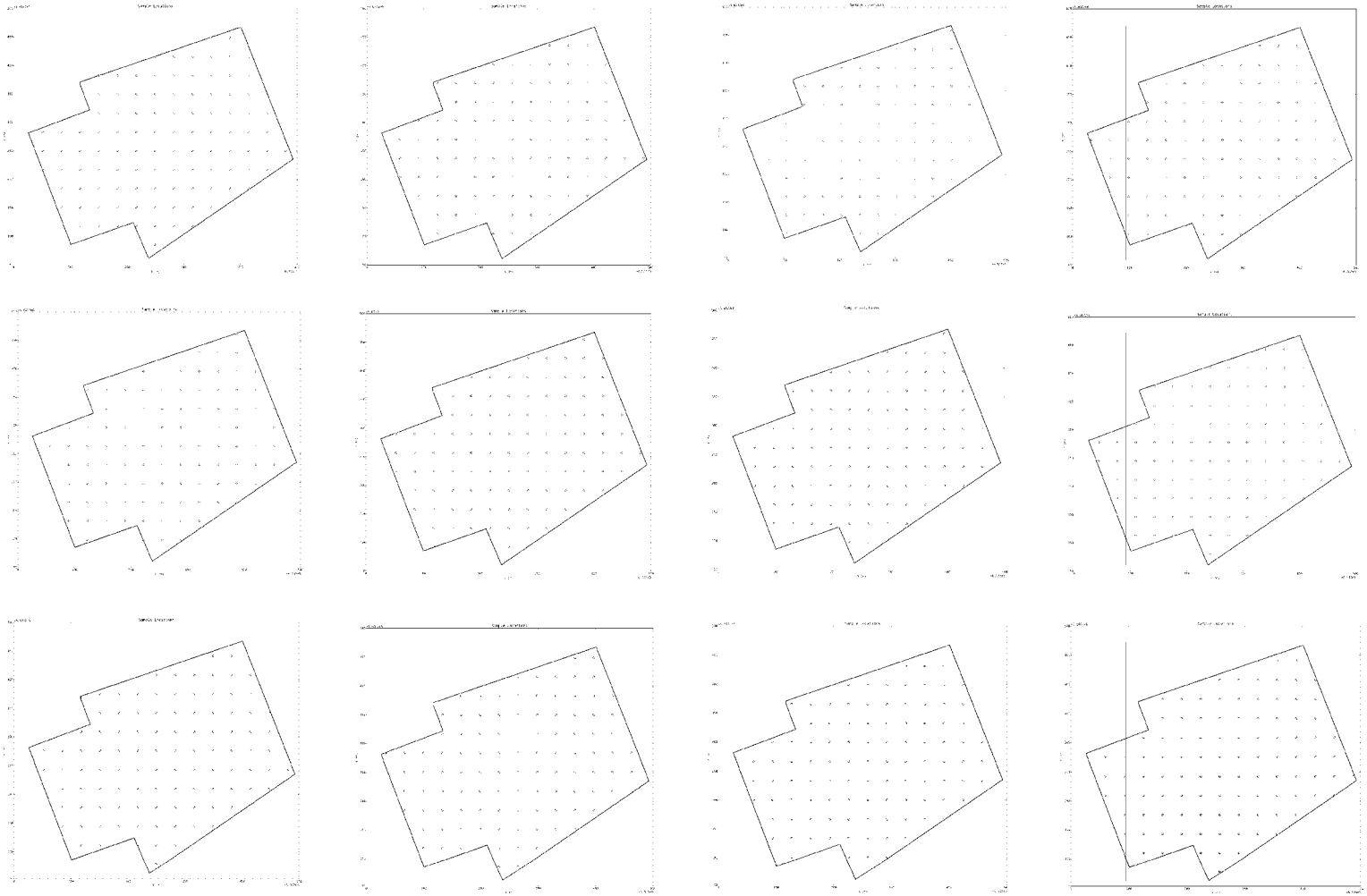

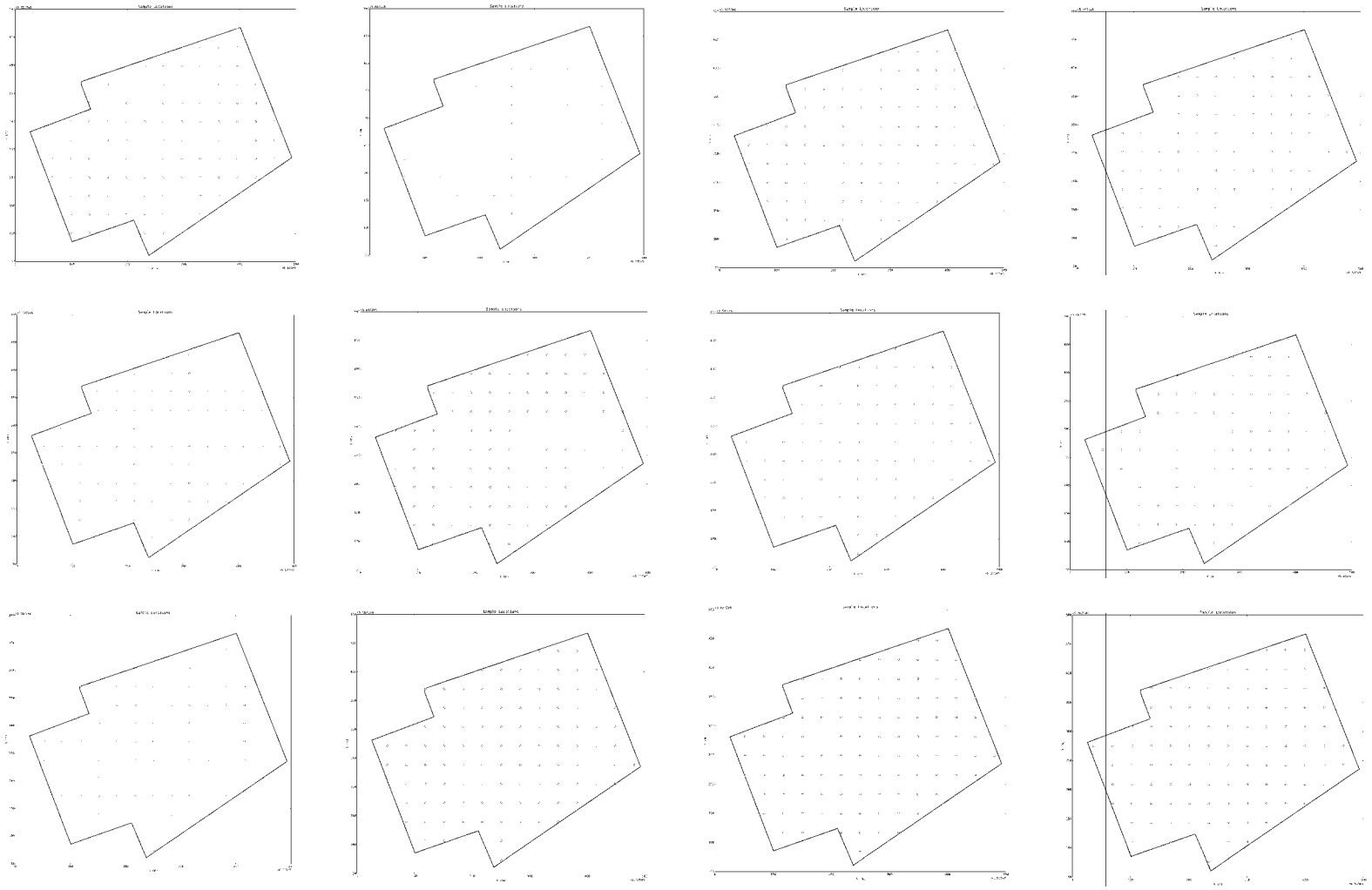

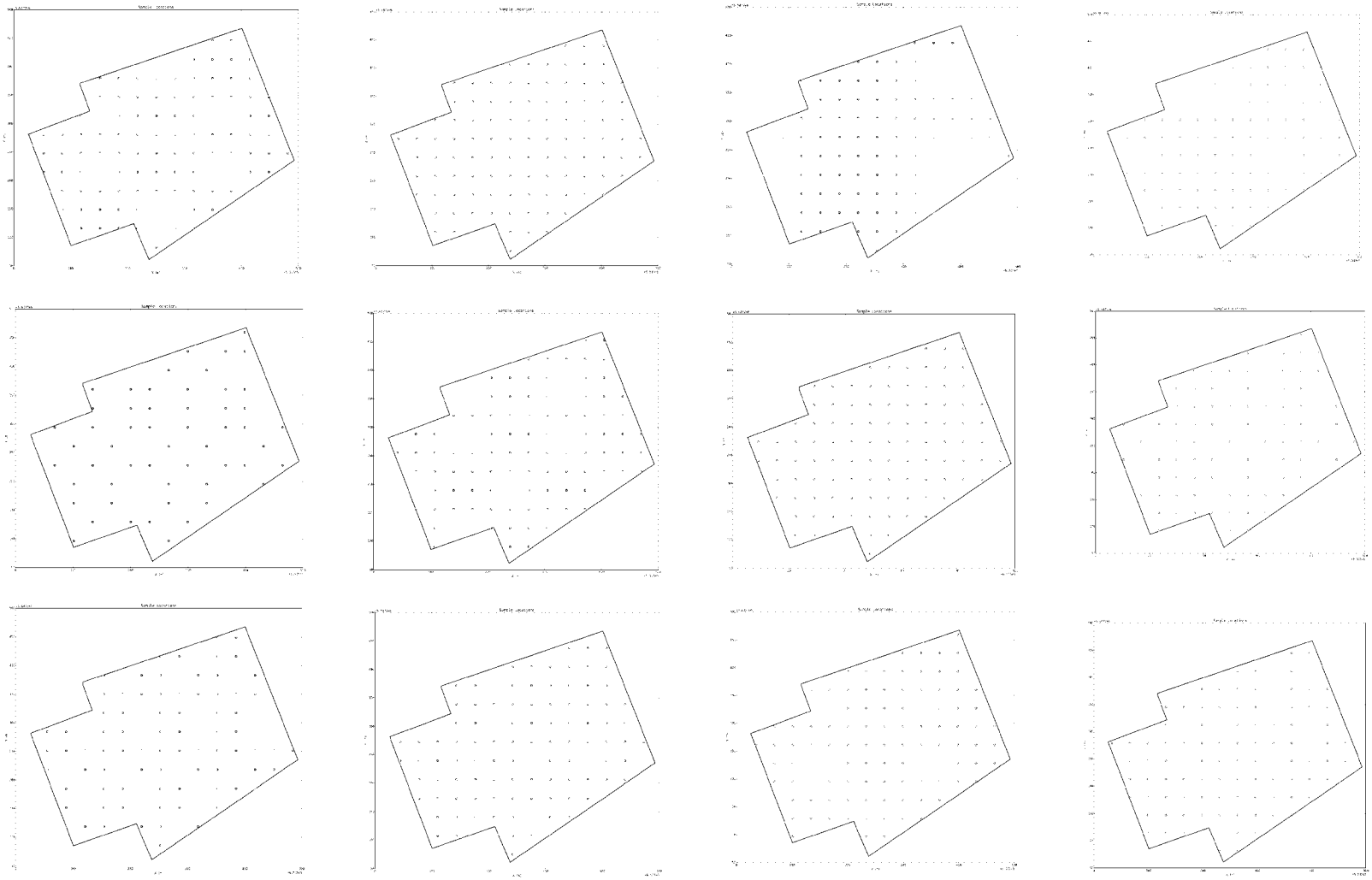

Curriculum Vitae

Personal information

Full name:	Meisam Rezaei
Date of birth:	06/12/1982, Khomein, Iran
Nationality:	Iranian
Affiliation:	1) Department of Soil Management, Faculty of Bioscience Engineering, Ghent University, 9000 Ghent, Belgium; 2) Unit Environmental Modeling, Flemish Institute for Technological Research (VITO NV), 2400 Mol, Belgium 3) Department of Biology, Faculty of science, Antwerp University, 2610 Wilrijk, Belgium
Contact details:	Tel: +3292646038(Gent office), +3214336896 (VITO office), Cell phone: +32486446398, Fax: +3292646247, E-mail: Meisam.rezaei@ugent.be; Meisam.rezaei@vito.be; Meisam.rezaei1@gmail.com

Education and training

2012- now	**PhD Candidate in Bioscience Engineering,** Ghent University, 9000 Ghent, Belgium ***Thesis:*** Characterization and Modeling of Water Flow in Sandy Soils for Irrigation Optimization. Supervisors: *Piet Seuntjens, Wim Cornelis, Ingeborge Joris*
2009-2011	**Reasercher:** Soil and Water Research Institute of Iran, Karaj, Iran ***Research Topic:*** Study of Chemical Forms and Behaviour of Contaminants in Persian Gulf War Polluted Lands. Advisors: *Kambiz Bazargan, Karim Shahbazi*
2005-2008	**Master in soil engineering:** Faculty of Water and Soil Engineering, Gorgan University of Agricultural Sciences & Natural Resources, Gorgan, Iran ***Thesis:*** Effect of zeolite amendment on adsorption and desorption kinetics of ammonium, phosphate and potassium in Rahmat Abad Soil Series of Golestan province. Supervisors: *Seyed Alireza Movahedi Naeini, Farhad Khormali*
2001-2005	**Bachelor in Soil Science:** Soil Science Department, Ferdowsi University of Mashhad, Mashhad, Iran

Awards and fellowships

2008	**First rank master student,** Gorgan University of Agricultural Sciences & Natural Resources, Gorgan, Iran
2012	**PhD scholarship:** Ministry of Science, Research and Technology (MSRT) of Iran
2016	**Postdoctoral researcher,** Antwerp university and VITO, Belgium

Research interest

Soil physics, Vadose zone hydrology, Contaminant hydrology, Modeling of water flow, chemical transport and interaction between water/fluid flow in the porous media, Land and water management

Publications

International/national peer reviewed

- **Rezaei, M.,** Seuntjens, P., Joris, I., Wesley Boënne., Van Hoey, S., Campling, P. Cornelis, W. 2016. Sensitivity of water stress in a two-layered sandy grassland soil to variations in groundwater depth and soil hydraulic parameters. *Hydrology and Earth System Sciences*. 20 (1): 487-503.
- **Rezaei, M.,** Seay, T., Seuntjens, P., Joris, I., Wesley Boënne., Van Meirvenne, M, Cornelis, W. 2016. Predicting saturated hydraulic conductivity in a sandy grassland using proximally sensed apparent electrical conductivity. *Journal of Applied Geophysics*. 126: 35-41.
- **Rezaei, M.,** Seuntjens, P., Shahidi, R, Joris, I., Wesley Boënne., Al-Barri, B., Cornelis, W. 2016. The relevance of in-situ and laboratory characterization of sandy soil hydraulic properties for soil water simulations. *Journal of Hydrology*. 534: 251–265.
- **Rezaei, M.,** Movahedi Naeini, S.A.R. 2009. Kinetics of potassium desorption from a loess soil, soil mixed with zeolite, and the Clinoptilolite Zeolite as influenced by calcium and ammonium. *Journal of Applied Science.* 9(18):3335-3342.
- **Rezaei, M**., Movahedi Naeini, S.A.R. 2009. Effects of ammonium and natural zeolite on potassium adsorption and desorption kinetics in a loess soil. *International Journal of Soil Science*. 4: 27-45.
- Bagherifam, S., Lakzian, A., **Rezaei, M**. 2010. Uranium Removal from Aqueous Solutions by Iranian Natural Zeolite – Riched Clinoptiolite. *Journal of Water and Soil*. 24 (2): 208-217. In Farsi.
- **Rezaei, M.,** Movahedi Naeini, S.A.R. and Khormali, F. 2010. Potassium Quantity – intensity (Q/I) curves for two soils as affected by Zeolite additions. Pajuhesh and sazandegi journal. 91: 27-34. In Farsi.
- **Rezaei, M.** and Movahedi Naeini, S.A.R. 2010. The effect of ammonium presence on adsorption and desorption kinetics of potassium in soil, zeolite and mixture of zeolite and soil. *EJANG*. 2 (2): 29-48. ejang@gau.ac.ir. In Farsi.

Conference Papers

- **Rezaei, M.,** Seuntjens. P., Joris, I., Boënne, W., De Pue, J., Cornelis, W. 2016. Quasi 3D modelling of water flow in the sandy soil. *Geophysical Research Abstract. Vol. 18, EGU2016-15295. 17-22 April, Vienna, Austria. Oral.*
- **Rezaei, M.,** Seuntjens, P., Shahidi, R., Joris, I., Boënne, W., Cornelis, W. 2016. Sensitivity of soil water content simulation to different methods of soil hydraulic parameter characterization as initial input values. *Geophysical Research Abstract. Vol. 18, EGU2016-15225. 17-22 April, Vienna, Austria. Poster.*
- **Rezaei, M.,** Seuntjens, P., Shahidi, R, Joris, I., Wesley Boënne., Cornelis, W. 2016. How soil water simulations using a hydrological model are affected by in-situ and laboratory hydraulic parameter sets. *Eurosoil 2016 Istanbul. Oral.*
- **Rezaei, M.,** Seuntjens, P., Joris, I., Boënne, W., Cornelis, W. 2014. Estimation of the spatial distribution of soil hydraulic characteristics using apparent soil electrical conductivity as proxy data. *TERENO International Conference. 29 Sep-2 Oct. Bonne Germany. oral*
- **Rezaei, M.,** Seuntjens, P., Joris, I., Boënne, W., Cornelis, W. 2014. An alternative tool to predict and upscale soil saturated hydraulic conductivity: apparent soil electrical conductivity. *In the 9th International Soil Science Congress on "The Soul of Soil and Civilization" in Side, Antalya, Turkey. 14-17 October. Abstract.*
- **Rezaei, M.,** Seuntjens. P., Joris, I., Boënne, Shahidi, R., W., De Pue, J., Cornelis, W. 2014. Effects of spatial variability of soil hydraulic properties on hydrological model for irrigation management purposes. *In the 9th International Soil Science Congress on "The Soul of Soil and Civilization" in Side, Antalya, Turkey. 14-17 October. Abstract.*
- **Rezaei, M.,** Seuntjens, P., Joris, I., Boënne, W., Van hoey, S., Cornelis, W. 2013. Optimizing Hydrus 1D for irrigation management purposes in sandy grassland. In proceeding of: *The 2nd European Symposium of Water Technology & Management. Leuven, Belgium. pp 122-126. Poster.*
- Bahreini Toohan, M., **Rezaei, M.,** Movahedi Naeini, S.A.R. 2008. Physical and nutritional amendment of topsoil using zeolite. *Iran International Zeolite Conference (IIZC), 29 April-1May. Tehran (In Farsi).*
- **Rezaei, M.,** Movahedi Naeini, S.A.R. 2008. The effect of soil incorporated zeolite on potassium quantity-intensity (Q/I) relations. *Iran International Zeolite Conference (IIZC), 29 April-1May. Tehran (In Farsi).*
- **Rezaei, M.,** Bahreini Toohan, M., Movahedi Naeini, S.A.R., Khormali, F. 2008. Zeolite applications for industrial waste water filtration. *Iran International Zeolite Conference (IIZC),* April 29-May 1, 2008, Tehran (In Farsi and English).
- **Rezaei, M.,** Akhzari, D., Keshavarzi, A., Alaodin, M.Z., Taheri, V., Movahedi Naeini, S.A.R. 2008. The effect of ammonium on potassium desorption by Zeolite. *Iran International Zeolite Conference (IIZC), 29 April-1May. Tehran (In Farsi)*
- Ghanei, M., **Rezaei, M.,** Pashaei Aval, A., Khormali, F., Mosaedi, A. 2007. Soil salinity and acidity maps for Aghghala agricultural lands (Golestan Province). *10th Iranian Soil Science Congress. Karaj. Iran (In Farsi).*
- **Rezaei, M.,** Ayubi, Sh., Ghergherechi, Sh. 2007. Estimating soil erosion from Ziarat areas of Golestan province by RUSLE model. *10th Iranian Soil Science Congress. Karaj. Iran (In Farsi).*

Books

- Movahedi Naeini, S.A.R. and **Rezaei, M.** 2009. Soil Physics; Fundamentals and Applications. Gorgan University of Agricultural Sciences and Natural Resources Publications, Gorgan, Iran. (In Farsi). 473p. ISBN: 978-964-8926-24-8

Reports

- **Rezaei, M.,** Seuntjens, P., Joris, I., Cornelis. W. 2015. Data assimilation of in situ soil moisture measurements in hydrological models: third annual doctoral progress report, work plan and achievements. 23p.
- **Rezaei, M.,** Seuntjens, P., Joris, I., Cornelis. W. 2014. Data assimilation of in situ soil moisture measurements in hydrological models: second annual doctoral progress report, work plan and achievements. 25p.
- **Rezaei, M.,** Seuntjens, P., Joris, I., Cornelis. W. 2013. Data assimilation of in situ soil moisture measurements in hydrological models: first annual doctoral progress report, work plan and achievements. 25p.

Regular courses followed

Title	Coordinator/Teacher	Organizers / Institute	Date/period
• *Contaminant transport in soil*	*Prof. Piet Seuntjens*	*Ghent University*	*2012-2013*
• *Soil physics*	*Prof. Wim Cornelis*	*Ghent University*	*2012-2013*
• *Land information system*	*Prof. Ann Verdoodt.*	*Ghent University*	*2012-2013,*
• *Intermediate academic English course*	*UTC*	*Ghent University*	*2012-2013*
• *Advanced Academic English: Conference Skills Presentation Skills in English*	*UTC*	*Ghent University*	*2013-2014*

Seminars workshop and summer school

Title	Coordinator/Teacher	Organizers / Institute	Date/period
• *Aquacrop workshop*	*Prof. Dirk Raes*	*KU Leuven University*	*16 to 20 July 2012*
• *ENVITAM course on HP1 (HYDRUS + PHREEQC)*	*Diederik Jacques*	*Gent university/SCKSEN*	*25-28 March 2013*
• *Let's talk science*		*Brussel/Gent/ Antwerp/ Hassalt universities*	*2-4 July 2014*
• *COMSOL Multiphysics Workshop-Fluid dynamic modeling*	*Frank de Pont*	*COMSOL Inc.*	*24 March 2016*

Projects

2009-2011	**UNCC projects at Soil and Water Research Institute of Iran**: Study of Chemical Forms and Behaviour of Contaminants in Persian Gulf War Polluted Lands • Sorption and Desorption of Heavy Metals by Contaminated Soils of Khuzestan Province • Determination of the best extractant for evaluation of heavy metals plant availability in selected contaminated soils of Khuzestan Province.
2016-2017	**Flemish Institute for Technological Research (VITO) and Antwerp University Project:** • Flow field distortion and contaminant exchange kinetics for the IFLUX design concept

رَّبِّ زِدْنِي عِلْمًا (طه، 114)

"O my Lord! advance me in knowledge. (Holly Quran: 20:114)"